CRANFIELD INSTITUTE OF TECHNOLOGY

SCHOOL OF INDUSTRIAL SCIENCE

PhD THESIS

LUISA QUINTINO

FUSION CHARACTERISTICS IN P-GMAW OF MILD STEEL

Supervisor: Professor R.L. Apps

April 1986

CRANFIELD INSTITUTE OF TECHNOLOGY

SCHOOL OF INDUSTRIAL SCIENCE

PhD THESIS

LUISA QUINTINO

FUSION CHARACTERISTICS IN PULSED-, GMAW OF MILD STEEL

Supervisor: Professor R.L. Apps

April 1986

ABSTRACT

The influence of process parameters on deposition and fusion characteristics of mild steel with Pulsed Gas Metal Arc Welding has been investigated using a transistorized power supply.

A simple model of melting behaviour has been developed which allows the prediction of dilution behaviour and explains the interplay between mass and heat in P-GMAW. In order to predict heat affected zone area, a model driven from the former one has also been developed.

Deposition characteristics were studied taking the care of studying the influence of each welding parameter at each time, whenever it was possible. Emphasis was given to shielding gas mixture which was found to significantly influence metal transfer mode and arc stability.

A systematic approach to choose process parameters in Pulsed Gas Metal Arc Welding with a constant current power supply is proposed.

It was found that mean current and welding speed play the most important role in determining fusion characteristics, thus, based on a simple model, methods of controlling these aspects are suggested. Emphasis was placed on understanding dilution behaviour.

It was found possibility to develop procedures allowing the independent choice of deposition rate and dilution behaviour and to give an account of many observations with simple models of melting phenomena.

The developed model is combined with calorimetric heat transfer measurements to investigate the result that only a small fraction of the total process power is required to melt the observed fusion areas. A "dual Heat" source fusion model is suggested where plate melting is largely in response to direct arc heating, providing means of optimising plate dilution and thereby reducing the risk of fusion defects.

A generalized representation of fusion characteristics is given which allows independent selection of required fusion characteristics to be assessed.

ACKNOWLEDGEMENTS

I want to express my gratitude to Dr. C. J. Allum for the assistance and the guidance during this project and my friend Zé Francisco for his enthusiasm and consistent encouragement.

I wish also to express my admiration and gratitude to my supervisor, Professor R. L. Apps, for his support and advice.

It is a pleasure to acknowledge the contribution of the staff of the "Underwater Welding Group" for the assistance during the experiments, of Mrs. Isabel Nunes, Mrs. Beatriz Nolasco and Mr. Carlos Marques for transforming a pile of untidy pages and drawings to the present form.

The financial support of the Gulbenkian Foundation is acknowledged especially the assistance of Mrs. Maria Raquel Almeida Dias.

I am also indebted to the Instituto Superior Técnico (Technical University of Lisbon) and the Instituto de Soldadura e Qualidade (Portuguese Welding Institute) for their support which enabled me to carry out this work.

I could not possibly forget the support of my parents and parents-in-law and, without doubt, this thesis would not have been completed without the tolerance and encouragement of my husband, Luis. This is deeply appreciated.

To my children Miguel and Margarida

LIST OF CONTENTS

LIST OF CONTENTS PAGE

LIST OF TABLES

TABLES

32 - Thermal diffusivity values obtained from equation (155)

33 - Values of θ_1 and θ_2 for beads deposited in V grooves

34 - Theoretical and experimental values of dilution in V grooves

35 - Theoretical and experimental values of dilution in V grooves

36 - Correction factor affecting dilution

37 - Calculated and experimental values of the product fusion area (A_F) x squared welding speed (v^2) in V groove.

38 - Calculated and experimental values of the product fusion area (A_F) x squared welding speed (v^2) in V grooves

39 - Correction factor affecting the product of fusion area and squared welding speed

40 - Effective plate heating voltage in V groove

41 - Weld metal recovery factor (η)

LIST OF PHOTOGRAPHS

PHOTOGRAPHS

1 - AWP M 500 synergic unit

2 - AWP M 450 PS synergic unit

3 - Influence of shielding gas composition on slag formation

4 - Influence of shielding gas composition on bead appearance (1.0 mm wire diameter, 25 mm plate thickness)

5 - Influence of shielding gas composition on bead appearance (10. mm wire diameter, 6 mm plate thickness)

6 - Influence of shielding gas composition on bead appearance (1.2 mm wire diameter, 25 mm plate thickness)

7 - Influence of shielding gas composition on bead appearance (1.2 mm wire diameter, 6 mm plate thickness)

8 - Influence of shielding gas composition on bead appearance (1.6 mm wire diameter, 25 mm plate thickness)

9 - Influence of shielding gas composition on bead appearance (1.6 mm wire diameter, 6 mm plate thickness)

LIST OF FIGURES

FIGURES

45 - Influence of background parameters on burn-off rate

46 - Influence of mean current on bead penetration, reinforcment height and width

47 - Influence of mean current on penetration for different heat inputs

48 - Influence of shielding gas composition and wire diameter on penetration

49 - Influence of shielding gas composition and wire diameter on width of the bead

50 - Influence of shielding gas composition and wire diameter on reinforcement

51 - Influence of electrode extension on penetration, width and reinforcement height

52 - Influence of heat input on penetration for a range of mean currents

53 - Influence of welding speed on penetration

54 - Influence of welding speed on reinforcement height on the bead

55 - Influence of welding speed on width of the bead

56 - Influence of peak current on penetration for 250 Amps current

57 - Influence of mean current on wetting angle and fusion angle

58 - Influence of mean current on bead shape factor

59 - Influence of shielding gas composition on bead wetting angle and mean arc voltage

60 - Influence of shielding gas composition on bead shape factor and fusion angle

61 - Influence of nominal heat input on wetting angle and fusion angle

62 - Influence of nominal heat input on bead shape factor

63 - Effect of arc current and welding speed on bead plate wetting angle

64 - Influence of welding speed on plate fusion angle

65 - Influence of welding speed on bead shape factor for different mean currents

66 - Bead shape in mild steel with an Ar/5% CO_2 shield for a 1.2 mm wire size

67 - Influence of peak parameters on bead shape factor

68 - Influence of mean current on plate fusion area for 1.2 mm wire size in an Ar/5% CO_2 shield on thick plate

69 - Influence of arc current on plate fusion area

70 - Influence of mean current on total fusion area and reinforcement area

71 - Influence of wire size and shield gas composition on plate fusion area

72 - Influence of wire size and shielding gas composition on total fusion area

73 - Influence of electrode extension on plate fusion area for mean currents of 100 and 150 A and 1.0, 1.2 and 1.6 mm wire diameters in an Ar/5% CO_2 shield

74 - Influence of electrode extensition on reinforcement area

75 - Influence of electrode extension on total area

76 - Influence of nominal heat input on plate fusion area

77 - Influence of nominal heat input on total fusion area

78 - Influence of welding speed on plate fusion area (A_F)

79 - Influence of welding speed on total fusion area (A_T) and reinforcement area (A_D)

80 - Influence of electrode extension on dilution for mean currents of 100 and 150 A and wire diameters of 1.0, 1.2 and 1.6 mm

81 - Influence of nominal heat input on dilution for a range of mean currents

82 - Influence of welding speed and arc current on dilution

83 - Influence of peak parameters on dilution

84 - Influence of welding speed on heat affected zone area

85 - Influence of I/v on heat affected zone area for two different shieldings

86 - Weld bead shape in a V groove

87 - Influence of shielding gas composition on wetting angle in V grooves

88 - Influence of shielding gas composition on wetting angle in V grooves

89 - Influence of the product mean current ($\bar{I}$) x welding speed (v) on dilution (60^o)

90 - Influence of the product mean current ($\bar{I}$) x welding speed (v) on dilution (90^o)

91 - Influence of the product mean current (I) x welding speed (v) on dilution (120^o)

92 - Average weld pool temperature for GMAW of mild steel

93 - Axial plasma velocity 7 mm from the electrode tip as a function of current

NOMENCLATURE

NOMENCLATURE

A_F - Plate fusion area

A_T - Total fusion area

A_D - Deposit area

A_{HAZ} - Heat affected zone area

A - Cross sectional area of the wire

a - Acceleration

C_p - Specific heat

C_D - Drag coeficient

c - Capilarity constant

C_{PL} - Specific heat of liquid metal

D - Detachment parameter

d - Wire diameter

d_A - Wire diameter of fusion area

e - Electron charge

F - Pulse frequency

F_P - Electromagnetic force

F_T - Surface tension force

F_g - Gravity force

F_E - Force due to vapourization and chemical reactions

F_d - Drag force

g - Gravitational acceleration

h - Reinforcement height

H_a - Anode heating

H_m - Heat needed to bring unit mass of metal from ambient temperature of liquid state

H_L - Heat content of electrode extension

H_c - Heat content at reference level

H_v - Latent heat of vapourization

H_r - Resistance heating

$\bar{I}$ - Mean current

I_p - Peak current

I_b - Background current

j - Current density

K - Thermal conductivity

K_L - Thermal conductivity in liquid

l - Electrode extension

m - Mass of the droplet

$\dot{m}$ - Mass melted per second

m_v - Mass of vapourized metal

n - Operating parameter

p - Penetration depth

P - Pressure

q - Heat input

Q_w - Heat required to melt the wire and super heat the droplet

r - Electrode radius

R - Distance

$\dot{R}$ - Resistance of wire extension

R_D - Radius of sphere

R_e - Reynolds number

r_a - Radius of fusion area

t - Time

T - Temperature

T_m - Melting temperature

T' - Temperature of electrons

t_p - Peak duration

t_b - Background duration

T_d - Droplet temperature

T_o - Initial temperature

T_c - Temperature at reference level

V - Voltage

v - Welding speed

V_{ET} - Effective voltage

$\bar{V}$ - Flow velocity

V_a - Anode fall

v_s - Velocity of fluid stream

v_{eff} - Effective velocity

v_d - Droplet velocity

W - Melting rate

W_a - Melting rate due to anode heating

W_r - Melting rate due to resistance heating

w - Width of the bead

Z_m - Melting efficiency

Z_m^* - Plate melting efficiency

$\bar{\alpha}$ - Modified burn-off factor

α - Burn-off factor

β - Burn-off factor

$\bar{\gamma}$ - Specific gravity

γ_s - Bead shape factor

δ - Dilution

η - Process efficiency

Θ - Wetting angle

$\dot{\theta}$ - Dimensionless temperature

ρ - Diffusivity

ρ_L - Diffusivity in liquid phase

ρ_m - Density of metal

ρ_g - Density of the flowing medium

ν - Kinematic viscosity

$\not{\phi}$ - Droplet volume

$\emptyset$ - Thermoionic work function

$\emptyset_o$ - Thermoionic work function of the cathode surface

μ - Viscosity

μ_o - Magnetic permitivity of vacuum

σ - Electrical conductivity

$\dot{\sigma}$ - Surface tension

Φ - Droplet volume

ζ - Plate fusion area

In the interest of clarity, all equations and other expressions have used the symbols, even when the original work quoted has adopted a different nomenclature.

When a relatively obscure symbol is used only once, it is defined in the text.

CHAPTER 1 - INTRODUCTION

CHAPTER 1 - I N T R O D U C T I O N

The MIG or GMA welding process was introduced to industry in the fourties. It was initially used for aluminuim and later developed for steel and other non-ferrous alloys. In the beginning power sources with constant current characteristics were used but the need of arc voltage control was soon felt. Subsequently, the constant potential power source was introduced and the self adjustment so available has been of great use in practice.

Fundamental research work in MIG welding was undertaken in the fifties and was related mainly to the study of the characteristics of the electrical arc, metal transfer and heat in the filler and base materials, but it is only recently that significant progress has been made in the study of the physical phenomena associated with metal transfer, heat and mass flow in this welding process. In conventional MIG welding, only limited control of metal transfer is possible, primarily due to limitations in power supply design; on the other hand this welding process is associated with poor fusion characteristics (fusion defects) and spatter. These problems were largely associated with the explosive nature of the short circuiting transfer mechanism used in most cases (e.g. positional welding) and to the inherent lack of process control available in the conventional equipments.

In the sixties the use of pulsed current was presented as an alternative technique for overcoming the high current at wich the onset of spray transfer occurs in steels and for welding thin aluminium, but until recently, precise control of pulse characteristics was not possible with the commercialized equipment. Recently, the appearance of comercial solid state power supplies presented the possibility of occurately controlling process parameters and resulted in renewed interest in MIG welding.

At the center of present development is the capability of controlling current waveform parameters in open arc pulsed current MIG welding accurately and independently such that these may be varied in a continuous manner. The potential of such control techniques has been recognised on an international scale and a range of pulsed GMAW control techniques using synergic and/or voltage control is currently available. Emphasis so far appears from the available literature to have been directed at

transfer characteristics and little has been stated about fusion. However, fusion characteristics are of basic importance in the development of any welding procedure since the nature of fusion is not only associated with weld soundness an essential requirement, but also has metallurgical implications and hence may affect mechanical properties.

In Pulsed GMA Welding the characteristics of welding are intricately linked to power supply specifications. The problem of choosing welding parameters for a given application therefore requires specification of a wide range of variables, often with individually competing effects. Previously, operator "preference" and "trial and error" solutions often determined the welding parameters adopted. However, in present situation, a clearer idea must be required of how mass and heat combine to influence fusion characteristics.

In this work, the effects and interactions of some of the variables in pulsed GMAW of mild steel are examined. Emphasis is placed on how wire and shielding gas composition affect bead and deposition characteristics. Other variables included in the study are electrical stick-out, mean current and welding speed. The interplay between mean current and welding speed is considered for GMAW and methods are suggested for controlling fusion behaviour. The aspects of penetration are considered and a suggestion to explain the experimental results obtained is assessed. Attention was largely focused on bead on plate welds in mild steel but experiments were also undertaken in V grooves.

GMAW has potential uses ranging from thin sheet to heavy section narrow gap welding and also finds application in surfacing. This range of applications leads to the requirements for a general understanding of how process parameters affect fusion behaviour. Here, it is found possible to develop procedures allowing the independent choice of deposition rate and dilution behaviour. A simple model of melting behaviour is developed where particular emphasis is placed on dilution behaviour and predictions are compared with experimental results. Consideration are also given to the result that only a small fraction of the total process power ($\simeq$5%) is required to create the observed plate fusion.

Results suggest that a "dual heat" source fusion model where plate melting is largely in reponse to direct arc heating; such a model suggests means of optimising plate dilution and thereby reducing the risk of fusion defects.

CHAPTER 2 - LITERATURE SURVEY

CHAPTER 2 - L I T E R A T U R E S U R V E Y

2.1 - DEVELOPMENT OF ARC WELDING

The first attempt to use the intense heat obtained with a carbon arc for welding took place in 1881 by Auguste de Meritens. In 1885, Bernardos used a carbon graphite electrode to obtain an arc. This welding process was used to make tanks, casks, pipes, etc. Two years later, Slaviaroff announced a process in which the carbon electrode was replaced by a metal rod which gradually melted and added fused metal to the weld. Despite this advance in the technology, commercial application of the metal-arc process in the following years was slow, because satisfactory metal electrodes were not available.

In 1907, Kjellborg, of Sweden, developed a covered electrode where a thin cover was used for stabilization of the arc. This was the beginning of manual metal arc welding, a process that is to this day, widely used in industry.

During World War I, welding technology was quickly developed. Ships and planes began to be built using welding. Nevertheless, in spite of the large field of applications of arc welding, further developments were slow until the thirties. By this time, in manual metal arc welding, new electrode coatings and improved AC welding transformers gave improved arc stability and weld quality. Mechanised arc welding was introduced with the submerged arc welding process which gives high deposition rates with acceptable weld quality.

Nevertheless, with none of these slag shielded processes, it was possible to have welds without atmospheric contamination in reactive metals, like aluminium and magnesium.

To overcome this difficulty, Hobart and Denver developed a gas shielded welding process, in which helium and a tungsten non-consumable electrode were used. Subsequently, argon shielding gas has prooved more popular and the process was called "Tungsten inert gas welding (TIG)".

The TIG process was unsatisfactory for welding thick sections of highly conductive materials. The use of a consumable electrode enabled this difficulty to be overcome and led to the appearance of the "gas metal arc welding process (GMAW)" in which applications were quickly developed for ferrous and non-ferrous metals and alloys.

In 1950, carbon dioxide was used as shielding gas for steel welding. This process was adopted by automative shops and other metal working plants for applications where the quality of the weld was not particularly critical. In order to obtain high quality welds, argon or argon and oxygen or argon and carbon dioxide mixtures were used.

In the last 25 years, developments in arc welding have been significant and opened a large field for research. In the seventies, one of the most important progress was the rise of highly stable power supplies which opened chances of examine arc welding process characteristics in much greater detail.

2.2 - GAS METAL ARC WELDING

2.2.1 - General description

GMA welding is a process in which an electrical arc is drawn between a consumable wire electrode and the plate. The melted metal is shielded from atmospheric contamination by a gas or gas mixture; fully inert gases have been used in which case the process is called "Metal Inert Gas" welding (MIG); but for steels active gases (CO_2, O_2) have been used either totally or mixed with inert gases in which case the process is termed "Metal Active Gas" welding (MAG).

This process can also be termed as GMAW (Gas Metal Arc Welding) and sometimes with a designation related with the transfer mode, (i.e.):

- pulsed arc - (GMAW - P)
- short-circuiting - (GAMW - S).

The equipment for GMA welding comprises mainly of a power supply, a shielding gas supply, a welding torch and a wire feed system. A control system is employed to initiate and terminate the shielding gas and cooling water,operate the welding contactor and control the wire feed speed.

2.2.2 - Equipment for GMAW

2.2.2.1 - Conventional equipment

Usually the conventional equipment operates in constant

flat V-I characteristics which is better for short-circuiting transfer type.

On this type of power source, the voltage is set at the power source and the current is determined by the wire feed speed, which is usually set at the wire feeder. Increasing the wire feed speed, increases the current and vice-versa. Arc length plays an important part in GMAW, however when using this constant voltage power source and a wire feeder which delivers the wire at a constant speed, arc length changes due to inevitable operator error, or plate irregularities but it is automatically compensated due to the characteristics of this process (self-regulation). In order to compensate the described changes, mean current is altered during the welding operation, thus leading to alterations on the process characteristics.

The gas flow is controlled by a flowmeter. The welding gun, which can be water cooled or air cooled, is normally equipped with a trigger switch that controls all the functions necessary to make the weld.

Most of the wire feeders available are designed for use with constant potential power sources. The welding current is controlled by increasing and decreasing electrode feed speed for a given setting of the power source. The control of the wire speed can be mechanical, electro-magnetical or electronic.

The introduction of the new technologies in welding equipment has had a significant impact in the last ten years and the most significant step has been the commercialization of transistorized power sources for GMA welding. The pulsed MIG process has been the main beneficiary of transistorized control, providing the industry with high performance equipment that enable accurate control of the process.

2.2.2.2 - Power source developments

It has taken quite a long time to apply to welding the "new" electronic technology. In this field, phase-control thryristor equipment was, until recently, considered "up market". Nevertheless, recently a search for new GMA welding power sources that enable a greater control of the process, e.g. response time, accuracy and repeatability mainly in view of mechanized applications, began.

During the recent years, the most important developments in this field have been: SCR phase control enabling welding voltage/wire feed speed to be preset and maintained during the operation; series regulator enabling high efficiency of feedback circuits, thus accurate and repeatable output; secondary chopper with most of the features of the series regulator but less accurate and less expensive and the use of small invertors (ref.8).

2.2.2.3 - Solid state power supplies

During the past ten years, the flexibility and high response of the transistor power source have been exploited in order to develop new welding techniques in GMA welding. For example, to improve arc stability and to provide a more flexible short-circuiting GMAW process, a technique has been developed which has two essential features: the short circuiting parameters can be set quite independently of the arcing parameters and all parts of the current wave form are accurately controlled (ref. 5,6,9). This improves stability and induces less spatter; nevertheless it is the use of pulse current and vertical V-I characteristic that is the most important step ahead in this field. In this technique, the transistor power source capabilities were used to set, precisely, the requirements for metal transfer. The basic unit pulses, for various combinations of material, wire diameter, etc., where the parameters are pre-programmed into the welding control unit (refs. 24, 25, 26, 27). The operator selects the appropriate programme for each case, sets the wire feed speed and the power source delivers the optimum parameters to maintain the correct burn-off rate. Feedback is obtained from a tacho - generator mounted on the wire which monitors directly the wire feed speed (synergic control). Arc length control has been found to be desirable also in some cases (self--regulating control).

A large range of these equipments is presently available which goes from the fully-programmable wave forms to the so-called "one--knob" machines (ref. 22).

These "one-Knob" machines are provided with a control sistem that enables the control of the process to be entirely achieved by a single adjust-

ment, i.e., the power supply can simply be turned on at any desired current level and the welding conditions (e.g. stability, droplet size, etc.) can be made independent of welding current. Heat input, bead size or,in one word, welding characteristics are chosen or changed during welding by means of one-knob adjustment. These type of equipment is well-suited for use in automated or robotic welding systems.

The "one-knob" machines, although the simplest to use, can present important limitations for certain operations where control is required over more than one variable (mean current). These are, nevertheless, commercially available equipments with different degrees of control possibilities, the more sophisticated ones being fully programmable.

Computerized systems are presently being incorporated in welding power supplies enabling higher performance of the equipments and better accuracy and control of the welding process.

2.2.2.4 - Developments in wire feed systems (refs. 10, 11)

Most wire feeders employ a similar form of mechanical drive: the wire is guided into a pair of driven rools with their axes at right angles to the wire, the wire is pinched between the rolls, using an adjustable pressure screw or toggle, and is driven into a second guide tube towards the welding head. These systems have several disavantages, including the scarring of the wire if there is any misalignment between the guides and the drive rools. The control of roll pressure is critical: too low and the rolls will slip on the wire, too high and the motor may stall.

In order to avoid some of these problems, new wire feed systems have appeared in the last ten years, e.g. the use of three conventional rolls mounted at 120^{o} to each other. Two of the rolls being from a single drive, while the third is edle. Pressure may be applied to the rolls independently or simultaneously through spring loaded, free-floating lever arms. This allows the rolls to be self-aligning, which means that, not only permits the wire to be self-feeding when starting a new reel of wire, but also makes it virtually impossible for the wire to become misplaced from between the rolls. One wire feeder can also accept a range of wires with diameter ratios of 1 to 4 without changing the components.

The planetary system (Fig. 1) is another recent development which allows the use of different diameters without the need to change the feed rolls: hard, soft or flux-cored are accomodated with the same feed rolls by changing the main pressure (ref. 12).

Wire feed has always been one of the major problems in GMAW, since, as the torch is hand held the wire must go through a flexible conduit and irregularities in the wire feeding create problems on process characteristics (e.g. arc stability). Modern wire feed circuits incorporate speed feedback to ensure minimum variations of speed.

2.2.3 - Shielding gas mixtures

Shielding in GMA welding has an important role in what concerns the process characteristics, since not only the transfer mode (detachment and size of the droplets), but also the metallurgical aspect, penetration and surface quality are significantly influenced by the composition of this mixture (refs. 14, 16) and the type of shielding (ref. 15).

The first protective gases to be used were inert ones: argon (used in Europe) and helium (used in USA). The physical properties of these gases are summarized in Table 1.

Comparation of ionization potential values indicate that the formation of plasma with an helium shield is more difficult than with an argon shield since, the higher the ionization potential, the more difficult is to initiate an arc. High ionization pottentials can also result in poor arc stability, thus helium shields can lead to less stable arcs.

Thermal conductivity of the gas has been reported to affect the shape of the weld bead, making helium weld beads broader than argon's. Higher flow rates should be used with helium shields since its density is one-tenth that of argon (ref. 13).

Nevertheless, namely due to economical aspects, CO_2 was, for several years, the most important shielding for GMAW of steels. This gas presents several important limitations to the process, e.g. it is only possible to be used with short-circuiting transfer mode; the dissociation of oxygen leading to intense oxidation.

For steel welding, mixtures of argon and carbon dioxide

or oxygen are being used with good results (ref. 14), leading to improved arc stability reduced spatter and an increased operating range. Mixtures of 5 to 20% CO_2, for carbon steel are common the higher levels being preferred. In order to increase heat input, helium additions can be used.

The recent development on GMAW process showed the importance of the composition of the protective gas, thus a considerable effort is being undertaken to optimize shielding gas for MIG welding applications.

2.2.4 - Developments of MIG welding process

2.2.4.1 - Flux cored process (refs. 17, 18, 19)

Tubular wires usually used for hard facing have been known for many years and are used for GMA welding. The core consists of flux or powdered metal, giving several advantages:

- ingredients in the core have fluxing, deoxidizing and scaverging actions, generate protective vapours and sometimes provide alloying aditions;
- higher deposition rates in flat or horizontal-vertical positions (thinner wires have been developed for positional welding);
- better tolerance to joint gap variations, reduced risk of lack-of-sidewall fusion defects.

Some wires need a supplementary gas shield, usually Ar and CO_2 mixtures, others provide their own shielding by means of decomposition and vapourization of the flux core. The use of the supplementary gas shielding allows a greater tolerance to variations in welding parameters; the reduced requirements on the flux for shielding (compared with self-shielded wires) has led to a marked reduction in the risk of porosity defects. Nevertheless, the use of shielding gas precludes the application of these wires for site work.

The self-shielded wires were initially developed from the CO_2 shielded flux cored wire and offered a process which could be operated on site. Smaller wire diameters can also be used which led to

a greater use of cored wires for positional welding and thinner sections. The high fume generation by these wires limits its use in inside applications but it is, of course, not a great problem in site work.

The metal cored wires, in which the core contains metal powders and deoxidants enable lower fume generation and higher metal recovery rates.

Efforts have been undertaken during recent years in order to improve the quality of the wire and the weld metal properties, so that flux cored wires are finding an increasing number of applications in general fabrication. Its performance with pulse current and vertical characteristics is being studied.

2.2.4.2 - AC current (refs. 20, 21)

Attempts have been undertaken in the past to apply AC current to GMA welding and have usually been abandoned on the grounds of lack of stability under normal operating conditions. The use of AC MIG welding (as with AC-TIG welding) requires very high values of open circuit voltage in order to stablize the arc. These voltages are not available in commercial equipments and would lead to safety problems in manual welding. It is possible, nevertheless, to develop additional systems in order to avoid, or at least partially avoid, this problem.

The most significant advantage that can be gained is an increase in deposition rate since the heat generation is greater when the electrode is negative. The aim is then to choose welding parameters (current cycle) in order to improve deposition rate, but in a way that the metal is transferred when the electrode is positive in order to have a stable arc. However, because of problems in equipment design, no actual commercial equipments are available.

2.2.4.3 - Pulsed current MIG

The pulsed MIG welding process has been know for the past thirty years and commercial equipment has been available for nearly 20 years. Nevertheless, it is only recently that its use in industry has widely increased. Using pulsed current (see Fig. 2), it is possible to obtain a transfer mode characterized by fine droplets crossing an

open arc with low mean currents (refs. 25, 39). This type of transfer can occur normally only for high values of current. It allows also a greater torch to work piece variations with a stable arc and low degree of spatter and leads to beads with less risk of sidewall fusion defects at the low current levels. This technique is attractive as an alternative for short-circuiting transfer. Nevertheless, the use of conventional equipment with a flat V-I characteristic with pulsed current created problems related to operational stability of the process and quality of the beads obtained.

The first available equipments had two major difficulties:
- only multiples or sub-multiples of main frequency were possible;
- the shape of the current wave was sinusoidal.

These resulted in difficulty in precisely controlling the pulse energy in relation to metal transfer (refs. 9, 17, 22).

In the past few years, development of electronically controlled thyristor and transistor power supplies has significantly changed this position. It is now possible to produce square wave shapes in which all the pulse energy is used effectively to provide metal transfer and the pulse and background can be chosen in order to produce both, the metal transfer characteristics and required weld pool heat input. This allowed the attainment of stable arcs and small, low current weld pools, suitable for thin materials or for positional welding, but using open arc transfer of small droplets of metal from the electrode wire tip or the weld pool. With the advent of these solid state power supplies, it became possible to provide a nominally square wave current, in which the amplitudes and durations could be independently varied. The requisite pulse parameters can be determined for any viable wire and shielding gas composition whislt another important possibility is the generation of pulse wave forms with any practical frequency. In addition, the use of control system such as synergic control or self-regulating control (see section 2.5) available in most of the commercial equipments for pulsed GMAW, enable the accurate choice of welding parameters and excellent reproducibility, not only with a given set but also between different sets (refs. 9, 17, 22, 23, 24).

The use of solid state power supplies with pulse current, constant current characteristics and control systems is one of the most

important developments in arc welding during the last decade, thus this is the area where the present work is developed.

2.2.5 - Innovations on control system

The use of conventional equipments with a flat V-I characteristic creates several problems, namely related with stability of the arc and quality of the welds obtained, mainly due to the fact that the current intensity is left uncontrolled.

The use of pulsed current, giving a pulse transfer mode, with these constant potential power supplies was suggested twenty years ago. This technique leads to low spatter, higher deposition rates and better quality welds (e.g. less side wall defects) than the short circuiting mode; nevertheless, this technique is not widely practised mainly due to difficulties in choosing the correct pulse parameters and maintaining it during the welding operation and the poor tolerance of the welding arc to joint fit up variations. In an attempt to ocercome these limitations quite significant advances have recently been made in the development of the power source control systems.

In 1971, Reinks (ref. 7) presented the design and construction of a versatile, multi-purpose, low-cost add-on pulse control system which operated with commercial type weld power supplies. This equipment provided the modulated gas metal-arc process which led to good quality weldments in all positions and enabled the automatization of some welding techniques usually done manually. Nevertheless, accuracy and repeatability of welding conditions were not yet achieved and this, associated with a slow response of the system, made the search for control systems that enabled the control of pulse shape (duration and magnitude) together with easier setting of parameters,continue. Fedback control is an useful technique which can be applied most effectively with electronic power sources. The output of the system is measured and compared with the desired output parameters, any differecnce between the two values will cause an "error" signal to be generated, this is fedback to the power control system which adjusts the output to correct the imbalance (ref.8).

This type of control applied to the solid state power supplies gives the possibility to accurately control the welding process. The most important development in this field is the "one-knob" control where by

the adjustment of all the parameters is achieved.
In the power supplies actually on the market, this one-knob control is obtained by means of a synergic control (wire feed speed control of mean current) on a self-regulating control (voltage control of mean current).

The basic main systems of control in these power supplies are silicon controlled rectifiers, transistor series regulator, secondary choppers and primary invertors, which, in terms of output, enables a slower or faster answer, more or less precise.

2.2.5.1 - Synergic control

On the equipments with "synergic" control, the power supply and the wire feeder are linked in a way such that mean current is determined by the wire feed rate or vice-versa (see Fig 3, ref 22). If the wire feed speed is increased, a tachogenerator signal from the wire feed motor determines the mean current required from the power supply and the structure of $\bar{I}$ is then determined according to a set of rules called the "logic". For a given feed speed (or mean current), the pulse amplitude and duration together must be adjusted so that at least one droplet is detached with each pulse. The mean current, determined by combination of the four pulse parameters, must be that giving a burn-off rate equal to the wire feed rate to maintain a constant arc length.

The volume of the detached droplets is determined by the relationship between wire feed speed and frequency. Background parameters have to be defined in order to maintain a stable arc. The adjust of all parameters is difficult in practice. Furthermore, even minor changes in the wire feed, could lead to degeneration of the established welding condition, causing arc and metal transfer instability, burn-backs or stubbing which would result in defective welds if the equipment was not provided with a control system (ref. 24, 25, 26, 27).

With the synergic control system, the "logic" contains a combined relationship between the wire feed speed and all the revelant pulse parameters. The approach to find this relationship was based on two criteria:

- balance between wire feed speed and burn-off rate to maintain a constant arc length, and

- control of metal transfer by the repeated application of a current pulse.

Two basic types of"synergic" welding are presently commercially available and the ways in which pulse wave forms change are shown on Fig. 4. On type I logics, mean current is increased by changes on I_p, I_b and T_b with fixed T_p and I_e (I_p - I_b) (peak current increases with mean current) which means, from detachment data avilable that multiple peak detachments are expected at high mean currents and background detachments at low mean currents. Droplet size will therefore change if a sufficiently wide range of mean currents is emcompassed. For type II logics, mean current is increased by varying t_b with all the other pulse parameters constant. The droplet size may be also changed as it increases with t_b but the droplet detachment should be always of the same kind as I_p^2 t_p is constant (ref.23).

With these systems, the voltage floats so that if the welding torch is moved away from the work the arc length will change. To stabilize the arc length (especially when welding low resistive materials) an additional voltage control may be required.

2.2.5.2 - Self-regulation - Voltage control of mean current

In this control type, a reference voltage is set which nominally corresponds to arc length and it is compared with the actual arc voltage. If, for any reason, the arc length (voltage) changes the power supply output is automatically modified to affect the burn-off rate and restore the pre-set voltage (see Fig. 5) (ref. 22).

This change can be achieved by changing some of the pulse parameters and there are sets, designed for research purposes, where this control can be achieved in several different ways, e.g. AFC - automatic frequency control (where I_p, I_b and t_p are fixed and t_b can change), AWC - automatic width control (where I_p, I_b and F are fixed and t_p and t_b can change with constant $t_p + t_b$), AAC - automatic amplitude control (where I_b, t_p and t_b are fixed and t_p can change), AAWC - automatic amplitude/width control which is a combination of the last two (ref. 28).

Nevertheless the most commonly used system, in practical applications, is by changing pulse frequency under constant peak conditions and constant background current. This type of control is simple and effective and possesses many of the features (by a different mechanism) as the conventional self-adjusting arc. The only limitation is the

changing of the stick-out that can occur, thus leading to changes in mean current. More sophisticated versions of this control technique employ a current dependent reference voltage thereby taking account of the rising voltage-current characteristic of an arc of fixed length.

2.2.5.3 - Adaptative control

In this system, the required arc length is achieved by a closed loop control of arc current by arc voltage. High and low voltage levels are set (which in effect define an average arc current) and when these levels are reached arc current changes to a low or high value respectively. When arc length or wire feed speed are changed the time spent in both, high and low current phases change too, in order to maintain the average set arc length.

2.2.5.4 - Thermal pulsing control (ref. 17)

Thermal pulsing is a different type of process control, as it is used to control weld pool behaviour. The essential characteristic of this technique is a high current level initially applied for rapid penetration of the joint, but which, if continued, would cause excessive penetration and eventually burn-through. The current level is, after a controlled time period, dropped to a low or pilot arc level to enable the weld pool to solidify.

The use of this control system in GMA welding means that the wire feed must be switched between high and low levels, in synchronism with current pulses, to ensure that the metal transfers in a stable way. Commercial thermal pulsing systems normally operate with repeatedly stopping and starting of the arc. This is called the "interval" welding technique which is very attractive at low pulse frequencies (e.g. 0.5 - - 5 Hz), where welding can be carried out in short lengths.

This technique has advantages when welding thin sheets particularly in position.

2.2.5.5 - Backface penetration control

This control leads to further process control. A closed loop control is arranged between a radiation signal from the weld backface and the process parameter being controlled.

2.2.5.6 - Computerised control (refs. 30, 31)

A synergic controlled power source must be pre-programmed to deliver the correct pulse current level, pulse time, background current level and time to detach a droplet synchronously with each pulse of current. The synergic relationship varies according to the wire material composition, wire diameter and shielding gas composition, thus synergic power sources are pre-programmed for various combinations of wire type and shielding gas composition. Using a computerized control there is a wide choice of pulse parameters and the parameters found to be the most suitable for a specific task can be stored for subsquent use.

The computer controlled power sources are ideal for mechanised applications.

2.2.6 - Brief summary

From the last section, it can be seen that many efforts have been made to improve the MIG welding process.

Two basic aims have guided these developments, improve transfer and deposition characteristics and automation of the process. In order to accomplish the first one, several ideas have been proposed, e.g. the use of AC current or pulsed current. The development of control techniques, such as synergic control and self-regulating control enable a continuous operational adjustement of welding parameters and surely represent a step ahead in the automation of the MIG process.

Two features are immediately apparent. First the ease of operation whereby the necessary relationship with wire feed is simply pre-programmed in an electronic control, which, in turn, acts as the reference for the transistor power supply. Secondly, again taking synergic control as the example, synergic pulsing with its wide and stable range in wire feed speeds makes operation with modulated feading viable. Previously only limited forms of modulation, e.g. thermal pulsing had been attempted in MIG welding.

There is no doubt that the new power supply technology offers far greater control and reproductibility than has hithero been possible with MIG welding. Nevertheless, there are still a number of difficulties to be resolved. The choice of the correct welding parameters for each case has to be done on the grounds of the understanding of the

process behaviour, which has to be based on fundamental research of MIG welding technology. The use of empirical data with insufficient theoretical foundations for these developments can be a limited benefit. This is all the more serious when automation is concerned since in mechanised welding operations, where a high integrity joint is demanded,the setting of the welding parameters which must be pre-programmed according to the approved welding procedures, has to be accurate, any deviation from these parameters could well introduce defects.

The use of computers in arc welding either associated with power supplies or integrated in automatized or robotized systems or applied to seam tracking systems, etc., is opening an entire new field of possibilities in the performance of arc welding techniques.

2.3 - METAL TRANSFER IN GMA WELDING

2.3.1 - Modes of transfer

2.3.1.1 - IIW classification (ref. 32)

Different forms of metal transfer in GMA welding depend on the forces involved. These forces depend on several parameters, e.g.: magnitude and type of current, current density, electrode composition, electrode extension, shielding gas, power supply characteristics.

According to the International Institute of Welding classification, the metal transfer modes in MIG/MAG welding are the following:

A - free flight transfer,
A.1 - globular transfer
- drop transfer
- repelled transfer

A.2 - spray transfer
- projected transfer
- streaming transfer
- rotating transfer

A.3 - explosive transfer.

B - bridging transfer

B.1 - short-circuiting transfer.

Each of these transfer modes are defined as follows (Fig. 6):

- Free flight transfer

Characterized by the free flight of droplets through the arc space. No mechanical or electrical contact between the wire tip and the pool occurs.

- Globular transfer

This is characterized by droplets substantially larger than the electrode diameter detaching themselves at low frequencies.

- Drop transfer

The electrode tip melts until the weight of a droplet exceeds the restraining force of surface tension. This happens in low current density processes.

- Repelled transfer

The arc concentrates on a small region of the molten tip where a large drop is formed at the electrode tip due to the repelling electromagnetic forces. This happens, for example, in CO_2 welding of steel.

- Spray transfer

Characterized by droplets smaller than the electrode diameter detaching themselves at high frequencies, the dominant factor is the electromagnetic force.

- Projected transfer

Droplets are detached before growing too large and projected with considerable velocity. The forces involved are partly gravitational but mainly electromagnetic forces. The molten tip of the electrode has no tapered shape.

- Streaming transfer

The tip of the electrode takes the form of long cone of liquid metal from the end of which a stream of fine droplets is projected.

- Rotating transfer

The end of the wire softened by Joule and arc heating are twisted by electromagnetic forces causing high frequency rotation of the electrode tip, the droplets detaching themselves at a high rate in a tangencial direction in relation to the end of the electrode. This is achieved with high current densities and a long electrode extension.

- Explosive transfer

A liquid balloon is formed at the electrode tip by formation of gases in the molten metal, the pressure breaking the ballo into small spatter.

- Bridging transfer

This is characterized by the contact between the electrode tip and the weld pool.

- Short-circuiting transfer

This is a bridging transfer associated with an electrode short circuit. Electromagnetic forces and surface tension drag the liquid metal from the electrode tip into the pool.

2.3.1.2 - Other transfer modes

Recent studies of GMAW transfer modes (ref. 43) detected a new transfer mode, the drop spray, which is not referred in IIW classification.

In drop spray, the transfer mode occurs between globular and spray stream transfer modes, for a narrow range of currents and it is characterized by regular spherical droplets detaching one by one from the electrode tip. The arc is narrow with the root covering the bottom hemisphere of the droplet, with low spatter and low fume generation.

This type of transfer, which is easily achieved with pulse

current has been recognized and is nowadays widely used.

2.3.2 - Acting forces

The frequency of drop transfer and the drop mass influence the regularity of the weld. Droplet detachment and the way in which the droplet crosses the arc, are mainly determined by the following forces:

- gravitational force,
- drag force,
- electromagnetic force,
- surface tension,
- vaporization force,
- explosive force.

Several efforts have been undertaken in order to calculate these forces and to define their balance for the several metal transfer modes (refs. 34, 35, 36, 38).

Recently, in 1983, Waszink and Graat (ref. 37) experimentaly investigated the forces acting on a drop of weld metal. The experimental results obtained were in good agreement with the theoretical expressions of gravitational force, drag force and electromagnetic force.

For the drop spray transfer mode used in this work, Ma (ref. 43) developed a force balance; surface tension and electromagnetic force are the most important for drop formation and detachment.

Force balance in GMAW has indeed been a large and deep field of research for a long time and the results obtained are quite complicated and diverse; nevertheless, as this is not a relevant area for the present work, there is no point of discussing it deeply.

2.3.3 - Detachment model

In order to explain the metal transfer process, it is necessary to establish a quantitative relationship between the geometric dimensions of the wire tip and the movements of the liquid metal. This type of model enables the connection between the theoretical analysis and the physical phenomena. A variety of models of this type have been proposed by several authors (ref. 36, 41, 42, 48), presenting differences in the formation and shape of the droplets for the several IIW metal transfer modes.

More recently (ref. 43, 44) two relevant models appeared, applicable to the transfer modes obtained with the modern power supplies (see Figs. 7, 8, 9, 10).

Detachment models are a rather complicated matter which is not further discussed here as it is not of major importance for this project.

2.3.4 - Metal transfer in pulsed GMAW

In pulsed GMAW any current normally producing globular transfer can be modulated to generate a current waveform of alternating low level background and high level pulse current in order to obtain a desired deoplet transfer mode (refs. 45-58). The background current serves primarily to sustain the arc, whereas the pulse current is adjusted to exceed the critical value of current and thus transfer a small droplet from the wire tip. The pulse wave form is therefore chosen in order to produce series of small droplets, at a mean current which would normally produce globular transfer.

It is considered that the best transfer mode is characterized by: one "droplet" detaching in the end of the peak and with an equivalent diameter equal to that of the wire (ref. 56).

The square wave current shape (see Fig. 2) is characterized by peak current (I_p), background current (I_b), peak duration (t_p) and background duration (t_b) (ref. 49).

The mean current ($\bar{I}$) and frequency (F) are given by:

$$\bar{I} = \frac{I_p\ t_p + I_b\ t_b}{t_p + t_b} \qquad (1)$$

$$F = \frac{1}{t_p + t_b} \qquad (2)$$

The transistorized power supplies presently available employ more or less square wave current shapes with high peaks in order to detach the droplet and the lower possible backgrounds to maintain a stable arc.

The study of the influence of pulse paramerer on metal transfer mode in GMAW has been undertaken by a number of workers (refs. 48-58).

The main conclusions obtained through these works were that drop detachment is principally determined by I_p and t_p with background parameters playing only a minor role. For many materials (mild steel, stainless steel, aluminium) it was found that one droplet per pulse is detached if

$$I_p^{\,n}\, t_p = \text{constant} \qquad (3)$$

where n is constant depending on the wire material (see Fig. 11).

Wire diameter has a significant influence on the one drop detachment zones too, as shown on Fig. 12 .

Similar relationships may also be found where two or more droplets occur in a peak by identifying new constants on the right hand side of the expression, nevertheless the most controlled transfer mode is achieved when only one droplet detaches per pulse since subsquent detachments can be different (see Fig. 13).

To achieve small droplet transfers I_p should be chosen above the spray transition current (i.e. the steady current at which droplets assume an equivalent sphere diameter equal to that of the wire).

Amin (ref. 49) found a value for n = 2.3, from experiments with 1.2 mm wire in mild steel and 1.6 mm wire in aluminium. According to the same reference, droplet detachment time (T_d') and droplet volume (v') can be related by the expression

$$v' = \frac{\pi\, d^2\, W\, T_d'}{240} \qquad (4)$$

Background parameters play the major role in arc stability. Generally, background current must be above 20 A and background duration less than 30 ms in order to have a stable arc.

Ma and Apps (ref. 56), in 1983, identified a new metal transfer mode, the drop spray, using pulsed current. This type of transfer, which occurs in a narrow current DC range, is characterized by regular droplets with low spatter and fume formation, it is projected and can be used in all welding positions. This type of transfer is easily achieved in pulsed current, provided the parameters are correctly chosen. The dominant forces acting on the electrode tip are surface tension and electromagnetic with droplet detachment occuring by metal vaporisation at the neck of the droplet.

2.3.5 - Brief summary

Much research has been undertaken in metal transfer mechanisms. Several models were suggested to calculate and interpret the phenomena associated with the appearance of the molten droplet on the wire tip and its transfer to the weld pool. The theories proposed vary and the models are often completely different from one another. The systematic theory which links the mechanism model, acting forces and their calculation together with welding variables has not been established. The use of transistorized power supplies and pulse current allowed a step forward in the understanding of metal transfer mode in MIG welding. The IIW classifications of metal transfer modes, despite its importance, is nowadays inadequate since recent experimental work, especially with pulse current, has led to results favouring a transfer mode not considered in this classification.

The identification of a very stable form of transfer, drop spray, which is also associated with a higher efficiency than other transfer modes is possibly the most important result of the latest investigations in this field. The aim, nowadays, is to choose the correct welding parameters in order to have this type of transfer. With continuous current however this is a quite difficult task since this type of transfer is only possible within a narrow range of currents. However in the pulse current mode, drop spray transfer is easy to obtain provided the parameters are correctly chosen. In The present research, work has been undertaken in order to find the correct parameters for specific material / gas composition.

2.4 - MELTING RATE

The electrode melting rate is produced by the heat generated by the anode or cathode reactions (depending on the polarity), by the resistance of the wire to the flow of current and in a small portion, by radiation from the arc stream or the weld crater (ref. 59 - 64).

The wire feed speed is then related with current density in the wire and electrode extension, by an expression of the form:

$$W = K_1 j + K_2 l\, j^2 \qquad (5)$$

where K_1 and K_2 are coeficients dependent on electrode wire characteristics.

2.4.1 - Anode heating

The heat developed at the anode is contributed by electrons from the arc entering the anode. Individual components are the "heat of condensation" of the electrons (IØ), the kinetric energy occuring due to acceleration of the electrons across the anode potential drop (IV_a) and the thermal energy of the electrons. The anode heating can be expressed as (ref. 64):

$$Ha = I\ (Ø + Va + \frac{5KT'}{2e}) \qquad (6)$$

The contribution of anode heating to the melting rate of the electrode can be calculated by isolating the contribution of the ohmic heating of the electrode, i.e. by determining the melting rate with zero electrode extension. In Fig.14 the relationship between melting rate and electrode extension is represented for different welding currents. Since this relationship is linear it is possible to extrapolate to zero electrode extension. (ref. 60).

The rates of melting due to anode heating, taking from this chart, are plotted as a function of welding current on Fig. 15 . This figure shows that the melting rate due to anode heating is proportional to the current and can be defined by:

$$W_a = C_a\ I \qquad (7)$$

where C_a is a constant. Equation (7) is similar to the first term of expression (5).

2.4.2 - Electrical resistance heating

The electrode wire is heated according to Ohm's law as it is fed through the stick-out, and is defined by:

$$W_r = C_r \frac{l}{A}\ I^2 \qquad (8)$$

This expression is similar to the second therm of the equation (5).

2.4.3 - Radiation energy

The heat developed by radiation from the arc stream or the weld crater does not significantly influence melting rate (ref. 60).

2.4.4 - Welding variables

From what has been stated, it is possible to conclude that anode heating is a function of current, anode drop and electrode work function. Experiments (ref. 64) to calculate V_a, ϕ and KT'/e gave the following values:

$$V_a = 0 \text{ to } 3 \text{ V}$$

$$\phi = 3.8 \text{ to } 4.5 \text{ V}$$

$$\frac{5}{2}\frac{KT}{e} = 1.3 \text{ to } 2.0 \text{ V}$$

The total of these three terms, i.e., $V_a + \phi + \frac{5\ KT'}{2\ e}$ has been taken as 5.1 to 9.5 V by various workers in the field (ref. 64). (It is important to note that direct measurements of anode potential drop are very difficult).

It was thought until recently that the shielding gas composition would influence anode heating, but Halmøy (ref. 65) proved theoretically that this influence is not significant. It was found also (ref. 60) that electrode heating due to anode reactions is independent of the electrode extension. Ohmic heating for a given material is dependent on stick-out, wire diameter and welding current.

The melting rate of an electrode is controlled by a number of factors; for positive wire direct-current arcs, melting rate (or burn-off rate) is defined by the well-known experimental relationship.

$$W = \alpha I + \beta\ l\ I^2 \qquad (9)$$

2.4.5 - Melting rate in pulsed GMAW

Melting rate in pulsed GMAW is mainly governed, as in DC welding by anode heating and electrical resistance heating. The influence of pulse structure on burn-off rate (using the DC theory averaged over pulse time - for a square wave) is given by (ref. 22):

$$W = \frac{W_b T_b + W_p T_p}{T_b + T_p} \qquad (10)$$

where W_b and W_p are contributions made during background and peak times respectively. These may be written as:

$$W_b = \alpha I_b + \beta l I_b^2 \qquad (11)$$

$$W_p = \alpha I_p + \beta l I_p^2 \qquad (12)$$

After substituing (11) and (12) in (10)and since mean current ($\bar{I}$) is given by equation (1) we obtain

$$W = \alpha \bar{I} + \beta l (I_p^2 t_p + I_b^2 t_b) F$$

Ohmic heating during background duration is usually negligible compared to that during the peak (i.e. $I_p^2 t_p >> I_b^2 t_b$) so that W then becomes

$$W \approx \alpha \bar{I} + \beta l I_p^2 t_p F \qquad (13)$$

This equation differs from that of a continous current as the joule heating term for pulsed current is proportional to the square value of peak current and is therefore more pronounced. Earlier work (ref. 49) disregarded the joule heating term and used $W = K\bar{I}$ as the basis of the synergic MIG process. This approach worked over a limited current range but an expression to include the joule heating was required for higher resistive wires.

2.4.6 - Brief summary

The melting rate of a MIG welding wire has been clearly explained and quantified as dependent on two sources of heat:

- anode heating and
- joule hetaing.

The proportion in which each of these sources contributes to wire melting depends on several factors, such as current type (i.e. DC cur-

rent, pulse current) and type of material. For example in aluminium, a low resistive material, only anode heating is responsable for melting the wire while in titanium, a high resistive material, the joule heating plays the most important role.

In steel wires such as mild steel, the contribution of ohmic heating for melting rate of wire electrode takes about 50% in usual welding condition.

Despite the knowledge of material behaviour, there are still some gaps in this field, such as systematic approach to the influence of shielding gas composition and wire diameter on melting rate. Further work is then required in order to clarify the points referred above.

2.5 - HEAT BALANCE OF MELTING PROCESS

The aim of this section is to emphasize the work done on the several forms of heat, heat sources, etc., involved in the welding process and its influence on the process characteristics. The major heat source is, of course, the welding arc and so emphasis has been placed on its description.

Empirically, it is possible to say that the heat developed in the arc region melts the wire, superheats the droplets and melts base material, thus these items are considered separately in this survey.

2.5.1 - Welding arc (ref. 64, 76-78)

An arc is initiated by an electrical discharge between two electrodes and can be formed only under conditions where the continuity can be maintained by processes occuring within the arc itself.

The literature on physics of the welding arc is mainly based on inert gas welding arcs with non consumable tungsten cathode. The considerations and results are usually considered to be applicable to consumable electrode arcs except for metal transfer. An electric welding arc can be divided in three regions: the anode, the cathode and the arc column.

There are two characteristic curves which can be determined to provide information about the arc: the arc voltage - current relationship which gives the general external behaviour of the arc, and the arc potencial across the arc length . The fall in

voltage with increasing current at low currents (up to 30 - 60 Amps) is not fully understood but several suggestions have been made such as that the temperature of the arc is higher and more electrons are presented at high temperature making current conduction easier, i.e. less potential required. After the voltage increases with current in a nearly linear way depending on the type of arc (Fig. 16).

The change in arc potential along the arc length gives information about the internal structure of the arc (Fig. 17). It is possible to notice three regions of different potential gradient along the length of the arc. The arc consists mainly of gas at high temperature, which is called the arc column or arc plasma, in which the current is carried by electrons and ions provided by thermal ionization of the gas. Near the electrodes the gas can no longer exist at a high temperature, because of the cooling effect of the electrodes; the maintenance of the current requires a high potential drop so that the cathode and anode drop regions are formed.

2.5.1.1 - The arc column

The arc column, which is composed of charged electrons and ions and neutral particles (atoms and molecules in the excited and non-excited states), is characterized by two features:

- high temperature (such that the gas is sufficiently ionised to be conductive,
- high flow velocity (from the electrode to the work piece).

The temperature is maintained if sufficient energy is generated to compensate for that lost by conduction, convection and radiation.

The temperature distribution and the amount of gas which flows through the arc and becomes heated must, in some manner, determine the heat and mass transfer from the arc column to the weld metal and that these factors are in turn related to the amount of electrical energy which is converted into heat in the column. The energy dissipated in VI watts is converted into heat in the column. The energy dissipated is VI watts per unit length, where V is the voltage gradient along the column. The problem is then to formulate the way in which this energy is transferred to the surroundings by the various heat transfer processes.

The relative importance of conduction and convention may be

assessed from the Peclet number P_e

$$P_e = \rho_m \, v \, L \, C_p/K \qquad (14)$$

where L is a typical length.

Values of P_e near 10 indicate that convection dominates while for low values heat flow is primarily by conduction.

In the arc column, the electrons travel towards the anode and positive ions towards the cathode. The number of electrons and positive ions in each volume unit of the column is approximately equal so that the arc column is electrically neutral and consequently the electric field is constant (aprox. 10 v/cm, ref. 64).

The stability in the arc column is closely related to its electrical conductivity. Low ionisation energy and high arc temperature is of advantage. The arc temperature is strongly dependent on thermal conductivity. The lower the thermal conductivity at constant arc current and effective ionisation energy, the higher the arc temperature. Gases with relatively low thermal conductivity (e.g. Ar) led to stable arcs and, on the other hand, gases with high thermal conductivity (e.g. He) rather unstable arcs.

The arc temperature is of importance in what concerns metal transfer, on Fig. 18 (ref. 64) are shown isotherm maps for argon arcs.

The average temperature of metal vapour arc is 6000 to 7000^{o} K (ref. 78) but in the centre much higher temperatures can be reached.

The mass flow in the arc column in GMA welding is electromagnetically induced. The velocity distribution in the plasma jet has been measured by several different ways and the results obtained are shown in Fig. 19.

2.5.1.2 - Cathode fall region (refs. 64, 72, 74)

The electrical connection between the cathode and the arc column is a region in which a significant potential drop is observed. The order of this voltage drop is 4.8 to 5.3 V (ref. 64). The cathode fall region is of importance in welding, because it is there that the electrons must be produced to flow into the arc plasma and the ease of production and maintenance of this electron supply determines to a large extent the stability of the arc.

Several suggestions have been made to explain the cathode drop region. The first one postulated that electrons were supplied from the cathode at high temperature by thermionic emission and accelerated in the cathode drop, thus gaining kinetic energy which was there lost by collisions with athoms or molecules in the arc column. The thermal ions so produced were accelerated towards the cathode and on impact gave up their kinetic energy of neutralization so maintaining the cathode at the high temperature necessary for the emissions of electrons. This occurs in thermionic cathodes (tungsten or carbon), but this approach can not apply for low-melting point electrodes. In non-thermoionic cathodes, the temperature is too low for thermoionic emission of electrons.

Mechanisms which might augment the field current as surface roughness, surface layers of positive ions, elevated temperature and variation of fields strength with time, can explain cold emission Various other mechanisms have been postulated but the processes occuring in the cathode drop region are not still very well understood.

Finkelburg and Maecker (ref. 75) suggested three alternative types of mechanisms to explain the cathode fall region based on experimental behaviour in three possible extreme cases. In practice two of these mechanisms can occur at the same time or the mechanisms may change from one type to another. These mechanisms are:

1 - thermal emission,

2 - plasma emission,

3 - field emission.

The first, which is characterized by the lack of a well--defined cathode spot and a low current density (10^3 amp/cm^2) occurs in the non-consumable tungsten-electrode process.

The plasma emission mechanism is associated with current densities from 10^4 to 10^7 amp/cm^2 and is characterized by a stationary cathode spot and marked contraction of the arc column immediately adjacent to the cathode. This mechanism occurs in low current high pressure arcs.

The third cathode theory, which is associated with a well--defined but non-stationary cathode spot, moving around with velocities of the order of 10^4 cm/s. The current density is of the order of 10^5--10^8 amp/cm. This type of cathode machanism is predominant in welding with consumable electrodes.

The energy balance at the cathode is of importance in welding. In broad terms it is possible to say that the energy expended in the cathode drop region is used to provide the current carrying stream of electrons which enter the column with energy $\frac{5KT'I}{2e}$ and to heat any gas or vapour flowing through the cathode drop while the remainder finds its way into the cathode by unspecified mechanisms. There is some confusion in the literature of gas discharge tubes and electron tubes regarding the mean kinetic energy carried by the particles, 2 k T and 3/2 KT are the most used values, nevertheless 5/2 KT is the correct value (ref. 104). The processes occuring in the cathode drop region are not very well understood mainly because there is the problem of making physical measurements in very small regions at exceedingly high temperatures and the very high localized energy dissipation produces a state of matter which is difficult to analyse theoretically.

2.5.1.3 - Anode fall region (ref. 74, 78, 80)

Near the anode the temperature changes from the high value of the column to a lower value that characterize the anode. Due to this fact there is a destabilization of the continuity of the ion flow, the concentration of positive ions decreases, resulting in the negative space charge which is responsible for the anode potential drop.

Although, some attempts have been undertaken in order to explain the anode drop region the theory is still incomplete. Nevertheless, in the anode drop region, three phenomena must occur:

- the temperature must fall from that of the column to that of the anode,
- a supply of ions must be produced to flow into the arc column,
- the ions so produced must be accelerated and raised to the arc column temperature.

Gas and vapour streams can have a very marked effect on the anode drop if they have a velocity of the same order or greater that the ion's velocity (10 cm^2/s).

The anode drop is very difficult to measure or estimate but general values have been suggested (ref. 64):

- Busz-Penckert and Findenburg - 5 to 10 V

- Sugawara - 4.2 V for 10 A arc

- Hamilton and Guile - 4 to 7 V in argon
  2.5 to 10 V in air

and anode current density has been estimated at 100 A/cm^2 to 10^5 A/cm^2.

The energy balance at the anode is particularly important in welding since it influences the melting of metal to form a weld pool in straight-polarity and the melting of the electrode in reverse-polarity. The heat entering the anode has been estimated as:

$$H_a = I \phi + I V_a + \frac{5 K T}{2 e} I \qquad (15)$$

2.5.1.4 - Brief summary

The physics of the welding arc has been a matter of much research work since its discovery and several authors have attempted to explain the phenomena associated with it. Interactions of mass, heat and metal transfer have been basic problems in arc welding since the introduction of the process, yet little is known of the principles and processes involved, due to the fact that the metal arc welding system is complex and difficult to investigate experimentally.

Theories presented to explain the cathode drop region are various and there is still some confusion namely when these theories are applied to a given welding process. The anode drop region is better understood as a result of the awareness of the role of anode and cathode jets.

Most of the experimental work on the physics of the welding arc has been on inert gas shielded arcs with non-consumable tungsten cathode. It is generally assumed that the process derived from a tungsten cathode arc can be used to explain those occuring in a consumable electrode arc, except for metal transfer. This is an empirical approach with severe limitations. Another fault in this field is the fact that the influence of the composition of the shielding gas has not been considered in most cases. Therefore, the theories presented are not completely clear and further work is required to correctly explain the missing details.

2.5.2 - Heat balance on the wire

2.5.2.1 - Introduction

Since the primary function of the arc column is to maintain the passage of the current, a current balance equation has to be obeyed. This in turn requires that a region of conducting gas should be maintained at the necessary high temperature so that an energy balance equation must be fulfilled.

2.5.2.2 - Wire melting and droplet heat content

Erokin and Rykalin (ref. 81) proposed a heat balance equation which explained the relatiohship between the heat consumed on wire melting and the heat source

$$Q_d + Q_6 + Q_7 = Q_2 + Q_3 + Q_4 + Q_5 \qquad (16)$$

where Q_d is the arc heating, Q_6 is the arc column heating to the drop, Q_7 is the heat developed by chemical reactions between the drop and the gases, Q_2 is the heat for melting the electrode metal, Q_3 is evaporation, Q_4 is the superheating of liquid metal, Q_5 is the heat lost from a drop surface. This is a general equation that needs to be detailed. Wire melting rate is a variable that significantly influences the quality of MIG welding. Droplet temperature is of importance too, namely in what concerns fusion characteristics of a MIG welding bead.

The investigation of wire melting rate and heat content of the droplets should be based on the analysis of heat balance occuring on the wire tip. Several approaches (ref. 60-71) were undertaken on heat balance of metal transfer; all these approaches conclude that the heat developed in the arc was mainly due to anode heating and resistance heating (see Section 2.2.4). This amount of heat is consumed in melting the wire and losses (e.g. evaporation, superheating, etc.). The attempts undertaken led to expressions to calculate these amounts of heat.

Lesnewich (ref. 60) in 1958, proposed a dual heat source--anode heating (Ma) and resistance heating (Mr) - to explain wire melting rate, where Ma = Ca I and Mr = Cr L I^2, Cr and Ca being constants dependent on electrode characteristics. An empirical equation was developed to cal-

culate melting rate for reverse polarity DC arcs.

Wilson et al (ref. 61) calculated the ohmic heating of a wire assuming constant values of specific heat and of the temperature coefficient of the resistivity. In fact, these are not constant and vary with temperature and this must be included in a realistic calculation.

In 1977, Jelmorini (ref. 82) suggested that the heat balance (H) is composed of anode heating (Ha) and Joule heating (Hr) and was consumed on wire melting (Hw) and evaporation (He). Two years later, Halmøy (ref. 65) found a relationship between Joule heating, wire melting rate, current and stick-out by graphical integration:

$$H_L = a \frac{l\ j^2}{W} - b \qquad (17)$$

where a and b are constants depending on material characteristics.

As this result is based on theoretical curves of the relation between the heat content per unit volume with temperature and resistivity with temperature, direct measurements were undertaken which showed a slightly different relationship. This can be due to the rapid heating of the wire; nevertheless this work is an important contribution mainly in what concerns Joule heating calculations.

Recently (1982), Waszink et al (ref. 44, 67) found that the heat flow rate is dependent on current and melting rate and present simple physical models which describe the transport of heat through the liquid.

The relationship between the heat balance process that occurs at the wire tip and the welding parameters was established for GMAW-DC positive. The total power, P, supplied to the wire is given by

$$P = I^2 R + I \phi$$

The ohmic power developed in the solid part of the wire is, in general, not sufficient to raise the temperature of the material from room temperature to melting point and to melt it, thus there must be a flow of heat from the anode spot to the solid, through the liquid tip. If this power is Q, the melting rate is the determined by $I^2 R + Q$ and it was found that the value of Q is different in the globular and spray transfer modes.

The work presented in these papers is a real contribution to the fundamental research of GMAW and the first referring to metal transfer modes, but it referred to the IIW classification. Another shortcoming of this work is the calculations of temperature being based on a mathematical

model. Temperature distribution in the electrode extension is difficult to measure thus several mathematical models have been proposed with obvious limitations and furthermore all are based on small current ranges.

Further work is needed in order to find directly the temperature distribution along the wire and then correctly explain and determine the heat generated at the wire.

Droplet temperature also plays an important part in what concerns the heat balance. Its value determines for a great part the temperature of the weld pool and therefore its size. Several attempts have been undertaken to measure droplet temperature and the heat transferred through the droplet.

Voropai et al (ref. 85) examined droplet formation and described a method to determine the form of the free surface of electrode metal droplets during their formation at the electrode tip and in the course of transfer to the weld pool and to solve the reverse problem to determine the forces acting on the droplet. The method described made possible the prediction of new methods of controlling the characteristics of the process of consumable electrode-welding, nevertheless this method and the equations obtained are complicated, theoretical and lack of experimental confirmation.

Pokodnya (ref. 83) measured the heat contents of droplets in MIG welding in a CO_2 shield by calorimeter tests. He experimentally determined the influence of the electrode polarity and found that the heat content of the droplets was lower when the electrode was negative, 2000^{o} C - 2500^{o} C for mean current from 200 A to 400 A, while for the same parameters droplet temperatures around 2800^{o} C were found when the electrode was positive.

Ando et al (ref. 41) calculated heat content of droplets and droplet temperature using Lesnewich approach of melting rate and reached the value of 2700^{o} C for steel droplets. This value was confirmed experimentally with calorimeter measurements. While Heiro (ref. 84) concluded, based on experimental tests, that droplet temperatures could be varied by careful selection of welding parameters in pulsed-arc welding and that these temperatures are markedly dependent on pulse energy, he found values between 2300^{o} C and 2600^{o} C for the droplet temperature.

Jelmorini's (ref. 82) results gave T_{dr} as 2400^{o} C for the range of currents 120 - 290 A. In this case, the temperature was measured by means of a thermocouple arrangement after it had passed through the arc

and Halmoy concluded that droplet temperature is just above the melting point of the material and keeps constant along the process.

Waszink (ref. 44) states that droplet temperature is determined by part of the power generated at the anode surface, i.e. $I\emptyset - Q$, if heat losses by evaporation and Joule heating in the drop are neglected. He presents the relationship of droplet temperature with mean current, stick-out and wire diameter for globular and spray transfer modes. T_{dr} is almost constant (aprox. 2200^{o} C) within the globular transfer mode and it varies (aprox. 2000 - 2600^{o} C) for the spray transfer mode with a maximum value for $\frac{Il}{a} \times 10^{6} = 7$ A/m. Despite some discrepances between the referred works, it is obvious that it is agreed that droplet temperature is significantly above the melting point and most of the works point out values of 2500^{o} C $\pm$ 10%.

2.5.2.3 - Brief summary

In conclusion, it may be stated that many workers have suggested the relationship between heating sources and heat comsumption such as arc heating, Joule heating, wire melting and drop heating. Nevertheless, some problems still remain unexplained, e.g. the distribution of temperature in wire extension, the ratio of the heat energy distribution between the heat consumption on melting and superheating. Thus the quantification of the several heat sources involved in metal transfer and its dependence on welding parameters has not been completely achieved yet.

2.5.3 - Heat and fluid flow on plate

2.5.3.1 - Introduction

If the arc is considered as an energy source, Q_a, and the energy is transferred from the source to the welded plate, giving an absorbed energy in the plate, Q_p, then the difference between Q_a and Q_p depends on the efficiency of heat transfer, η, and this is process dependent where:

$$Q_p = \eta\, Q_a \qquad (18)$$

and

$$Q_a = I \,.\, V \qquad (19)$$

this

$$Q_p = \eta I \ V \qquad (20)$$

or

$$Q = \eta H \quad \text{where } H = I \ . \ V \qquad (21)$$

A number of determinations of the heat efficiency factor have been made for the GMAW process with reported values in the range 65 to 70% (refs. 100, 102). The fundamental relationship linking the four major weld variables current (I), voltage (V), weld speed (v) and amount of energy absorbed by unit length (q) is given by

$$q = \eta \frac{I \ V}{v} \qquad (22)$$

In recent years, there has been a growing recognition of the fact that fluid motion in weld pools may play an important role in affecting both the heat transfer phenomena and ultimately the mechanical properties of the weld metal.

2.5.3.2 - Heat flow in the weld pool

The temperature distribution and the temperature-time cycles involved in arc welding determine the shape of the fusion boundary, the metallurgical transformations of the material and distortion problems. An important factor is then the estimation of the heat required to form the weld in terms of the thermal constants, metal thickness, welding speed, etc. These requirements have led to investigations of heat flow in arc welding (refs. 81,86-102). These investigations have been primarily of a theoretical nature and to carry out the analysis approximations have had to be made so that the problem can be formulated mathematically. Heat losses (radiation and convection) are considered small and so most of the approaches of the problem are based on conduction of the heat. . . . Here some of the most significant contributions in this field are reported.

Forty years ago, Rosenthal (ref. 99) presented the first solution for a travelling point source of heat which has been the basis for subsequent studies of heat flow in welding. He proposed the following equation for point sources moving across the surface of a semi-infinite body for three dimensional heat flow:

$$T - T_o = \frac{q}{2 \pi K} \frac{1}{R} \exp \frac{-v}{2 \rho} (R + x) \quad (23)$$

Rykalin (ref. 81) took a similar temperature distribution equation to the one proposed by Rosenthal taking in account the effect of heat losses to the surroundings and proposed that for moving point sources at high speed this expression could be simplified, the temperature distribution for a deposit on thick plate being given by:

$$T (t, Y_o, Z_o) = \frac{q}{2 \pi K vt} \exp \{- \frac{Y_o^2 + Z_o^2}{4 \rho t}\} \quad (24)$$

Rosenthal and Rykaline found plate thickness to be of significance as regarded the type of heat flow. Two cases are specially emphasized in the literature - 3D and 2D (three and two dimensional heat flow). Here only 3D case is discussed as it is the one employed in this work. The solutions presented so far are based on a number of simplifying assumptions:

(a) the physical coefficients (thermal conductivity, specific heat and density) of the material are constant;
(b) adiabatic conditions exist, i.e. no heat losses from the plate, except by surface convection in the case of thin sheet;
(c) there is no heat created by Joule effect;
(d) the heat source is considered a point source;
(e) conditions are steady-state, i.e. during a long weld run with established welding parameters;
(f) the solid in infinite;
(g) no metal transfer occurs across the arc or into the plate surface.

Obviously, these assumptions are unrealistic but they do allow that the analytical solutions presented above could be given.

Numerical techniques (refs. 90, 91) can provide an alternative method for predicting heat flow characteristics, but, for thick plates, the complexity of the triaxial co-ordinate system requires considerable mathematical expertise, as well as a very large digital computer. It is believed that analytical solutions offer simple solutions and provide ample scope for the introduction of corrections (refs. 80, 89, 102, 98).

Ushio et al(ref. 90) proposed the physical situation represented on Fig.21 where the heat condition inside the fusion boundary was given by:

$$\frac{\delta^2 T}{\delta x^2} + \frac{\delta^2 T}{\delta y^2} + \frac{\delta^2 T}{\delta z^2} = - \frac{v}{\rho L} \frac{\delta T}{\delta z} \qquad (25)$$

where T must satisfy the following boundary limit conditions:

$$\lim_{r \to 0} 4 \pi r^2 K_L \frac{\delta T}{\delta r} = 2 q$$

$$\lim_{r \to \infty} T = T_o$$

where $r = \sqrt{x^2 + y^2 + z^2}$

T_o is room temperature

and

$$T = T_f$$

$$P = - L \rho v (\vec{\nu} \vec{z}) = K_L \left(\frac{\delta T}{\delta \nu}\right)_L - K \left(\frac{\delta T}{\delta \nu}\right)_s \qquad (26)$$

and on the fusion boundary

$$f(x,y,z) = 0$$

where $\vec{\nu}$ is the unit vector in the direction of the outward normal to the boundary, Z is the unit vector in the direction of positive Z, P is the rate of emission of latent heat of solidification per unit area of the bondary and the problem is so resolved into the mathematical one to obtain the temperature distribution and the fusion boundary satisfying these equations.

Methods of solution are presented and calculations undertaken. Further experimental tests were undertaken and the agreement with theoretical considerations was proved to be acceptable.

In the case of welding in mild steel, the experimental data of pool width agree with the theoretical one, but the ripple lag length and pool length obtained by experiment are larger than those obtained by theory. This case can be attributed to convective heat transfer

in molten pool due to fluid dynamic motion of molten metal.

Oreper, Eajar and Szekely (ref. 91) considered a idealized stationary weld pool in GTA welding in order to define the principal conditions that govern heat transfer and convection. The model chosen is a reflection of actual operating practice and the conclusions drawn by computer results were proved to be of practical relevance. The problem was stated by the following equations:

i) the equation of continuity

$$\nabla V' = 0 \qquad (27)$$

ii) the equation of motion

$$\rho (V' \nabla) V' = - \Delta p + \mu \nabla^2 V' + F_b \qquad (28)$$

where the body force (F_b) is given by:

$$F_b = J \times B - \rho_m g \beta (T - T_0) \qquad (29)$$

which incorporates both the electromagnetic and bouyancy forces where V is the velocity vector and β is the coefficient of volume expansion.

The development of these equations have led to a model that shows that surface tension driven flows dominate convection in the arc weld pool. As such this model is more correct than others which have neglected this factor.

Apps and Milner (ref. 80) suggested that same error in Rykaline's approach lay in neglecting the latent heat of fusion released on solidification of the weld pool. They recommended the introduction of the term $\rho_m l_{arc} v_d A$ to take these effects into account in the thermal history.

Adams (ref. 89) recognised this problem of latent heat release and using the location of the fusion boundary as a parameter, he rewrote the basic Rosenthal's equation as:

$$\frac{1}{T_p - T_o} = \frac{2 \pi K \rho \zeta}{q v} \{2 + (\frac{v r}{2 \rho})^2\} + \frac{1}{T_m - T_o} \qquad (30)$$

for thick plate.

Grosh et al (ref. 95) obtained analytical solutions for the basic differential equation of heat flow which took into account certain variations of the thermal properties of a solid when heated by a moving point source. The variations considered were of a type where thermal conduc-

tivity and thermal diffusivity are similar functions of temperature.

$$K = K_o \, f'(T) \qquad (31)$$

$$\rho = \rho_o \, f'(T) \qquad (32)$$

The latent heat of metallurgical transformations was neglected as well as heat losses from the surface to the solid by convection and radiation.

Christensen(ref.102)generalized Rosenthal's approach. He established that the heat input q (cals) to be expected, approximately, under given conditions, could be stated in terms of arc volt-amperes, VI, and a coefficient for arc efficiency:

$$\eta = \left(\frac{4.18\ q}{VI}\right) 100\% \qquad (33)$$

He generalized Rosenthal's temperature charts for the particular set of material properties, heat input and welding speed under consideration. The dimensionless parameters λ, Ψ, ζ and ρ were proposed to represent the radius vector R of any point with respect to the source.

$$\lambda = \frac{vx}{2\rho}, \quad \Psi = \frac{vy}{2\rho}, \quad \zeta = \frac{vz}{2\rho}, \quad \rho = \frac{vr}{2\rho} \qquad (34)$$

where x, y, z, are the co-ordinates and $\dot{\theta}$ was considered as the dimensionless parameter representing the rise of temperature above ambient $(T-T_o)$:

$$\dot{\theta} = \frac{T - T_o}{T_c - T_o} \qquad (35)$$

The conditions of welding were defined by an operaying parameter (n):

$$n = \frac{qv}{4\pi\rho^2 C_p \gamma (T_c - T_o)} = \frac{qv}{4\pi\rho^3 (H_c - H_o)} \qquad (36)$$

These terms were introduced into Rosenthal's equation for moving point sources moving across the surface of a semi-infinite body giving:

$$\frac{\dot{\theta}}{n} = \frac{1}{\rho} \exp^{-(\rho+\lambda)} \qquad (37)$$

where ρ, λ are dimensionless parameters given by $\rho = \frac{vR}{2\rho}$, $\lambda = \frac{vx}{2\rho}$.

From this expression, values of ρ and λ were computed for a series of chosen $\frac{\theta}{n}$ contours (see Fig. 20). This type of chart is generally applicable to all combinations of materials and welding conditions with the limitations and assumptions incorporated in the point source equation.

Experimental data gave good agreement with the theoretical Rykalin (ref. 81) approach.

Recently Eajar and Tsai (ref. 98) considered a distributed heat source travelling across a semi-infinite plate. Green's function for a distributed heat source Q^* was used:

$$G\,(w/w',\ y/y') = \frac{2\,e^{\frac{-v}{2}\{(w-w')^2 + (y-y')^2 + z^2\}^{1/2}}}{\{(w-w')^2 + (y-y')^2 + z^2\}^{1/2}} \qquad (38)$$

where w', y', z', is the location of the heat source, w, y, z is the point of interest and the temperature distribution over the surface of interest is

$$T - T_o = \int\int G\,(w/w',\ y/y')\,\{e^{-\frac{v}{2\rho}(w-w')}\ \frac{Q^*(w',\ y')}{K}\}\ ds' \qquad (39)$$

In order to simplify these expressions the authors considered a heat source Q with a distribution parameter σ which has dimensions of length and can be considered as the half width of the arc. Q is then given by:

$$Q\,(x,y) = \frac{q}{2\,\pi\,\sigma^2}\ e^{-(x^2 + y^2)\ /\ 2\,\sigma^2} \qquad (40)$$

where σ is a distribution parameter and q is the heat input and the temperature distribution

$$T - T_o = \frac{q}{\Pi\ \rho_m\ c\ (4\ \pi\ \rho)^{1/2}} \cdot \int_0^t \frac{dt'(t-t')^{-1/2}}{2\,\rho(t-t') + \sigma^2} \cdot \cdot$$

$$e^{-\frac{(x-vt')^2 + y^2}{4\,\rho\,(t-t') + 2\sigma^2} - \frac{z^2}{4\rho\,(t-t')}} \qquad (41)$$

The solution on dimensioneless form is:

$$\dot{e} = \frac{n}{\sqrt{2\,\Pi}} \int_0^{\frac{v^2 t}{2\rho}} d\tau \; \frac{\tau^{-1/2}}{\tau + u^2}$$

$$e^{-\frac{\zeta^2 + \Psi^2 + 2\zeta\tau + \tau^2}{2\tau + 2u^2} - \frac{\gamma^2}{2\tau}} \qquad (42)$$

where the dimensionless variables are:

$\zeta = vw/2\rho$, $\Psi = v\,y/2\rho$, $\gamma = \frac{vz}{2\rho}$ - dimensionless distances

$\tau = v^2\,t'/2\rho$ - dimensionless time and $u = v\sigma\,/2\rho$ - dimensionless distribution parameter.

The experimental verification of the predictions was undertaken and gave a good approach despite the simplifying assumptions. This theory gives an accurate function relationship between both parameters and materials parameters which is, nevertheless, of limited application (GTAW) and complicated.

The determination of the actual heat flow conditions which do not depend only on the thickness of the material but is influenced by thermal properties, preheat, welding process, heat input and geometrical factors is of importance.

Since the fusion boundary provides a reliable record of one isotherm (assuming homogeneous weld metal), Wells (ref 79)and Lancaster (ref.33) attempted to correlate the heat input term q to the dimensions of the weld bead. They arrived at the following equations for 3D case:

$$q = d_A K\, T_m \left(1 + \frac{4}{5}\,\frac{v d_A}{4\rho}\right) \qquad (43)$$

This equation proves useful for determining the relationship between v and d for constant arc energy. It is a simple equation with practical use which can be used to predict fusion characteristics. There is also considerable literature dealing with practical observations concerning weld pool formation but, up to the present, it has been rather difficult to develop a meaningful and simple relationship between theoretical models and experimental observations.

2.5.3.3. - Fluid flow in weld pools

GTA welding with low currents is the case where the fluid flow patterns are simplest in welding, because the surface is relatively undisturbed by the arc force and the form of the molten pool is more or less hemiphesrical.

Oreper and Szekely (ref. 87) considered GTAW and made a mathematical formulation for the transient development of the fluid flow in a liquid pool generated by a spatially variable heat flux acting on a solid metal plate. Electromegnetic, buoyancy and surface forces were considered. The results obtained for temperatures profiles and velocity fields are shown on Figs. 22, 23.

Bradstreet (ref. 97) presented a schematic picture of a fluid flow in the weld pool as shown on Fig. 24 for GMA welding. Tracer technique and also high speed cinematography were used and it was found that the reverse stream along on the wled pool surface was relatively weak and the dominant effect was rearward flow. Three metal streams are combined to form the weld pool:

- one originated from filler metal running along the centreline of the weld pool,
- the other two originated from the parent metal and flowing initially along the edges of the weld pool.

Lancaster (ref. 64) concluded recently that the forces that generate weld pool circulation are:

i) the axi symmetrical J x H force due to a current source at a centre of the weld pool. This would generate toroidal flow, but such flow has only been observed in simulated weld pools in a static container;

ii) asymmetric electromagnetic forces due to current flow outside the weld pool;

iii) drag forces due to the plasma jet;

iv) the stagnation pressure due to the plasma jet or the inertia force due to the impigement of metal drops. This causes a crater on the front of the weld pool.

This led to the suggestion that the general pattern of metal movement is

as follows: metal from the filler metal is mixed with metal from the lower part of the arc crater and swept back along the lower surface of the weld pool; some of it then moves foward along the pool surface towards the arc. The metal solidifying at the edges of the pool is mainly metal from the base metal.

The model - dual heat source model - presented in this work is in accordance-with this general pattern of metal movement.

2.5.3.4. - Brief summary

Heat and fluid flow in weld pool have been widely investigated and several authors proposed qualitative and/or quantitative theories in order to explain the phenomena involved. Most of the literature on this subject is from a quite early date and again here TIG welding was the major beneficiary. More or less complicated models can be found but there is a lack of simple modelling with practical use in this field.

In the context of the above sections, the major problems in the appication of heat flow theory to the welding situation are:

i) the selection of real values of the thermal properties and the consideration of their variation with temperature;

ii) the consideration of the latent heat of fusion in the solidifying weld pool and the heat evolution or absortion due to solid state metallurgical transformations;

iii) in practice heat is not supplied in a point or line source;

iv) in many situations, it is difficult to know whether heat flow is purely 2 or 3 dimensional or a combination of these flow types.

The assumption of a point source of heat for the welding arc (undertaken by most of the authors) is debatable, nevertheless, the theories based on this conviction are in fairly good agreement with experimental results within the observed cases (ref. 90, 102).

Only recently, Eagar and Tsai (ref. 98) proposed a heat balance based on a distributed heat source on a semi-infinite plate; again it is impossible to have an accurate approach since a number of simplifying assumptions remain, for example, the fact that a Gaussian heat source was considered for developing the theory when the heat distribution of arcs is not really Gaussian.

Several authors (ref. 80, 89) tried to overcome problems i) and ii) but the results have not been treated together in an attempt to obtain better correlation between theory and practise.

The mode in which heat is transferred from the arc to the weld pool, the losses associated and the way it is consumed in the weld pool has not been clearly explained.

Other approaches, even more empirical, but based on the theories already developed, could be of some help in trying to find simple models for the phenomena associated with heat and fluid flow on the weld pool.

2.5.4 - Weld bead dimensions

2.5.4.1 - Penetration and bead shape

Most of the work referred to in section 2.5.3 was undertaken in order to calculate weld bead dimensions. Christensen's (ref. 102) approach led to the following dimensionless parameters:

- cross sectional area (a_m) of fused and recristalized zones

$$a_m = (v/2\rho)^2 A_m \qquad (44)$$

where A_m is the experimental area of expressed in terms of radius vector $\dot{\rho}_m$ at maximum contour width

$$a_m = \frac{\pi}{2} (1 + 2\dot{\rho}_m) \left(\frac{\dot{\rho}_m}{1 + \dot{\rho}_m}\right)^2 \qquad (45)$$

- width (ψ_m) and depth (ζ_m) of fused and recrystalized zones

$$\psi_m = \zeta_m = \frac{\dot{\rho}_m}{1 + \dot{\rho}_m} \left(\sqrt{1 + 2\dot{\rho}_m}\right) \qquad (46)$$

The results obtained using these approaches and its comparison with experimental data are shown in Fig. 25.

Ushio et al's (ref. 90) approach proposed a computerized formula in order to calculate molten pool length and width. Theoretical and experimental results are in good agreement, in most of the cases, as shown in Fig. 26.

Eajar and Tsai (ref. 98) used a dimensionless operating parameter n defined as:

$$n = \frac{q\ v}{4\ \pi\ \gamma\ \rho_m\ C_p\ (T_c - T_o)} \qquad (47)$$

and a dimensionless distribution parameter u as:

$$u = \frac{v}{2\ \rho} \qquad (48)$$

which give the welding conditions for the several process shown in Figs. 27, 28, 29, 30.

The travelling distributed heat source theory provides the first estimate of weld pool geometry based upon fundamental of heat transfer. The agreement between theory and experiment is improved considerable over previous models. The theory provides a model that can be used to asses how changes in the process or in the material will influence the weld geometry.

Penetration is, nevertheless, the weld bead dimension where most attention has been focused. Changes in GMA weld pool shape and depth of penetration can create significant welding problems, particularly when high precision automatic welding is required, so penetration and the area of penetration are the two major parameters relating to fusion defects.

Several workshave been undertaken in order to find the possibility of controlling these two parameters.

Friedman, E. (ref. 96) studied the effect of weld pool distortion on penetration and concluded that the propensity of a weld bead to fully penetrate the thickness of the weldment is enhanced by weld puddle depression. Another important conclusion was the influence of current, which, when increased, results in more heat input thus causing more melted material and increase in penetration. This leads to increase in arc pressure (arc pressure is proportional to the square of the arc current) producing a greater degree of puddle depression. For partial penetration welds depression of the top surface varies linearly with arc pressure.

Friedman also stated that the understanding and controlling of surface tension was essential for controlling weld puddle shape change, as well as enhancing penetration.

Essers and Walter (ref. 100) studied the effect of several heat sources (current, radiation, convection, filler metal) on penetration and concluded that it was the heat in the transferring droplets which

determined the mass of the work piece that is melted, i.e. penetration and areas of penetration.

In GMAW and plasma-GMAW, the results indicate that the penetration was a function of the magnitude of γ P (the sum of the momentums per second), where γ is the number of droplets reaching the weld pool per second, P is the momentum of the droplets (P = mv), as shown on Fig. 31 and that γ P increases with increase in current. The transfer mode is not referred in this work but it can be of relevance.

Cowdery (ref. 101) studied the effect of pulsed current on penetration using GMAW with a pulse frequency of 50 Hz in aluminium and mild steel. The results obtained showed that penetration increases as

i) the pulse duration decreases;
ii) the arc length is reduced;
iii) the wire feed speed increases.

Another important result of this work was the relationship found between penetration and travel speed which is shown in Fig. 32. This is, nevertheless, a limited work with results within a narrow range of parameters.

Oreper, Eajar and Szekely (ref. 91) developed a model (see section 5.3) that allows the prediction of shape and penetration of the weld pool under various process conditions and base metal compositions in, at least, a qualitative sense. This work is an important contribution but it is limited for GTA welding. Despite the several works published in this field, most of them from an early date, there is nothing published directly related with pulsed GMAW and work in this field is needed mainly if automatisation and robotisation are envisaged.

2.5.4.2 - Brief summary

From what was presented above, it is clear that some considerable effort has been made to explain the mechanism of penetration and bead shape. Most of the models presented were developed for TIG welding.

Oreper et al's (ref. 87) model can be extended to take account of flow in the presence of significant surface depression and in a travelling mode. Eajar and Tsai's contribution (ref. 98) in this field was the only one considering process conditions and base metal compositions.

One of the most significant contributions in GMAW was made by Essers and Walter (ref. 100) who indicate that the heat content of the

transfering droplets is the main factor determining the cross-sectional area of penetration while the impact of the droplets governs the depth of penetration. Nevertheless, wettability, dependent on the various surface tension forces involved, has a significant effect too on penetration and mainly on the shape of the weld bead the transfer mode considered in this work is not referred to and it can be of relevance. The good agreement of most of these models with experimental results gives confidence that more difficult models, i.e. more complete with less simplifying assumptions, may provide a realistic discription of heat flow in arc welding. Nevertheless, these quite complicated models are of no use in day-to-day practical situations.

A gap that seems to appear in this subject is the lack of literature referring to multipass welding which is the usual situation in practical uses.

As a conclusion, it is possible to say that a clear idea about the mechanism of penetration and bead shape has not yet been achieved and that the prediction of these factors, surely of major benefit in practical use is, so far, impossible.

Pulsed GMAW has, so far, been outside such considerations and surely work in this field is pressing.

2.6 - CONCLUSIONS

Conventional MIG welding is associated with spatter and poor fusion characteristics which can only be overcome within narrow tolerance bands.

For stable welding, it is essential to maintain a constant arc length which is achieved by matching wire feed speed with burn-off rate and the metal transfer mode from the wire tip to weld pool has to be of the "spray" type. A spray transfer mode is produced in DC MIG welding only above a critical wire feed speed (or current) which is impossible to use when welding in position or on thin plates or materials which are sensitive to high energy inputs. The lower current range produces globular or short-circuiting transfer modes which leads to poor transfer characteristics as mentioned above.

Pulsed current appeared initially as a technique to overcome these difficulties but, until recently, precise control of pulse characteristics, as demanded by the arc, was not possible with commercial

power supplies.

Since the beginning of the seventies, new concepts in electric arc welding equipments have been developed and solid state devices have been substituted for the traditional electromagnetic amplifiers. These new equipments, now commercially available, opened a large range of possibilities in GMA welding, especially in pulsed GMAW which has been the major beneficiary of this technique.

Research work has been mainly directed to metal transfer characteristics with the objective of controlling these characteristics by means of pulse parameters. Nowadays, the control of metal transfer in GMAW by the application of a current pulse is well established for mild steel, stainless steel and aluminium, as well as for a variety of other ferrous and non-ferrous materials.

An interesting prospect is the use of these new equipments with tubular consumables (e.g. flux cored wires). This may lead to reducing the lowest heat input achievable with a given consumable, manipulating droplet size and detachment rate and perhaps influencing weld properties through the control of reaction rates.

The problem of choosing welding parameters for a given application can arise, as it requires the specification of a wide range Variables such as gas/wire combinations, mean current, pulse parameters, often with competing effects.

In the present work, astep forward is taken in the examination of the effects and interactions of the possible variables in pulsed GMAW specially in what concerns wire size and shielding gas composition. Previously emphasis was placed on studying the possibilities of controlling metal transfer but little or not research work was undertaken on fusion characteristics. Nevertheless, specially in a process that gained reputation of being prone to fusion defects, the possibility of controlling aspects such as penetration, fusion area and dilution, is of basic importance for its development. The study of the influence of welding parameters on fusion characteristics in pulsed GMAW of mild steel is undertaken in this work with the objective of controlling these aspects. The result of this work has been to further explain interactions between process parameters and welding characteristics and to provide a sounder base for further development in controlled Gas Metal Arc Welding.

CHAPTER 3 - DESIGN OF RESEARCH PROGRAMME

CHAPTER 3 - D E S I G N O F R E S E A R C H P R O G R A M M E

3.1 - BASIC AIMS

The basic aims of the present work were:

1 - to further develop the study of the influence of welding parameters on deposition characteristics in pulsed GMA welding of mild steel,

2 - to investigate the influence of welding parameters on bead characteristics in pulsed GMA welding in mild steel,

3 - to establish a simple model based on the knowledge obtained above which enables the control of plate fusion area and dilution in pulsed GMA welding,

4 - to develop the model referred to above to enable prediction of heat affected zone dimensions,

5 - to apply the model to beads deposited in grooves,

6 - to explain penetration mechanisms based on the experimental results obtained.

3.2 - EXPERIMENTAL PROGRAMME

A sketch of the experimental programme undertaken is presented in Fig. 33.

3.3 - RELATION OF EXPERIMENTAL RESULTS AND THEORETICAL CONCEPTS

It is important in new research that experimental results should be explained by the development of the appropriate theoretical concepts.

In this work, an experimental programme was designed step by step first based on earlier investigations in P-GMAW and further based on the analysis of the results that were being obtained.

The results of the different sets of experiments were analysed each time based on the development of theoretical concepts in order to find the correct explanation of the relations obtained. Theories on heat flow in arc welding and forces involved in the welding process, on fluid flow on the molten pool were considered at various stages so that a complete

and correct explanation of the results would be achieved.

It was an aim of this work to interpret both practically and theoretically all the results obtained and to relate then to operational characteristics and welding variables.

An important objective was to express the results in the simplest way, clearly, in order for them to be easily applicable in practice.

CHAPTER 4 - EQUIPMENT AND MATERIALS

CHAPTER 4 - E Q U I P M E N T A N D M A T E R I A L S

4.1 - EQUIPMENT

4.1.1 - Power sources

Two synergic transistor power sources were used as described below.

4.1.1.1 - AWP M 500

The AWP M 500 synergic unit (photo 1) is a transistorized power supply that provides control of voltage and current to within ± 1 per cent at maximum output. The main technical characteristics of this power source are shown in Table 2.

4.1.1.2 - AWP M 450 PS

The AWP M 450 PS synergic unit (photo 2) is a transistor controlled power source that provides a high degree of stability and repeatability. The main technical characteristics of this power source are shown in Table 2.

4.1.2 - Wire feed unit

The wire feed unit used with the AWP M 500 was a BOC T.F. 2.0. It provides a continuously variable feed speed from about 0.8 m/min to 16 m/min. The wire feed unit used with the AWP M 450 PS was a Millermatics S-54 D which provides a continuously variable wire feed speed from 0.5 to 15 m/min.

4.1.3 - Welding torch

With the AWP M 500 a Union Carbide ST12 water cooled heavy duty MIG torch was used. The torch was mounted very close to the wire feed unit in order to get accurate feed. The welding torch employed with the AWP M 450 PS power source was a Tweco 400 unit, air cooled with a 5/8 in. gas shroud.

4.1.4 - Test rig

The test rig consisted of a transverse table capable of moving in one direction in a horizontal plane with speed continously variable from about 0.5 to 8.0 mm s^{-1}. An hydraulic control system permitted lateral and vertical movements of the torch enabling it to be accurately positioned in relation to the workpiece.

4.1.5 - Control of arc length and stick-out

Arc length and stick-out were controlled by projecting a magnified arc image (magnification of 5) on a calibrated screen. A 135 mm local distance lens were used.

4.1.6 - Water cooling system

Two water cooling systems a Transcooler and a Thermal Arc were used for cooling the torch and the power units respectively. The AWP 450 PS power source has an internal water cooling system.

4.1.7 - Gas supply

Gas flow was monitored and regulated by means of a tapered tube and float device. This employed a linear scale, each division corresponding to 10 ℓ/min, with an accuracy of ± 10%.

4.1.8 - Photographs

Black and white 35 mm photographs of the equipment and of some weld beads were taken using the following settings:

- shutter speed 1/125 sec,
- lens aperture f16,
- lens focal distance - 50 mm.

4.1.9 - Current and voltage measurements

Welding current and voltage were measured using the power supply meters with the AWP M 500. These meters working by means of a non-inductive shunt were independently calibrated and gave an accuracy of ± 1%.

With the AWP 450 PS the voltage was measured by an independent voltimeter with an accuracy of ± 0.1%.

During some of the experiments the pulse structure was recorded using a Transient Recorder, viewed on an oscilloscope and printed on an ultra violet oscillograph (U.V.O.).

4.1.10 - Measurements of weld bead cross-sectional areas

The bead-on-plate areas (total, reinforcement and fusion) were measured from traces obtained on a Vickers projection microscope with a five times magnification lens using an ALLBRIT planimeter and a computerized based GP 7.2 digitizer system. The areas of the beads deposited on V grooves were measured using the digiter system referred above.

4.2 - MATERIALS

4.2.1 - Shielding gas

The gas mixtures used were the commercial available:

Ar
Ar/1% O_2
Ar/2% O_2
Ar/5% CO_2
Ar/20% CO_2
CO_2
85% He/1.5% CO_2/13.5% Ar (Helishield 1).

4.2.2 - Wire electrodes

The filler materials used were:

- 1.0 mm, 1.2 mm and 1.6 mm mild steel Bostrand LW1 wires with the nominal composition shown in Table 3, according to the specification BS 2901; Part 1; A 18.

4.2.3 - Base materials

The base materials used were 6 mm, 25 mm and 35 mm thick mild steel (C - 0.25, Mn - 1.25) bars of 60 mm x 25 mm. In the 35 mm bars, V grooves of 60^o, 90^o and 120^o where machined with a 15 mm depth.

CHAPTER 5 - EXPERIMENTAL PROCEDURE

CHAPTER 5 - E X P E R I M E N T A L P R O C E D U R E

5.1 - GENERAL PROCEDURE

5.1.1 - Materials preparation

The mild steel bars were degreased and cleaned of dust and surface oxides immediatley before welding.

5.1.2 - Power supply voltage / current characteristics

A vertical voltage / current characteristic was used for all the experiments in order to obtain a stable current. The power supply was used in the open arc reverse polarity mode (electrode positive) for all the work.

5.1.3 - Measurement and control of arc length and electrode extension

After choosing a given arc length and electrode extension the contact tube / plate distance was set by moving the torch up or down. The arc length was then controlled by projecting a magnified image upon a calibrated screen. In order to keep the arc length constant, wire feed speed was regulated to the appropriate value with arc voltage floating. This task was sometimes difficult due to wire hunting, specially for the fine wires (possibly due to high wire feed rates). Some additional difficulties were found for very low welding speeds due to the molten material that appeared on the front of the arc and for very high mean currents due to the depression in the weld pool. The arc length defined is the apparent arc length since the actual length is somewhat variable due to depression of the weld pool by the arc force and to the transfer of electrode material.

For the present work an apparent arc length of 5 mm was used.

5.2 - INFLUENCE OF WELDING PARAMETERS ON DEPOSITION CHARACTERISTICS

5.2.1 - Introduction

The main purpose of the experiments was to investigate the influence of the welding parameters on the arc running characteristics,

burn-off rate and metal transfer characteristics. The choice of the welding parameters in each case was sometimes quite difficult to make since it was impossible, speciallyin pulsed GMAW, to investigate one parameter at a time due to the links between them and to the competing individual effects than often existed.

Most of the experiments were of a bead-on-plate nature in mild steel, i.e. mild steel wires with the diameters 1.2 mm mainly, but also 1.0 mm and 1.6 mm were melted under several gas shielding mixtures and deposited on top of mild steel bars of 25 mm and 6 mm thickness. Some experiments were undertaken also in V grooves with three different angles in mild steel with a 1.2 mm wire burning in a Ar/5% CO_2 shield.

During the experiments, arc running characteristics, i.e. arc stability and shape, spatter and fume generation, were observed and measurements of wire feed speed were registered using the display of the equipment.

5.2.2.- Mean current

The underlying basis of the parameter selection for experiments performed was the adoption of conditions relating to one droplet per pulse, detaching at the peak and having an equivalent spherical diameter near 1.2 mm.

The requirement of droplet detachment during a pulse peak is reasonable as this is the intended purpose of the peak (there are, however, reports that detachment outside the peak may have beneficial effects when welding aluminium and its alloys,(ref. 104)but the requirement of just one droplet per peak is a less obvious choice since in many situations satisfactory conditions exist with more than one droplet. Differences may exist between first and subsequent detachments however and therefore one droplet per pulse is though to give the most controlled form of transfer (see Fig. 16). The specification of droplet characteristics is restricted here to that of droplet volume (ref. 42).

This choice was made too on the grounds that one droplet per peak minimizes peak energy and hence allows maximum background energy for a given current. This is not important at high mean currents as enough power can be dissipated during the background period to guarantee arc stability. However at low mean currents (less than 100 A depending on wire size) the power in the background has a marked effect on process

stability.

Clearly, a volume corresponding to a sphere of diameter 1.2 mm is arbitrary, nevertheless the range of practical value is not large. Values much in excess of wire diameter are of limited practical interest while fine droplets charac eristics of streaming transfer are not evident in pulsed welding. According to ref. 42, droplets near the size of the wire diameter are usually compatible with satisfactory arcing conditions.

In order to standardise asmany influences as possible, the peak parameters used were I_p = 350 A and t_p = 4 ms. This condition is compatible with one droplet per pulse (see Fig. 1). The experiments were carried out with a 1.2 mm wire diameter burning in a Ar/5% CO_2 shield. Stick-out was kept constant at 15 mm for a plate / contact tip distance of 20 mm. Bead-on-plate deposits were done with mean current changes using increments of current of 20 A between 50 A and 200 A.

During the experiments, arc running characteristics were observed with emphasis on arc shape alterations and measured mean current voltage and welding speed.

5.2.3 - Shielding gas composition

Beads were deposited on mild steel plates moving at 1.53 mm/ /sec beneath a machine torch mounted perpendicularly to the work, using various gas mixtures. Mean current was set at 100 A with a pulse structure defined by I_p = 350A, t_p = 4 ms, I_b = 38 A, t_b = 16 ms. Stick-out and arc length were kept constant at 15 mm and 5 mm respectively. Special emphasis was placed on observing changes in arc running characteristics whilst wire feed speed was measured using the machine's wire feed meter.

For these tests, only commercially available gases were investigated and those used were Ar, Ar/1% O_2, Ar/2% O_2, Ar/5% CO_2, Ar/20%CO_2,CO_2,85% He/13.5%,Ar/1.5% CO_2 (Helishield 1). It was appreciated at the outset that some of these are not suitable for pulsed GMAW of mild steel (e.g. CO_2, Ar). However, such gases were included with a view of examining their influence on particular aspects and as a matter of completeness to compare with the other gases rather than establishing their suitability as welding shields.

5.2.4 - Wire diameter

Wire diameters of 1.0, 1.2 and 1.6 mm were used in an Ar/5% CO_2 shield. Experiments were performed as described in the last section. It may be seen from Fig. 15 that I_p = 350 A and t_p = 4 ms should be compatible with one droplet per pulse for all wire diameters used here.

In order to obtain suitable droplet sizes, a pulse frequency corresponding to 50 Hz per 100 A (mean current) is required for a 1.2 mm wire, provided that peak parameters have been chosen to give one droplet per pulse. A relation 50 Hz/100 A was applied to all wire sizes in order to standardise as many influences as possible.

5.2.5 - Electrode extension

Electrode extension was varied between 10 mm and 25 mm whilst holding the arc length and the mean current constant. This procedure was undertaken for three different values of mean current with 1.0, 1.2 and 1.6 mm wires in an Ar/5% CO_2 shield. Peak parameters and frequency were kept constant at I_p = 350 A, t_p = 4 ms and F = 50 Hz. Wire feed speed was measured using the equipment's meter and arc running characteristics were observed.

5.2.6 - Nominal heat input

Nominal heat input is defined as

$$q = \frac{\bar{I}V}{v} \text{ KJ/mm} \qquad (49)$$

(heat input rate per unit length)

A range of mean current (70 - 250 A) and travel speeds (0.8 - 8 mm/sec) were employed corresponding to nominal heat inputs of 0.5 to 5 KJ/mm. All heat inputs are nominal values calculated prior to welding on a basis of a 30 V arc. Peak structure was fixed (350 A, 4 ms), all the beads were deposited on a thick plate with a 1.2 mm wire burning in an Ar/5% CO_2 shield. Stick-out and arc length were kept constant at 15 and 5 mm respectively.

5.2.7 - Welding speed

Beads were deposited with welding speeds between 0.7 and 8 mm/sec, for a 15 mm stick-out and 5 mm arc length. Peak structure was kept constant (350 A, 4 ms) and background parameters were chosen on a basis of 50 Hz per 100 A. Deposition characteristics were registered.

The experiments were carried out according to the following procedures:

i) the shielding gas / wire diameter combination of Ar/5% CO_2 and 1.2 mm was investigated for mean currents of 100, 150 and 200 A;

ii) for the same wire with helium base shield (13.5% Ar/85 % He/1.5% CO_2) a range of mean currents was investigated;

iii) procedure described in ii) was repeated for 1.0 and 1.6 mm wires with an Ar/5% CO_2 shield.

5.2.8 - Peak parameters

For a 250 A mean current and a 125 Hz frequency, weld runs were deposited on steel bars using a 15 mm electrode extension for a 20 mm plate/contact tip distance. Deposition characteristics were investigated using:

i) increments of peak current of 50 A for a fixed peak duraction;

ii) increments of peak duration of 1 ms for fixed peak currents.

The maximum peak current was limited to 500 A by the output of the power supply.

5.2.9 - Background parameters

Experiments were undertaken with a fixed mean current using the approach shown on Fig. 34.

i) constant frequency and constant peak and background durations;

ii) constant frequency;

iii) constant peak parameters,

for a 1.2 mm wire in an Ar/5% CO_2 shield with a 15 mm stick-out and a 5 mm arc length. Arc running and burn-off characteristics were observed.

5.3 - INFLUENCE OF WELDING PARAMETERS ON BEAD CHARACTERISTICS

5.3.1 - Introduction

The main purpose of these experiments was to investigate the influence of welding parameters on fusion characteristics, which are of basic importantce in the development of any welding procedure.

The fusion characteristics considered of importance were depth of penetration, width of the beads, wetting angle, shape of the bead, total fusion area and plate fusion area. For all sets of experiments these were measured and these measurements led to the study of the dilution (see Fig. 35) which was defined as

$$\delta(\%) = \frac{A_F}{A_F + A_D} \times 100\% = \frac{A_F}{A_T} \times 100\% \qquad (50)$$

5.3.2 - Mean current

Wire diameters of 1.0, 1.2 and 1.6 mm in Ar/5% CO_2 and Helishield 1 were used within the mean current range of 75 to 250 Amps. Peak structure was fixed at (350 A, 4 ms) with background conditions chosen on the basis of a 50 Hz per 100 A rule. This procedure gave satisfactory droplet transfer with drop volume that was insensitive to mean current. For example, at 200 A the frequency was 100 Hz with a background duration of 6 ms and a background current level of 100 A. By adopting this procedure, possible influences of peak current and droplet size on fusion were standardised. All the work was confined to bead-on-plate (25 mm thickness) with mild steel.

From all the beads obtained macrograph samples were taken and from the respective traces penetration, width, reinforcement height, wetting angle, fusion and total areas were measured.

5.3.3 - Shielding gas composition

Bead characteristics were investigated for the gas mixtures Ar, Ar/1% O_2, Ar/2% O_2, Ar/5% CO_2 and Helishield 1 for 1.0, 1.2 and 1.6 mm wire diameters. Weld runs were deposited with a mean current of 100 A defined by I_p = 350 A, t_p = 4 ms, I_b = 39 A, t_b = 16 ms for 15 mm

stick-out and 5 mm arc length. Table speed was held constant at 1.53 mm/s for all the gas mixtures. Photographs of the weld runs were taken to illustrate the result of these experiments.

5.3.4 - Wire diameter

Wire diameters of 1.0, 1.2 and 1.6 mm were used with the gas mixtures Ar, Ar/1% O_2, Ar/2% O_2, Ar/5% CO_2 and Helishield 1 for 100 A mean current and 1.53 mm/s welding speed. Bead characteristics were observed as referred on 5.3.1 for wire diameters of 1.0, 1.2 and 1.6 mm with an Ar/5% CO_2 shield for mean currents from 75 to 250 A and welding speeds of 0.75 mm/s to 8 mm/s. A wire diameter/gas shielding combination of 1.2 mm/Helishield 1 was used for mean current (75-250 A) and welding speed (0.75 - 8 mm/s) ranges as described above.

5.3.5 - Electrode extension

Experiments were undertaken with electrode extension of 10 mm, 15 mm, 20 mm and 25 mm for mean currents of 100, 150 and 200 A with wire diameters of 1.0, 1.2 and 1.6 mm in an Ar/5% CO_2 shield. Arc length and table speed were held constant at 5 mm and 1.53 mm/s respectively. Measurements of beads size were undertaken in order to find possible differences.

5.3.6 - Nominal heat input

It is usually considered that heat input is a major parameter in determing bead characteristics. In order to establish its effect on bead characteristics (namely penetration and plate fusion area), experiments were performed for a range of values from 0.5 KJ/mm. For each value of heat input, several values of mean current (70 to 250 A) with proportional values of welding speed (0.7 mm/s to 8 mm/s) were investigated. Peak parameters and mean current/frequency relationship were held constant at I_p = 350 A, t_p = 4 ms, $\bar{I}/F$ = 2 in order to standardise metal transfer characteristics and its effect on bead shape.

Beads were deposited on 25 mm plates with a 1.2 mm wire burning in an Ar/5% CO_2 shield. Stick-out and arc length were kept constant at 15 mm and 5 mm respectively. Special emphasis was placed on measuring penetration and plate fusion area.

5.3.7 - Table speed

Bead characteristics were investigated from cross sections of welds deposited with I_p = 350 A, t_p = 4 ms, $\bar{I}/F$ = 2.15 mm electrode extension and 5 mm length under the conditions given below:

i) Travel speed was varied within a range of 0.8 to 8 mm/s for a fixed mean current with an Ar/5% CO_2 shield and a 1.2 mm wire. This procedure was undertaken for three different values of mean current (100, 150 and 200 Amps).
For the very low speeds some difficulty was found on maintaining the stick-out of 15 mm and/or the plate/contact tip distance of 20mm due to the fused metal that ran in front of the arc;

ii) Varying travel speed from 0.8 to 8 mm/s over the current range 65 to 325 A for 1.0 and 1.6 mm wires in an Ar/5% CO_2 shield and for the 1.2 mm wire for Helishield 1.

5.3.8 - Peak parameters

In order to study the influence of metal transfer characteristics (number and size of droplets detached), peak parameters were changed maintaining all other welding parameters constant for a fixed mean current (250 A), frequency (125 Hz), wire diameter (1.2 mm), gas mixture (Ar/5% CO_2), stick-out (15 mm) and arc length (5 mm). Peak current was varied over the range of 500 to 300 A for fixed peak duration and this method was adopted for peak durations from 1 to 6 ms using increments of 1 ms (t_p = 1 ms was investigated only as a matter of completeness once the power supply characteristics indicate 1 ms rise time). Bead size, especially penetration, fusion and total areas, were observed.

5.3.9 - Background parameters

Another way of changing metal transfer characteristics is to change frequency for a fixed current since $\bar{I}/F$ is the relation "defining" droplet volume. Magnitude of background current and duration were changed in order to study the influence of frequency on bead characteristics for a fixed mean current and fixed peak parameters.

Other approaches were undertaken in which background parameters and peak parameters were changed for a constant frequency and where peak and

background intensities were changed for a fixed frequency and for fixed peak and background durations. For all the experiments, mean current, wire size, shielding gas composition, stick-out and arc length were kept constant with the following values: 100 A, 1.2 mm, Ar/5% CO_2, 15 mm 5 mm respectively.

Measurements of bead size were done as described above.

5.4 - CALORIMETRIC STUDY

In order to gain a better understanding of plate heating phenomena a limited calorimetric study was undertaken.

Several beads were deposited on 15 mm thick plate for mean current values of 100, 150 and 200 Amps and welding speeds of 2, 4 and 6 mm/s. Wire diameters of 1.0, 1.2 and 1.6 mm together with Ar/5% CO_2 and 13.5% Ar/85% He/1.5 CO_2 (helishield 1) gas mixtures were used.

Using a calorimeter designed for the purpose, the temperature of plates before and immediately after welding was measured, i.e. the welding plates were quenched in a water calorimeter and the temperature was measured after stirring the water.

The weight of the plates before and after welding was measured using a balance.

All the experiments were undertaken for fixed plate conditions (I_p = 350 A and t_p = 4 ms) while stick-out and plate/contact-tip distance were held at 15 and 20 mm respectively.

5.5 - INFLUENCE OF WELDING PARAMETERS ON THE DIMENSIONS OF THE HEAT AFFECTED ZONE

5.5.1 - Introduction

Heat affected zone characteristics are of great importance in welding since they are related with the mechanical and metallurgical properties which govern the weld behaviour. This aspect is of basic importance when welding certain alloys and particularly hardenable alloy steels. In order to be able to relate welding parameters and heat affected zone dimensions, it is necessary to understand heat flow theory since it can indicate the essential variables which govern the formation of heat affected and fusion zones.

5.5.2 - Mean current and travel speed

Emphasis was placed on determining the effect of different mean current/ welding speed combinations on heat affected zone area (A_{HAZ}) defined as the area between the surface of the palte and the 723° C isotherm (A_1) (see Fig. 36).

Mean currents of 100, 150 and 200 A were used with table speeds from 0.75 to 8 mm/s for 1.2 mm wire with Ar/5% CO_2 and Helishield 1 gas mixtures.

Electrode extension and arc length were hold constant at 15 and 5 mm respectively. Peak parameters and mean current/frequency relationship used were: I_p = 350 A, t_p = 4 ms and $\bar{I}/F$ = 2.

5.6 - INFLUENCE OF WELDING PARAMETERS ON THE CHARACTERISTICS OF THE BEADS DEPOSITED IN GROOVES

5.6.1 - Introduction

V grooves are possibly the most common preparation used in welded construction, thus the relationship between welding parameters and fusion characteristics on these beads is of practical importance.

When welding in a V groove, most of the difficulties (e.g. operating conditions, fusion defects, etc.) are more critical on the first pass. An important parameter for fusion characteristics in V grooves is the angle of the groove since it influences heat flow.

In this work, attention was directed to the fusion characteristics and bead shape of this first pass in beads deposited in V grooves of several angles by means of measuring plate fusion areas, deposited area, wetting angle, width and height of the bead.

5.6.2 - Shielding gas composition

Ar/2% O_2, Ar/5% CO_2, Ar/20% CO_2 and He_1 were used for shielding welds deposited in V grooves of 60, 90 and 120° for 150 and 200 A mean current and a welding speed of 2 mm/s.

V grooves were machined in 35 mm thick mild steel to give a depth of 15 mm, in which the weld bead was deposited. An 1.2 mm wire was used with a contact tip/plate distance of 20 mm and an average arc length of 5 mm.

After welding the beads were sectioned, polished, etched and traces were done where wetting angle, bead width and height were measured with the aim of studying the influence of shielding gas composition on bead shape.

5.6.3 - Mean current and travel speed

Mean current values of 150, 200 and 250 A were used with welding speeds varying in the range of 2 to 7 mm/s for two different gas shields: Ar/5% CO_2, Helishield 1.

The peak parameters and mean current/frequency relationship used were the same of those for all the other experiments in mild steel: I_p = 350 A, t_p = 4 ms, $\bar{I}/F$ = 2.

The work preparation described in section 6.1 was used here again.

From the samples obtained fusion area and deposited area were measured.

CHAPTER 6 - EXPERIMENTAL RESULTS

CHAPTER 6 - E X P E R I M E N T A L R E S U L T S

6.1 - DEPOSITION CHARACTERISTICS

6.1.1 - Arc running characteristics

Arc running characteristics have been described in terms of stable operation, which is a subjective assessement and arc voltage which is measured in each experiment.

6.1.1.1 - Shielding gas composition

The "best" running characteristics visually were associated with 1.2 mm wires burning in argon/oxygen and argon/CO_2 mixes. In pure CO_2 shields large globules formed (increasing in size with wire diameter) producing asymmetrical transfer and spatter. A degree of light spatter was also observed with Helishield 1. This was associated with very fine droplets jumping from the wire tip.

Shielding gas composition has a significant effect on arc voltage as shown in Fig. 37.

6.1.1.2 - Wire diameter

With fine wires (1.0mm) arc hunting often occurred (probably due to high wire feed rates); this was less evident with 1.2mm diameter wires. With 1.6mm wires, wire melting sometimes appeared to occur in a slightly asymmetric manner, i.e. not uniformly across the wire tip. Heavy spater was generelly absent from all the wires (with the exception of CO_2 shields).

The influence of wire diameter on arc voltage is not significant as shown in Fig. 37.

6.1.2 - Burn off rate

Burn-off rate (W) for a square wave current is approximately given by:

$$W = \int_{cycle} W(t)\ dt \approx (W_p T_p + W_b T_b)\ F \qquad (51)$$

W(t) is the instantaneous burn-off rate.

The corresponding steady current behaviour (ref. 105) is:

$$W_p \approx \alpha I_p + \beta \ell I_p^2 \qquad (52)$$

and

$$Wb \approx \alpha I_b + \beta \ell I_b^2 \qquad (53)$$

where α and β are treated here as constants for a given wire size describing average arc and resistive heating efects respectively
ℓ is the electrical stick-out length.

The average burn-off rate for a square wave pulsed current may then be expected to approximately obey:

$$W = (\alpha I_p t_p + \beta \ell I_p^2 t_p + \alpha I_b t_b + \beta \ell I_b^2 t_b)\ F \qquad (54)$$

In order to evaluate and discuss relationships between theoretical and experimental values some simplification of this expression was considered (see Chapter 8).

6.1.2.1 _ Mean current

The influence of mean current on deposition was examined for the Ar/5% CO_2 gas mix with 1.2 mm wire and a stick-out of 15 mm. Results are shown in Fig. 38. The relationship is linear with a slope of 2.85 m/min per 100A. Results obtained with similar conditions for 1.0 and 1.6 mm wires are shown in the same figure.

6.1.2.2 - Shielding gas composition

Burn-off characteristics obtained with all the gas mixes are shown in Fig. 39 for a range of wire sizes at a fixed mean current of 100 A. Shielding gas composition has little influence on burn-off rate.

Arc voltage, a parameter that depends on the gas mixture, has of course also a small effect on burn-off rate, and there is a slight trend to higher burn-off rates with increasing voltage for a given wire size, e.g. for a 1.2 mm wire burn-off rate increases from 3 m/min in argon at about 20 volts to 3,4 m/min in helium near 33 volts.

Such data may also be expressed in terms of mass deposition rate per unit current (see Fig. 40). Deposition rate was calculated from burn-off rate.

$$\dot{m} = W \times A \times \rho_m \times 60 \ (kg/hr) \qquad (55)$$

where

$$A = \pi d^2/4$$

Fig. 40 shows that deposition rate is generally 1.6±0,3 Kg/hr/100 A for all gases wire and sizes.

6.1.2.3 - Wire diameter

The results obtained on the influence of wire diameter on wire melting rate are shown on Fig. 38. Wire melting rate increases with wire size and the deposition rate of 1.0, 1.2 and 1.6 mm wires are similar being typical around 1.6 Kg/hr/100 A with a scatter of ± 0.3 Kg/hr/100 A (see Fig. 40).

6.1.2.4 - Electrode extension

The influence of electrode extension on burn-off rate was examined in an Ar/5% CO_2 shield for 1.0, 1.2 and 1.6 mm wires for three different mean currents (see Fig. 41, 42 and 43). The results show that burn-off is very sensitive to electrode extension in pulsed GMAW, e.g. increasing the stick-out by 6 or 7 mm for a 1.2 wire the deposition rate increases about 0.3 Kg/hr/100 A.

6.1.2.5 - Nominal heat input

Nominal heat input is a parameter that depends on mean current and/or welding speed.It's influence on burn-off rate is not very significant.

Nevertheless, there is a trend for higher heat inputs to be associated with slightly lower burn-off rates.This can be due to differences in the stick-out, since these experiments were undertaken with very low table speeds and so with molten material travelling on the front of the arc. In order to stabilize the arc for these very low values of speed lower values of stick-out were used. Arc length was slightly altered too. Consequently, the results show that it is worthless to consider the influence of nominal heat input as "one" parameter on burn-off rate.

6.1.2.6 - Table speed

Welding speed has only a small influence on burn-off rate. This slightly decreases for the lower values of welding speed. The differences can be due, as explained above, to the effect that bead size has on arc length/electrode extension and hence process power.

6.1.2.7 - Peak parameters

In order to study the influence of peak parameters on burn--off rate the relation $I_p^2 t_p$ (D) was considered. The results are shown in Fig. 44. The relationship is linear with a slope of 2.5×10^{-2} ms ($\pm$ 0.15×10^{-2}).

6.1.2.8 - Background parameters

Background parameters didn't significantly influence burn-off rate as shown in Fig. 45.

6.2 - BEAD CHARACTERISTICS

6.2.1 - Bead Appearance

6.2.1.1 - Shielding gas composition

The "best" surface finish (surface ripple and fusion line straightness) was obtained with argon/oxygen mixtures.

It was observed that an easily detachable khaki coloured slag often formed at the plate/bead interface (this is associated with SiO_2 formation). The spacing of the slag islands changes markedly with shield gas composition being absent in pure argon shields and heavy in CO_2 shields (see photo 3). This suggests a criterion for classifying gas shields in terms of SiO_2 formation. In increasing order this is Ar, Helishield 1, Ar/1%O_2, Ar/2%O_2, Ar/5%CO_2, Ar/20%CO_2 and CO_2.

6.2.1.2 - Wire size

In terms of surface ripple and fusion line straightness the best beads were made with 1.0 mm wire diameter(see Photos 4 and 5). In Photos 6,7,8 and 9 bead appearance obtained for all the gas mixtures and 1.2 and 1.6 mm wires (respectively) is shown, for thick and thin plates.

6.2.2 - Penetration, width and reinforcement height

Depth of penetration, width and reinforcement height of the bead were defined as shown on fig. 35 for thick and thin plates.

6.2.2.1 - Mean current

The results obtained on the influence of mean current on penetration width and reiforcement height are shown in Fig. 46.

It was found that penetration (p) increases more or less linearly with I such that for conditions used here:

$$p\ (mm) = 0.028\ I\ (A) - 1.35 \quad (200 \geq I \geq 75) \qquad (56)$$

Width and reinforcement also increase linearly with mean current, this is expected since the deposition rate increases too.

In Fig. 47 the influence of mean current on penetration is shown for a range of "nominal heat inputs. Again, dependance on arc current is roughly linear.

6.2.2.2 - Shielding gas composition

The results on bead penetration measurements for both thick and thin plate are shown in Fig. 48.

Shielding gases producing greatest penetration were Ar/5%CO_2 and Ar/1%O_2 mixes. Increasing the CO_2 and O_2 levels to 20% and 2% respectively appeared to have an adverse effect on penetration, which was particularly marked between 1% and 2%O_2. With Helishield 1 on thin plate the weld burned through.

The dependance of weld width on gas type is shown on Fig. 49.

On the 6 mm plate the narrowest beads were obtained with an argon shield with increasing value for Ar/1%O_2, Ar/5%CO_2, Ar/20%CO_2, Helishield 1,CO_2.On these deposits the mixture Ar, Ar/1%O_2, Ar/2%O_2, led to more or less the same width. Increasing the amount of CO_2 also increases the width of the bead.

The influence of shielding gas composition on reinforcement height is shown in Fig. 50. The values obtained showed the same relationship as width, the higher reinforcement being associated with the narrowest beads.

6.2.2.3 - Wire diameter

Wire size exerts a small influence on penetration (see Fig. 48). However there is a tendency for penetration to increase marginally with decreasing wire size. The only exception to the small influence of wire size is for pure argon shields. Here for both plate thicknesses decreasing wire size greatly increases penetration; a factor of 4 exists between the results with 1.6 and 1.0 mm wire diameters.

The influence of wire size on weld bead width is shown in Fig. 49. There is a tendency for the widest beads to be associated with the smallest wire size used. Nevertheless, for the parameters used, wire size exerts only a small influence on bead width.

Reinforcement height is not significantly influenced by wire size (see Fig. 50).

6.2.2.4 - Electrode extension

The influence of electrode extension on penetration, width and reinforcement height of the bead for a mean current of 100 A and 1.2 mm wire is shown in Fig. 51.

Results obtained with 1.0 and 1.6 mm wires for 100 Amps mean current and with all the wires for 150 and 200 A mean current (although not shown) indicate the same trend, i.e. penetration approximately constant for all the electrode extensions with width and reinforcement increasing with stick-out. This can be explained by the increase of burn-off rate (and deposited mass) with electrode extension.

6.2.2.5 - Nominal heat input

The influence of nominal heat input on penetration depth for a range of mean currents from 70 to 250 A is shown in Fig. 52. Penetration has very different values for the same nominal heat input, e.g. a factor of 5 exists for 2 KJ/mm. Thus it is not possible qualitatively or quantitatively to determine the influence of heat input as "one" parameter on penetration.

For width and reinforcement height the same conclusion can be taken.

6.2.2.6 - Welding speed

The influence of welding speed on penetration is shown in Fig. 53 for a range of mean currents (70 - 250 A). General features of behaviour indicated that a fourfold increase in speed (from 2 to 8mm/s) has little influence on penetration whereas penetration may increase by 100% between speeds of 1 and 2 mm/s. It may also be seen that maximum penetration is achieved for a speed of about 2 mm/s irrespective of the current used.

Results obtained on width and reinforcement height measurements are shown in Fig. 55 and Fig. 54; welding speed significantly influence width and reinforcement. These values are related to the amount of material deposited during the unit time (deposition rate) in the unit length. Low values of welding speed led to large amounts of deposited metal per unit length thus to the highest values of width and reinforcement height, which decrease with the increase of welding speed.

6.2.2.7 - Peak parameters

Penetration depth is 4.5 $\pm$ 0.5mm for all the peak parameters used here (see Fig. 56). This was quite a surprising result since for the conditions used metal transfer characteristics (number of droplet detachments per pulse and size of droplets) were changed. The explanation for this result is presented in Chapter 8.

Measurements of width and reinforcement height gave values of 14.7$\pm$ 0.9mm and 3.2 $\pm$ 0.2 mm respectively, the higher values being associated with the higher values of $I_p^2 t_p$, due to the influence of this parameter on deposition rate.

6.2.2.8 - Background parameters

Experiments were undertaken with I=150 Amps, I_p=250 A, t_p=4ms for a range of frequencies from 26 to 83 Hz. The results obtained gave values of penetration of 2.1 $\pm$ 0.3mm changing indifferently with the increase of background current and duration.

The same remark can be made about the values of width and reinforcement height which were 3.2$\pm$ 0.8 mm and 3.0 $\pm$ 0.6 mm respectively.

6.2.3 - Wetting angle, bead shape factor and fusion angle

Bead shape wetting angle (θ) and fusion angle (ζ) were defined as the angles between plate surface and a tangent to the bead surface and a tangent to the plate fusion boundary respectively (see Fig. 35).

Bead shape was defined by the expression (see Section 8.2):

$$\gamma_s = \frac{A_F}{w \times p} \quad \frac{4}{\pi} \qquad (57)$$

The values of wetting angle, fusion angle and bead shape give an important indication about the susceptibility to fusion defects of the beads, e.g. beads with high θ , low ζ and γ_s may present side wall lack of fusion.

6.2.3.1 - Mean current

The influence of mean current on wetting angle, bead shape and fusion angle is shown in Fig. 57 and Fig. 58. The results indicate that wetting angle decreases with increasing mean current, while fusion angle increases and bead shape factor is constant. This fact means that when increasing mean current "better" shapes are to be expected.

6.2.3.2 - Shielding gas composition

The gas mixtures Ar, Ar/1%O_2, Ar/2%O_2, Ar/5%CO_2, Helishield 1 arranged in this order represent decreasing bead plate wetting angle θ , as shown in Fig. 59, for thick (25 mm) and thin(6 mm) plates. As with other processes it was found that θ decreases with increasing voltage.

Shielding gas composition is an important parameter in influencing bead shape and fusion area as shown in Fig. 60. The "best" bead shapes were obtained for Ar and Helishield 1, for both thick and thin plates, but as, with an Ar shield wetting angle is very high, Helishield 1 is the gas mixture giving better fusion shapes from the gases examined here.

6.2.3.3 - Wire diameter

Measurements of wetting angle, fusion angle and bead shape calculations undertaken on the bead deposited with different wire diameters (1.0, 1.2 and 1.6 mm) on thick plate under the same conditions for Ar/5%CO_2 shield, I_p=350A, t_p=4ms, I=100A, F=50Hz, v=1.53 mm/s are presented in Table 4.

These results do not present an obvious trend.

6.2.3.4 - Electrode extension

Wetting angle is approximately constant for the electrode extensions investigated, increasing slightly with the increase of the stick-out. For 150 A mean current these values are shown on Table 5.

The results on the bead shape factor and fusion angle, for the same conditions, are shown in Table 5 and indicate that stick-out does not significantly influence this value.

6.2.3.5 - Nominal heat input

The influence of nominal heat input on bead shape factor, wetting angle and fusion angle was measured for two different mean currents within a range of heat inputs. The values found are shown in Figs. 62 and 61.

Wetting angle increases as heat input increases whereas bead shape factor and fusion angle are approximately constant. Nevertheless, the "best" bead shapes were associated with the lower current for the intermediate values of heat input examined.

Since heat input values are associated with welding speed values (for constant mean current) these results can be explained by changes in this parameter (see Section 6.2.3.6).

6.2.3.6 - Welding speed

Wetting angle increases with the decrease of welding speed as shown in Fig. 63 for three values of mean current.

Below 3mm/s, wetting angle is strongly influenced by speed. In this region, current has a small effect with a tendency for larger angles at highest currents. Below 1.0 to 1.5 mm/s beads exhibit very poor wetting characteristics as the wetting angle is then obtuse. For speeds above about 3mm/s wetting angle changes only slightly with welding speed (current then has the dominant influence). Fusion angle results are shown in Fig. 64. An interesting observation is the higher fusion angles being associated with the higher values of penetration, v=1.5 - - 2mm/s, which nevertheless present high wetting angles as referred above.

The influence of welding speed in the bead shape is presented in Fig. 65. For the same welding parameters ($\overline{I}$, I_p, t_p, shielding gas, etc.) speed does not significantly influence bead shape. For the parameters chosen for these experiments finger penetration was always obtained.

6.2.3.7 Peak parameters

Wetting angle does not change significantly with peak parameters (see Fig. 66). Measurements undertaken for all the peak structures investigated in this work gave a mean value of 40.5^{o}. A similar behaviour was observed on fusion angle (see Fig. 66).

The influence of peak parameters on bead shape is shown in Fig. 67. All the beads obtained were characterized by a finger penetration shape (see Fig. 66), with no significant trend in the relationship between bead shape factor and peak parameters.

6.2.3.8 - Background parameters

The influence of background parameters on wetting angle and fusion angle and bead shape factor is shown in Table 6 for I=150 A, I_p=350 A, t_p=4 ms. The results show that background parameters do not significantly influence either wetting angle or bead shape factor or fusion angle.

6.2.4 - Plate fusion area, reinforcement area and total fusion area

Plate fusion area, reinforcement and total fusion area are defined as shown in Fig. 35.

6.2.4.1 - Mean current

Plate fusion area increases significantly with mean current. The results obtained on thick plate with 1.2 mm wire in an Ar/5%CO_2 shield, I_p=350 A, t_p=4 ms and I/F=100/50 are shown in Fig. 68. This relation can be represented by the expression

$$A_F \ (mm^2) = K \ (I)^n \qquad (58)$$

where k and n are constants:

K=1.11 x 10^{-4}

n=2.35

In Fig. 69 the influence of mean current on plate fusion area is shown for different values of welding speed. The results shown are in fair agreement with those presented in Fig. 68 and close to the maximum values identified. At speeds of 4 mm/s and less, the increase in fusion area with current obeys approximately an I^2 law with a weaker dependence at higher speeds. For values of speed higher than 4 mm/s this depenence is more or less linear.

The influence of mean current on total fusion area and reinforcement area is shown in Fig. 70. Total fusion and reinforcement areas increase with current. For reinforcement area this relationship is approximately linear, as expected, since a similar kind of relationship exists between the volume of the deposited material and mean current (see Section 6.1).

6.2.4.2 - Shielding gas composition

The effect of gas mixtures on plate fusion is shown in Fig. 71, for thick and thin plate. On thick plate the largest fusion areas were obtained for gases containing CO_2, possibly due to the higher thermal conductivity of this gas (higher than Ar or Ar/O_2 mixes). The smallest fusion areas were obtained with the mix $Ar/2\%O_2$. On thin plate trends are less well defined but fusion area is as expected, generally higher than for the thicker plate.

One interesting result concerns plate burn through observed with all wire diameters in the helium rich mix although on thick plate fusion area was little different than in other gases). A possible explanation of this observation is the "buried arc effect" (e.g. as in Keyhole welding), where the high power developed in a helium column may be efficiently transferred to the pool when a depression is developed, power which would otherwise have been lost to the athmosphere.

The total fused metal area (see Fig. 72) is, of course, composed of plate fusion area and reinforcement area (the latter contribution is not shown here, explicity, but may be obtained from burn-off and recovery data in Chapter 8).

6.2.4.3 - Wire diameter

In thick plate, fusion area increases significantly as wire size is reduced (see Fig. 71), an effect observed for all the gases. This may be due to the inherently stronger convective action within the arc for fine wires. With thin plate, differences between wire sizes are less well pronounced but for the 5% and $20\%CO_2$ mixes the smallest wire is again associated with maximum plate melting.

Similar trends were observed for the total fused metal area (see Fig. 72). This was expected since the differences on reinforcement area are not significant (burn-off rate approximately constant).

6.2.4.4 - Electrode extension

The influence of electrode extension on plate fusion area is not significant, as shown in Fig. 73 for a 1.2mm wire and two different values of mean current (100 and 150 A) although higher values of total area and reinforcement area were found as electrode extension was increased (see Fig. 74 and 75). The results are due to the increase (see Fig. 42) observed in burn-off rate, as stick-out increases and to the higher amount of heat developed by Joule effect in the arc. The results shown that this higher amount of heat developed does not significantly influence plate fusion however this result is discussed in Chapter 8.

6.2.4.5 - Nominal heat input

The influence of heat input on plate fusion area is shown in Fig. 76. It is interesting that for the same mean current, an increase of heat input by a factor of 5 generates beads with fusion areas usually within a scatter of 5 mm^2 for mean values between 10 and 20 mm^2 (depending on mean current). Another interesting result is that for the same heat input, fusion area presents signficantly different values, e.g. for a heat input of 2 KJ/mm, A_F varies between 0.3 and 22.2 mm^2. These results will be discussed in a later section (see Chapter 8).

Data obtained on total fusion area is shown in Fig. 77. The increase observed in the total fusion area with heat input is, of course, due to the height of reinforcement area, which increases with the increase of mean current for a given welding speed and with the decrease of welding speed for a given mean current.

6.2.4.6 - Welding speed

The influence of welding speed on plate fusion area is shown in Fig. 78. Qualitatively, this influence is similar (but more pronounced) to that of penetration with maximum fusion occuring at speeds close to 1.5 mm/s.

Reinforcement area is significantly influenced by welding speed, so, for the same mean current, total fusion area is dependent on welding speed, showing the same trend as reinforcement area.

The results on reinforcement area and total area are shown in Fig. 79 for 100 A mean current.

6.2.4.7 - Peak parameters

For a mean current of 250 A peak parameters were changed within the overall possible range (300 A $\leq I_p \leq$ 500 A, 2ms $< t_p <$ 5ms) and plate fusion area measurements gave approximately constant results 24.5 ± 2.5 mm^2. The only exceptions were observed for the lowest peak conditions ($I_p \times t_p$) and continuous direct current where plate fusion area is 19 ± 1 mm^2.

Total fusion area and reinforcement area are approximately constant, for the range of peak conditions used on $A_T = 54 \pm 5$ mm^2 ; $A_D = 30 \pm 5$ mm^2.

6.2.4.8 - Background parameters

The measurements undertaken on the beads deposited with the fixed mean current and peak parameters within a range of background parameters of 50 to 170 A current and 8 to 24 ms duration gave approximately constant values i.e. 8.6 ± 1.4 mm^2. This is quite an unexpected result since for the values used droplet volumes changed from 1.02 mm^3 to 2.06mm^3 and droplet momentum was expected to significantly influence penetration and plate fusion area (ref. 100).

6.2.5 - Dilution

Dilution (δ), defined by the ratio of plate melting (A_F) to total melted area (A_T), (see Fig. 35) is an important parameters in welding

It may also be used as a rough measure of susceptibility to fusion defects and as a mean of comparing fusion characteristics with other processes. Dilution is of interest in surfacing applications and may also give an indication of interpass refinement in multilayer welding. Further and perhaps more significantly, it describes important aspects of the interplay between mass and heat, e.g. in situations where maximum plate melting is required for minimum mass deposition. Thus, attempts should be made to optimise dilution.

6.2.5.1 - Mean current

Dilution is sensitive to arc current for a given welding speed having a value near 20% for typical manual GMAW (see Table 7).

In this work an effort was made to gain an understanding of this behaviour which is presented in Chapter 8.

6.2.5.2 - Shielding gas composition

In Table 8 is shown the average values of dilution (averaged over wire size) for all the gases examined in this work. This table shows that typically only 15-20% of melting occurs at the plate, the rest being deposited mass and that shielding gas composition do not affect significantly this value.

From the results presented above, it is obvious that P-GMAW is a welding process with inherent poor fusion characteristics when compared with SMAW or GTAW. An interesting result is the quantitative value of melting efficiency (Z_m) defined as the percentage of process power used in raising the fused mass to melting:

$$Z_m = \frac{H_m \cdot W \cdot A}{I \cdot V} \times 100\% \qquad (59)$$

where H_m is the heat required to melt the unit volume of metal (=10.23 J/mm^3 for mild steel - ref. 100).

Average values of Z_m (averaged over wire size) are shown on Table 9. It may be seen that the total melting efficiency for argon rich gases is generally between 32-36% with lower values occuring in Helishield 1 (due to high arc voltage and attended column losses). However, the most noteworthy feature of these results is that only 5% of the arc power produces plate melting on thick plate. The component of Z_m corresponding to plate fusion (Z_m^*) is shown on Table 9.

6.2.5.3 - Wire diameter

The influence of wire diameter on dilution for an Ar/5%CO_2 shield is shown in Table 10.

Wire size has a minor influence on the dilution factor.

The results shown in Tables 7 to 10 are for bead-on-plate deposits. When welding in grooves as the interplay between mass and heat is changed, the results are quite different (see Section 6.4).

6.2.5.4 - Electrode extension

Electrode extension's influence on dilution is shown in Fig. 80 for different wire sizes and different mean currents (100 A, 150 A and 200 A). As expected, the fraction of melting occuring at the plate decreases with increase in electrode extension, since plate fusion area is approximately constant and total area increases with increase in the stick-out.

6.2.5.5 - Nominal heat input

Observing the results in Fig. 81 it is possible to conclude that the value of δ will decrease as heat input increases.

The results obtained on the influence of heat input on plate melting and dilution are, at first sight, quite unexpected since heat input is usually associated with fusion characteristics in a way that it would be expected that this interplay should be more significant. In Chapter 8 an explanation for these results is advanced.

6.2.5.6 - Welding speed

The influence of welding speed on dilution is shown in Fig. 82 for a range of mean currents from 70 to 250 Amps. The results show that there is a trend for dilution to increase with welding speed, but, with this representation, this behaviour is far from clear. Simple modelling considerations introduced in Chapter 8 show that a better representation of this data is given by the product I.v

6.2.5.7 - Peak parameters

In Fig. 83 is presented the relationship between dilution and peak current for several peak durations. Dilution decreases with the increase of peak current as was expected since plate fusion area is approximately constant and reinforcement area increases (see Section 6.2.4.7).

6.2.5.8 - Background parameters

The experiments undertaken by changing background parameters and frequency for a fixed mean current and peak parameters gave values of dilution almost constant as expected since background parameters do not significantly influence either plate or total fusion area (see Section 6.2.4.8).

6.3 - CALORIMETRIC STUDIES

Total heat transfer efficiency to the plate was measured by monitoring the temperature rise of a water calorimeter after quenching a welded sample. The welding technique consisted of depositing a single bead on thick strips of carbon steel and then immersing samples immediately on completion of welding (with a welding time of about 20s); results from these experiments are given in Table 19 where η is the total heat transfer efficiency and V_{ET} is an effective voltage associated with total heat transfer (i.e. $V_{ET}=\eta$ V). It may be seen (table 21) that the process efficiency is typically 14.5 for an Ar/5% CO_2 shield. However, in the helium rich gas, V_{ET} is considerably higher ($\simeq$22 V). The discussion of the results obtained is presented on Chapter 8.

6.4 - HEAT AFFECTED ZONE DIMENSIONS

6.4.1 - Influence of mean current and table speed

Heat affected zone area was measured for a range of welding speeds from 0.75mm/s to 8mm/s for 100, 150 and 200 Amps mean current. The results are shown in Fig. 84. Heat affected zone areas increase with the decrease of welding speed in an exponential way.

6.4.2 - Influence of nominal heat input

Influence of nominal heat input on heat affected zone area is shown in Fig. 85 for 1.2mm wire, Ar/5%CO_2 and 23% Ar/75% He/2%CO_2 respectively.

These results obtained show a trend for heat affected zone area to increase with the increase in heat input.

6.5 - BEAD CHARACTERISTICS OF DEPOSITS IN V GROOVES

Bead characteristics of deposits on V grooves are defined on Fig. 86.

6.5.1 - Shielding gas composition

Shielding gas composition has a significant influence on wetting angle as shown in Figs. 87 and 88 for two different mean currents. These figures show that higher wetting angles are usually

associated with low voltage arcs.

Shielding gas composition has also a significant effect on dilution as shown on Table 11.

6.5.2 - Mean current and welding speed

The product I x v was found to have a significant effect on dilution. The results obtained for 60, 90 and 120° V grooves are shown on Figs. 89, 90 and 91 for Ar/5%CO_2 and He_1 gas mixtures.

The higher possible values of dilution were obtained for bead-on-plate deposits. As the V groove angle decreases the values of dilution (maintaining all the other parameters constant) decreases too. This trend is more significant for the differences observed between the higher angles, i.e. bead-on-plate to 120°and 120°to 90°.

CHAPTER 7 - THEORETICAL CONSIDERATIONS

CHAPTER 7 - THEORETICAL CONSIDERATIONS

7.1 - DEPOSITION CHARACTERISTICS

7.1.1 - Introduction

The Gas Metal Arc Welding process is characterized by a consumeble electrode burning under a gas shield. The electrode, heated by electrical energy, melts at the tip in the form of droplets that travel, through the electric arc, to the weld pool. The deposition characteristics related mainly with size and speed of the droplets strongly influence these performances. The heat developed at the electrode tip and the forces acting on the droplet are the two major aspects influencing these characteristics.

7.1.2 - Heat balance at the electrode tip

The total power that contributes to electrode heating comes from two main sources: Joule or resistance heating generated by the passage of electric current through the wire and arc heating. The flow process is described by the melting rate (W) and the drope temperature (T_d), which are determined by the heat generated in the wire and the heat flow through it.

The heat supplied to the wire by the Joule effect depends on the resistance ($\dot{R}$) of the wire extension which is related with current, stick-out and wire diameter and can be calculated by:

$$H_r = I^2 \dot{R}$$

Previous work (ref. 61) shows that the resistance heating developed in the solid part of the wire is not sufficient to raise the temperature of material from room temperature to the melting point and then to melt it. Consequently, there must be a flow of heat from the anode spot to the solid through the liquid tip.

Usually in GMAW, the wire is positive with respect to the work piece. The energy gained from the arc at the anode is supplied by electron absorption and is given approximately by.

$$H_a = \pm \left(V_a + \Phi + \frac{5}{2} \frac{KT}{e}\right) I \qquad (60)$$

It should be noted that the electron thermal flux of power involves a factor of 5/2 and not 3/2 as normally used. This point has been made previously by J. Waszink (private communication) and steems from the manner in which the quasi-Maxwellian distribution of electron energy is averaged (ref. 104) giving a result different from the 3/2 random flux factor.

These quantities do not appear to vary much with current so that approximately

$$H_a = \text{constant} \times I \qquad (61)$$

Several values for this constant have been presented by various authors (ref. 62) varying from 5.3 to 6.38 V.

In the present work, energy sources of heat passing to the anode from the arc, heat conduction and radiation from the hot gas, energy from chemical reactions, neutral and excited atoms striking the anode and surface recombination of dissociated gas were neglected.

The heat energy generated as stated above is then consumed on wire melting, super heating the liquid metal and vapourisation. These aspects are governed by the following equations.

The heat consumed by the wire anode ($\dot{H}_a$) is at the rate

$$H_a = \pi a^2 W_a \rho \{H_m + (T_d - T_m) C_p\} \qquad (62)$$

and the heat consumed ($\dot{H}_r$) in the stick-out l (part of the electrode beyond the contact tube) is

$$\dot{H}_r = \frac{1}{\pi a^2 \sigma} = \pi a^2 W_r \rho \{H_m + C (T_d - T_m)\} \qquad (63)$$

The heat consumed to super-heat the droplet (ΔH) is given by

$$\Delta H = \dot{m} C_p (T_d - T_m) \qquad (64)$$

the heat consumed on vapourization is

$$\dot{H} = H_v \cdot m_v \qquad (65)$$

In this work all other amounts of heat consumed (radiation from the hot spots on the anode surface, heat conducted or convected away to the surrounding gas) were neglected.

From what has been presented above it is possible to write a heat balance equation:

$$\dot{H}_a + \dot{H}_r = \dot{H}_a + \dot{H}_r + \dot{H} + \dot{H}$$

which governs heat input and heat consumed at the electrode tip during welding.

The way this balance influences deposition characteristics is difficult to quantify but in order to have "good" deposition characteristics this heat balance must provide an equilibrium between wire feed speed (influenced by $\dot{H}_r$) and melting rate (influenced by $\dot{H}_a$ and $\dot{H}_r$).

7.1.3 - Forces acting on the wire tip and liquid metal

In GMAW, the dominant forces acting on the wire tip and molten metal during the metal transfer are electromagnetic force and the surface tension force.

The other forces, gravity, forces due to the vapourization and chemical reactions, drag force and forces due to gas eruptions are much less important.

In the following sections, expressions proposed by several authors to calculate these forces are presented.

7.1.3.1.- Electromagnetic force

The electromagnetic force is one of the most important influencing metal transfer and its changes can be critical in determining the mode of tranfer.

For a solid cylinder with constant current density across the section the magnetic force is given by

$$F_p = \frac{\mu_o I j}{4\pi} \left(1 - \frac{\dot{r}^2}{\dot{R}^2}\right) \qquad (66)$$

where μ_o is $- 4\pi . 10^{-7}$ and $\dot{r}$ is radial coordinate.

This force acting on a conductor whose input radius is R_1 (the radius of interface between solid wire and liquid drop) and output radius is R_2 (radius of the effective conductive cross section)

$$F_p = \frac{\mu_o I^2}{4\pi} \log \frac{R_2}{R_1} \qquad (67)$$

for a rigid body and is not applicable to the case of a liquid drop

where the magnetic force is transmitted by pressure and inertia forces.

7.1.3.2 - Surface tension

The weight of the maximum drop supported by surface tension is given by

$$F_\sigma = 2 \pi b \sigma \Psi \left(\frac{b}{c}\right) \qquad (68)$$

in which the function Ψ takes values between 0.6 and 1.0 and c is capillarity constant $c^2 = \frac{2\sigma}{\rho_m g}$.

7.1.3.3 - Gravity force

The force due to gravity is calculated by

$$F_g = m g \qquad (69)$$

7.1.3.4 - Forces due to vapourization and chemical reactions

Back thrust from vapour jets emitted at places of strong local heating can give rise to a drop repelling force.

For a hemispehrical tip (MIG welding) this force is given by

$$F_E = \frac{Q_o^2 I^2}{8\pi \rho_m R^2} \qquad (70)$$

where Q_o is mass flux due to evaporation per ampere and has the value of $0.02\ I^2$ dynes (with I in amperes).

7.1.3.5 - Drag force

The force exerted on a spherical body in a flowing gas in the direction of the flow can be written as

$$F_d = C_d \frac{\pi \bar{V}^2 \rho_g}{2} R_D^2 \qquad (71)$$

where $\bar{V}$ is flow velocity, R_D is the radius of the sphere, and C_d is a function of the Reynolds'number (R_e) and ρ_g is the density of the flowing medium.

$$R_e = \frac{R_D \bar{V}}{\mu} \qquad (72)$$

The values of R_e above 1.00 (which is the case of this work) the relationwhip between the drag coefficient and the Reynolds'number is given by Fig. 92.

7.1.3.6 - Gas eruptions

It appears from high speed cine films that development and eruption of gas from the electrode affect metal transfer. The main reaction involved is the burn-off of carbon according to

$$FeO + C \rightleftarrows Fe + CO\uparrow$$

In fact, the metallurgical situation is much more complicated, as several oxidation and deoxidation processes play a role, the course of which depend on the concentrations of the diverse components and/or temperature.
From what was been presented above it is obvious that the influence of the several forces on deposition characteristics is dificult or even impossible to quantify.

7.2 - FUSION CHARACTERISTICS

7.2.1 - Introduction

The applicability of GMA welding is often limited by occurrence of various defects, like undercutting, lack of fusion, etc. The correct understanding of metal flow in the weld pool and the formation of the weld bead, with the object of eliminating these defects is of major importance for the developments of this welding process. However, the physical behaviour of the weld pool may limit the range of welding parameters over which the process is operable.

It is in the area where physical phenomena have a direct influence on welding technology that a greater undestanding of these phenomena could improve the quality of joints and the applicability of GMA welding.

7.2.2 - Flow in the weld pool

Many works have been published on heat flow in the weld pool which were widely discussed on chapter 2.

According to various studies undertaken (ref. 64), the forces that generate flow in the weld pool seem to be as follows:

- the axi-symmetrical J x B force due to a current source at the centre of the weld pool. This would generate toroidal flow, but such flow has only been observed in simulated weld pools in a static container;

- asymmetric electromagnetic forces due to current flow outside the weld pool;

- drag forces due to the plasma jet;

- the stagnation pressure due to the plasma jet or the inertia force due to the impingement of metal drops. This causes a crater or depression in the weld pool surface and metal that is melted at the front of the weld pool is accelerated as it flows through the restricted cross--section around the crater.

Flow implies, within the weld pool, heat will flow in part by convection. Nevertheless, this does not invalidate the conclusion that conduction plays the most important role in weld bead formation, if the weld pool shape is not too far from the predicted assuming heat flow by conduction.

Equations of heat condection were used in most of the works (ref. 80, 81, 86, 89, 99, 102) in order to study heat conditions during welding. These approaches were based on simplifying assumptions, e.g. neglecting radiation and convection, neglecting the variation of physical properties with temperature, etc, nevertheless the results obtained are usually in good agreement with experimental observations. The small deviations from the idealised models sometimes observed, could possibly be explained by convection effects (ref. 102).

7.2.3 - Weld pool temperature

A point source of heat is infinitely intense and defined by the energy it transfers to the weld pool per unit time. This flux of heat q (cal/sec) may be stated in terms of arc volt-amperes, VI and a coefficient of arc efficiency (ref. 99):

$$\eta = \left(\frac{4.18\,q}{V\ I}\right) 100\% \qquad (75)$$

The generalization of this point source equation was undertaken by Christensen (ref. 102) who defined a non-dimensional parameter (n) in order to calculate the average weld pool temperature as

$$n = \frac{qv}{4\ \pi\ \rho^2\ C_p\ \gamma\ (T_c - T_o)} \qquad (76)$$

The average weld pool temperature for GMAW of mild steel is shown in Fig. 93 (ref. 64).

This expression allows the calculation of the approximate temperature on the weld pool, however the phenomena occuring in the weld pool are rather complex and not possible to be accurately considered in a simple analysis.

7.2.4 - Depth of penetration, width and reinforcement of fused zone

It is necessary in arc welding that a molten region of uniform depth and cross-section be formed in order to avoid fusion problems. It was considered that such a condition could only be maintained if a crater or depression was formed in the surface to be welded (ref. 66). In fact, results show that , e.g. with a 3 mm electrode, penetration was obtained in GMAW at 200 - 250 A, which is the current level at which the arc jet would be expected to form a depression, this always occur here due to the high values of pulse current.

The analysis of penetration profile is generally non-quantitative but some effort has been directed to the calculation of reinforcement bead profiles (ref. 64). An equation to calculate the cross-sectional profile has been presented based on the assumption that results of two dimensional and three dimensional analysis are quite close:

$$\sigma = -\ \frac{1}{\{a\ (1 + b)\}^{1/2}}\{(1 + b)/E\ (\phi,\ S) - E\ (\pi/2,\ S) - b\ F\ (\phi,\ S) -$$

$$- F\ (\pi/2,\ S) \qquad (77)$$

$$a = \frac{\rho_m g}{2} \qquad b = 1 - \frac{\sigma}{2 \rho_m g R_o^2} \qquad s = \left(\frac{2}{1 + b}\right)^{1/2}$$

$$K = \frac{\sigma}{\rho_m g R_o} \qquad \cos \Phi = \{a (y^2 - 2Ky)/2\}^{1/2}$$

where F (Φ, S) is the elliptic integral of the first kind, E (Φ, S) is the elliptic integral of second kind and K is the Boltzmann's constant.

This equation is quite complicated thus its manipulation lacks of practical use. Christensen's (ref. 102) non dimensional parameter which has been used by Edgar and Tsai (ref. 98) is possibly the most significant contribution in this field, nevertheless its application is also quite complicated.

From the points presented above on the existing theory on fusion characteristics it is obvious that simple model modelling with practical application in this field is lacking.

CHAPTER 8 - THEORETICAL APPROACH AND SIGNIFICANCE OF EXPERIMENTAL RESULTS

CHAPTER 8 - THEORETICAL APPROACH AND SIGNIFICANCE OF EXPERIMENTAL RESULTS

8.1 - DEPOSITION CHARACTERISTICS

8.1.1 - Introduction

The central aim of this work was to examine the effects and interactions for some of the possible variables in pulsed GMAW of mild steel.

Emphasis has been placed on how wire size and shielding gas composition affect deposition characteristics. Other variables included in this study were electrical stick-out and mean current where all the experiments have involved a bead-on-plate welding.

8.1.2 - Burn-off rate

The burn-off rate per ampere can be divided in two parts, one due to arc heating (W_a) and the other due to resistance heating (W_r). The theoretical equation governing these two aspects are:

$$W_a = \pi r^2 v_a \rho_m = \frac{\Phi + V_a + \frac{5}{2}\frac{KT}{e}}{\{H_m + (T_d - T_m) C_p\}} \qquad (78)$$

where $\frac{5}{2}\frac{KT}{e}$ is the thermal energy of electrons and v_a is melting rate due to anode heating

$$W_r = \Psi / \pi r^2 \{ H_m + (T_d - T_m) C_p \} \qquad (79)$$

The values of α and β (theoretical constants related with arc heating and resistive heating respectively) can be calculated. For mild steel, we have (ref. 79)

$H_m = 1308 \times 10^6$ J/Kg

$T_d = 2400^{o}$ C

$Tm = 1537^{o}$ C

$C_p = 8 \times 10^2$ J/Kg K

$\Psi = 125 \times 10^{-5}$ ohm.m

making

$$(V_a + \Phi + \frac{5}{2}\frac{KT}{e}) = 5.5 \text{ V}$$

$$\alpha = 2.7 \times 10^{-6} \text{Kg/A.S}$$

$$= 0.31 \text{ mm/A.S}$$

The experimental value of α found in this work is 0.27 mm/A.s for identical conditions.

A similar approach can be undertaken with β and the results obtained are

$$\beta = 6.4 \times 10^{-5} \text{ A}^{-2} \text{ s}^{-1}$$

which is close to measured values (5.93×10^{-5} A^{-2} s^{-1}).

Since the agreements are quite good, the expression to calculate W used in this work is

$$W = \alpha \bar{I} + \beta \ell \bar{I}^2 \qquad (80)$$

for D.C. current, where α and β are the constants describing arc and resistive heating effects respectively.

The average burn-off rate, for a square wave pulsed current, is then (see section 6.1.2):

$$W = \alpha(I_p t_p + I_b t_b) + \beta \ell F (I_p^2 t_p + I_b^2 t_b) \qquad (81)$$

In this work it was assumed that ohmic heating during the background duration is negligible compared to that during the peak (i.e. $I_p^2 t_p >> I_b^2 t_b$).

For the parameter used here (see Table 12) this approach is valid, e.g. not more than 15% of the ohmic heat is generated during the background (this value is 5% for $\bar{I}$ = 100 A and 12% for $\bar{I}$ = 200 A).

W then becomes:

$$W \simeq \alpha \bar{I} + \beta \ell \bar{I}_p^2 t_p F \qquad (82)$$

The factor $I_p^2 t_p$ (defined here as D) has previously been identified by a number of workers (ref.23,25)as the criterion determining one droplet per pulse conditions (a detachment parameter).

Most of this work was undertaken with fixed I_p and t_p, however D may of course be constant even when I_p and t_p vary. The expression for W now reduces to

$$W \simeq \alpha \bar{I} + \beta \ell DF \qquad (83)$$

Clearly if F is proportional to W or $\bar{I}$ then the burn-off rate will be linearly related to mean current for a given electrode extension and detachment parameter. This gives the explanation for the observed burn-off behaviour in pulsed GMAW (see Fig.38). Extrapolating the data shown in Figs. 41, 42 and 43 to zero extension ($\ell = 0$) allows α to be identified. β can also be calculated from the slope of these lines. Results are given in Tables 13 to 15 for 1.0, 1.2 and 1.6 mm wire diameters respectively.

Results for the 1.2 mm wire are in broad agreement with values previously identified from steady current experiments, e.g. $\alpha \simeq 0.3$ mm/As and $\beta \simeq 5 \times 10^{-5}$ A^{-2}/s (ref. 19). Values for other diameters are expected (see ref. 63) to vary as 1/A for α and $1/A^2$ for β, i.e. the products αA and βA^2 should be largely insensitive to wire diameter. Data given above is in broad agreement with this interpretation as may be seen from Table 16.

This data, combined with equation (82) may be used to estimate many aspects of deposition behaviour in pulsed GMAW.

For the present experiments expression 82 predicts that deposition rate ($\dot{m}$) (for 1.2 mm wire diameter) is given by

$$\dot{m} = 0.89\ (1 + 0.052\ \ell)\ \text{Kg/hr/100 A} \qquad (84)$$

(with ℓ in mm). Taking $\ell = 15$ mm gives

$$\dot{m} = 1.6\ \text{Kg/hr/100 A}$$

This is in excellent agreement with the data in Fig. 40

8.1.3 - Droplet volume

Droplet volume is one of the major factors influencing deposition characteristics.

According to ref. 43 the best transfer characteristics are associated with droplets with the same diameter as the wire detaching in the end of peak duration. The droplet volume (Φ) can be calculated by means of the following expression

$$\Phi = \frac{W.A}{F} \qquad (85)$$

In order to maintain a nominal droplet size, it is desirable to have F proportional to W. After substituting W from equation (83), Φ is identified as

$$\Phi = \alpha\ A\ (\bar{I}/F) + \beta\ \ell\ DA \qquad (86)$$

This gives a physical interpretation of why it is useful to adopt a "rule of thumb" frequency per amp relationship, i.e. by fixing $\bar{I}/F$ the drop size is fixed for a given stick-out, wire size and detechment parameter for any wire feed speed.

It should also be noticed that droplet volume increases with stick-out, an effect also observed in steady current welding (ref. 106). Equation (86) may be re-arranged to give $F/\bar{I}$, i.e.

$$F/\bar{I} = \frac{\alpha.A}{\Phi - \beta\ \ell\ DA} \qquad (87)$$

Experimental results indicate that the products $\alpha.A$ and $\beta.A^2$ are independent of wire diameter. It then follows that $F/\bar{I}$ should be increased with decreasing wire diameter as found experimentally.

The ratio of resistance heating to arc heating in pulsed GMAW is given by

$$\frac{\beta\ell\ DF}{\alpha\bar{I}} \quad \text{or substituting for } F/\bar{I} \text{ gives } \quad \frac{\beta\ell\ DA}{\Phi - \beta\ \ell\ DA} \qquad (88)$$

For values of D and F/I used here this ratio is in the range of 60% to 80% with a stick-out of 15mm and any wire diameter. The reason for this strong influence is associated with the high peak current levels adopted in pulsed GMAW (these produce squared effect on ohmic heating).

Expressions introduced above may be used to identify a new burn-off relationship for pulsed GMAW :

$$W = \bar{\alpha}\ \bar{I}$$

with

$$\bar{\alpha} = \frac{\alpha}{1 - \frac{\beta\ \ell\ AD}{\Phi}} \qquad (89)$$

Here $\bar{\alpha}$ is a modified burn-off factor which may or may not be constant as $\bar{I}$ is changed, depending on how D, Φ and ℓ are chosen.

In these experiments, ℓ , Φ and D were fixed as F was varied, hence linearity is expected (see Fig. 38).

The prediction of droplet volume (see eq. 86) is 1.125 mm^3 (drop diameter 1.29 mm) for the 1.2 mm wire investigated.

One other point worthy of note is that equation (89) places fundamental limitations on the combination of possible parameters in pulsed GMAW, i.e. as $\bar{\alpha}$ must, of course, be positive then

$$\Phi > \beta\ \ell\ AD \qquad (90)$$

The physical significance of this relationship is associated with resistive heating supplying most of the heat required to melt the wire and in effect, prohibiting further increases in wire extension, i.e. arbitrary choices of Φ, A and D then define the maximum value of ℓ.

8.1.4 - Droplet momentum

In order to have good control of metal transfer characteristics welding parameters are chosen to give one droplet detached in the edge of each pulse with a diameter equal to wire diameter. The place of detachment of the droplet has implications in its acceleration across the arc and impact on the pool. To minimize spatter, droplets are best transferred across the arc during the background period. Thus the preferred poirt of detachment is thoughtto be on the trailing edge of a pulse.

The acceleration a, of droplets due to the plasma stream in the arc may be obtained by:

$$a = \frac{3}{8} \frac{v_s^2 \rho_g}{R_d \rho_m} Cd \qquad (91)$$

where ρ_m, R_d and Cd have the usual meaning, ρ_g is the density of the flowing medium and v_s is the velocity of the fluid stream.

To compare the acceleration of the droplet when it crosses the arc under peak and background conditions used in this work, the values used (ref. 64) were:

$\rho_g = 6 \times 10^{-2}$ Kg/m^3 (density of the flowing medium)

$\rho_m = 6.5 \times 10^3$ Kg/m^3

$\nu = 3.4 \times 10^{-3}$ m^2/s

The value of the axial plasma velocity (v_s) was calculated using Fig. 94 but as the velocity falls off rapidly in a radial direction the mean effective velocity assumed (V_{eff}) was half of the axial value (ref. 64). Reynold's number was calculated using the expression

$$R_e = \frac{R_d v_{eff}}{\nu} \qquad (92)$$

and the drag coefficient C_d was taken from Fig. 92.

The values obtained are shown in Table 17, where v_d is the droplet velocity when it reaches the weld pool (the initial velocity was considered 1.5 m/s (see ref. 109).

The force (F) acting on the drop is given by:

$$F = \frac{\pi}{2} v_{eff}^2 \rho_g R_d^2 C_d \qquad (93)$$

and the droplet momentum (P) by:

$$P = mv_d \qquad (94)$$

Calculations gave much higher values of F and P for the detachments occuring during the peak ($F = 777.1 \times 10^{-6}$ Kg, $P = 14.7 \times 10^{-6}$ Kg.m/s) than during background ($F = 21.2 \times 10^{-6}$ Kg, $P = 7.8 \times 10^{-6}$ Kg.m/s) which implies that metal transferring during the peak lead to more instability and spatter than if it occurs during background conditions, this is in agreement with experimental results (ref. 43).

8.2 - FUSION CHARACTERISTICS

8.2.1 - Introduction

GMAW has potential uses ranging from thin sheet to heavy section narrow gap welding, and also finds application in surfacing. This range of applications leads to the requirements for a general understanding of how process parameters affect fusion behaviour. In this section, emphasis is placed on understanding dilution behaviour as this is a good indicator of general fusion characteristics. Simple models of melting and penetration behaviour are developed and predictions compared with experimental results.

8.2.2 - Plate fusion area and dilution

8.2.2.1 - Development of model

A simple starting point is to consider plate melting as the result of heat transfer by thermal conduction from a moving point source of heat (q) (see Fig. 95).

From ref. 33, 79

$$q \approx \pi \, d_A K \, T \left(1 + \frac{v \, d_A}{5\rho}\right) \qquad (95)$$

where d_A is the equivalent diameter of the fused plate region as defined from the fused plate area by:

$$A_F = \frac{\pi\left(\frac{d_A}{2}\right)^2}{2} \qquad (96)$$

A heat conduction model, first used by Wells (ref. 79) based on the assumptions that radiaction and convection losses are neglected, is developed for determining fusion characteristics in pulsed GMAW. By adopting this approach bead geometric factors are smoothed out.

Eliminating "d_A"from equations (95) and (96) gives:

$$A_F = \pi \left(\frac{5\rho}{4v}\right)^2 . \left\{1 + \left(\frac{2q\,v}{5\,\pi\,K\,T\,\rho}\right) - \sqrt{1 + 2\left(\frac{2q\,v}{5\,\pi\,K\,T\,\rho}\right)}\right\} \quad (97)$$

The point source of heat q appearing above may be written as $I.V_E$ where V_E is an equivalent voltage associated with heat transfer to the plate and plate melting.

The deposited bead area (A_D) is given by

$$A_D = \frac{W}{v} . A \quad (98)$$

"A" is the wire cross-sectional area and W the burn-off rate has the form

$$W = \bar{\alpha}\,\bar{I} \quad (99)$$

where $\bar{\alpha}$ is a burn-off factor dependent on pulse parameters (see section 8.1.3).

Dilution behaviour is now readily examined since by definition

$$\delta = \frac{A_F}{A_D + A_F} \quad (100)$$

and equations (95) to (100) give:

$$\frac{A_F}{A_D} = \theta_2 \left(\frac{1 + \theta_1 M - \sqrt{1 + 2\,\theta_1 M}}{M}\right) \quad (101)$$

with $M = \bar{I}.v$

$$\theta_1 = \frac{2\,V_E}{5\,\pi\,K\,T\,\rho}, \qquad \theta_2 = \frac{\pi}{\bar{\alpha}\,A}\left(\frac{5\rho}{4}\right)^2 \quad (102, 103)$$

Equations (100) and (101) suggest that, for given material factors (plate, wire and gas), δ is a function of only M, i.e. $\bar{I}.v$

The form of the experimental $\delta(M)$ curve given in section 6.2.5.6

is assymetric in nature tending towards $\delta \sim 50\%$ at very high values of M. Such behaviour is also predicted by equation (101) i.e. for $\theta_1 M >> 1$ equation (101) gives:

$$\frac{A_F}{A_D} = \theta_1 \cdot \theta_2 \qquad (104)$$

The maximum value of δ (λ_1 say) is therefore determined by $\theta_1 \cdot \theta_2$ such that

$$\lambda_1 = \frac{\theta_1 \theta_2}{1 + \theta_1 \theta_2} \qquad (105)$$

Equations (100) and (101) may also be used to predict the initial slope of the δ (M) curve and hence characterise δ (M) behaviour. By differentiating equation (100) and using equation (101) it can be shown that the initial slope (λ_2 say) is

$$\lambda_2 = \frac{d\delta}{dM} \quad (M = 0) = \frac{\theta_1^2 \theta_2}{2} \qquad (106)$$

where λ_1 and λ_2 are illustrated in Fig.96.

The consistency of the model presented here may be checked by estimating values of θ_1 and θ_2 from thermal properties and process considerations and subsequently comparing values of λ_1 and λ_2 so obtained with those found experimentally. However this involves assumptions concerning V_E and so the converse approach is adopted. Measured values of λ_1 and λ_2 (taken from Fig. 97) are used to determine θ_1 and θ_2 and hence V_E and α .

Equations (105) and (106) give:

$$\theta_1 = \frac{2 \lambda_2 (1 - \lambda_1)}{\lambda_1} \qquad (107)$$

and

$$\theta_2 = \frac{\lambda_1^2}{2 \lambda_2 (1 - \lambda_1)^2} \qquad (108)$$

The plate diffusivity is now identified from θ_2 (i.e. see equation (103)

as

$$\rho = \frac{4\,\lambda_1}{5\,(1-\lambda_1)}\sqrt{\frac{a\,\bar{\alpha}}{2\,\lambda_2\,\pi}} \qquad (109)$$

and effective plate heating voltage is, by Θ_1,

$$V_E = 2\,K\,T\,(2\,\pi\,a\,\bar{\alpha}\,\lambda_2)^{1/2} \qquad (110)$$

where $\bar{\alpha} = 4.9 \times 10^{-5}\,ms^{-1}\,A^{-1}$ has been used).
λ_1 and λ_2 are identified from Fig. 97

$$\lambda_1 \approx 0.5$$

$$\lambda_2 \approx 1.12 \times 10^{-3}\,A^{-1}.\,mm^{-1}/s$$

The plate diffusivity (ρ) can now be calculated:

$$\rho = 7.1\ mm^2/s$$

Thermodynamic data (ref. 107) give $\rho \approx 5\text{-}6$ mm/s for a characteristic temperature between that of the plate and melting point and so this estimate is reasonable. The value of K corresponding to this value of ρ is $K \approx 30$ W/m K (ref. 107) V_E can now be estimated and it is found that

$$V_E \approx 6 \text{ volts.}$$

Measured arc voltages are typically 22 - 30 V for the present combination of process parameters, which implies that only 20 - 27% of the total process power contributes to plate heating and melting. The process efficiency is, of course, much higher and measured here as 60 - - 70%. However, such a result is not unreasonable as typically only 3 - 8 % of the total process power is required to melt observed plate fusion areas.

8.2.2.2 - Comparison of experimental and predicted values

8.2.2.2.1 - Plate fusion area

A powerful test of the model is to estimate plate fusion areas since deposition characteristics can be accurately predicted.

Equations (98), (99.) and (101) then give:

$$A_F\ v^2 = a\ \bar{\alpha}\ \theta_1\ (1 + \theta\ M - \sqrt{1 + 2\ \theta_1\ M}) \qquad (111)$$

Data presented in section 6.2.4 is shown in Fig.98 in the form suggested by equation (111), i.e. $A_F\ v^2$ against $M = \bar{I}.v$.

Predictions of A_F are also presented in section 6.2.4.6, Fig.78 as a function of welding speed for a range of arc currents. It can be seen from these graphs that reasonable correlation exists between experiment and theory although the model is, of course, unable to account for the dip in fusion area.

8.2.2.2.2 - Dilution

To apply equations (100) and (101) to the prediction of fusion characteristics θ_1 and θ_2 must be know. θ_1 and θ_2 defined by the values of λ_1 and λ_2 obtained above as (from equations 107 and 108):

$$\theta_1 = 2.24 \times 10^{-3}\ A^{-1}\ mm^{-1}\ s$$

$$\theta_2 = 4.46 \times 10^{2}\ A\ .\ mm\ .\ s^{-1}\ s$$

where

$$\theta_1\ .\ \theta_2 = 1$$

Predicted and experimental dilutions using these values are shown in Table 18. This level of agreement is regarded as satisfactory for the present type of model.

Experimental data represented in the manner suggested by equations (100) and (101) (δ against $\bar{I}.v$) is shown in Fig.99 for a 1.2 mm diameter wire burning in an Ar/5% CO_2 shield. The general form of the curve is such that saturation behaviour occurs at a high $\bar{I}.v$ value where δ is near 50%. To check this trend (observed for $\bar{I}.v < 2000$ A.mm/s) a further test was conducted with a 400 A DC arc at 8 mm/s i.e. $\bar{I}.v = 3200$ A.mm/s. The result achieved was $\delta = 56\%$ (with $A_p = 28$ mm² and $A_F = 36$ mm²) in line with the previously identified trend (and predicted by this theory).

Experiments with other wire diameter and gas mixes (see Fig. 99) show similar behaviour where the saturation dilution increases slightly with increasing wire diameter and is greater in a helium rich shield than in Ar/5% CO_2.

Fusion characteristics predicted above indicate that the values of and V_E used, give useful representations of behaviour.

Results also indicate that improved agreement with experiment is achievable by using a slightly higher value of V_E than 6V. This is possibly a result of using thermodynamic data to identify K which may have a higher "effective value" due to weld pool convection.

8.2.3 - Penetration

8.2.3.1 - Development of model

Consider the forces exerted by arc and mass transfer to the pool

$$F_{(arc)} \approx \frac{\mu_o I^2}{4\pi} \chi \qquad (112)$$

where χ is a geometric factor of order unity (ref. 108) and μ_o is $4\pi \times 10^{-7}$ henry/m

$$F_{drop} \approx m \cdot v_d \cdot F \qquad (113)$$

v_d has two components: one associated with initial transfer from the wire and the other with acceleration across the arc. In pulsed current welding the initial velocity will be a function of peak current level while the final velocity will depend on arc flow conditions during droplet transit time. In the present experiments droplets were detached, one per pulse, at the end of the peak duration. Transfer occurred entirely within the following background period, i.e. taking an initial velocity of 1.5 m/s (ref. 109) and an arc length of 5 mm gives a transit time of 2-5 ms. This is much shorter than the duration of the background period. The final velocity is therefore expected to be little different from the initial velocity and largely determined by the peak current (ref. 109). For the

present experiments droplet mass and peak current were fixed while frequency was increased in direct proportion to mean current. F (drop) is therefore proportional to mean current, i.e.

$$F(\text{drop}) = \rho_m A v_d \bar{\alpha} \bar{I} \qquad (114)$$

where the usual notation has been used.

For pulsed current welding, arc force is associated with the mean value of I^2 . To a first approximation the mean value of I^2 is $I_p^2 t_p F$ since $I_p^2 t_p >> I_b^2 t_b$. Using the notation $D = I_p^2 t_p$ (see section 8.1) gives

$$F_{(arc)} = \frac{\mu_o D \chi F}{4\pi} \qquad (115)$$

Hence the arc force is also proportional to pulse frequency and therefore, mean current.

Estimates of these forces are obtained for a 1.2 mm wire diameter with $v_d \approx 2$ m/s, $\chi \approx 2$, $I_p = 350$ A, $t_p = 4$ ms, $\bar{I}/F = 2$, $\bar{\alpha} = 4.9 \cdot 10^{-5}$ m/s A.

Then

$$F(\text{drop}) \sim 8.6 \cdot 10^{-7} \bar{I} \text{ (N)}$$

$$F(\text{arc}) \sim 4.9 \cdot 10^{-5} \bar{I} \text{ (N)}$$

total arc force is therefore about 50 times greater than the droplet force. However the axial pressures associated with these forces are of a markedly closer ratio. The pressure exerted by droplets is roughly

$$P(\text{drop}) \sim \frac{F_{drop}}{A} \approx 0.76 \bar{I} \text{ (N/m}^2\text{)} \qquad (116)$$

A number of related approaches to estimating arc pressures exist, e.g. examining gas flow stagnation pressure at the pool centre, considering the average arc force. The latter case is used here where the radial distribution of pressure is assumed to be a similar form as the current distribution (see ref. 108).

Instantaneous arc pressure over the region of droplet entry is approximately:

$$P\ (arc) \approx F\ (arc)\ .\ \frac{j}{I} \qquad (117)$$

Experiments with gas tungsten arcs indicate that j is largely insensitive to arc current having a value near 10 A/mm^2. This result is used in calculations made here. The average arc pressure (average over a pulse cycle) is then

$$P\ (arc) \approx \left(\frac{\mu_o I^2 \chi}{4\pi} \frac{j}{I} \right)_{ave} = \frac{\mu_o \bar{I} \chi j}{4\pi} \qquad (118)$$

or

$$P\ (arc) \approx 2\ \bar{I}\ N/m^2 \qquad (119)$$

The precise balance of arc and droplet pressures is difficult to estimate closely due largely to uncertainties in j. Despite this, the above discussion indicates that arc effects are certainly not negligible (as previously indicated, ref. 97) and probably dominant.

The head (h) of liquid capable of being sustained by this total pressure is (neglecting surface tension) given by:

$$2.76\ \bar{I} \gtrsim \rho_m\ g\ h \qquad (120)$$

where h(max) is 4.1 mm at 100 A and 8.2 mm at I = 200 A.

Clearly if the arc is to act on the plate then h must exceed reinforcement height, i.e. the arc pressure must be capable of displacing the deposited mass. This in turn is influenced by welding speed. For a semi-circular deposit the critical speed at which arc pressure is just capable of displacing deposited mass, and there by allowing the arc to act on base metal, is

$$v_c \approx \frac{W\ .\ a}{A_D} = \frac{2\ W\ .\ a}{\pi\ h^2} = \frac{2\ W\ .\ a\ (\rho_m g)^2}{\pi\ P^2} \qquad (121)$$

where P is the total pressure (arc and drop)

$$v_c = \frac{2\ \bar{\alpha}\ a(\rho_m g)^2\ \bar{I}}{(2.76\ \bar{I})^2\ \pi} \qquad (122)$$

or

$$v_c = \frac{217}{\bar{I}} \quad (mm/s) \qquad (123)$$

The minimum speed at which an arc acts directly on to base plate material is therefore 3 mm/s at 70 A and 0.7 mm/s at 250 A.

At speeds greater than v_c a pool depression is expected, and hence finger penetration is likely to occur (i.e. the position of the equivalent point source of arc heating is then below the plate surface).

The predictions of this section are, of course, very approximate and incapable of directly predicting penetration behaviour. Instead emphasis has been placed on illuminating the mechanism of penetration in pulsed current GMAW and indicating how this may be manipulated.

The above expressions indicate that mean current is the dominant factor in controlling penetration (at a given welding speed), i.e. the structure of mean current is of little consequence (except with regard to the total arc force).

8.2.3.2 - Comparison of experimental and predicted values

The results obtained with different peak parameters which lead to changes in droplet volume, place and frequency of detachment and so significant changes in droplet momentum and in the value of the forces acting on the droplet when it reaches the weld pool, gave no significant changes in penetration and shape of the bead.

The region of v = 1 to 3 mm/s is in agreement with observed maxima in penetration and plate fusion area (for the current range examined here, 70-250 A). Both these results lend further weight to the hypothesis that plate melting is largely due to direct arc action on the plate.

8.2.4 - Bead shape

The quantitative definition of the fusion area shape is a difficult task and this is certainly true for the results obtained (see Fig. 66) since all the shapes look very alike.

Depth and width of the bead are, of course, not enough to define it; in this work the definition of this shape was done by means of wetting angle, fusion angle and a shape factor defined as follows.

For the perfect bowl penetration (semi-circle) which is the "best" possible plate fusion area shape, the relation X between fusion area and the area of a circumscript rectangle is given by:

$$X = \frac{A_F}{w \times p} = \frac{1}{2} \frac{\pi p^2}{2 \cdot D_r \cdot D_r} = \frac{\pi}{4} \qquad (124)$$

where D_r is the radius of the semi-circle (which is equal to penetration p) and the smaller side of the semi-circunscript rectangle.

The factor γ_s given by the following expression:

$$\gamma_s = \frac{A_F}{w \times p} \quad \frac{4}{\pi} \qquad (125)$$

will give a quantitative approach of how close the shapes obtained are to the best possible shape (perfect semi-circle with $w = 2 D_r$) for a given penetration depth, i.e. as γ_s decreases the tendency for a "finger" penetration shape increases.

From the results shown in section 6.2.3 it is possible to conclude that bead shape factor hardly changes for some of the conditions examined due to the"finger" penetration shape obtained in those cases. Nevertheless the correlation between wetting angle, fusion angle and bead shape factor gives an useful indication on bead shape.

8.2.5 - Generalised representation of fusion characteristics

Aspects of fusion characteristics have been presented and modelled in section 8.2.2 and 8.2.3. These deal with the influence of mean current and welding speed on deposition rate, plate fusion area, dilution and bead wetting angle. With these results it is possible to describe the current and speed dependence of all the characteristics on just one graph.

Such a graph is constructed by plotting lines of constant dilution (I . v = constant) on a chart of mean current against welding speed. Lines of constant deposited bead size (I/v = constant) are superimposed on this chart. Further, the dominant role of welding speed on bead wetting angle (see Fig.100) allows the speed to define wetting angle to within $\pm 5^{o}$ while the current axis defines deposition rate (1.55 Kg/hr/100 A for the conditions below). A chart of this form is presented for a 1.2 mm

wire in an Ar/5% CO_2 shield with a 15 mm electrode extension (see Fig.100). The lines of constant I.v may also be interpreted in terms of heat input, deposition rate or bead size by means of simple scaling factors:

- deposited bead area A_D (mm^2) $= 0.55\ (\bar{I}/v)$
- plate fusion area A_F (mm^2) $= \dfrac{\delta \cdot A_D}{1 - \delta} = \dfrac{0.55 \cdot \delta \cdot (\bar{I}/v)}{1 - \delta}$

- heat input q (KJ/mm) $= V \cdot (\bar{I}/v)$
  (where V is arc voltage - typically 25 volts)
- deposited mass in (g/mm) $= 4.31 \cdot (\bar{I}/v)$
- deposited mass in (kg/hr/100 A) $= 1.55$

Additional information may be displayed on such charts by noting:

i) the lowest mean current correponding to satisfactory metal transfer is about 60 A;

ii) the maximum comfortable manual welding speed is generally near (4 mm/s);

iii) the largest pool size capable of being maintained in overhead welding is about 30 mm^2.

Clearly these limitations are dependent on a wide range of factors and may, under som circunstances require modification. They should however provide a starting point in the practical use of such a chart. Other factors can also be introduced although this is not done here, e.g. metallurgical implications of dilution on reheating, influence of heat input structure on solidification, etc.

Some immediate implications of Fig.100 are that:

1. a narrow range of possibilities exist for a reducing dilution below 10%,particularly if bead shape is important;
2. the maximum dilution achievable manually in all positions is less than about 35%;
3. automated welding has significant attractions for improving dilution characteristics by moving at higher speeds than are achievable manually.

One use of such a chart is to indicate the possibilities of achieving a desired bead/fusion characteristic, for example, 20% dilution with 1.2 KJ/mm. For a 25 V arc this gives $I/v \approx 50$ A.mm/s and from the chart $\bar{I} \approx 110$ A, $v \approx 2.2$ mm/s. The corresponding deposition rate, bead size and fusion area are 1.7 kg/hr, 28 mm^2 and 6-7 mm^2 respectively. The chart also indicates that this condition is probably "all-positional" with a wetting angle close to 70^o and penetration close to the maximum possible for this current. These conclusions are in good agreement with data previously introduced (see Figs. 38, 47, 53, 63, 78). If the required condition is not possible then consideration should be given to changing the wire size/gas composition and proceeding as above.

8.3 - STRUCTURE OF PLATE HEATING

8.3.1 - Introduction

Considerations in section 8.2.2 indicate that only 20 - 27% of the total process power is associated with raising the plate to melting temperature and then causing melting. Furthermore, typically only 3 - 8% of the arc power is required to melt the volume of metal corresponding to observed plate fusion. This later result is a simple statement of factual observation. However the former result is curious as clearly much more than 20 - 27% of the arc power is transferred, in one form or another to the plate. To gain a better understanding of the significance of this result calorimetric tests (see sections 8.5.4 and 8.6.3)were undertaken, thereby allowing a detailed energy balance to be conducted.

8.3.2 - Total heat transfer efficiency

Total heat transfer efficiency to the plate was measured by monitoring the temperature rise of a water calorimeter after quenching a welded sample. Pulse parameters previously introduced were used for these experiments. Results obtained are given in Tables 19 and 20.

Table 19 shows that the process efficiency is typically 60 - 70%. Combining these results with voltage data (Table 20) allows an "effective voltage" (V_{ET}) associated with total heat transfer to be obtained, i.e. $V_{ET} = \eta V$. These values are given in Table 21.

It can been seen that V_{ET} is largely insensitive to arc current and typically 15 volts in Ar/5% CO_2 and 22 Volts in Helishield 1. These values are much higher than the effective plate heating and melting voltage ($V_E \sim 6V$) found in section 8.2.2.

8.3.3 - Wire heating

In the present context it is also of interest to compare observed burn-off rate with those predicted by equation (83) (values of α and β being taken from Table 16). Results are given in Table 22 in the form $W/\bar{I}$ where experimental values have been averaged over $\bar{I}$.

The agreement is generally very good. This suggests that equation (83) may be used to isolate arc and resistive heating components of wire melting. To express the arc and resistive heating components as equivalent voltages requires that we first consider the heat associated with wire melting rates.

The heat required to just melt the wire and superheat detaching droplets is

$$Q_W = \dot{m} \{H + C_{PL}(T_d - T_m)\} \qquad (126)$$

with

$$H = \int_{T_0}^{T_m} C_p \, dT + L \qquad (127)$$

where H = 1.311 MJ/kg (ref. 100), C_{PL} = 800 J/kg^{o} C (ref. 43), T_m = 1535^{o}C. There is a good deal of experimental evidence in steady current welding (see refs. 82 - 85) to suggest that T_d is insensitive to arc welding with a value close to 2400^{o}C ($\pm$ 100^{o}C). It is assumed here that such a result also holds in pulsed current welding. Combining this data gives the heat consumed at the wire (Q_W):

$$Q_W = 2.0 \times 10^6 \dot{m} \ (W) \qquad (128)$$

where $\dot{m}$ is in kg/s and can be found from data given in Table 22. Furthermore, the Ohmic and arc heating components of wire heating are also known from equation (83). Consider first the total heat appearing at the wire, Q_W may be expressed as an equivalent wire heating voltage by simply writing

$Q_W = \bar{I}\ V_{EW}$.

Then

$$V_{EW} = 2\ (\frac{\dot{m}}{\bar{I}})\ 10^6 \text{ (volts)} \qquad (129)$$

or

$$V_{EW} = 2\ \frac{W}{\bar{I}}\ .\ \rho_m\ .\ A \times 10^6 \qquad (130)$$

where ρ_m and A have the usual meaning.

Results from Table 22 now allow V_{EW} to be identified as shown on Table 23.

From equation (83) it is readily shown that the percentages of total wire heating associated with arc heating are 58%, 55% and 67% from 1.0, 1.2 and 1.6 mm wire diameter respectively. Using the results of Table 23 then gives the equivalent anode and resistive heating potentials (see Table 24).

These figures show that arc heating is insensitive to wire size while resistive heating decreases with increasing wire diameter. (The insensitivity of Ohmic heating potential to arc current is due entirely to the pulse structures used here, i.e. $F/\bar{I}$ = constant). This type of behaviour is expected. The arc heating components given above are similar to those found by other workers (e.g. 6.3 (ref. 43), 4 (ref. 65), 6 ± 0.5 (ref. 44). V_{EW} has three electrical heating components, i.e.

$$V_{EW}\ (\text{arc}) \approx \Phi + Va + \frac{5\ K\ T}{2\ e} \qquad (131)$$

where $\Phi = (4.4\ e\ V)e$ and K have the usual meaning.

T is the plasma electron temperature just outside the metal. Close to the droplet tip arc composition is likely to be dominated by metal vapour with a lower temperature than in the column. Taking T for a metal vapour arc as 5000 K gives

$$V_{EW}\ (\text{anode}) \approx 5.5 + Va \qquad (132)$$

Comparing V_{EW} with results given in Table 23 then implies that the anode fall voltage is close to zero. Such behaviour has previously been reported in GMAW (ref. 44) and also suggested for other types of arc

(ref. 37). One other possibility is that V_a is almost exactly balanced by vapourisation and contact tip losses (effects not considered above).

8.3.4 - Plate heating and melting

The heat appearing at the plate as a result of arc effects, $V_{ET}(arc)$ (i.e. excluding deposited metal) is approximately given by the difference between total plate heating and heat developed at the wire (i.e. by subtracting the data of Tables 21 and 23, where the droplet temperature is assumed to change little in transit through the arc). Results are shown in Table 25 where

$$V_{ET}\ (arc) \approx V_{ET} - V_{EW} \qquad (133)$$

The Ar/5% CO_2 results presented in Table 25 are very close to values of V_E identified directly from plate fusion in Sections 8.2.2, i.e. 6 volts. This implies, for the Ar/5% CO_2 shielding gas, that the arc supplies, through cathode heating and arc heating, just enough power to produce the observed plate melting (and associated heating). In view of the observation that large deposits produce little plate fusion at low speeds (where the deposit then acts as shield between arc and plate) it is tempting to suggest that plate fusion area is determined by arc heating and not by droplet heat transfer as suggested by Essers and Walters (ref. 100) (see Chapter 2). A possible mechanism by which this could occur is suggested later in this section.

Experimental values of V_{ET} (arc) given in Table 25 suggest that dilution behaviour may be significantly affected by shielding gas composition. To estimate the effect anticipated consider equation (108) which gives the maximum dilution as:

$$\lambda_1 = \frac{1}{1 + (\theta_1\ \theta_2)^{-1}} \qquad (134)$$

where $(\theta_1\ \theta_2)^{-1} = 1$ for a 1.2 mm wire in an Ar/5% CO_2 shield.

In general

$$(\theta_1\ \theta_2)^{-1} = \left(\frac{8\ K\ T}{5p}\right) \cdot \frac{\bar{\alpha} \cdot A}{V_E} \qquad (135)$$

The term in brackets is independent of gas type (as is $\bar{\alpha} \cdot A_f$, see section 8.1.2) and so, for a given wire, the influence of shielding gas in confined to V_E. Therefore

$$\frac{(\theta_1\ \theta_2)^{-1}\ (\text{Helishield 1})}{(\theta_1\ \theta_2)^{-1}\ (\text{Ar/5\% } CO_2)} = \frac{V_E\ (\text{Ar/5\% } CO_2)}{V_E\ (\text{Helishield 1})}$$

$$\approx \frac{6.3}{13.5} = 0.47$$

$$\lambda_1\ (\text{Helishield 1}) \approx 0.68$$

This result is in good agreement with measured value of λ_1 for Helishield 1 ($\lambda_1 \approx 0.65$, see Fig. 99). It is interesting to note that an increase of only 15% in λ_1 occurs when V_E is more than doubled. Values of λ_1 obtained in the above manner for 1.0 and 1.6 mm wire diameters are 45% and 55% respectively (where data from Tables 22 and 25 have been used). The respective experimental values are 40% and 55%. Agreement is again good.

A physical interpretation of this behaviour is given in Fig. 101 (i.e. as to why only a fraction of the total plate heat input contributes to melting and associated plate heating, i.e. arc heating). This figure shows droplets entering the pool and displacing liquid metal (and hence heat) to the reinforcement region. Clearly once a drop has entered the pool its identity is lost and the heat so deposited may be regarded, in the first approximation, as a point source situated at the centre of mass of the liquid region. At a similar level of approximation arc heating may be regarded as a point source situated near the point of droplet entry. These two heat sources will then be positioned as shown schematically in Fig.101 In view of the distance of q (droplet) from the melting front, and the different flow paths available, it is suggested that the plate fusion area is governed principally by q (arc). The heat affected zone size should however be influenced by the total heat input, q (arc)+ q (mass).

The qualitative model given above raises further questions associated with relative pool and droplet mean temperature. If the droplet temperature is lower than that of the pool then some of the arc power at the melting front may be absorbed by the droplet mass and hence lower the arc contribution. The converse is expected if droplet temperature is higher than pool temperatures. Taking the difference between droplet and pool temperatures as ΔT allows the effective contribution of droplet heating to V_E (say V_E (drop))to be estimated from

$$V_E \text{ (drop)} \approx \rho_m . A . C_{PL} . \Delta T . \frac{W}{\bar{I}} \qquad (136)$$

Using data previously introduced gives

$$V_E \text{ (drop)} \approx 3.4 . 10^{-3} . \Delta T \qquad (137)$$

As an estimate of this effect consider the example where pool and droplet temperature are 2000^{o} C and 2400^{o} C respectively:

V_E (drop) $\approx$ + 1.4 Volts

It should be noted that this is the deposited mass contribution at the "point of source" position of the arc. The rest of the deposited mass contribution appears to act from the centre of mass of the liquid region.

8.4 - HEAT AFFECTED ZONE DIMENSIONS IN PULSED GMA WELDING

8.4.1 - Introduction

Heat affected zone characteristics are of great importance in welding once they are related to mechanical and metallurgical properties which govern the behaviour of the welded construction. This fact is of basic importance when welding certain alloys and particularly hardenable alloy steels. In order to be able to relate welding parameters and heat affected

zone dimensions it is necessary to use heat flow theory since it can indicate the essential variables which govern the formation of heat affected and fusion zones. In the following sections, a model is developed to define this relationship in order to allow control of heat affected zone dimensions. In this section, the developed model is checked for two different cases.

8.4.2 - Development of model

Considering, as already done for plate melting (seection 8.2.2), that the formation of the heat affected zone in welding is due to thermal conduction from a moving point source of heat, then (ref. 102)

$$T = \frac{q}{2 \pi K r} e^{\frac{- v (r-x)}{2 \rho}} \qquad (138)$$

where T is the temperature distribution relative to the electrode when a weld run is made on the surface of a thick plate and the variables have the usual meaning and r and x are defined in Fig. 102.

We can see that for low temperature isotherms, (Fig. 102), like the $T = 750^{o}$ C defining heat affected zone dimensions, r and y have different values, so equation (138) has to be rearranged.

Considering a and b as:

$$a = \frac{2 \pi K T}{q} , \qquad b = \frac{v}{2 \rho} \qquad (139 \text{ and } 140)$$

and substituing in equation (138)

$$ar = e^{- b (r-x)} \qquad (141)$$

From Fig. 102

$$r^2 = y^2 + x^2 \qquad (142)$$

differentiating equation (141) and (142) and making

$$\frac{dr}{dx} = r' \quad \text{and} \quad \frac{dy}{dx} = y' \qquad (143)$$

$$ar' = - b\, ar\, (r' - 1) \qquad (144)$$

and

$$rr' = 2yy' + 2x \qquad y' = 0 \qquad (145)$$

After some mathematical arrangements

$$x = \frac{(br)^2}{b\,(1 + br)} \tag{146}$$

making

$$\eta = \frac{br}{1 + br} \tag{147}$$

and substituing in equation (144)

$$\exp.. \eta = \frac{a}{b}\,\frac{\eta}{1 - \eta} \tag{148}$$

and in equation (138)

$$y = \frac{\eta}{b}\,\left(\frac{1 + \eta}{1 - \eta}\right)^{1/2} \tag{149}$$

As the heat affected zone area is approximately a semicircle

$$A_{HAZ} = \frac{\pi\, d^2}{8}$$

and

$$d = 2y$$

so

$$A_{HAZ} = \frac{\pi}{2}\,\frac{\eta 2}{b^2}\,\left(\frac{1 + \eta}{1 - \eta}\right) \tag{150}$$

8.4.2.1 - Application of the model to a conduction limited pool

In order to check this model we can consider a steady point heat source so that a conduction limited pool would be obtained.

Then

$$r \to 0$$

which means that

$$b \to 0 \quad \text{and} \quad \eta \to 0$$

from equations (148) and (149), we get

$$\eta\,(1 + \frac{a}{b}) = 1 \tag{151}$$

and

$$A_{HAZ} = \frac{\pi}{2a^2} = \frac{q^2}{8\,K^2\,T^2} \tag{152}$$

which is the expected expression (ref. 33).

8.4.2.2 - Application of this model to fusion zone dimensions

In section 8.2.2 a similar approach was undertaken in order to relate fusion zone dimensions with the welding parameters.

Using the chart where $A_F \cdot v^2$ was plotted against $\bar{I} \cdot v$ we have the values shown on Table 26.

From equations (1 48) and (1 50) and remembering that $0 < \eta < 1$ (eq.(1 47), we get the values shown on Table 26.

We have from section

$\rho = 7.1\ mm^2/s$

$K = 30\ W/m^oC$

$V_E = 6.3\ V$

$T = 1\ 500^o\ C$

so we can calculate the values of $\frac{a}{b}$ for the two chosen points in Table 2.6 and find from Table 2.7 the values of $A \cdot v^2$.

The result is presented in Table 28.

The results are in good agreement with the experimental ones in Table 2.6, thus the model can be applied to fusion area.

8.4.2.3 - Application of this model to heat affected zone dimensions

In order to apply this model to heat affected zone some assumptions are needed. From section 8.3.4 we infer that plate heating may be represented as two point sources of heat (Fig. 101) where arc heat acts at the point of droplet entry to the pool and the bulk of droplet heating acts as a point source situated at the weld pool's centre of mass. The relative positions of these two points sources are dependent on welding speed.

Heat affected zone area is dependent on these two point heat sources.

From ref. 98 we get that for this specific case (heat affected zone area and high values for the operating parameters), the effect of a distributed heat source is similar to the one of a point heat source, so due to this fact and to the relative dimensions of the heat affected zone and the distance between the two points sources, we can consider they enter the plate at the same point.

If we look at the two extreme cases, we have for very low welding speeds (Fig.103-A) the arc on the top of the melted deposit material and for high welding speeds(Fig.103-B) the arc entering the plate before the reinforcement mass.

For the mean values of welding speed we shall have a behaviour between these two which is represented in Fig. 104.

Thus a useful approach is to consider that the heat point source acts in the center of mass of the reinforcement zone.

Considering a semi-infinite body the area that is heated by this point source is equal to

$$A_H = A_{HAZ} + \frac{A_D}{2} \qquad (153)$$

being A_{HAZ} the area between the plate surface and the 750° C isotherm and being A_D the area of the deposited material which is given by

$$A_D = \frac{W \cdot A}{v} \qquad (154)$$

From equation (150) and Table 27 and making $q=I\ V_E$, we obtain the values shown on Table 29. In Fig. 105, the experimental values of $A_H v^2$ were plotted against I.v. From this chart, we get the values of colum 1 and 2 in Table 30. In order to find the values in column 3, 4 and 5 we need the values of (diffusivity) and K (thermal conductivity) for T=750° C. From the data available we can find values for ρ from 5 to 8 mm/s and for k from 24 to 50W/m° C.

If the extreme values are used (subcolumns A and B) we can calculated the maximum and minimum value of V_E. The values in column 4 in Table 30 were taken from Table 29. Thus the calculated values of V_E for an Ar/5%CO_2 gas mixture and mild steel with a 1.2mm wire diameter are between 10.8 and 21 V. For the same materials with a Helishield 1 mixture they are between 18.9 and 30 V.

From Table 21, we find that V_{ET}=14.9 for Ar/5%CO_2 and V_{ET}=22.1 V for Helishield 1 which are more or less equal to the media of V_E values presented above (15.9 and 24.4 respectively), thus as good agreement is obtained this model can be applied to approximately predict heat affected zone dimensions.

8.5 - SIGNIFICANCE OF EXPERIMENTAL RESULTS ON BEADS DEPOSITED IN GROOVES

8.5.1 - Introduction

The model developed on Section 8.2 has to be rearranged in order to be aplicable for beads deposited in grooves since in this case the moving

point source of heat (q) develops heat for melting a plate creating a bead with the shape presented on Fig. 86.

The amount of plate material melted will be dependent on a new parameter the V groove angle since it affects heat flow.

In this section a similar approach as the one undertaken for bead-on-plate deposits is developed in order to find the correction factors to introduce that will enable the model to be applied to any V grooves.

8.5.2 - Application of the model

First thermal diffusivity was calculated using the expression:

$$\rho = \frac{4\ \lambda_1}{5\ (1 - \lambda_1)} \sqrt{\frac{a\ \bar{\alpha}}{2\ \lambda_2\ \pi}} \qquad (155)$$

The values of λ_1 and λ_2 were taken from Figs. 89, 90 and 91 and are shown on Table 30.

The values of thermal diffusivity obtained using Table 31 and equation (155) are shown on Table 32. The values for ρ in the tables are in the range of 5 to 6 mm/s (ref. 107) so the approach is reasonable.

The next step is to calculate the theoretical values of dilution and fusion area using the approach presented on last section and compare the results with the experimental ones. The values obtained are shown on Tables 33, 34 and 35.

For values of $M \geq 250$ δ_{theor} is different from δ_{exp} so the model must be corrected with adequate coefficients given by the expression

$$\bar{F} = \frac{\delta_{exp}}{\delta_{theor}} \qquad (156)$$

These coefficients are presented on Table 36

The use of a correction factor of $\bar{F} = 1.75$ will enable a good approach for theoretical and experimental values of dilution for any V groove (see Figs. 89, 90, 91.

Another interesting testing of the model that can be done (as before) is the calculation of fusion area using the expression

$$A_F\ v^2 = a\ \bar{\alpha}\ \theta_2\ (1 + \theta_1\ M - \sqrt{1 + 2\ \theta_1 M}\ )$$

and Fig. 106. The obtained results are shown on Tables 37 and 38

The values obtained for the corrective factor $\bar{f}$ defined by the expression

$$\bar{f} = \frac{A_F \, v^2_{(exp)}}{A_F \, v^2_{(theor)}} \qquad (157)$$

are shown on Table 39.

Again a mean value for ($\bar{f}$) will enable the applicance of this expression to any V groove (see Fig.106).

The calculations of V_E using expression (110) gave the values shown on Table 40. These values and the ones found for beads deposited on plate were plotted on the chart presented on Fig.107 against V groove angle. The results obtained show that the effective plate heating voltage is dependent on V groove angle and decreases as this angle decreases for the observed values.

The results presented in this section can be theoretically predicted by the following expression:

$$q = \pi \, K \, d \, T \, N \, (1 + \frac{dv}{4\rho}) \qquad (158)$$

where N is a factor affecting heat input depending on V groove angle (ζ)

$$N = f(\zeta) = \frac{\zeta}{\pi}$$

then

$$\frac{q\zeta}{q\pi} = \frac{\zeta}{\pi} \quad \text{or as } q = IV_E \qquad (159)$$

$$\frac{V_E \zeta}{V_E \pi} = \frac{\zeta}{\pi}$$

Substituing the obtained values (see Table 40) on this expression, it is possible to show that the agreement is good for $\zeta = 120^0$ while, for the values of $\zeta = 60^0$ and 90^0, the effective voltage is higher than the value indicated by this expression. This is due to the fact that, for smaller V groove angles, the arc is trapped inside the groove being less the heat dissipated to the exterior, thus leading to more effective plate heating.

CHAPTER 9 - GENERAL DISCUSSION

CHAPTER 9 - G E N E R A L D I S C U S S I O N

9.1 - INTRODUCTION

The aim of this section is to emphasize the results and explain the approaches undertaken which are considered to be of particular importance and to compare these with previous investigations.

9.2 - DEPOSITION CHARACTERISTICS

Mild steel burn-off characteristics in P-GMAW have been widely studied as mentioned on sections 2.6.1 and 2.8.1. In this work, emphasis was placed on the study of the influence of welding parameters namely mean current, stick-out, shielding gas composition and wire diameter on the deposition characteristics of the wire. The obtained results show basically that neither the shielding gas composition nor the wire diameter significantly influence deposition rate. Nevertheless, an interesting observation was the small trend to higher voltages ($Ar/20\%CO_2$, He_1) being associated with slightly higher burn-off rates. Such behaviour may be understood in terms of the analysis of Waszink et al (ref. 44). They consider wire melting phenomena and show that this is dominated by the work function effect (independent of gas type) and infer that anode fall potential (an effect influenced by gas composition) is probably small in consumable arc processes.

In practice any deposition advantage due to gas and wire size is easily off-set by simply changing slightly other welding parameters, eg. mean current, stick-out. Burn-off is very sensitive to electrical extension in pulsed GMAW, whereas (ref. 105) in pulsed GMAW electrode extension is very significant due to the resistance heating during the period of peak current I_p.

The values of burn-off rate were used to calculate the true deposition rate which must also account for mass losses(vapourization/ /spatter) or mass gains (carbon pick-up, etc.) during transfer to work. An examination of bead reinforcement areas for the three wire sizes and two plate thicknesses used, yielded the average recovery factors (each of six experiments) for each gas shown on Table 41.

While some values are a little over 100% (perhaps due to experimental error) the only notable feature is the low value of CO_2. This is probably due to the degree of heavy spatter accompanying transfer. The apparent anomaly between the linear burn-off rate and the strong influence of ohmic heating may be explained by generalizing burn-off results obtained for steady current welding to pulsed current situations. This also leads to an expression-eq. 83 (see section 2.1.2) whereby deposition rate may be predicted for any pulse structure mean current and electrical extension.

A result that ought to be emphasized is the systematic approach to estimating pulse parameters shown on Appendix I, which easily enable the calculation of pulse parameters for a given case.

9.3 - FUSION CHARACTERISTICS

The basic idea that governed this part of the work was to develop a simple model that explains the nature of plate melting and enables the prediction of fusion characteristics in GMAW. Emphasis was placed on the study of dilution, fusion area and penetration.

The choice of welding parameters in GMAW is complicated by the range of criteria often applied to bead geometry. Factores affecting bead geometry often compete so that desired conditions cannot be achieved with this process, eg. all-positional manual GMAW with dilution levels above about 40% are indicated to be unattainable (1.2 mm wire, Ar/5% CO_2) with this process (although achievable with SMAW and GTAW); typical manual conditions give dilutions near 20% where lack of fusion type defects may occur particularly if bead shape is poor.

In order to analyse the nature of plate heating and melting in GMAW, it is essential to understand the nature of heat flow for the proper appreciation of the heat effect in fusion welding.

The welding arc is considered as a moving point source of heat which liberates heat over a small area on the metal surface and that, once steady conditions have been achieved the temperature distribution relative to the heat source is stationary(the type of approach used in this work was undertaken by several authors eg. A.A. Wells (ref. 79)

and Lancaster (ref. 33). Several expressions based on this assumption have been accepted to be reasonably accurate (ref. 35).

Thus the temperature distribution is given by

$$T = \frac{q}{2\pi KR} \exp - \frac{v}{2\rho}(R - x)$$

where q is heat rate and v is the velocity of the heat source.

This equation predicts an infinite temperature at the heat source, which is, of course, impossible. In GMAW as metal is transfered to the weld pool, a substantial amount of flow occours in the weld pool so the heat transfer is partly convectional. Consequently the effective thermal conductivity of the liquid metal is increased and temperature gradients correspondingly reduced, as compared with predict values.

The weld boundary provides a permanent record of the maximum lateral extent of the melting point isotherm, so that measurements of the weld width may be used to verify heat flow theory. The theoretical relationship between heat input and the product of welding speed and weld width divided by the thermal difusivity of the metal is given by:

$$q = \pi\, d\, K\, T_m \left(1 + \frac{4}{5} \frac{vdA}{4\rho}\right) \qquad (160)$$

for our case (3D). This expression is used in this work to develop the model to predict dilution (δ) and fusion area (A_F) and analyse the nature of plate heating (V_E). Other approaches of the former equations have been used (ref. 90, 98, 99, 102). An observation that must be done is the fact that the inherent variability with temperature of the thermal properties of mild steel or the metals in general can present a problem whenever accurate results are essential.

Attempts to relate welding parameters and fusion characteristics were undertaken by Ushio et al (ref. 90) who found the same trends and concluded that a 10% error is made in the width of the bead when latent heat and the difference of the thermal diffusivity are ignored and Christensen et al (ref. 102) who defined an operational parameter as

$$n = \frac{qv}{4\rho^2 \pi K (T_m - T_o)}$$

related with bead dimensions (cross-sectional areas, width and depth) in a dimensionless way. This operating parameter n is proportional also to the parameter M=I.v used in this work and the relationship between n and bead characteristics present the same trends observed in this work (see section 2.5.4).

Eagar and Tsai's (ref. 98) approach was based on a distributed heat source (considered of several dimensions) and related with bead characteristics by means of an operational parameter defined in a similar way as Chistensen's. Again the results show the same trends.

In this work it was considered that other forms of heat transfer (eg. convection, radiation) play only a relatively minor role in heat transfer in GMAW.

Using a conduction based model the nature of plate heating and melting was investigated and it was found possible to give a quantitatively first order description of how plate fusion area and bead dilution behave as process parameters are varied (mean current, welding speed, wire size and shielding gas composition).
As a general rule it is observed that dilution is maximised by using high currents at high speeds. In particular it was found possible to represent dilution behaviour as a function of I.v and hence construct a generalised chart enabling the independent selection of welding parameters (see section 8.2.5). Clearly the conventional expression for heat input has little influence on such behaviour as well as for bead fusion. The significance of heat input on bead characteristics is therefone largely restricted to deposition behaviour, here deposition is largely determined by I/v and arc voltage plays only a small role.

It was observed that, typically only 5% of the total process power is required to melt the plate fusion area, which represents a low melting efficiency of base material in GMAW. The calorimetric studies indicate that about 65% of the process power is transferred to the weldment while fusion area measurements indicate that only 20-30% of the process power is associated with plate melting and heating.

A detailed heat balance reveals that this is precisely the contribution made by arc heating and it is suggested that plate melting occurs largely in response to arc heating with a relatively small contribution from droplet heat transfer depending on relative pool

and droplet temperatures. To account to this behaviour it is further suggested that plate heating may be represented as two point sources of heat where arc heat acts at the point of droplet entry to the pool and that the bulk of droplet heating acts as a point source situated at the weld pool's centre of mass.

The model presented in this work indicates that only limited opportunities exist for manipulating plate fusion characteristics in GMAW. This conclusion explains why the problem of fusion in GMAW has never been satisfactory solved by all the experimental work undertaken during the last decades.

The results of the investigation referred to above indicate a "dual heat" source fusion model (see section 8.3) where plate melting is largely in response to direct arc heating which is mainly dependent on mean current.

In fusion welding, when metal transfer is absent, penetration depth is linked to arc pressure causing puddle depression (ref. 96). In GMAW, Essers and Walter (ref. 100) found that despite the significant influence of mean current on penetration, it was the droplet momentum that played the most important role governing the depth of penetration. Cowdery (ref. 101) studied penetration aspects in pulsed MIG welding of aluminium using a sinusoidal current wave and concluded that wire feed speed, pulse magnitude and arc length influence penetration depth.

The results obtained in this work show that only small changes on depth of penetration are observed when pulse structure(peak parameters and background parameters) are changed at a given mean current.

The shape of the bead, defined by the factor (γ_s) changes with arc voltage which significantly influence wetting angle (θ) and fusion angle (ζ). On the other hand, penetration depth is very sensitive to changes in mean current, increasing with increasing mean currents and is significantly influenced by welding speed.

An operationally important result is that for the range of current used here, maximum plate fusion and penetration occur for welding speeds between 1.5 - 2mm/s. Below 1.5mm/s, these characteristics are extremely sensitive to welding speed while above 3mm/s only small changes occur (although strong finger penetration may be developed).

This suggests that plate fusion and penetration are optimized at any given current by welding speed between 1.5-3mm/s.

Plate melting and penetration area are particularly low in the presence of "bead role-over" even when large beads are deposited. Here a molten cushion shields the plate from the direct action of an arc. Such behaviour suggests that plate melting and penetration behaviour may be largely determined by arc effects (arc heating and arc force) and not primary by deposited mass effects as has been previously suggested (ref. 100).

An attempt is undertaken in this work in order to explain the general influence of arc effects on penetration mechanisms. For the experiments performed the total arc force greatly exceeds that due to droplet impact on the pool and axial pressure is estimated to be roughly four times that exerted by droplets over the region of droplet entry. The model based on these forces indicates that welding speeds above 1-3 mm/s (depending on I) are required if the deposited mass is to be displaced thereby allowing the arc to act directly on plate material. This range of speeds corresponds to the observed maxima in plate penetration and fusion and thereby confirms the arc heating hypothesis.

The heat balance of the system investigated shows that typically 5-6 volts appear at the wire tip as arc heating and that the anode fall potential is probably negligible. Wire heating due to resistive influences is in the range 2.8 - 4.1 V per 15mm of stick-out, depending on wire size and is significant because of the high peak levels adopted (these having a squared effect).

Models presented in this work may be manipulated to suggest ways of influencing fusion characteristics depending on the choice of welding parameters (e.g. mean current, pulse structure, welding speed, wire size, shielding gas composition, wire melting factors). Thus, an important practical result of this work is the generalized representation of fusion characteristics (fig. 100) in a clear and simple form thus enabling an approximate prediction to be easily found.

These modelling considerations on bead-on-plate mild steel weldments are of a general nature and were found to be applicable to other preparations such as V grooves. The results obtained in V groove deposits indicate that there is a trend for heating arc efficiency (V_{EA}) to decrease with the decrease of the included angle, nevertheless

it was found that this tends to be less significant for the lower angles. When the included angle tends to zero degrees, i.e. for closed V grooves, the arc is trapped inside the groove thus an opposite effect of the one described above is expected, i.e higher heat efficiencies. This means that heat efficiency (V_{EA}) should start to increase as V groove angle decreases from a given angle on which was found to be between 60^{o} and 90^{o} for an Ar/5% CO_2 shield.

A further operationally important result is that the lowest plate melting efficiency associated with the less penetrating welds was obtained for included angles around 60^{o} for an Ar/5% CO_2 shield. For He_1, as already found on the bead-on-plate results (see section 8.3), the arc heating efficiency (V_E) is significantly higher (and so plate melting); thus the lowest possible values of V_E should be observed for included angles less than 60^{o}.

As a general rule it is observed that dilution and fusion area are maximized for high currents and welding speeds and minimized by using low currents at low speeds for bead-on-plate weldments in thick and V grooves weldments in thick plate of mild steel.

An important result that is worthwhile emphasize here, is the validity of associating plate melting largely with arc heating and as the modelling considerations which led to this conclusion were of a general nature the models should be applicable to other materials and combinations of materials (plate/wire).

9.4 - HEAT AFFECTED ZONE CHARACTERISTICS

The influence of welding parameters on dimensions of the heat affected zone was studied too, based on a model for conduction of heat from a moving point source.

The type of approach undertaken for fusion zone (eq. 160) was impossible to apply here since the relationship used was not applicable for the 750^{o} isotherm. For low isotherms, like the one defining heat affected zone boundary, the expression

$$T = \frac{q}{2 \pi K R} e^{\frac{-v (R - x)}{2\rho}}$$

has to be rearranged since the shape of this isotherm is quite different from the shape of fusion boundary (see section 8.4).

The results show that heat affected zone dimensions increase as mean current and welding speed increase in a similar way as observed for fusion zone dimensions. Again this trend has already been proposed by several authors (ref. 98, 102).

The model developed associated with the results obtained in this work, show that heat affected zone formation is due to the action of arc heating and wire heating and a mean value of 60% of the process power was found to be associated with heat affected zone formation. This conclusion is substanciated by calorimetric studies undertaken (see section 6.3), which indicate that a similar fraction (65%) of the process power is transferred to the weldment.

CHAPTER 10 - CONCLUSIONS

CHAPTER 10 - C O N C L U S I O N S

1 - Mathematical models are proved to be applicable in P-GMAW and offer great advantages in optimizing welding parameters.

2 - Plate fusion behaviour may be indicated by conduction theory where arc effects (heating and force) play the dominant role.

3 - The models presented enable the prediction of dilution and plate fusion area for any mean current and welding speed.

4 - From an operational point of view, the most significant results concern the possibility of representing fusion characteristics quite generally on just one chart (see Fig. 100). This allows independent selection of required fusion characteristics to be assessed and may be of operational value in surfacing and welding procedural developments.

5 - The model developed indicates that only limited opportunities exist for manipulating plate fusion characteristics in GMAW (apart from the choice of $\overline{I}$ and v). With regard to maximising dilution these are: increasing arc cathode heating by, for example, using helium rich gases and by a choice of wire size or pulse structure so as to minimize the factor $\overline{\alpha}$. a.

6 - Maximum penetration and plate fusion area (for a given arc current) occur at welding speeds of 1.5 - 2mm/s. This is associated by observation and calculation with the lowest speed at which arc action is directed effectively on to the plate. At lower speeds a cushion of metal appears to shield the arc heat from the plate. For speeds higher than 3mm/s, penetration and fusion area values are independent of welding speed. Penetration and fusion area are significantly influenced by mean current.
The relative low plate dilution levels of about 20%, coupled

to poor bead shape, may give rise to fusion defects. Indeed, in all-positional manual welding it is difficult to achieve dilution levels above 30% or for that matter to reduce levels below 10%. Attractions therefore exist for the automatized application of this process (using high welding speeds and high currents). A maximum plate dilution of near 50% depending on wire size and shielding gas composition may be obtained by optimizing $\bar{I}.v.$

7 - As a general rule, it is possible to state that heat efficiency related to plate melting decreases with decreasing included angles in V grooves.

8 - A model was developed which enables the prediction of heat affected zone area for any mean current and welding speed. About 60% - 65% of the process power is associated with heat affected zone formation. Heat affected zone is then due to the effect of arc heating and heat transfer from the droplets.

9 - Shielding gas mixture strongly influences metal transfer characteristics and arc stability the "best" running characteristic being with Ar/1%O_2, Ar/2% O_2 and Ar/5% CO_2 (from the mixtures examined). Higher voltages were observed for Helishield 1 and increasing with increasing amounts of O_2 and CO_2 in Argon.

10 - Taking all data into consideration, it indicates that the "best" gas (of those examined) for general applications is Ar/5% CO_2. However, many situations may exist where other gas mixtures may be preferred. Burn-off depends on mean current, stick-out and pulse structure in P-GMAW. An expression is proposed in order to enable the prediction of burn-off rate in P-GMAW. Burn-off parameters depend on wire size with the products αA and βA^2 insensitive to wire diameter.

11 - From the practical point of view, the systematic approach to pulse parameter selection applicable to constant current power supply characteristics, presented on Appendix 1, is a significant result.

REFERENCES

1. Anon — The Procedure Handbook of Arc Welding 12th Edition, The Lincoln Electric Company

2. Anon — AWS Welding Handbook 7th Edition, Vol.2

3. Stewart,J.P. — The Welder's Handbook Reston Publishing Company, Inc., USA 1981

4. Milner,D.R. Apps, R.L. — Introduction of Welding and Brazing Pergamon Press, London 1968

5. Watkins,P.V.C. — The Transistor Controlled DC Welding Power Source Welding Institute Research Report, Oct/75

6. Needham,C. — Transistor Power Supplies for High Performance Arc Welding Welding Institute Research Bulletin,Vol.18, 3, Mar/77

7. Reinks,F. — Development and Evaluation of a Modulated Power Control for Fusion Welding Welding Journal, Vol.50,5, May/71, pp222S-230S

8. Norrish,J — A Review of Recent Developments in Welding Annual Assembly of Australia, Welding Institute, Oct/85

9. Lucas, W. — Exploitation of Transistor Power Sources in Arc Welding Welding Institute Research Bulletin, Vol.18, Nov/77

10. Needham,J.C. — Precision Wire Feed Systems Welding Institute Research Bulletin, Vol. 21, 11, Nov/80, pp340-346

11. Rider,G.
Albert, P.
Pulsed Wire Feed CO_2 MIG Welding Facilities Repair Work
Welding and Metal Fabrication, Vol. 46, 4, May/78, pp253-262

12. Samokovhsky,D.A.
Development of a Planetary Wire Feeder for MIG/MAG Welding
Metal Construction, Vol. 14,6, Jun/82, pp337 - - 339

13. Quintino, L.
Oliveira Santos,J.F.
Influence of Shielding Gas Composition on GMAW of Stainless Steel
III Doc XII C - 885 - 85

14. Müller
Gas, Mixtures of Gas for Use in Shielded Arc Welding
Institute of Special Branches of Production Technique, Technical University, Dresden

15. Anon
Dual Shielding Welding
Welding and Metal Fabrication, May/68

16. Van Witzenburg
Comparaison entre les Gas de Protection en Soudage MAG des Aciers Ordinaires
Revue de la Soudure, 3 - 1970/115

17. Lucas, W.
Trends in MIG Process Development
Exploiting MIG Welding Developments
Welding Institute, 1983

18. Jones, R.L.
Evaluation of the Production Welding Aspects of Flux-cored Wires
Welding Institute Research Repost, 174, Feb/82

19. Stular, P.
Metal Transfer with Cored Electrodes on Various Shielding Atmospheres
Symposium Physics of the Welding Arc, Welding Institute, 1962, pp98-102

20. Lucas,W.
Alternative Current MIG Welding
Advances in Welding Processes
4th International Conference, Harrogate, May/78, ppl17-126

21. Lucas,W.
Needham, J.C.
Why not AC MIG Welding?
Welding Institute Research Bulletin, Vol. 16, 3, Mar/75

22. Allum, C.J.
Welding and Technology Data Pulsed MIG Welding
Welding and Metal Fabrication, Feb/85, pp24-30

23. Allum, C.J.
MIG Welding - Time for a Reassessement
Metal Construction, Jun/83, pp347-353

24. Brown
Programmed MIG Welding
British Welding Journal, Vol. 1, 6, Jun/68
pp286-293

25. Amin, M.
Synergic Pulse MIG Welding
Metal Construction, Jun/81, pp349-353

26. Amin, M.
Watkins
Synergic Pulse MIG Welding
Welding Institute Research Report, Aug/77

27. Needham, J.C.
Synergic Pulse MIG Welding
The Welding Institute Research Bulletin, Vol. 8, 9, 1977

28. Lopes, A.A.
Cruz,J.M.
Freitas, J.M.
Oliveira Santos,J.F.
Quintino, L.
Electronic Arc Welding Power Source for DC/AC+DC: Pulsarc III (MMA, TIG and MIG/MAG)
Conference on Developments and Innovations for Improved Welding Production
Welding Institute, Birmingham, 1982;pp30-1-30-5

29. Rodrigues, A.C.
Power Electronics Provides Advances in Process Adaptation
Symposium "Using Synergic MIG Sucessfully", Oct/84, Cranfield Institute of Technology

30. Rehfeld
A New Microprocessor Controlled System for Monitoring and Analysing Arc Welding Processes
IIW, Doc. 212 - 769 - 79

31. Amin,M.
Microcomputer Control of Synergic Pulsed MIG Welding
Welding Institute Research Report, Dec/81

32. Classification of Metal Transfer on Arc Electric Welding Process
Welding in the world, Vol. 15, 5/6, 1977
ppl13-117

33. Lancaster — The Metallurgy of Welding Brazing and Soldering
George Allen & Unwin, Ltd., London 1974

34. Needham, J.C.
Cooksey
Mulner — Metal Transfer in Inert Gas Shielded Arc Welding
British Welding Journal, Feb/60, ppl05

35. Lancaster — Metal Transfer in Fusion Welding
Conference on Arc Physics and Weld Pool Behaviour, Welding Institute, London 1979, ppl35-146

36. Amson — Lorentz Force in the Molten Tip of an Arc Electrode
British Journal Applied Physics, 1965, Vol. 16, ppll69-1179

37. Waszink — Experimental Investigation of the Forces Acting on a Drop of Weld Metal
Welding Research Supplement, Apr/83, ppl08-116

38. Serdjuk, G.B. — Magnetic Forces in Arc Welding Metal Transfer
Symposium "The Physics of the Welding Arc", London 1962, Session 5, 3

39. Boughton
Matani — Two Years of Pulsed Arc Welding
Welding and Metal Fabrication, Oct/67,pp410-420

40. Buchinsk
Potapevskii — Selecting the Parameters of the Welding Conditions for Pulsed Arc Welding with a Consumable Electrode
Avt. Svarks, Vol. 30, 6, 1977

41. Ando
Nishiguchi — Mechanism of Formation of Pencil - Point like Wire Tip in MIG Arc Welding
IIW Doc. 212 - 156 - 68

42. Pintard — Contribution à l'Etude du Transfer de Metal dans le Soudage MIG
Comunication presentée à la Societé des Ingenieurs Soudeurs, Dec/64 - pp278-287

43. Ma, J.
Apps, R.L.
MIG Transfer Discovery of Importance to Industry
Welding and Metal Fabrication, Sep/82, pp307-313

44. Waszink,J.K.
Van den Heuvel
Heat Generation and Heat Flow in the Filler Metal in GMA Welding
Welding Research Supplement, pp269S-282S

45. Needham, C.
Arc and Transfer Characteristics of the Steel/CO_2 Welding Process
BWRA report, Oct/67

46. Paton
Sheiko
Controlling Metal Transfer in Arc Welding with a Consumable Electrode
Art. Svarks, 1965, 5, pp1-7

47. Partington
Needham
Controlled Transfer Characteristics on the Inert Gas Metal Arc Process. Effect of Duration and Current Amplitude of Current Pulse
BWRA report, p/16/66

48. Hiltunen
Pietikainen
Investigations and Observations on Material Transfer in MIG Welding
Conference on Arc Physics and Weld Pool Behaviour
Welding Institute, London 1979, pp147-162

49. Amin
Pulse Current Parameters for Arc Stability and Controlled Metal Transfer in Arc Welding
Metal Construction, May/83, pp272-278

50. Paton
Sheiko
Automatic Control of Pulsed Arc Welding with a Consumable Electrode
Art. Svarks, 1967, n. 1, pp3-8

51. Matsuda
Ushio
Itonaga
Yokoo
Pulsed CO_2 Arc Welding
IIW Doc. 212 - 586 - 84

52. Needham
Metal Transfer Characteristics with Pulsed Current
British Welding Journal, May/65, pp229-241

53. Needham
Pulse Controlled Consumable Electrode Welding Arcs
British Welding Journal, Apr/65, pp191-197

54. Partington — Controlled Metal in the Open Arc MIG Process. Effect of Pulse Duration and Amplitude
Welding Institute Research Report, 1966

55. Lenivkin — The Determination of Regions of Controllable Metal Transfer in Pulsed Arc Welding with a Consummable Electrode
Svar. Droiz. Vol. 23, 12, 1976, ppl0-l4

56. Ma, J.
Apps, R.L. — Analysing Metal Transfer during MIG Welding
Welding and Metal Fabrication, Apr/83

57. Matsuda
Ushio
Tonaka — Metal Transfer Characteristics in Pulsed GMA Welding
Transation of JWRI, Vol. 12, 1, pp9-17

58. Boughton
Lucey — The Use of Pulse Current to Control Metal Transfer in Welding
British Welding Journal, Vol. 12, 5, Apr/65, ppl59-166

59. Fu
Ushio
Matsuda — Melting Characteristics of some Steel and Aluminium Alloys in GMA Welding
Transation of JWRI, Vol. 12, 2, 1963, pp7-13

60. Lesnewich — Control of Meltong Rate and Metal Transfer in Gas Shielded Metam Arc Welding
Welding Journal, Aug/85, pp3435-3535

61. Wilson
Clausen
Jackson — The Effect of I^2R Heating on Electrode Melting Rate
Welding Journal, Jan/56, pp 1s-8s

62. Müller
Greene
Rothschild — Characteristics of Inert Gas Shielded Metal Arcs
Welding Journal, Aug/51, pp717-727

63. Milner
Salter
Wilkinson — Arc Characteristics and their Significance in Welding
British Welding Journal, Feb/60, pp73-88

64. Lancaster — The Physics of Welding
Pergamon, London 1984

65. Halmøy, E. — Wire Melting Rate, Droplet Temperature and Effective Anode Melting Potential. Conference on Arc Physics and Weld Pool Behaviour. Welding Institute, London, 1979, pp49-57

66. Sprargen, Bela Lengyel — Physics on the Welding Arc and the Transfer of Metal in Arc Welding. Welding Research Supplement, Jan/43, pp2s-42s

67. Waszink, Van den Heuvel — Measurements and Calculation of the Resistance of the Wire Extension in Arc Welding. Conference on Arc Physics and Weld Pool Behaviour. Welding Institute, London, 1979, pp227-239

68. Amson — Electrode Voltage in the Consumable Electrode Arc System. J. Phys. D. Appe: Phys., Vol. 5, 1972, pp89-96

69. Adrichem — Metal Transfer. IIW Doc. 212 - 171 - 69

70. Wilkinson, Milner — Heat Transfer from Arcs. British Welding Journal, Feb/60, ppll5-128

71. Paton, Potapewskii — Gas-Shielded Steady and Pulsed Arc Welding Process. (Review) Art. Svarka, 1973, ppl-10

72. Matsaumawa — Arc Characteristics in High Pressure Argon Atmosphere. Conference on Arc Physics and Weld Pool Behaviour. Welding Institute, London 1979, ppl23-133

73. King, Howes — Material Transfer in Arc Welding. Symposium "Physics of the Welding Arc", session 5, Paper 4, Welding Institute, London,1962, pp 180-188

74. Lucas, W. — Solid Wire AC MIG Welding. Welding Research International, Vol. 8, 2, 1978

75. Finkelnburg — Handbuch der Physik 1956. Vol. 22, pp254-444

76. Goldman, K.
Electric Arcs in Argon
Symposium "Physics of the Welding Arc", Session 2, Paper 1, Welding Institute, London, 1962, pp17-22

77. Lochte Hoetgerven, W.
The Electrical Arc between Carbon and Iron Electrodes
Symposium "Physics of Welding Arc", Session 1, Paper 1, Welding Institute, London 1962, pp1-13

78. Nestor, O.H.
Heat Intensity and Current Density Distribution at the Anode of High Current Inert Gas Arcs
Symposium "Physics of the Welding Arc", session 2, Paper 6, Welding Institute, London, 1962, pp50-61

79. Wells, A.A.
Heat Flow in Welding
Welding Journal, Vol. 31, 5, Research Spl., ay/52, pp236-267

80. Apps, R.L. Mülner, D.R.
Heat Flow in Argon Arc Welding
British Welding Journal, Vol. 2, 10, Oct/55

81. Rykaline Erokin
Calcul des Processes Thermiques de Soudage
Soudage et Techniques Connexes, Vol. 15,1/2,pp5-38

82. Jelmorini et al
Droplet Temperature Measurements in Arc Welding
IIW Doc. 212 - 411 - 77

83. Pokhodnya, I.K. Stripel, A.M.
The Heat Content of the Droplets of Electrode Metal in Gas Shielded Arc Welding
Art. Svarka, Vol. 20, 2, 1967, pp16-27

84. Heiro North
The Influence of Welding Parameters on Droplet Temperature during Pulsed Arc Welding
Welding and Metal Fabrication, Sep/76, pp482-485

85. Voropai Kolesnichenko
Modelling of the Form of Droplets of Electrode Metal in Welding with shielding Gases
Art. Svarka, 1979, 9, pp27-32

86. Myers Uyehara Borman
Fundamentals of Heat Flow in Welding
Welding Research Council Bulletin, Mar/76

87. Oreper
Szekely
Heat and Flow in Weld Pools
Journal of Fuid Mechanics, Vol. 147, 1984,pp53-79

88. Danilov
Chernyshov
On the Mechanism of Action of a Pulse of Current on the Weld Pool
Welding Production, n. 1, 1974, pp54-56

89. Adams, C.M.
Cooling Rates and Peak Temperatures in Fusion Welding
Welding Journal, Vol. 37, Research Supl., 1952 pp210-218

90. Ushio
Ishimura
Matsuda
Arada
Theoretical Calculation on Shape of Fusion Boundary and Temperature Distribution around Moving Heat Source
Transactions of JWRI,Vol. 6, 1, 1977, ppl-6

91. Oreper
Eagar
Szekely
Convention in Arc Welds Pools
Welding Journal, Nov/83, pp307s-312s

92. Demayantsevich
Distribution of Temperature in the Molten Metal Pool during Welding a Non-consumable Electrode
Automatic Welding, 11, 1972, pp5-7

93. Kopersak
Slivinshi
Durhno
Temperature Condition in Weld Pools
Welding Production, 11, 1974, ppl-3

94. Andeev
Temperature Distribution in the Weld Pool
Svar. Proiz., 11, 1974, ppl-3

95. Grosh, R.J.
Trabant, E.A.
Hawkins, G.A.
Quart. Appl. Math.,
1955, 13(2), ppl61

96. Friedman
Analysis of the Weld Puddle Distortion and its Effect on Penetration
Welding Journal, Jun/78, ppl61s-166s

97. Bradstreet
Effect of Surface Tension and Metal Flow on Weld Bead Formation
Welding Journal, Jul/68, pp313s-322s

98. Eagar, Tsai — Temperature Fields Produced by Travelling Distribution Heat Sources. Welding Journal, Dec/83, pp346s-355s

99. Rosethal, D. — Mathematical Theory of Heat Distribution during Welding and Cutting. Welding Research Supl., May/41, pp220s-234s

100. Essers, Walter — Heat Transfer and Penetration Mechanisms with GMA and Plasma GMA Welding. Welding Journal, Feb/81, pp 37s-42s

101. Cowdery — Penetration Characteristics on Pulsed MIG Welding: Effect of Pulse Shape at 50 Hz. Welding Institute Research Report, Dec/70

102. Christensen et al — Distribution of Temperature in Arc Welding. British Welding Journal, Feb/65, pp54-75

103. Anon — Physical Constants of some Commercial Steels at Elevated Temperatures. The British Iron and Steel Research Association 1953

104. Anon — Average Kinetic Energy of Diffusing Particles in Discharge and Electron Tubes. British Journal of Applying Physics, Vol. 12, Set/62

105. Trindade, E. — Msc. Thesis. School of Industrial Science, Cranfield, 1981

106. Nunes, J. — Msc. Thesis. School of Industrial Science, Cranfield, 1982

107. Switt, Hook, D.I., Gick, A.E.F. — CEGB RIM/N 637. Jun/72

108. Allum, C.J. — J. Phys. D. Appl. Phys 14, pp1041-1059, 1981

109. Allum, C.J. — Metal Transfer in Arc Welding as a Varicose Instability. J. Phys. D. Appl. Phys. 18, pp1447-1468, 1985

APPENDIX 1

APPENDIX 1

A systematic approach to estimating pulse parameters

An example is given below of an approach applicable to a constant current type power supply with continuously variable pulse settings.

Step 1. Choose a heat input appropriate to problem (say 83A)

Step 2. Choose an appropriate wire size - (say 1.2 mm)

Step 3. Choose peak conditions from Fig. 12. Say I_p = 350A, T_p = 4 ms

Step 4. Use $F/\bar{I}$ relationship (i.e. 50Hz/100 A) to find F, i.e. 41.5 Hz

Step 5. Find T_b from $F^{-1}-T_p$, i.e. 20.1ms

Step 6. Find I_b from $\bar{I} = F(I_p T_p + I_b T_b)$ i.e. 29A

Step 7. Choose wire extension (e.g. 15 mm) and calculate W from equation 83 and data of Table 14, i.e. W = 2.43m/min

The problem is now specified. In practice W would be "tuned in" to produce the desired arc length/electrical extension. It is also desirable to use arc voltage to control arc length in many situations. It should be emphasized that the above approach can only be expected to give a first approximation. Fine tuning can then be performed by entering the routine at some point and again systematically varying parameters. For example, if arc jet is too strong ot too weak, alternative values of I_p and t_p must be chosen by returning to Step 3. Subsequently, proceed to Step 7. For example, if droplets are too large or too small return to Step 4, change the $F/\bar{I}$ combination and proceed to Step 7, etc.

	ARGON	HELIUM
IONIZATION POTENCIAL (eV)	15.8	24.6
THERMAL CONDUCTIVITY (cal/ s/^{o}C)	0.406×10^{-4}	3.32×10^{-4}
DENSITY (relative to air)	1.38	0.137

TABLE 1 - Physical properties of argon and helium

	M 500	M 450 PS
INPUT VOLTAGE	380/440 3 Phase 50 Hz Maximum open circuit voltage 55 V DC	380/420/440 3 Phase 50/60 Hertz
OUTPUT CHARACTERISTICS	Arc voltage DC current--voltage relationship variable between constant current and constant voltage	Output slope - constant current (max. average 350 A)
WELDING CURRENT CONTROL	Current levels in range 0-500 A in 1 A steps with accuracy of ± 0.5%	Current levels in range 0-450 A in 1 A steps with accuracy of 1%
PULSED CURRENT CONTROL	Pulse peak and background 0-500 A in 1 A steps,peak time and background time 0.001 to 9.999 secs in 0.001 second steps	Pulse peak and background current 0-450 A in 1 A steps, peak time 0.1 to 99.9 m/sec in 1 m/sec steps
REPRODUCINILITY AND ACCURACY	Current: ± 1% at full scale setting Timming: ± 0.5% for each control	Current: ± 2% at full scale setting Accurancy maintained for line voltage Variation of ± 6%
SHORT CIRCUIT CONTROL	Max short circuit current - 500 A	Max. short circuit current: 450 A

TABLE 2 - Characteristics of the power sources

C	Mn	Si	S	P
0.12 max	0.90-1.60	0.70-1.20	0.040 max	0.040 max

TABLE 3 - Chemical composition of the filler materials

	1.0	1.2	1.6
θ	77	100	82.5
γ_s	0.49	0.54	0.46
ζ	13	7	6

TABLE 4 - Wetting angle, fusion angle and shape factor for different wire diameters
($\bar{I}$ = 100 A, I_p = 350 A, t_p = 4 ms, ℓ= 15 mm, Ar/5% CO_2, v = 1.53 mm/s)

	10	15	20	25
θ	68	76	77.5	80
γ_s	0.61	0.59	0.65	0.52
ζ	14	17	14	12.5

TABLE 5 - Wetting angle, fusion angle and bead shape factor for different stick-outs
($\bar{I}$ = 150 A, I_p = 350 A, t_p = 4 ms, ℓ = 15 mm Ar/5% CO_2, v = 1.53 mm/s)

I_b (Amps)	t_b (ms)	F (f/z)	θ (^{o})	γ_s	ζ	ϕ (mm)
50	8	83	52	0.52	9	1.02
70	10	71.5	50	0.63	14	1.13
83	12	62.5	40.5	0.44	6	1.23
93	14	55.5	58	0.56	7.5	1.46
100	16	50	41	0.51	6.5	1.54
105	18	45.5	43	0.57	6	1.7
110	20	41.6	59	0.46	10.5	1.8
113	22	38.5	56.5	0.57	6	1.9
117	24	35.7	42.5	0.54	8	2.06

NOTE: The values of ϕ (droplet diameter) were used on the discussion presented in Chapter 8.

TABLE 6 - Influence of background parameters on bead characteristics.
(I = 150 A, I_p = 350 A, t_p = 4 ms, ℓ = 15 mm, Ar/5% CO_2, 1.2 mm wire)

$\bar{I}$	75	100	125	150	175	200
δ	0.10	0.15	0.19	0.23	0.24	0.30

TABLE 7 - Influence of mean current on dilution
(1.2 mm wire diameter, ℓ = 15 mm, Ar/5% CO_2, $\bar{I}/F$ = 2, v = 1.53 mm/s)

GAS	Ar	Ar/1% O_2	Ar/2% O_2	Ar/5% CO_2	Ar/20% CO_2	CO_2	He 1
Thin plate	0.18	0.18	0.19	0.21	0.18	0.23	burn through
Thick plate	0.13	0.15	0.11	0.15	0.17	0.13	0.16
Average	0.16	0.17	0.15	0.18	0.18	0.18	.16

TABLE 8 - Influence of shielding gas composition on dilution
(1.2 mm wire diameter, $\bar{I}$ = 100 A, ℓ = 15 mm, F = 50Hz, v = 1.53 mm/s)

GAS	Ar	Ar/1% O_2	Ar/2% O_2	Ar/5% CO_2	Ar/20% CO_2	CO_2	He_1
Z_m	28	32	34.5	32.5	31.5	25	22
Z_m^*	3.8	4.7	3.8	5.0	5.2	3.2	3.7

TABLE 9 - Influence of gas type on melting efficiency (Z_m) and on the fraction of process power contributing to plate melting (Z_m^*) (i.e. $Z_m^* = Z_m$ with A identified with plate fusion area) ($\bar{I}$ = 100 A, v = 1.53 mm/s, ℓ = 15 mm)

	Wire	1.0 mm	1.2 mm	1.6 mm	Average
δ	Thin plate	0.23	0.21	0.22	0.22
	Thick plate	0.16	0.15	0.13	0.15

TABLE 10 - Influence of wire size on dilution ($\bar{I}$ = 100 A, F = 50 Hz, ℓ= 15 mm, Ar/5% CO_2, v = 1.53 mm/s)

	60°		90°		120°	
GAS MIXTURE \ $\bar{I}$	150	200	150	200	150	200
He_1	0.20	0.29	0.15	0.26	0.28	0.30
Ar/20% CO_2	0.13	0.22	0.12	0.23	0.23	0.33
Ar/5% CO_2	0.04	0.14	0.12	0.05	0.15	0.24
Ar/2% CO_2	0.11	0.22	0.07	0.09	0.13	0.13

TABLE 11 - Influence of shielding gas composition and V groove angle on dilution factor (δ) for mean currents of 150 and 200 A

MEAN CURRENT	FREQUENCY	I_b (A)	T_b (ms)
100	50	38	16
150	75	64	9.3
200	100	100	6.0
250	125	157	4.3

TABLE 12 - Background parameters calculated from 50Hz/100 A relationship with I_p = 350 A, t_p = 4 ms

PARAMETER	$\bar{I}$ (A)			AVERAGE
	100	125	150	
α (mm A^{-1} s^{-1})	0.47	0.47	0.47	0.47
β (A^{-2} s^{-1})	8.86×10^{-5}	9.24×10^{-5}	9.31×10^{-5}	9.14×10^{-5}

TABLE 13 - Burn-off parameters (α,β) for 1 mm wire diameter

PARAMETER	$\bar{I}$ (A)			AVERAGE
	100	150	200	
α (mm A^{-1} s^{-1})	0.28	0.27	0.27	0.27
β (A^{-2} s^{-1})	5.6×10^{-5}	5.56×10^{-5}	6.63×10^{-5}	5.93×10^{-5}

TABLE 14 - Burn-off parameters (α,β) for 1.2 mm wire diameter

PARAMETER	$\bar{I}$ (A)			AVERAGE
	100	150	200	
α (mm A^{-1} s^{-1})	0.22	0.17	0.16	0.18
β (A^{-2} s^{-1})	1.22×10^{-5}	1.14×10^{-5}	1.22×10^{-5}	1.19×10^{-5}

TABLE 15 - Burn-off parameters (α,β) for 1.6 mm wire diameter

PARAMETER	WIRE DIAMETER			AVERAGE
	1.0	1.2	1.6	
α A (mm^3 A^{-1} s^{-1})	0.37	0.31	0.36	0.35
β A^2 (mm^4 A^{-2} s^{-1})	5.64×10^{-5}	6.71×10^{-5}	7.6×10^{-5}	$(6.65 \simeq 0.9)10^{-5}$

TABLE 16 - Influence of wire size on α and β

I	10^3 R_D (m)	V_{eff}	Re	C_D	a (m^2/s)	a + g (m^2/s)	v_d (m/s)
38 A	0.6	5	1	25	3.6	13.4	1.54
350 A	0.6	103	18.2	2.16	132.2	142	1.89

TABLE 17 - Calculation of droplet velocity (ref. 64)

$M - \bar{I}.v$ (A mm/s)	δ (calculated)	δ (experimental)
100	0.09	0.10
250	0.16	0.20
500	0.22	0.29
1000	0.29	0.37
2000	0.34	0.40

TABLE 18 - Comparation of experimental and predicted dilutions

	Ar/5% CO_2			HELISHIELD 1
MEAN CURRENT (A) \ WIRE DIAMETER (mm)	1.0	1.2	1.6	1.2
100	58	72	72	70
150	64	65	53	66
200	55	62	56	64
AVERAGE (%)	59	66	60	67

TABLE 19 - Influence of arcing parameter on heat transfer efficiency (η%)

	Ar/5% CO_2						HELISHIELD 1	
WIRE DIAMETER (mm)	1.0		1.2		1.6		1.2	
MEAN CURRENT (A)	V (V)	W m/min	V (V)	W m/min	V (V)	W m/min	V (V)	W m/min
100	23.6	4.6	22	2.8	20.2	1.33	31.2	2.9
150	26.7	7.0	24.5	4.3	22.3	2.20	33.6	4.6
200	29.1	10.2	26.7	6.0	25.0	2.80	34.4	6.4

TABLE 20 - Process data corresponding to heat transfer experiments
(V - mean voltage, W - wirefeed speed, ℓ=15 mm with 5 mm arc)

	Ar/5% CO_2			HELISHIELD 1
WIRE DIAMETER (mm) / MEAN CURRENT (A)	1.0	1.2	1.6	1.2
100	13.7	15.8	14.5	21.8
150	17.1	15.6	11.8	22.3
200	16.0	13.4	14.0	22.2
AVERAGE (V)	15.6	14.9	13.4	21.1

TABLE 21 - Influence of process parameters on V_{ET}

WIRE DIAMETER (mm)	Ar/5% CO_2		HELISHIELD 1	
	$W/\bar{I}$ (mm/s)			
	Expt.	Theory	Expt.	Theory
1.0	0.79 (0.05)	0.81	--	--
1.2	0.51 (0.02)	0.49	0.48 (0.02)	0.49
1.6	0.23 (0.02)	0.27	--	--

TABLE 22 - Comparison of experimental and theoretical burn-off behaviour

WIRE DIAMETER (mm)	Ar/5% CO_2	HELISHIELD 1
	V_{EW} (volts)	
1.0	9.8	---
1.2	8.6	8.6
1.6	8.6	---

TABLE 23 - Equivalent wire heating voltages ($W/\bar{I}$ taken from equation (132))

WIRE DIAMETER (mm)	EQUIVALENT ARC HEATING POTENTIAL AT THE WIRE V_{EW} (arc) (Volts)	EQUIVALENT RESISTIVE HEATING POTENTIAL AT THE WIRE V_{EW} (Ohmic) (Volts)	TOTAL WIRE HEATING POTENTIAL V_{EW} (Volts)
1.0	5.7	4.1	9.8
1.2	4.7	3.9	8.6
1.6	5.8	2.8	8.6

TABLE 24 - Equivalent arc and resistive heating potencials at the wire

WIRE DIAMETER (mm)	Ar/5% CO_2	HELISHIELD 1
	V_{ET} (arc)	
1.0	5.8	---
1.2	6.3	13.5
1.3	4.8	---

TABLE 25 - Equivalent voltage, V_{ET} (arc) associated with arc heating influence at the plate

$\bar{I} \times v$ (A . mm/s)	$A_F \times v^2$ (mm/s)
500	≃ 70
1000	≃ 230

TABLE 26 - Values taken from Fig. 98 to be use in equations (147) and (148)

η	a^2/b	$\frac{2A_F b^2}{\pi}$
0	∞	0
0.1	8.14	0.012
0.2	3.27	0.06
0.3	1.73	0.17
0.4	1.01	0.37
0.5	0.61	0.75
0.6	0.37	1.44
0.7	0.21	2.78
0.8	0.11	5.76
0.9	0.05	15.39
1.0	0	∞

TABLE 27 - Intermediate calculation obtained from equations (147), (148) and (150)

($a = \frac{2\pi K T}{q}$, $b = \frac{v}{2\rho}$)

$\bar{I} \times v$	$\frac{a}{b}$	$\frac{A_F v^2}{2\rho^2 \pi}$	$A_F v^2$
500	1.338	~ 0.2	~ 63
1 000	0.669	~ 0.85	~ 269

TABLE 28 - Results on the applicance of the model to fusion area

$\frac{A v^2}{\rho^2}$	$Iv \left(\frac{V_E}{K T \rho}\right)$
0.075	1.54
0.377	3.84
1.068	7.27
2.32	12.44
4.71	20.61
9.04	33.97
17.46	59.86
36.17	114.27
96.64	251.4
∞	∞

TABLE 29 - Intermediate calculation values taken from Table 27 ($q = \bar{I} V_E$)

	1	2	3		4		5		6	
	$I \cdot v$	$A_H v^2$	$\frac{A_H v^2}{\rho^2}$		$Iv \left(\frac{V_E}{K T \rho}\right)$		$\frac{V_E}{K T \rho}$		V_E	
			A	B	A	B	A	B	A	B
Ar/5% CO_2	100	70	2.8	1.1	~ 14	7.5	0.14	0.075	12.6	21
	300	250	10	3.9	~ 34.5	18	0.12	0.06	10.8	18
	500	450	18	7	~ 63	26.5	0.13	0.05	11.7	15
	1000	975	39	15.2	~ 116	53.5	0.12	0.05	10.8	15
HELISHIELD 1	100	80	3.2	1.2	~ 16	8	0.16	0.08	14.4	24
	300	475	19	7.4	~ 66	28	0.22	0.09	19.8	27
	500	825	33	12.9	~ 105	47	0.21	0.09	18.9	27
	700	1400	56	21.9	~ 160	74.5	0.23	0.1	20.7	30

TABLE 30 - Calculation of V_E (values on column 4 were taken from Table 29)

	60	90	120
λ_1 (He_1)	0.43	0.40	0.475
λ_1 (Ar/5% CO_2)	0.325	0.25	0.40
λ_2 (He_1)	$5.3.10^{-4}$	$6.67.10^{-4}$	$1.39.10^{-3}$
λ_2 (Ar/5% CO_2)	$3.48.10^{-4}$	$2.5.10^{-4}$	$5.93.10^{-4}$

TABLE 31 - Values taken from Figs. 89, 90 and 91 used in the calculation of thermal diffusivity (eq. 155)

	60	90	120
ρ (He_1)	7.7	6.04	5.68
ρ (Ar/5% CO_2)	6.04	4.93	6.76

TABLE 32 - Thermal diffusivity values obtained from equation (155)

V groove angle		60^{o}	90^{o}	120^{o}
He_1	θ_1	$1.405.10^{-3}$	2.10^{-3}	$3.073.10^{-3}$
	θ_2	537	3332	294.5
$Ar/5\% CO_2$	θ_1	$1.45.10^{-3}$	$1.5.10^{-3}$	$1.6.10^{-3}$
	θ_2	333.1	222.2	416.9

TABLE 33 - Values of θ_1 and θ_2 for beads deposited in V grooves

$$(\theta_1 = \frac{2\,\lambda_2\,(1-\lambda_1)}{\lambda_2}\,,\quad \theta_2 = \frac{\lambda_1^{\,2}}{2\,\lambda_2\,(1-\lambda_1)^2})$$

	δ (calculated)			δ (experimental)		
M \ V groove	60	90	120	60	90	120
100	4.5	5.3	9.7	5.0	7.0	15.0
250	9.1	10.3	17.1	12.5	17.0	31.0
500	14.0	15.2	23.4	25.0	26.0	41.0
1000	19.6	20.3	29.2	38.0	36.0	47.0
1750	24.0	24.1	33.2	43.0	40.0	47.5

TABLE 34 - Theoretical and experimental values of dilution in V grooves

(He_1, ℓ = 15 mm, $\bar{I}/F$ = 2, I_p = 350 A, t_p = 4 ms)

	δ(calculated)			δ(experimental)		
M	60	90	120	60	90	120
100	3.0	2.1	4.4	2.5	2.5	5.0
250	6.1	4.4	8.9	8.0	7.0	13.0
500	9.6	6.9	13.5	17.5	12.5	24.0
1000	13.7	10.0	18.7	31	21.0	35.0
1750	17.0	12.5	22.7	32.5	25.0	40.0

TABLE 35 - Theoretical and experimental values of dilution in V grooves
(Ar/5% CO_2, ℓ = 15 mm, $\bar{I}/F$ = 2, I_p = 350 A, t_p = 4 ms)

	Ar/5% CO_2	He_1
60	1.83	1.72
90	1.88	1.7
120	1.72	1.65

TABLE 36 - Correction factor affecting dilution

	$A_F \cdot v^2$ (calculated			$A_F \cdot v^2$ (experimental		
M	60	90	120	60	90	120
300	18.5	20.9	37.3	50	45	70
400	30.2	33.6	58.5	75	65	100
750	84.2	89.6	148.3	200	155	280
1000	130.9	136.9	221.7	350	250	480
1250	182.5	188.3	300.1	520	380	710
1750	296.4	299.6	467.2	835	710	1140

TABLE 37 - Calculated and experimental values of the product fusion area (A_F) x squared welding speed (v^2) in V groove (He_1, ℓ = 15 mm, $\bar{I}/F$ = 2, I_p = 350 A, t_p = 4 ms)

	$A_F \cdot v^2$ (calculated			$A_F \cdot v^2$ (experimental		
M	60	90	120	60	90	120
300	12.1	8.6	17.9	20	15	40
400	19.8	14.0	29.2	35	25	60
750	54.8	38.5	79.9	125	80	160
1000	85.1	59.8	123.5	200	120	265
1250	118.6	83.1	171.3	305	275	375
1750	192.2	134.5	276.0	515	425	620

TABLE 38 - Calculated and experimental values of the product fusion area (A_F) x squared welding speed (v^2) in V groove (Ar/5% CO_2, ℓ = 15 mm, $\bar{I}/F$ = 2, I_p = 350 A, t_p = 4 ms)

	Ar/5% CO_2	He_1
60	2.33	2.64
90	2.35	1.98
120	2.13	2.11

TABLE 39 - Correction factor affecting the product of fusion area and squared welding speed

	60	90	120
V_E (He_1)	4.1	4.6	6.7
V_E (Ar/5% CO_2)	3.3	2.8	4.1

TABLE 40 - Effective plate heating voltage in V groove

GAS	Ar	Ar/1% O_2	Ar/2% O_2	Ar/5% CO_2	Ar/20% CO_2	CO_2	He_1
RECOVERY FACTOR (η)	100	100	106	103	102	88	103

TABLE 41 - Weld metal recovery factor (η) given by

$$\eta = \frac{\text{reinforcement area x welding speed}}{\text{wire cross-sectional area x wire feed speed}} \times 100\%$$

PHOTOGRAPHS

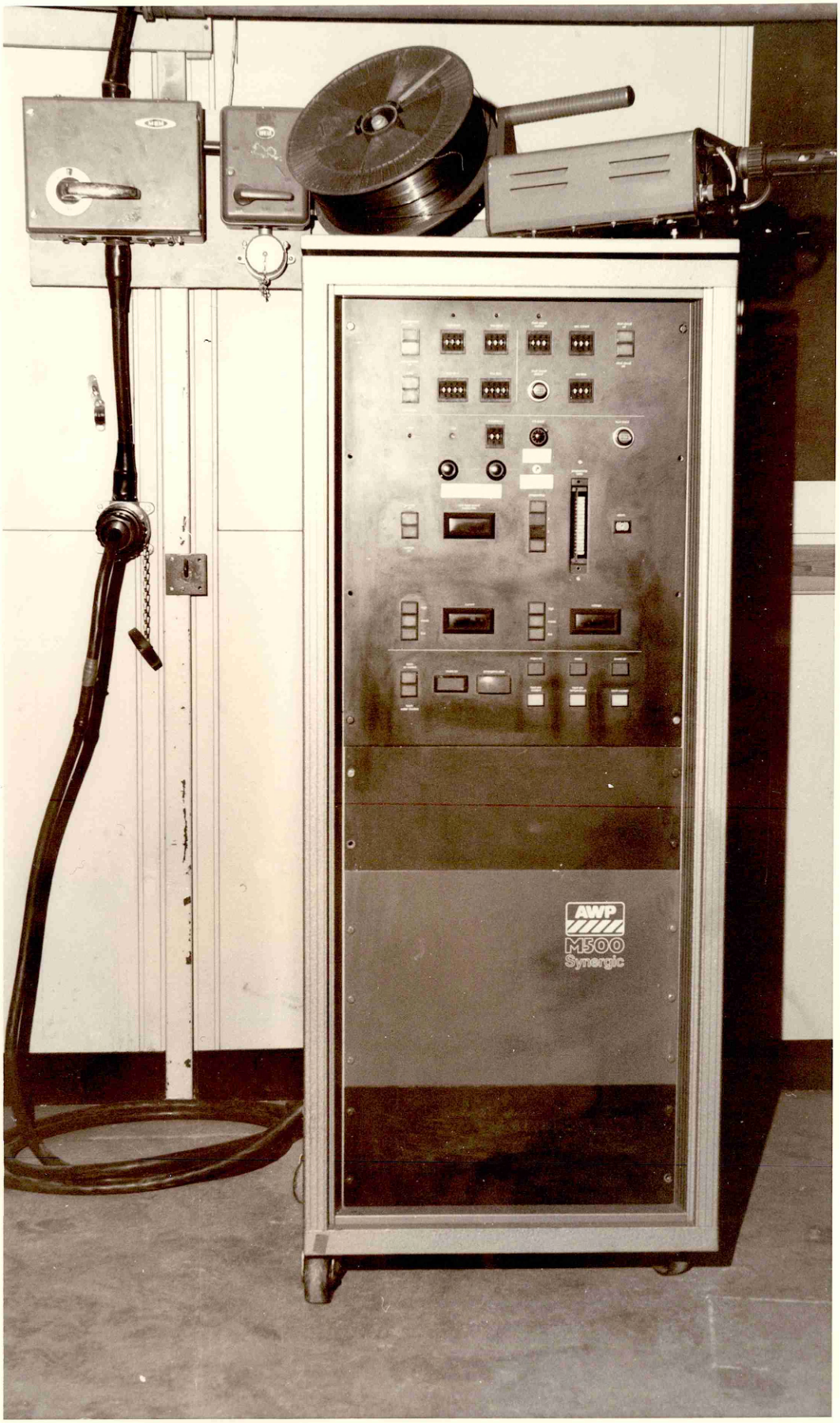

PHOTO 1 - AWP M 500 synergic unit

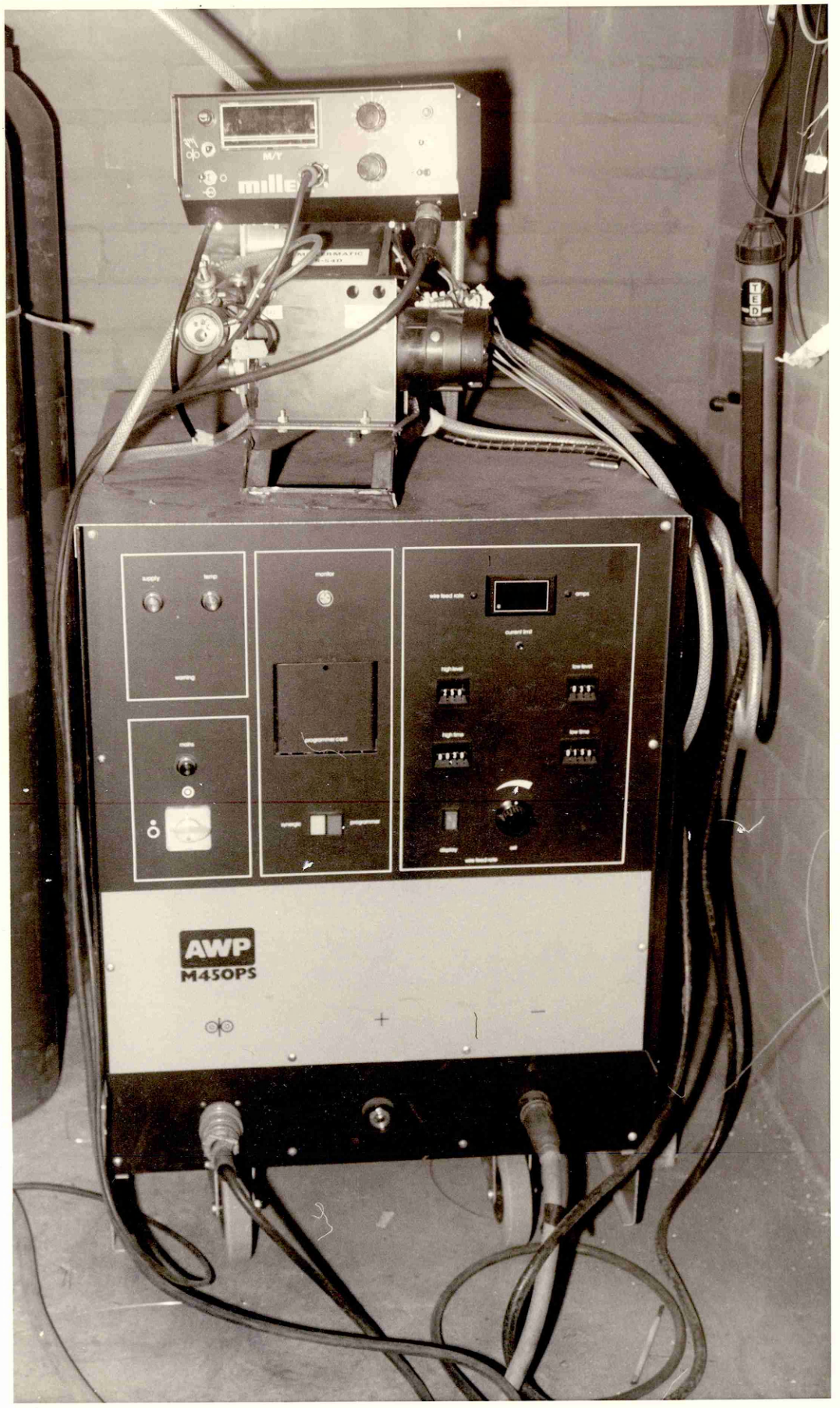

PHOTO 2 - AWP M450 synergic unit

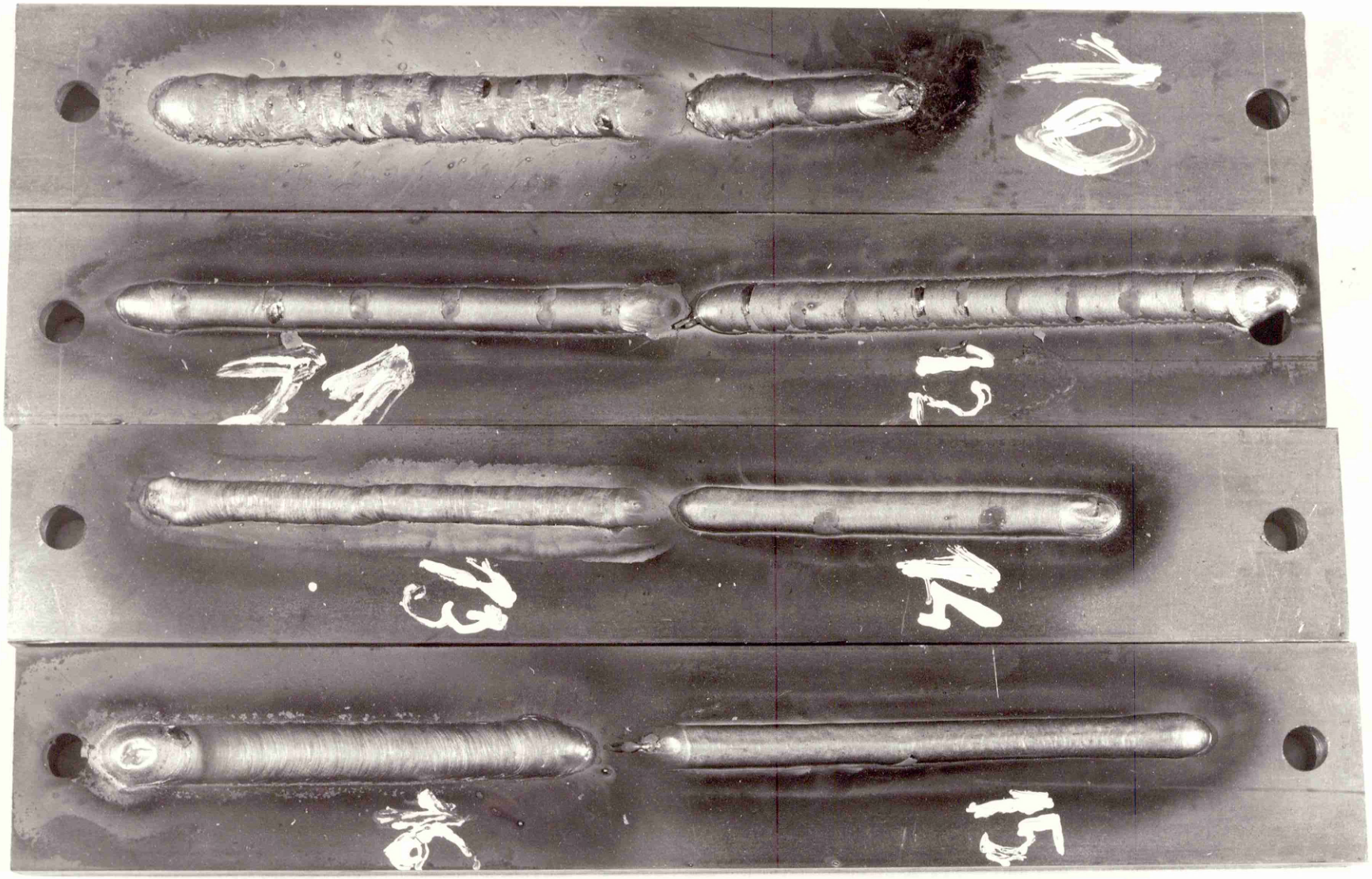

PHOTO 3 - Influence of shielding gas composition on slag formation
(I=100 A, l=15mm, v=1.53mm/s, 1.0 mm wire diameter with 0.82 Si, 1.5 Mn, 0.06 C)

Ar | Ar/1%O_2 | Ar/2%O_2 | Ar/5%CO_2 | Ar/20%CO_2 | CO_2 | Helishield 1

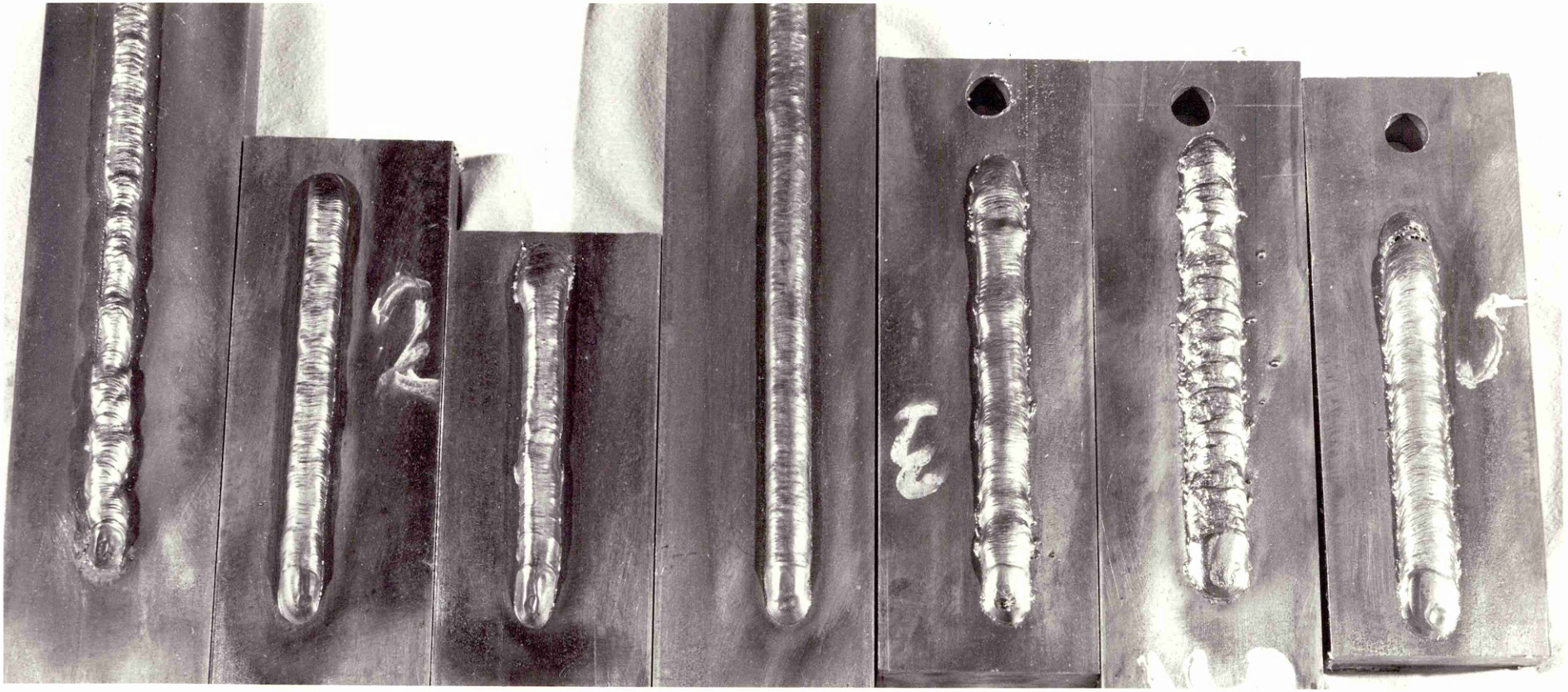

PHOTO 4 - Influence of shielding gas composition on bead appearence
(1.0mm wire diameter, I=100 A, 1=15mm, 25mm plate thickness)

Ar | Ar/1%O_2 | Ar/2%O_2 | Ar/5%CO_2 | Ar/20%CO_2 | CO_2 | Helishield 1

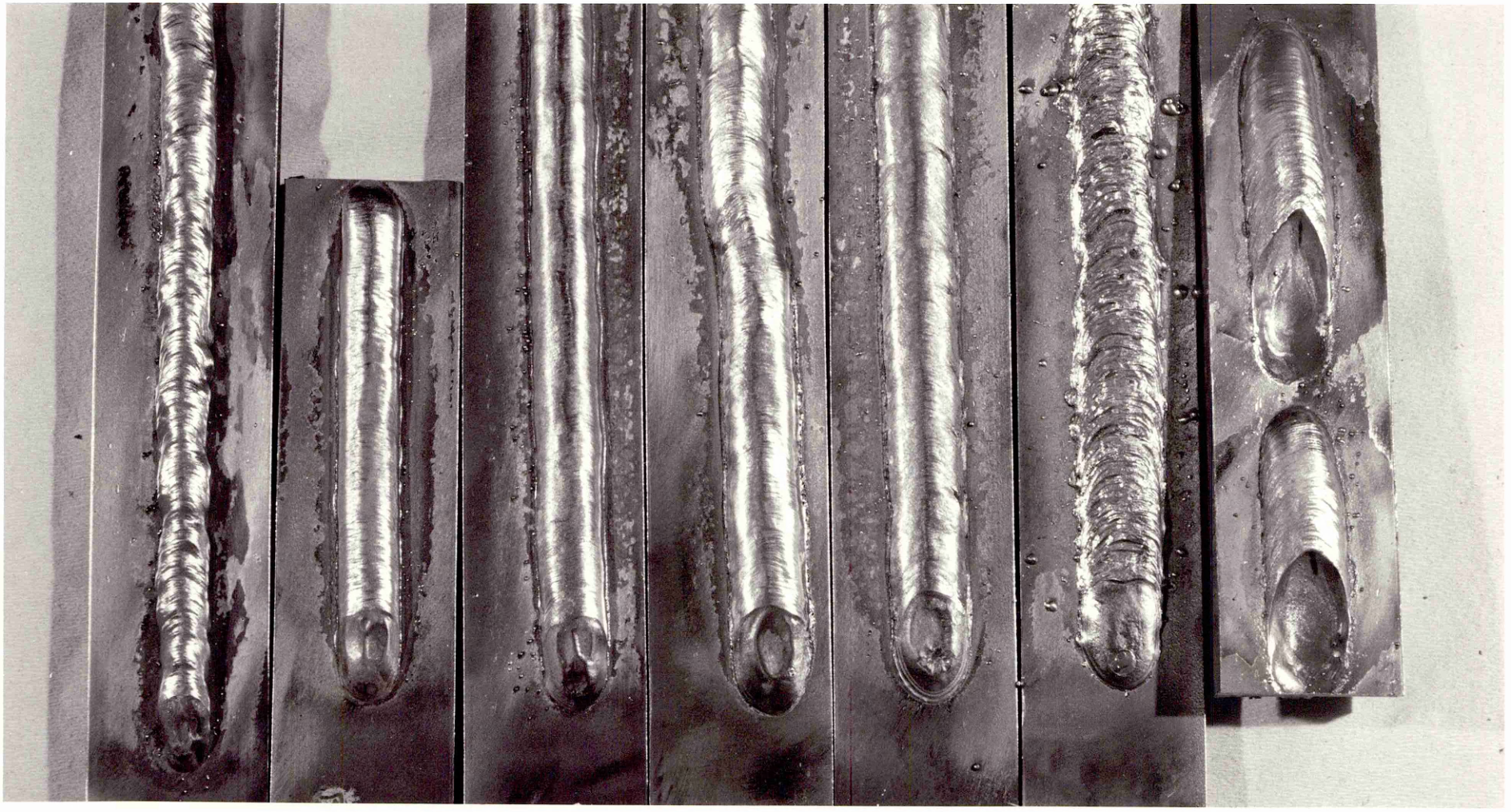

PHOTO 5 - Influence of shielding gas composition on bead appearance
(1.0mm wire, I=100A, l=15mm, 6mm plate thickness)

Ar | Ar/1%O_2 | Ar/2%O_2 | Ar/5%CO_2 | Ar/20%CO_2 | CO_2

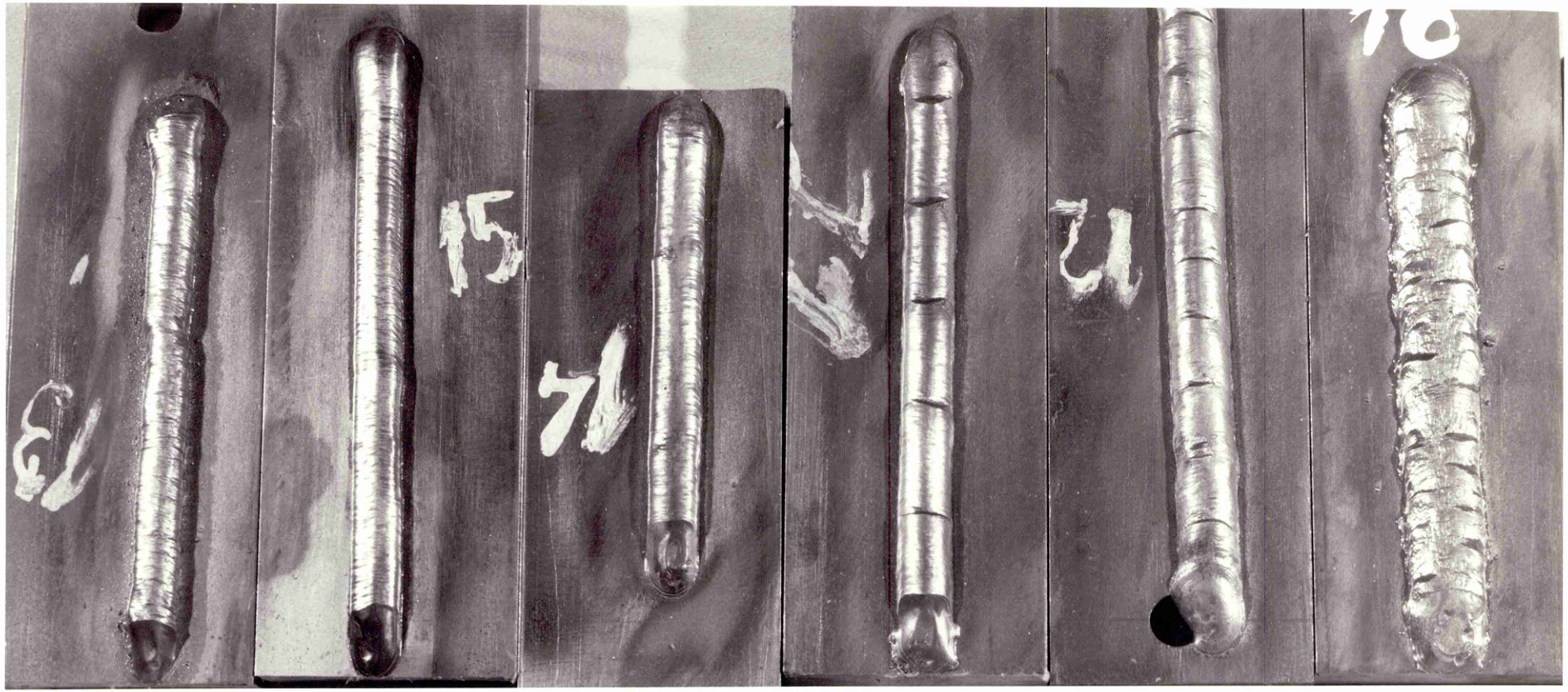

PHOTO 6 - Influence of shielding gas composition on bead appearance
(1.2mm wire, I=100A, l=15mm, 25mm thick plate)

Ar | Ar/1%O_2 | Ar/2%O_2 | Ar/5%CO_2 | Ar/20%CO_2 | CO_2 | Helishield 1

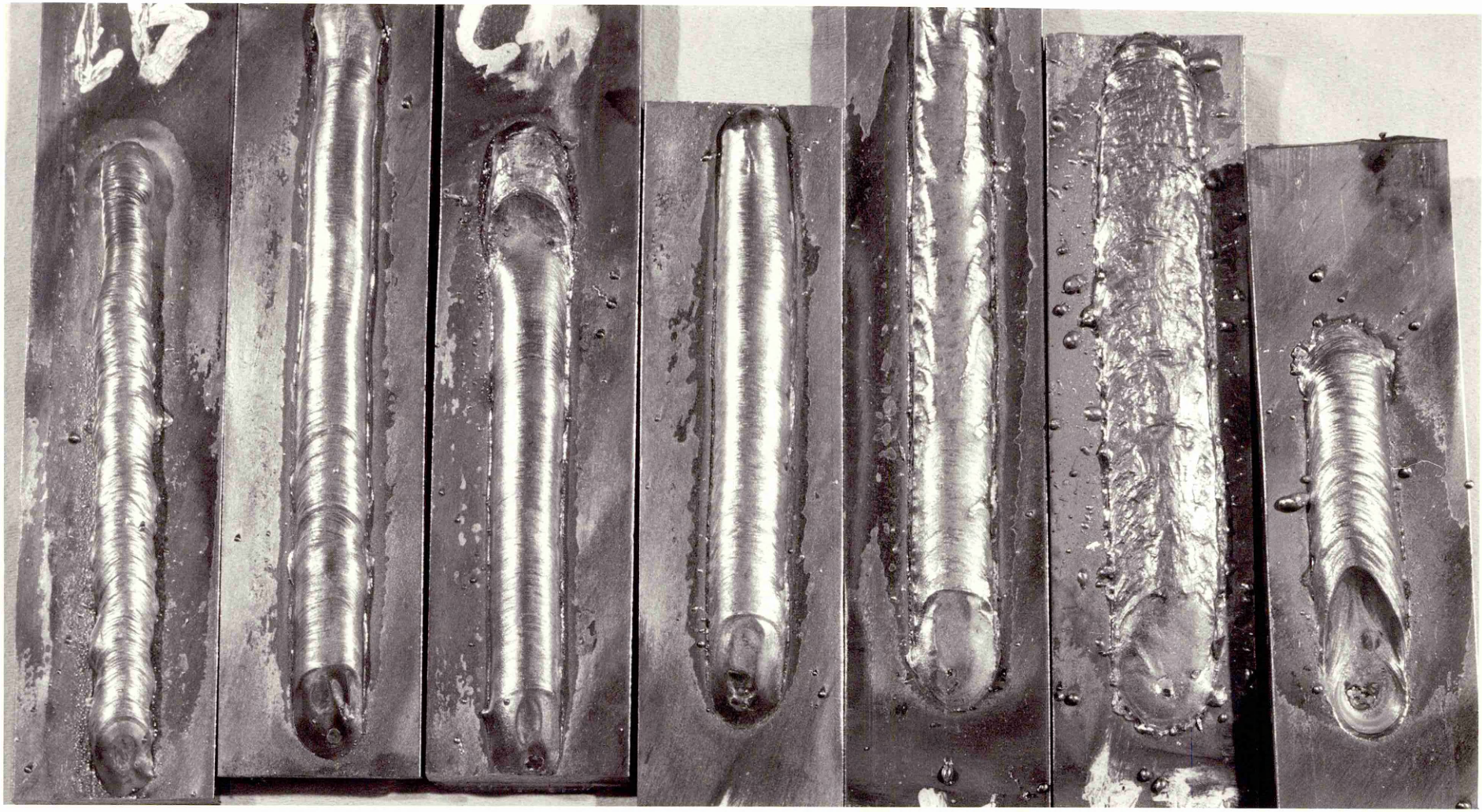

PHOTO 7 - Influence of shielding gas composition on bead appearance
(1.2mm wire, I=100 A, l=15mm, 6mm thick plate)

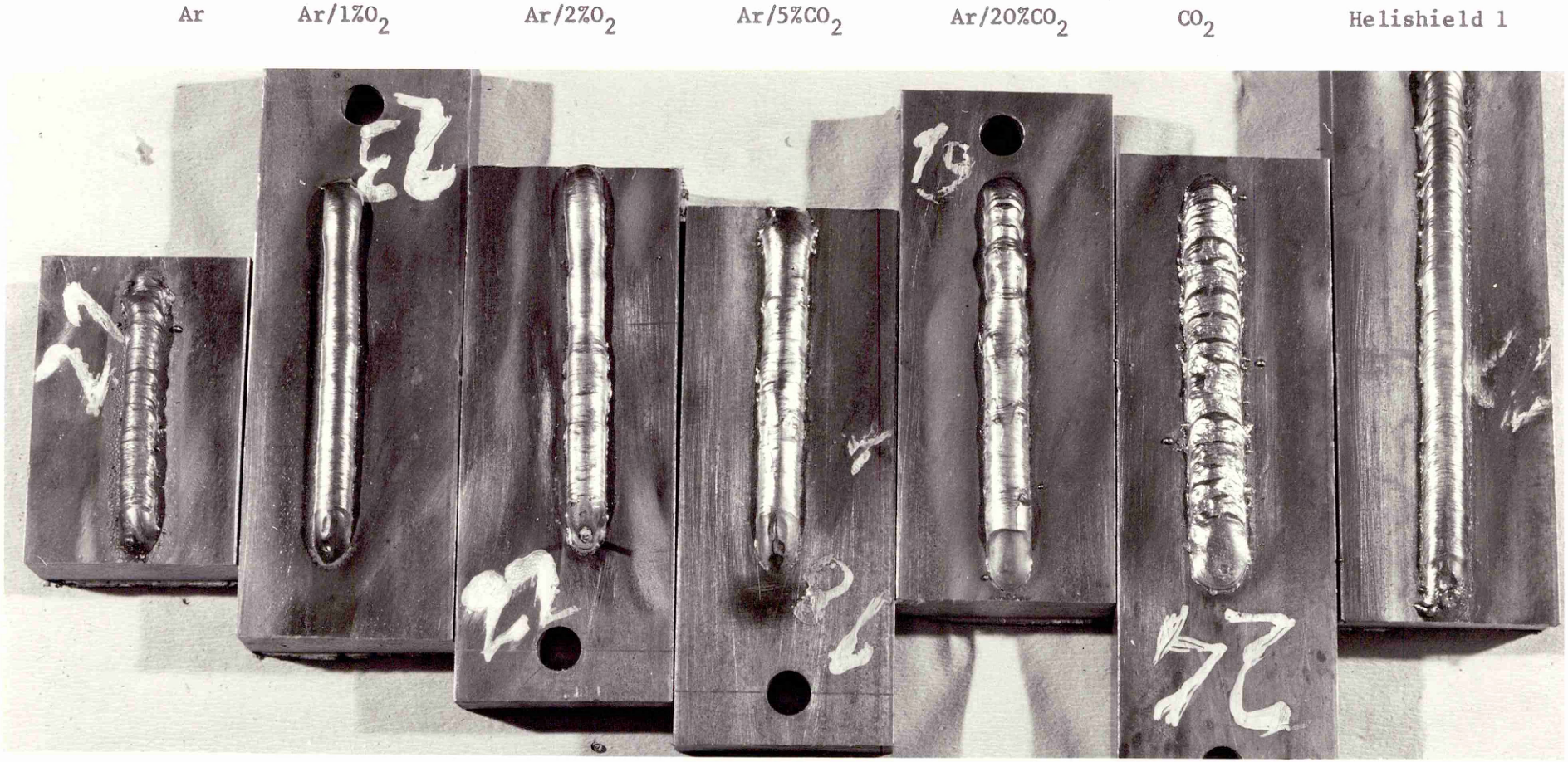

PHOTO 8 - Influence of shielding gas composition on bead appearance
(1.6mm wire, I=100A, 1=15mm, 25mm thick plate)

Ar | Ar/1%O_2 | Ar/2%O_2 | Ar/5%CO_2 | Ar/20CO_2 | CO_2 | Helishield 1

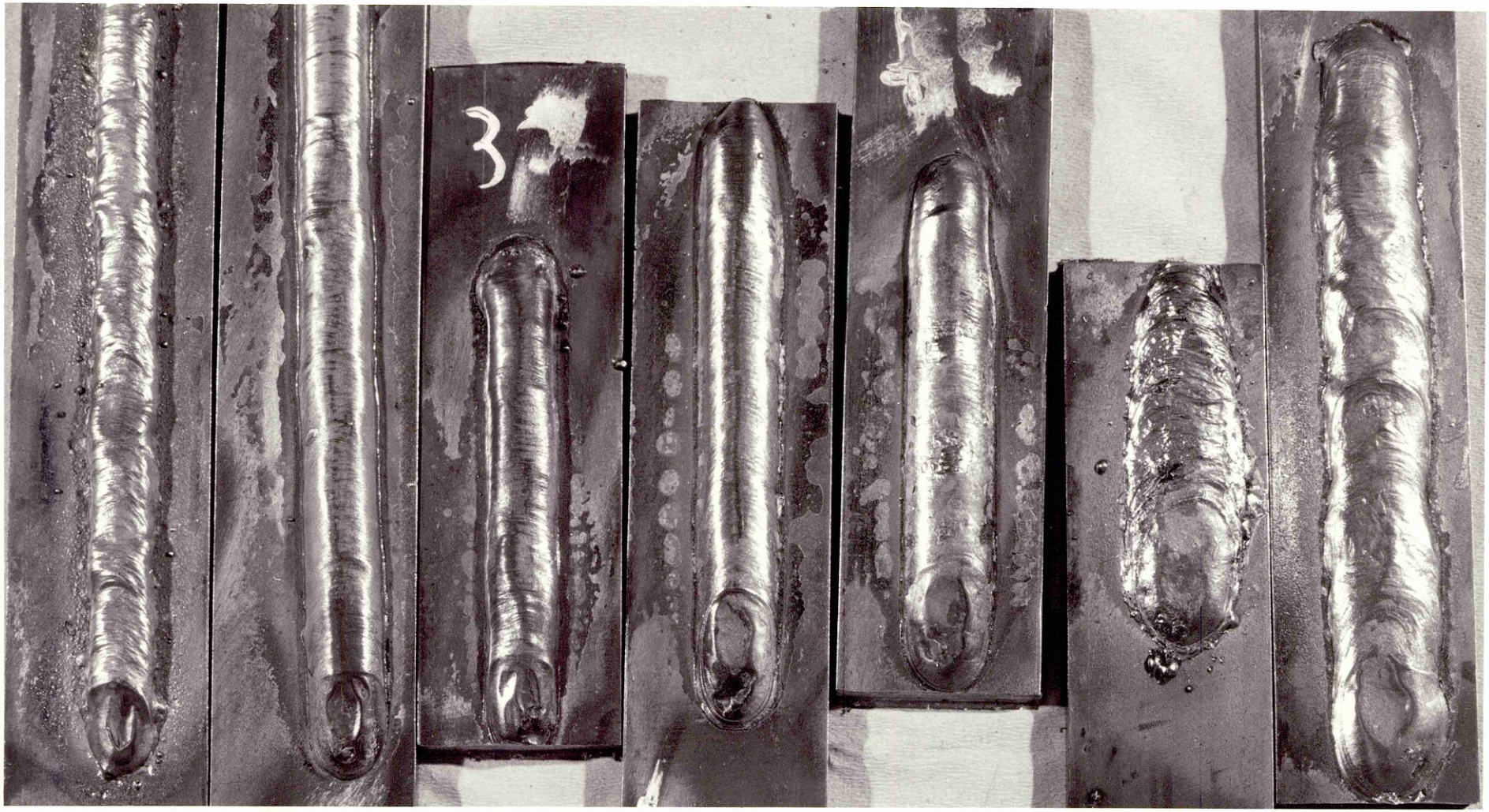

PHOTO 9 - Influence of shielding gas composition on bead appearance
(1.6mm wire, I=100A, l=15mm, 6mm thick plate)

FIGURES

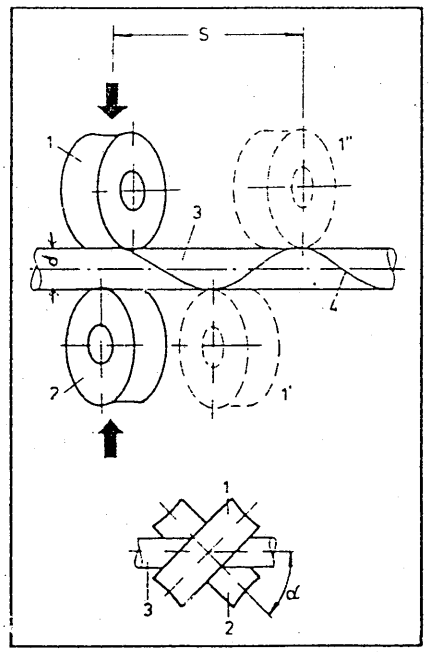

FIG. 1 - The planetary feeding principle: 1 and 2 - rollers; 3 - wire; 4 - thread lines; 5 - length gap for roller 1 to attain initial position again; α - angle between the rollers and the wire; d - wire diameter ($w = 2 \pi d n \tan \alpha$, where n is the speed of the motor) (Ref. 12)

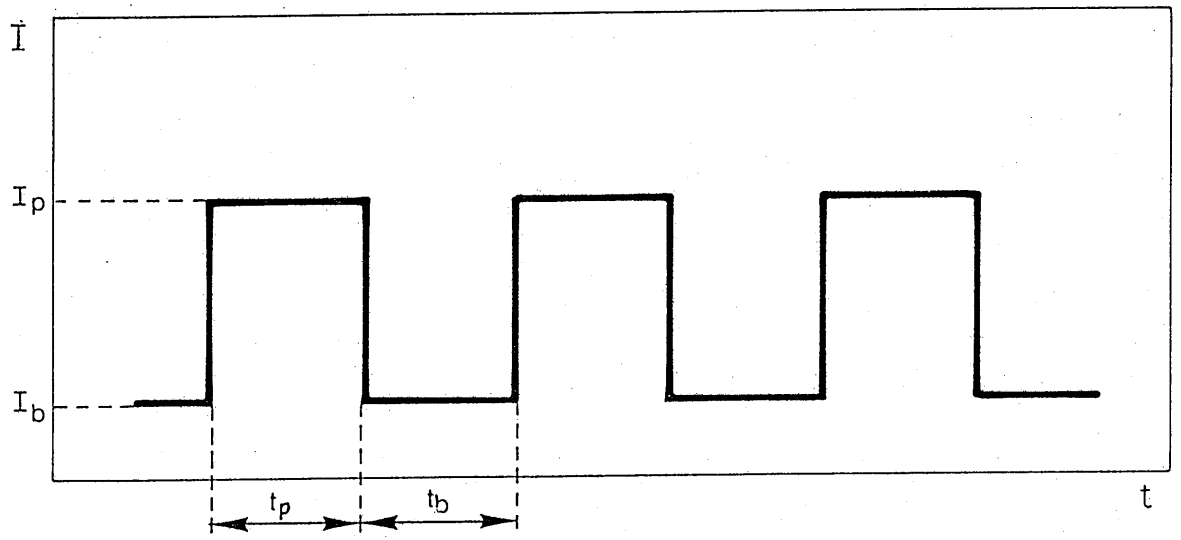

FIG. 2 - Pulsed current wave shape
(I_p - peak current, I_b - background current, t_p - peak time, t_b - background time)

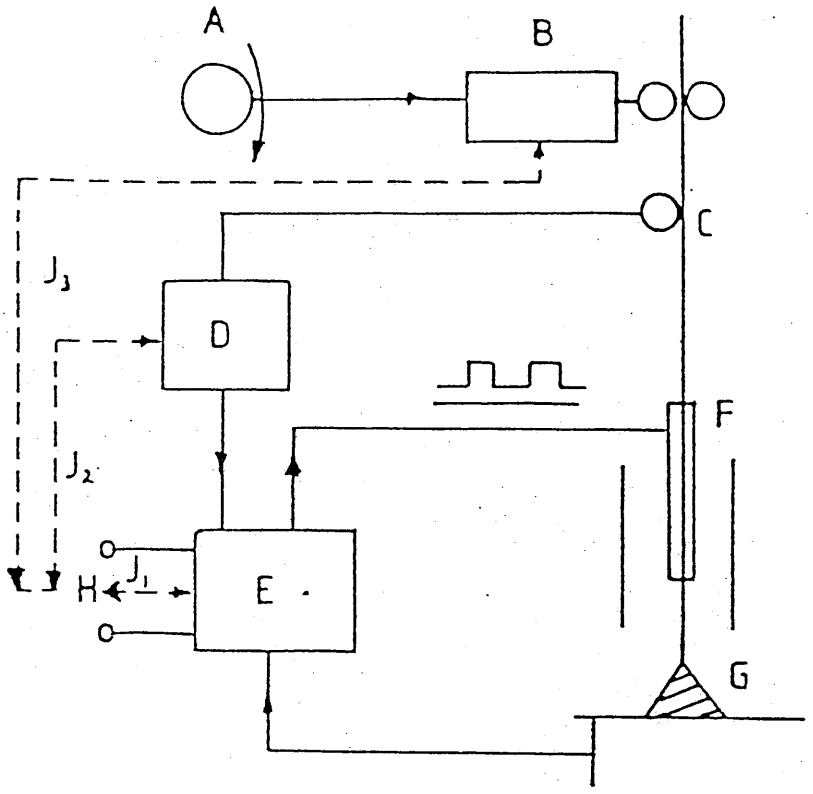

FIG. 3- SYNERGIC CONTROL (Ref. 22)

A - One Knob Control
B - Wire Feed Unit
C - Tacho Generator
D - Control Logic
E - Transistorised Power Supply
F - Contact Tube
G - Arc
H - Arc Voltage Sensor
J - Possible Voltage Feed Back Loops
for Arc Length Control

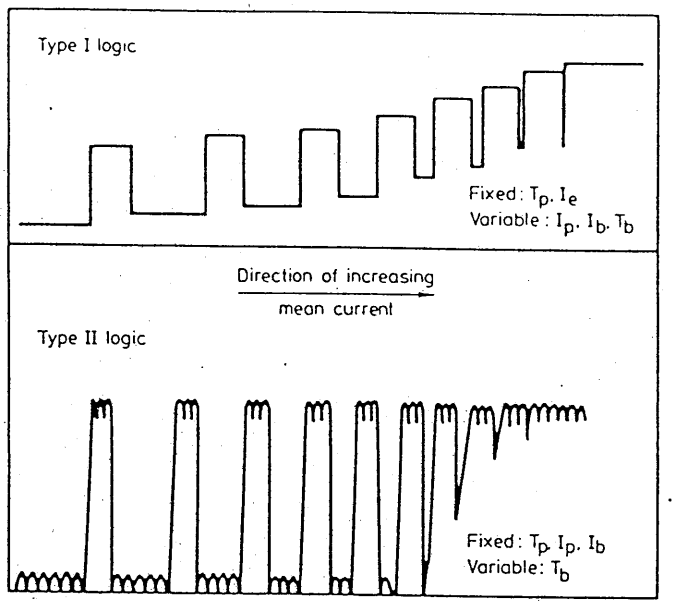

FIG. 4 - Changes in pulse shape as mean current is continuosly increased for synergic logics (Ref. 23)

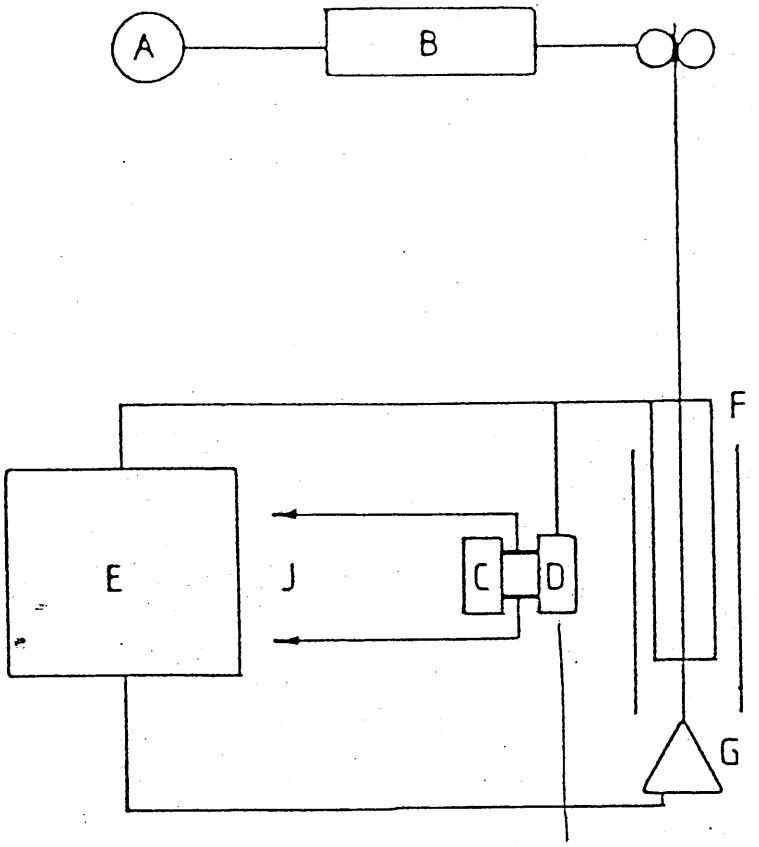

FIG. 5 - SELF REGULATING CONTROL (Ref. 22)

A - One Knob Control
B - Wire Feed Unit
C - Pre-Set Voltage Reference
D - Arc Voltage
E - Power Supply
F - Contact Tip
G - Arc
J - Voltage Error Signal (C-D) Used as a Command Signal to Power Supply (This usually controls pulse repeat frequency for constant I_p, I_b, T_p)

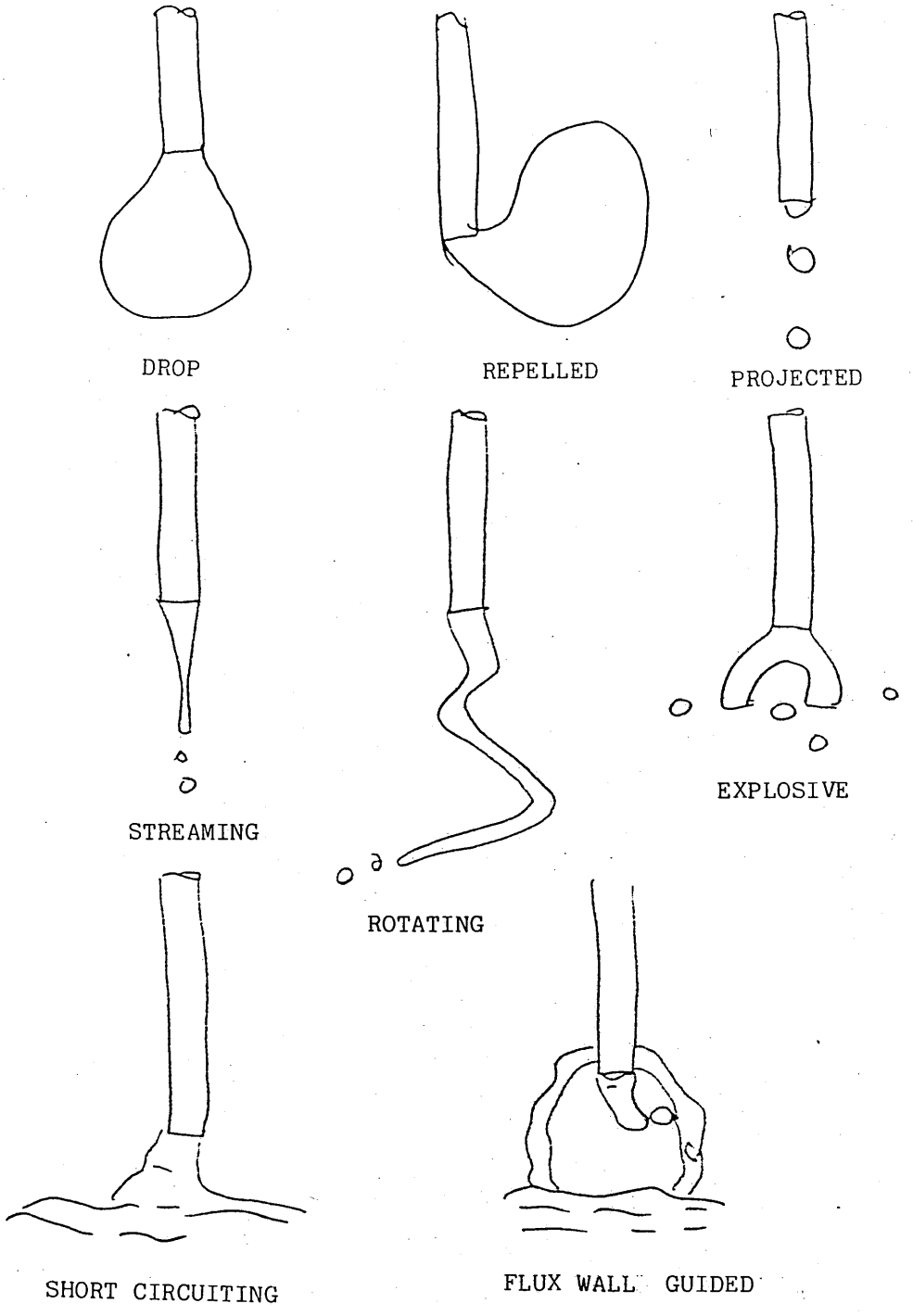

FIG. 6 - Metal Transfer Modes According to IIW Classification (Ref. 32)

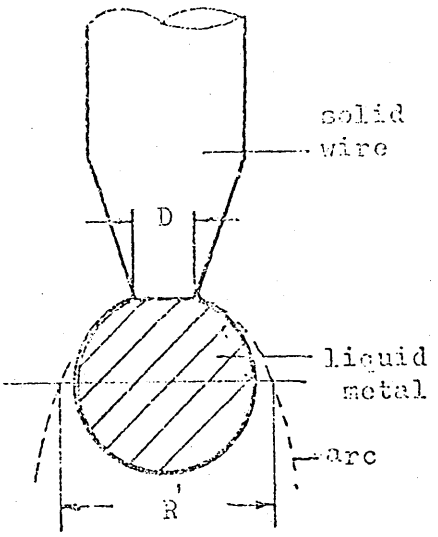

FIG. 7 - Model of drop spray transfer mechanism
(Ref. 43)

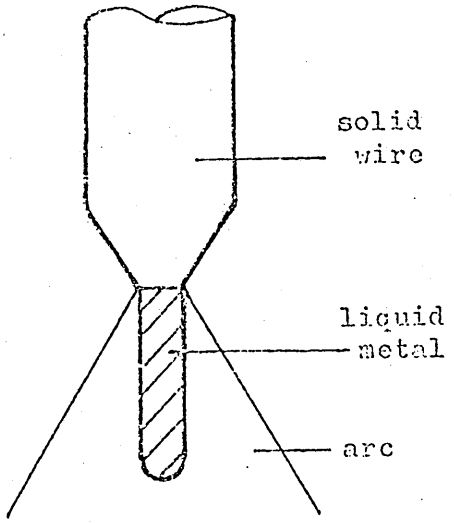

FIG. 8 - Model of stream spray transfer mechanism
(Ref. 43)

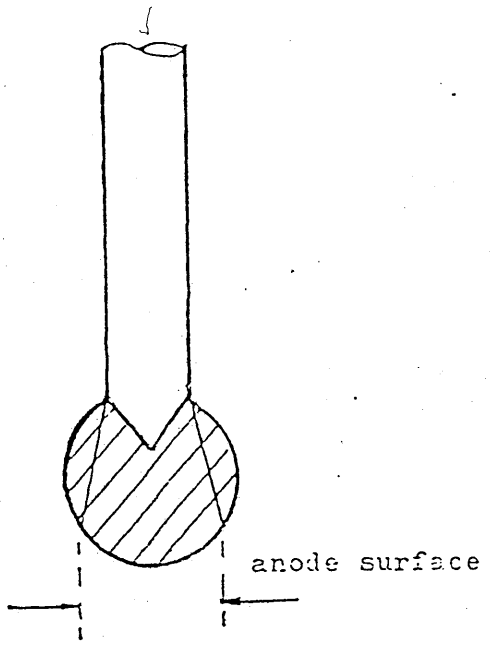

FIG. 9 - Model of globular transfer mechanism (Ref. 44)

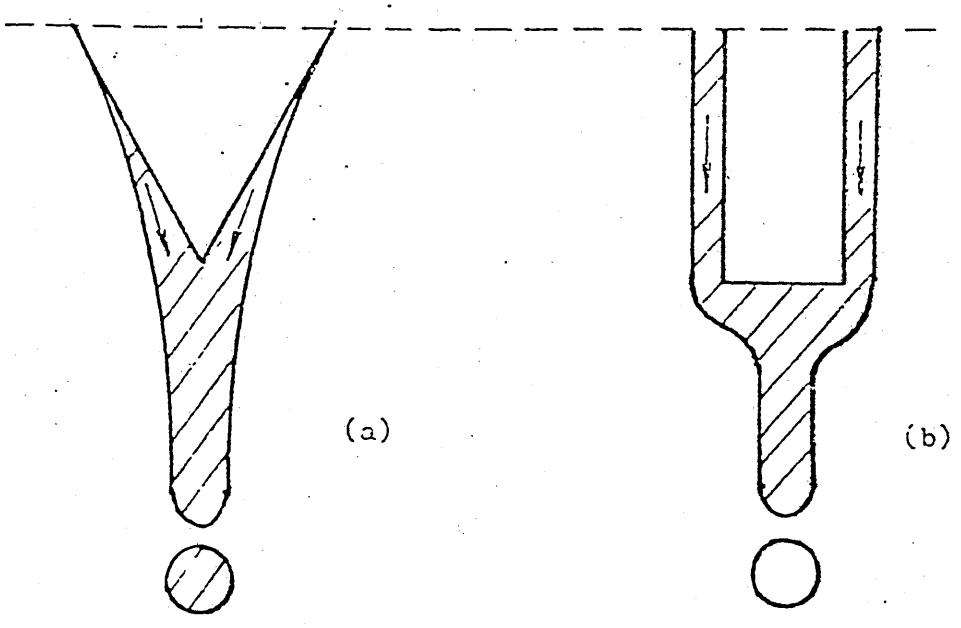

FIG. 10 - Model of spary transfer mechanism (Ref. 44)

(a) The real tip; a continuos flow of liquid metal goes downwards along the conical tip of the wire

(b) The model of spray transfer, the conical tip is replaced by a cylinder having the same length

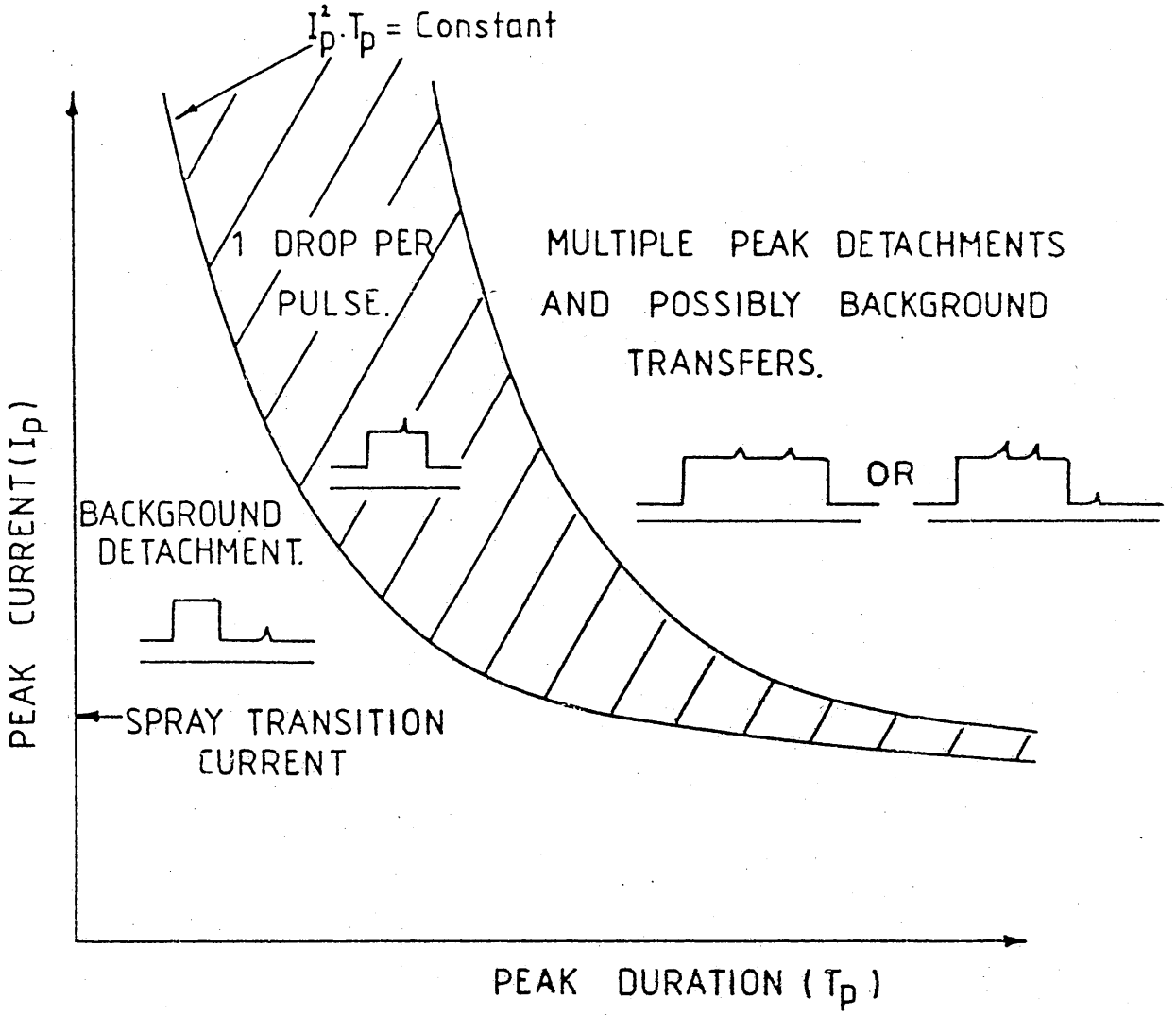

FIG. 11 - Influence of peak parameters on metal transfer (Ref. 22)

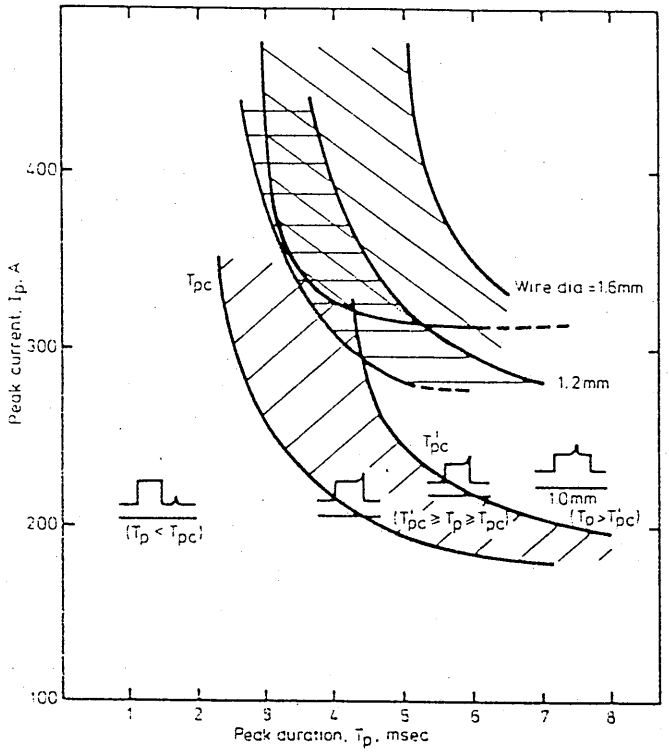

FIG. 12 - Influence of peak parameters on droplet detachment for mild steel wire in Ar/5% CO_2 for different wire diameters (ref. 23)

(T_{pc} and T'_{pc} are limits for one drop per peak detachments)

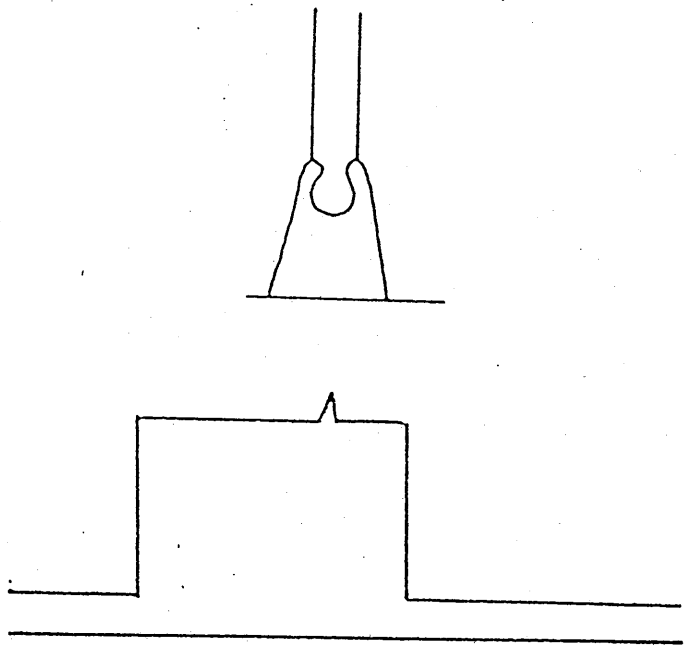

One drop per peak

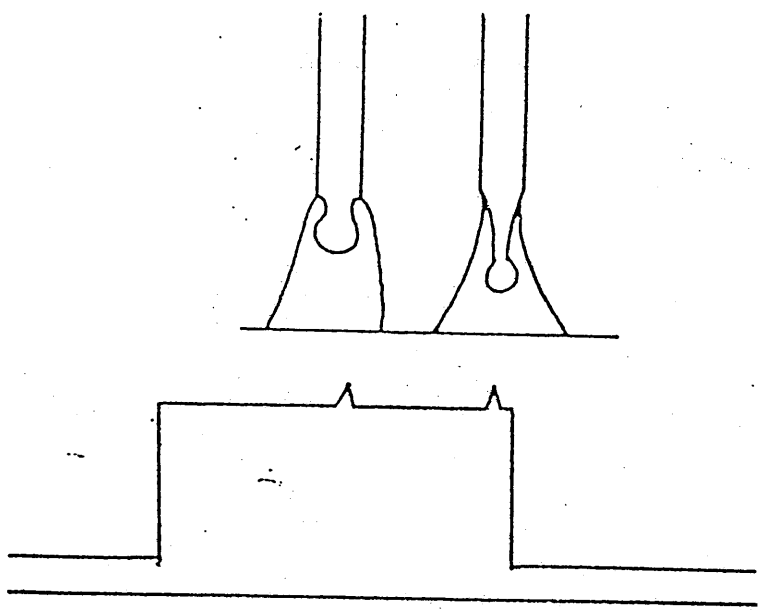

Two drops per peak

FIG. 13 - Possible difference between first and second detachments when two drops detach per peak (Ref. 22)

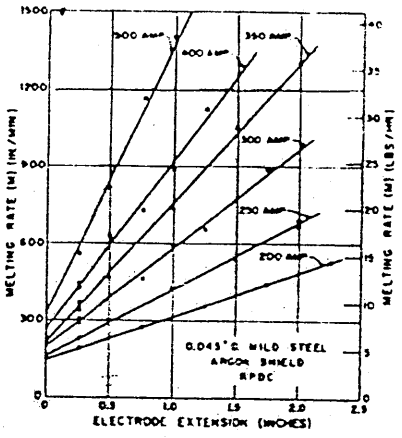

FIG. 14 - Effect of electrode extension and welding current on the electrode melting rate (Ref. 60)

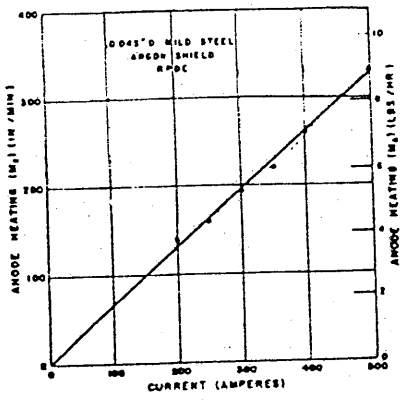

FIG. 15 - Effect of welding current on anode heating as measured by melting rate (Ref. 60)

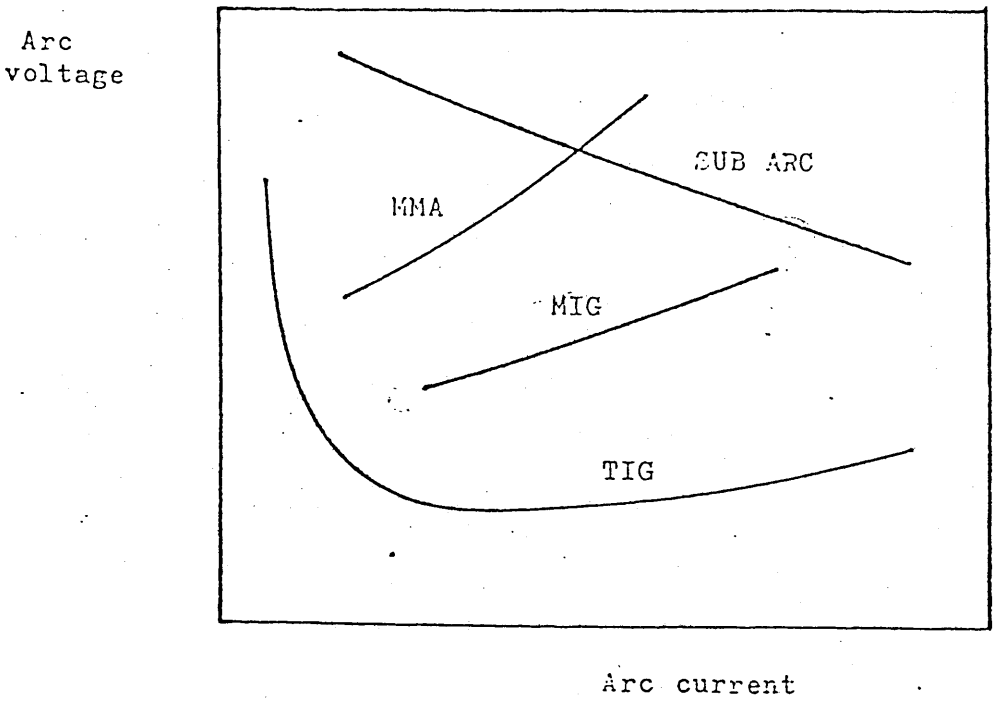

FIG. 16 - Typical arc characteristics of different processes

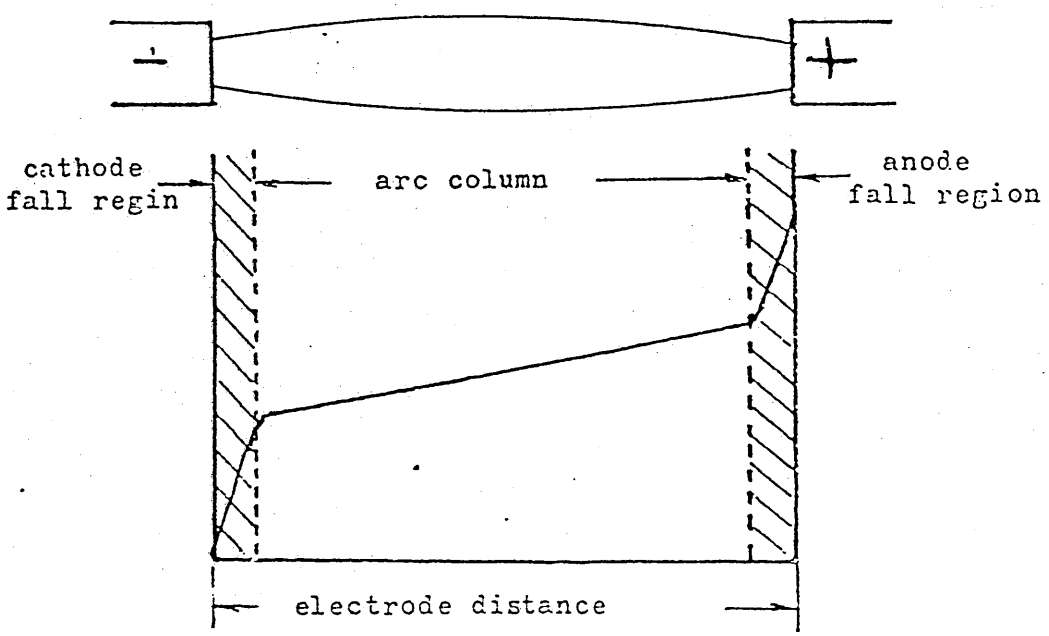

FIG. 17 - Schematic representation of the three different regions of the electric arc

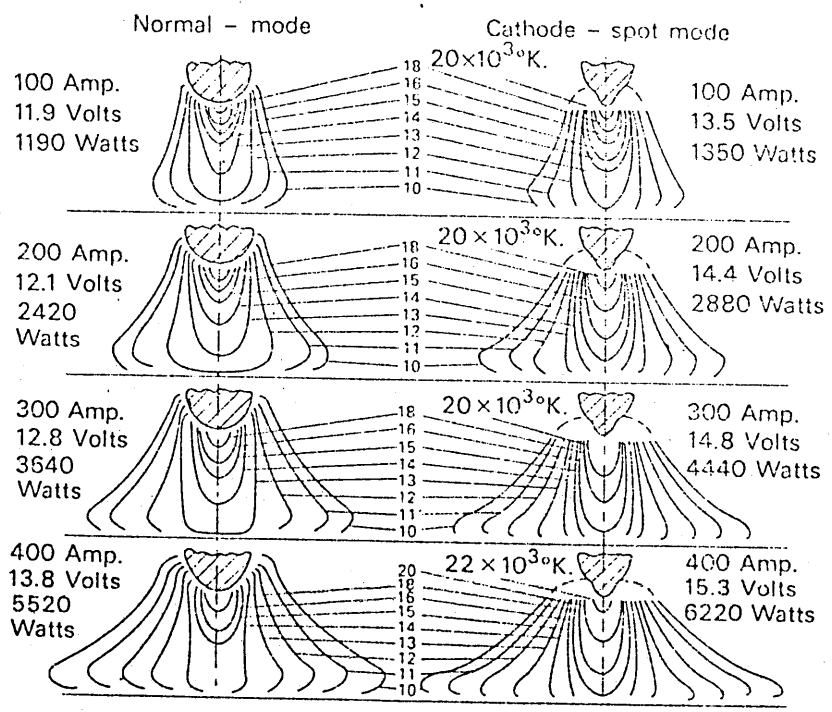

FIG. 18 - Isotherm maps of argon arcs.
(Jackson 1960)

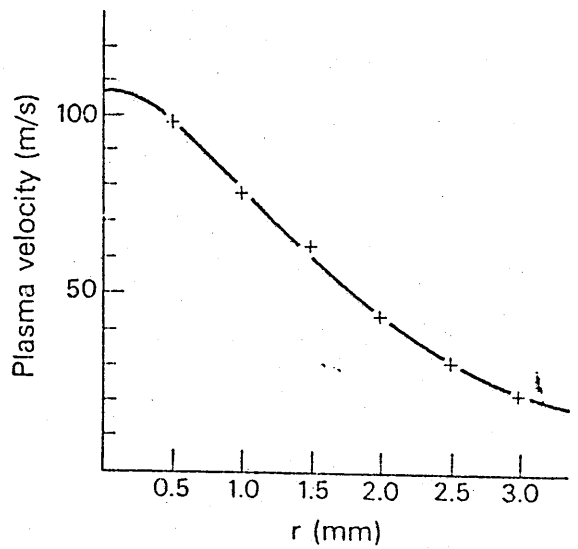

FIG. 19 - Axial velocity distribution in centre plane of arc.
(Seeger et al 1979).

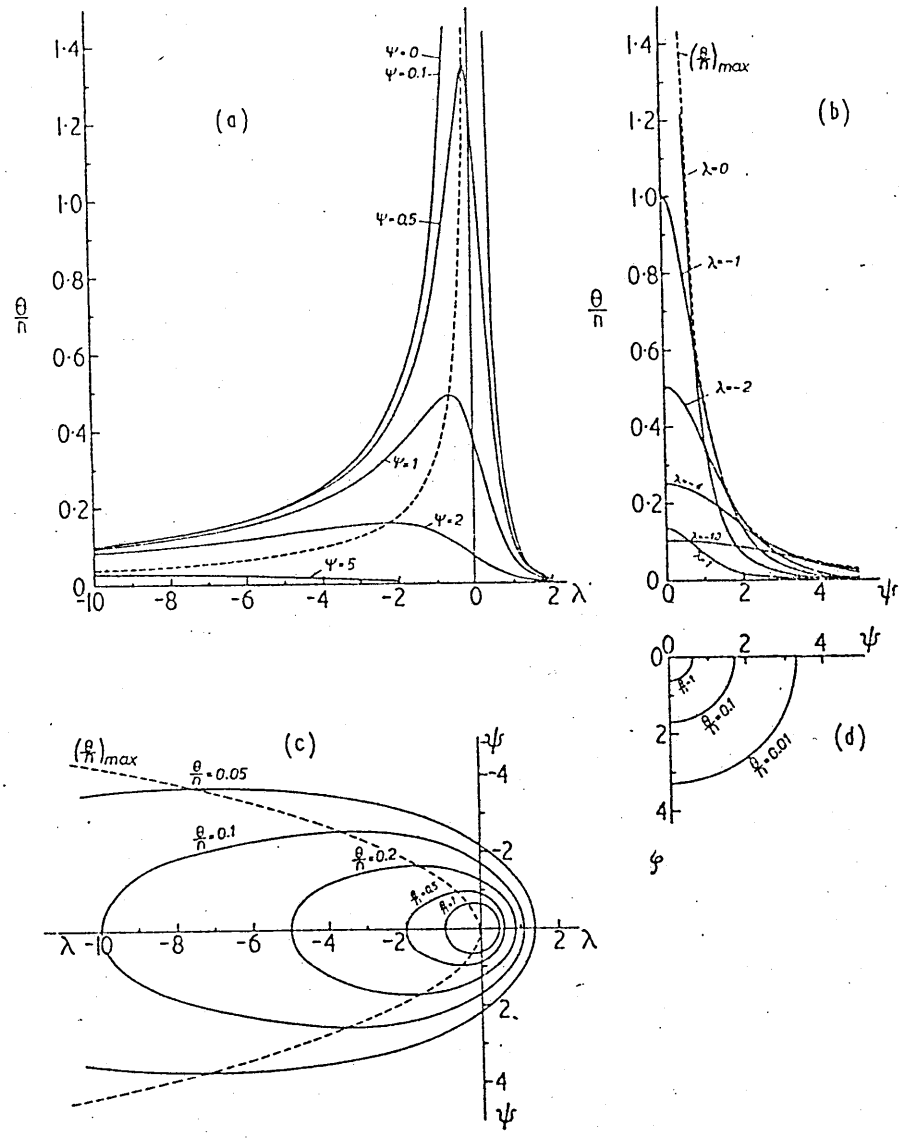

FIG. 20 - Dimensionless temperature distribution for point sources (ref. 102)

(a) Vertical sections parallel to the λ axis;
(b) Vertical sections parallel to the Ψ axis;
(c) Isotherms in the λ -Ψ plane at ζ = 0;
(d) Isotherms in the Ψ -ζ plane at λ = 0

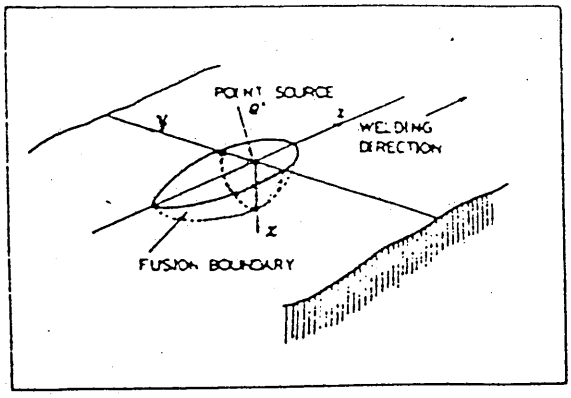

FIG. 21 - Physical situation for a steady state fusion boundary problem around moving point source and coordinate system (ref. 90)

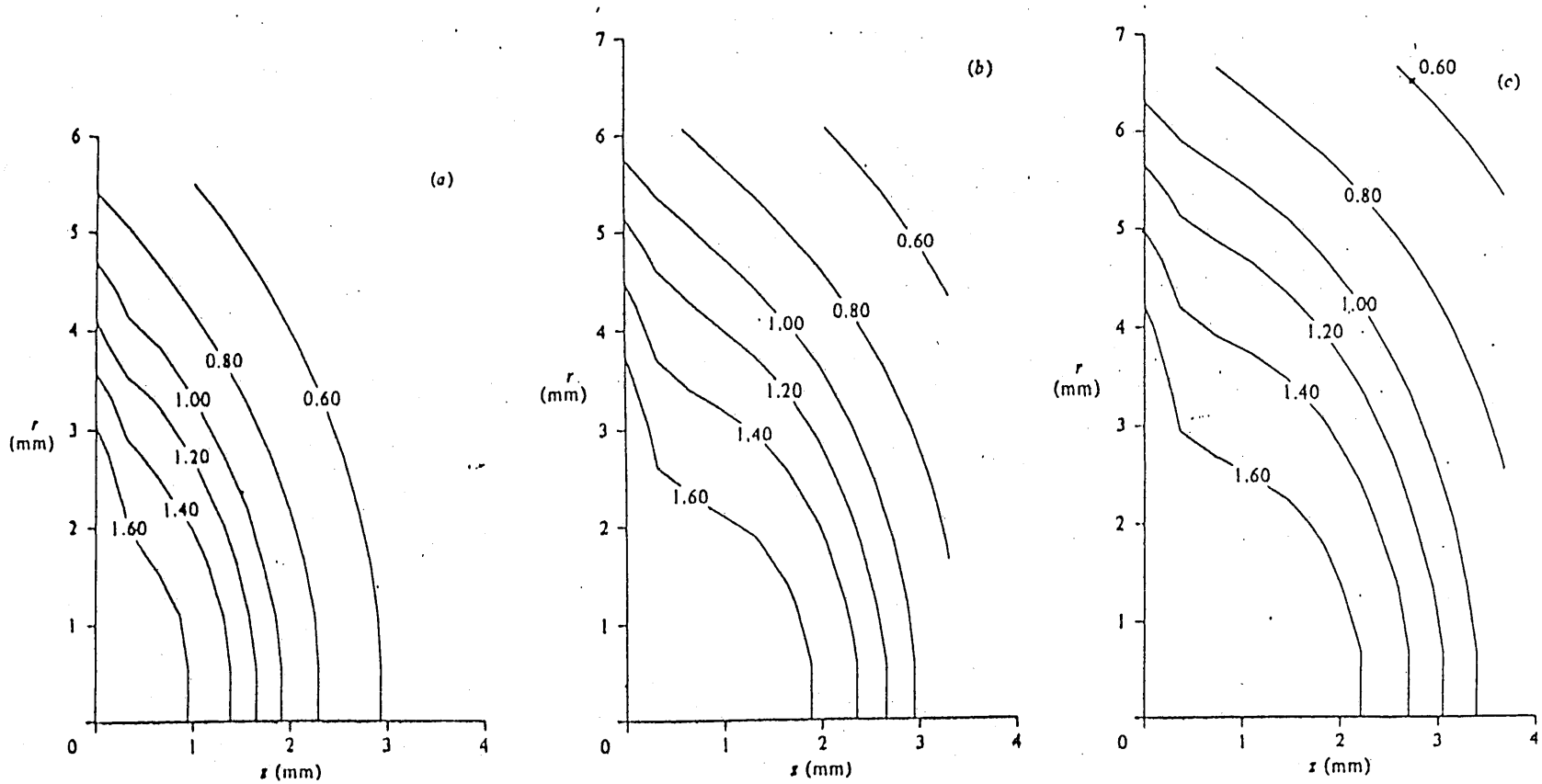

FIG. 2.2- Temperature profiles for combined buoyancy, electromagnetically and surface--tension-driven flow (normal-mode type of operation , $\delta\gamma/\delta T = 0.01$): (a) at 2.5 s; (b) 5 s; (c) 8s. (Ref.87)

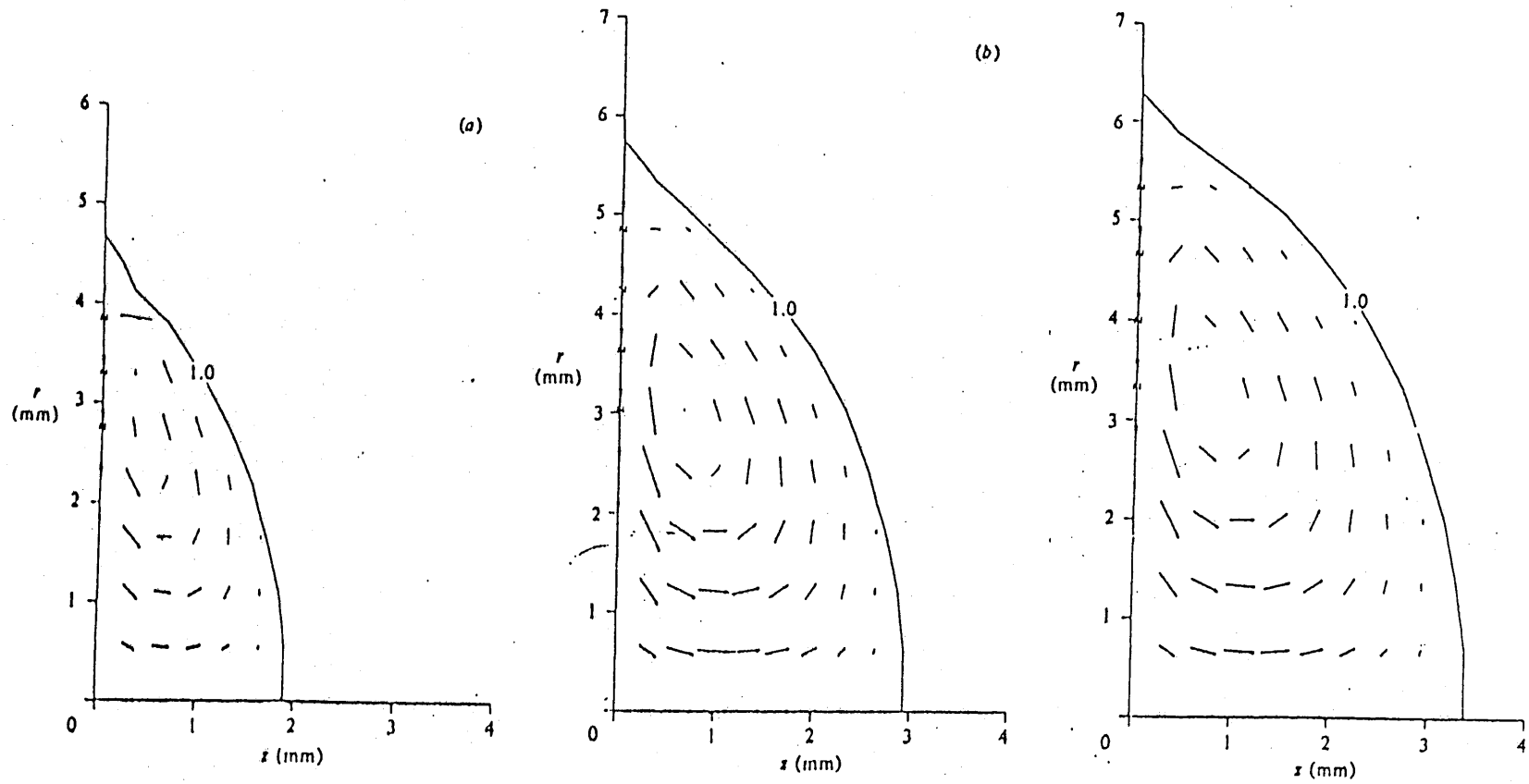

FIG. 23 - Velocity field for combined buoyancy, electromagnetically and surface-tension-driven flow (normal-mode type of operation, $\delta\gamma/\delta T = 0.01$): (a) at 2.5; (b) 5s; (c) 8s. (ref. 87)

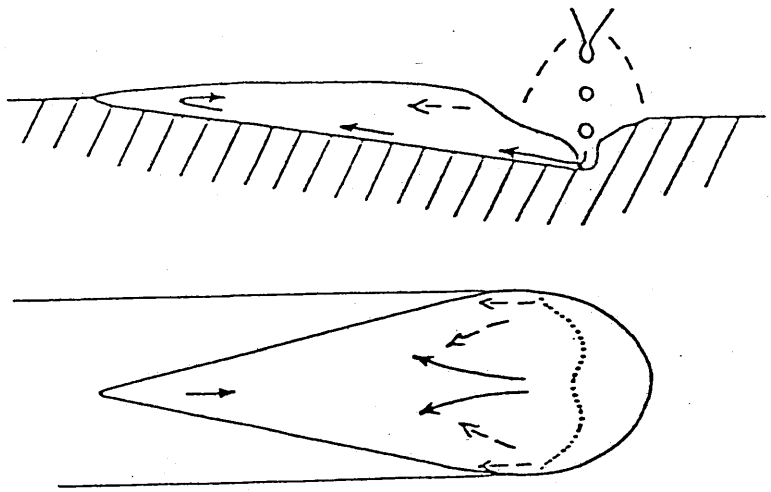

FIG. 24 - Flow of metal in the weld pool for GMAW. Full-line arrows-filler metal mixed with base metal from lower part of crater, dashed arrows - mainly base metal, dotted line - boundary between melted and solidifying metal (ref. 97)

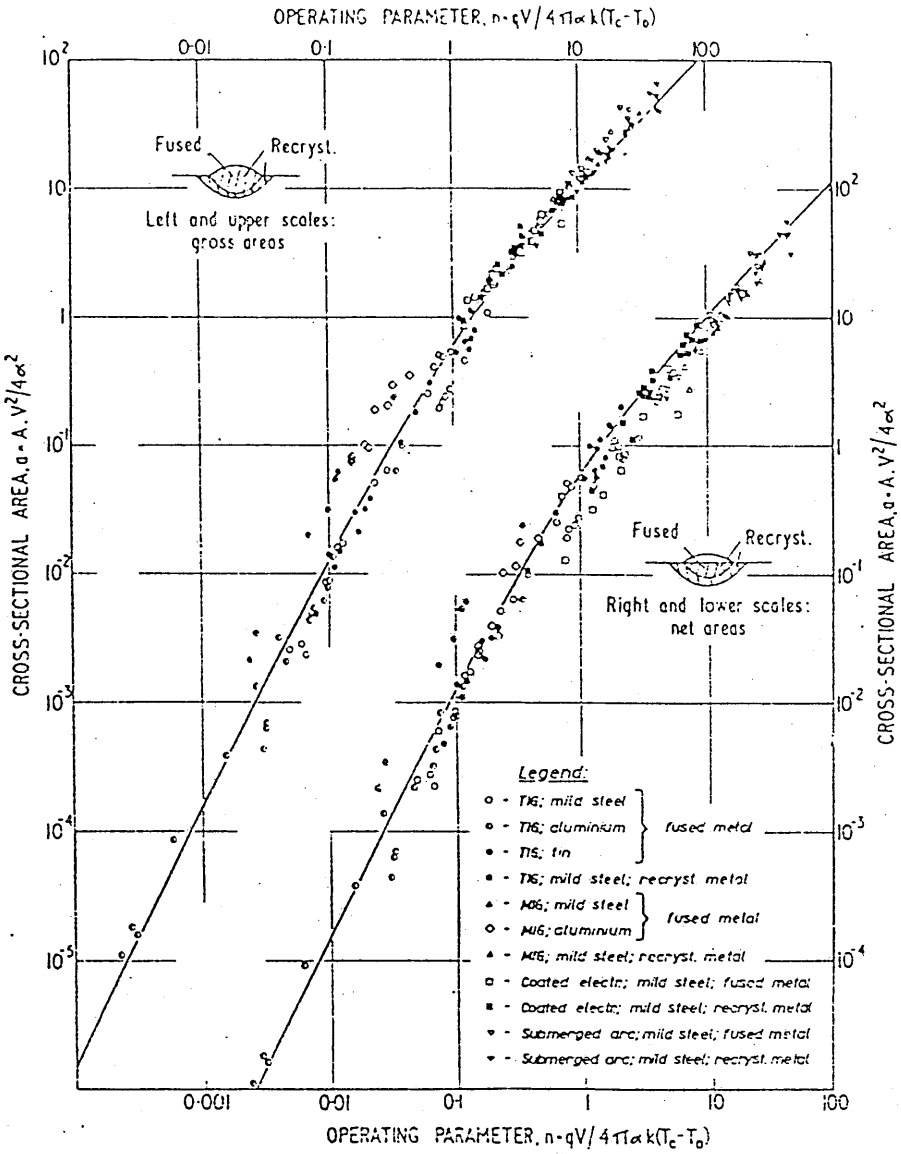

FIG. 25 - Fused metal and recrystalized metal cross-sections, calculated from equations 44, 45, 46 (ref. 102)

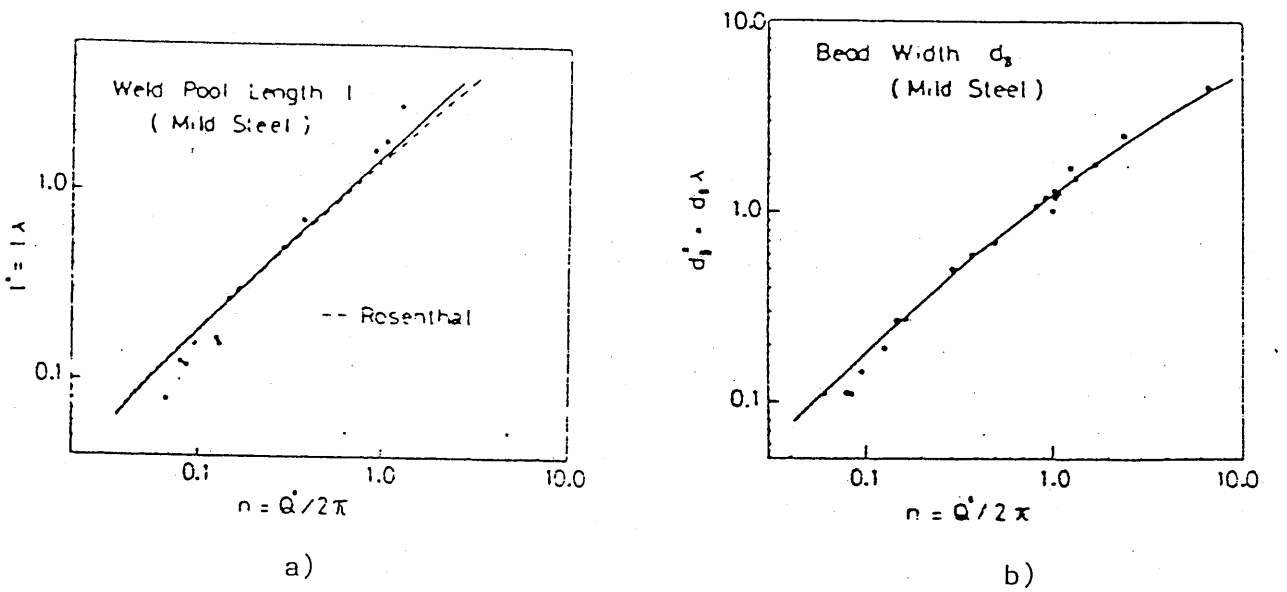

FIG. 26 - a) Comparison between computed and experimental molten pool length
b) Comparison between the computed and experimental width of the fusion boundary versus operating parameter n = Q/2 π
(Experimental plots are quoted from Christensen's data - ref. 90)

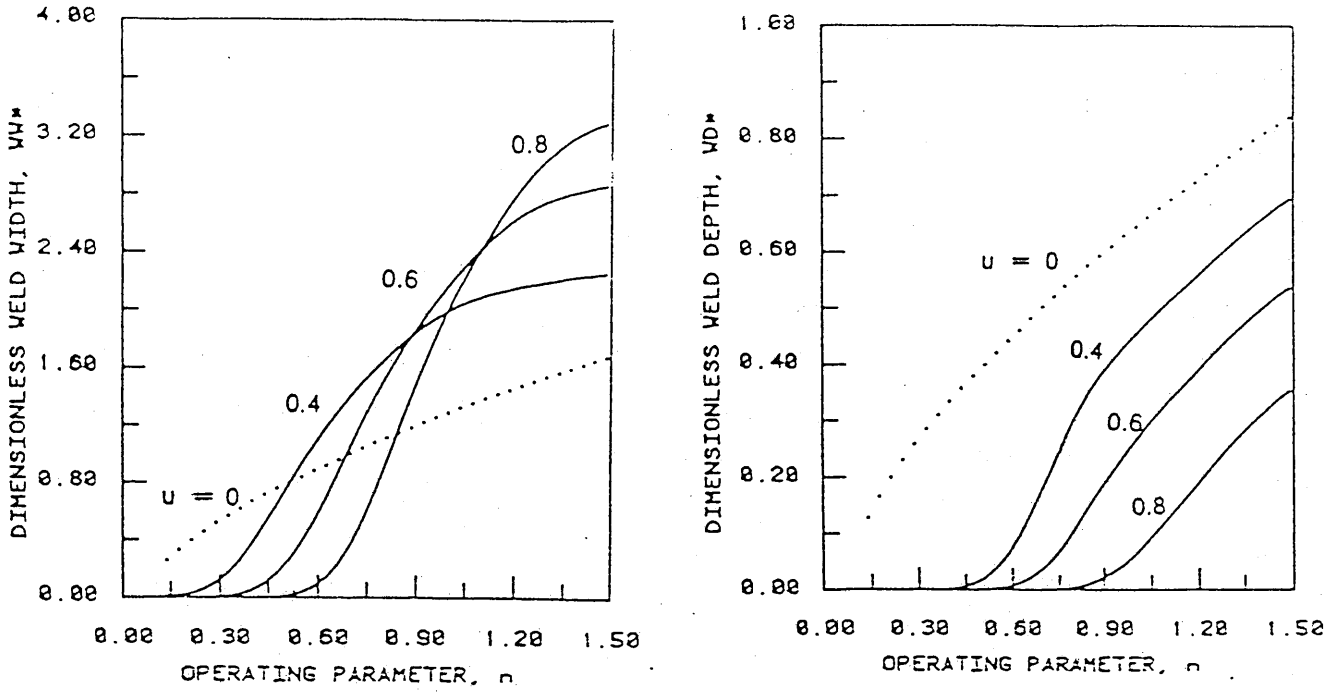

a) b)

FIG. 27 - a) Dimensionless weld width WW versus operating parameter, n, as a function of the dimensionless distribution parameter, u

b) Dimensionless weld depth WD vs. operating parameter, n, as a function of the dimensionless parameter, u. (Ref. 98)

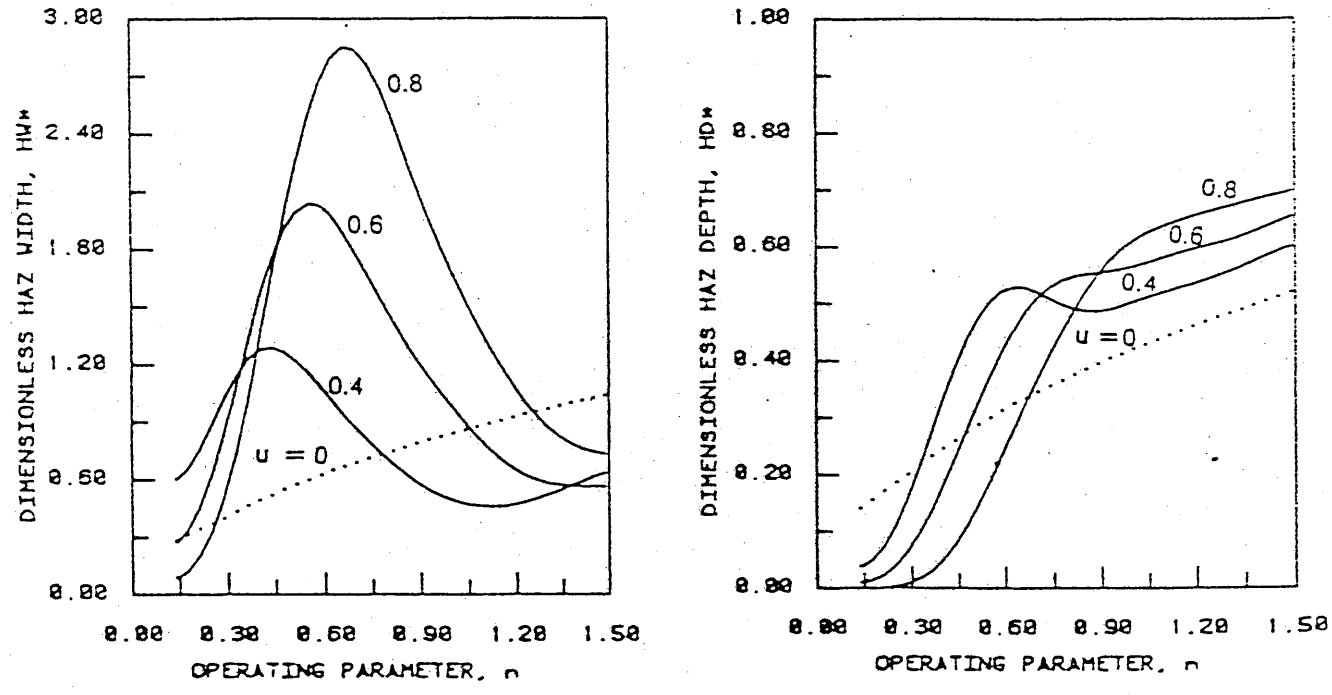

a) b)

. 28 - a) Dimensionless width of the heat affected zone, HW vs. operating parameter, n, as a function of the dimensionless distribution parameter, u

b) Dimensionless depth of the heat affected zone HD vs. operating parameter, n, as a function of the dimensionless distribution parameter, u (Ref. 98)

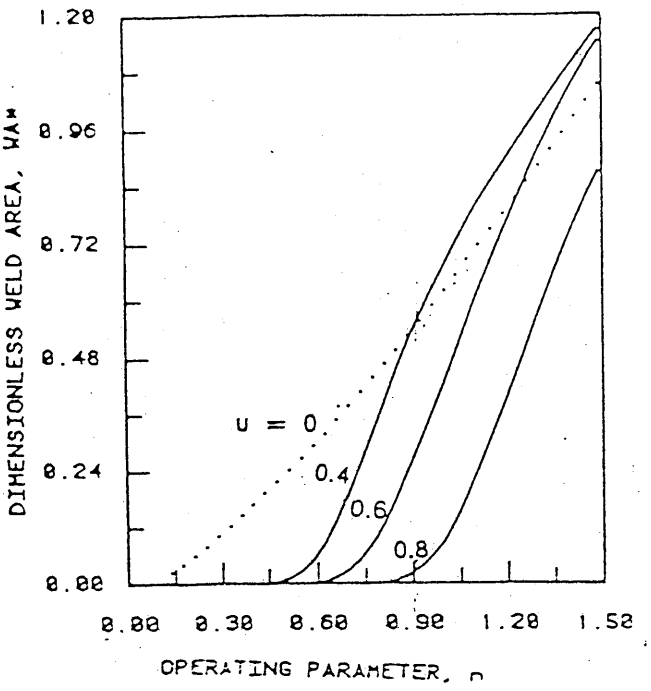

FIg. 29 - Dimensionless area of the weld metal WA vs. operating parameter, n, as a function of the dimensionless distribution parameter, u (Ref. 98)

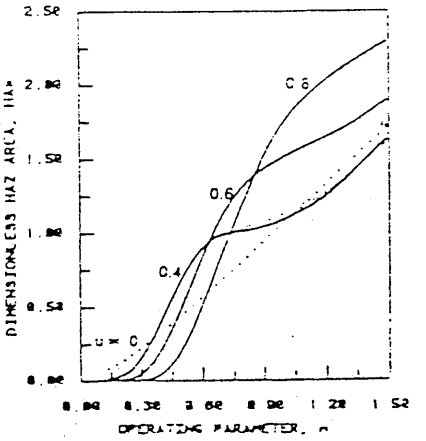

FIG. 30 - Dimensionless area of the heat-affected zone, HA Vs. operating parameter, n, as a function of the dimensionless distribution parameter, u (Ref. 98)

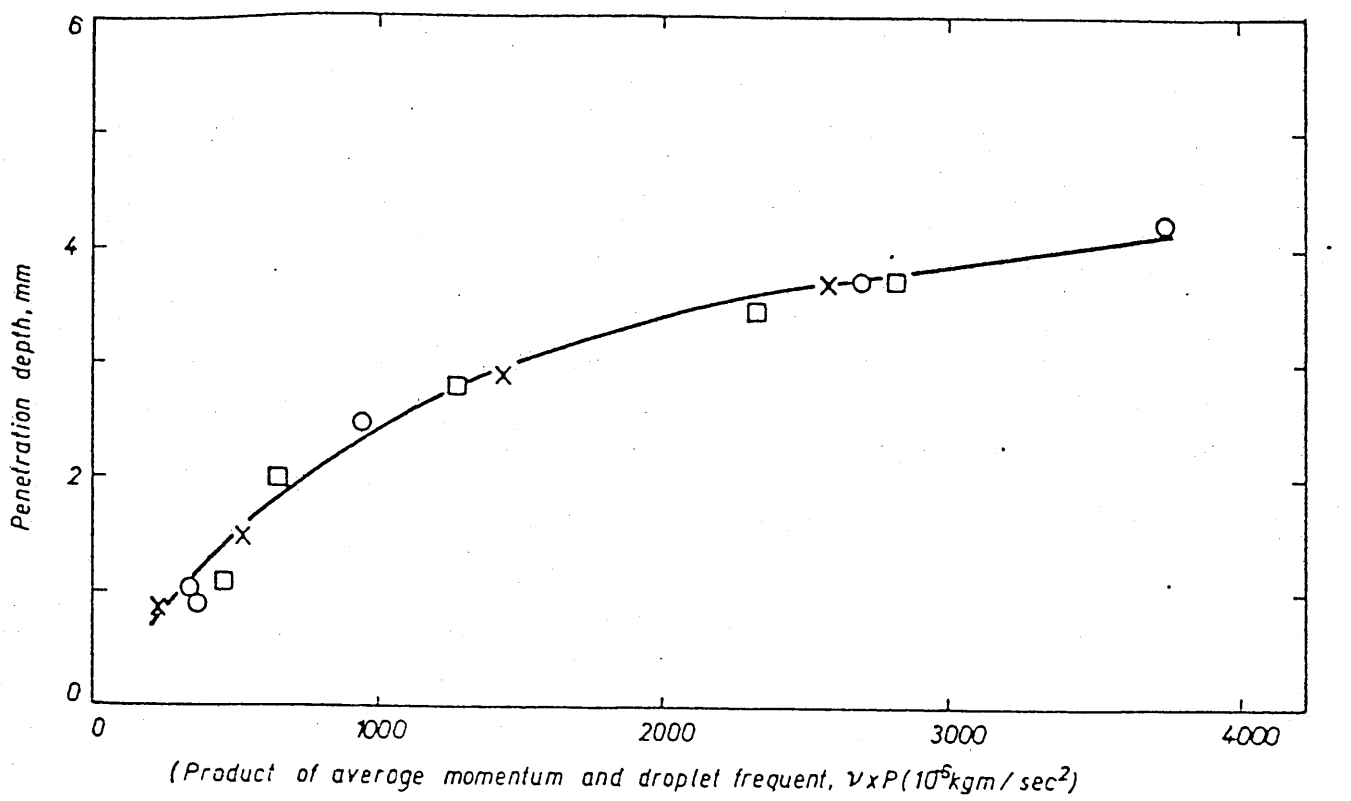

FIG. 31 - Depth of penetration of weld bead as function of ν p - 1.2 mm filler wire, positive polarity; - 1.2 mm filler wire, negative polarity; O - 1.6 mm filler wire, positive polarity (ref. 100)

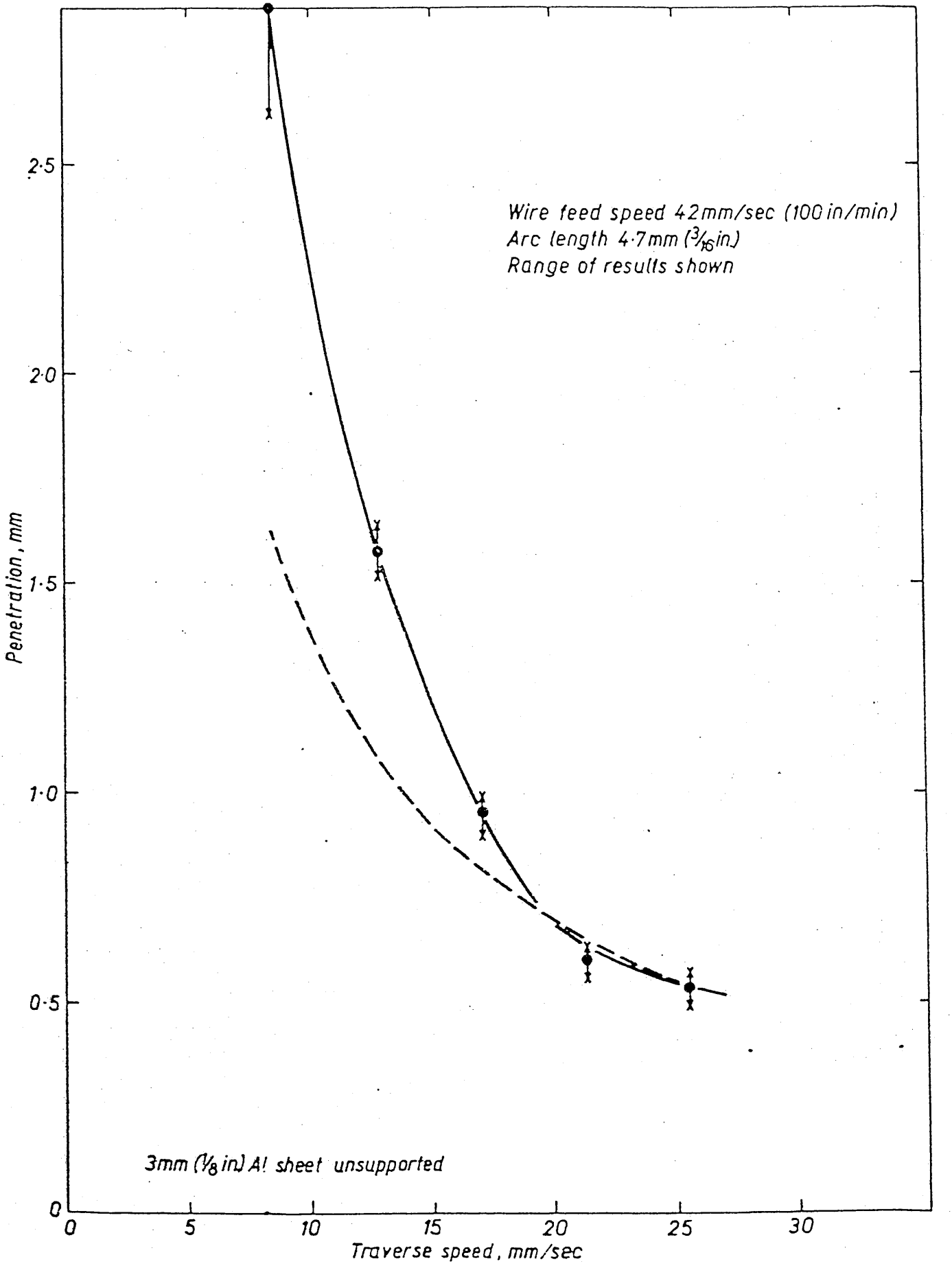

FIG. 3.2 - Penetration vs. travel speed (Ref. 101)

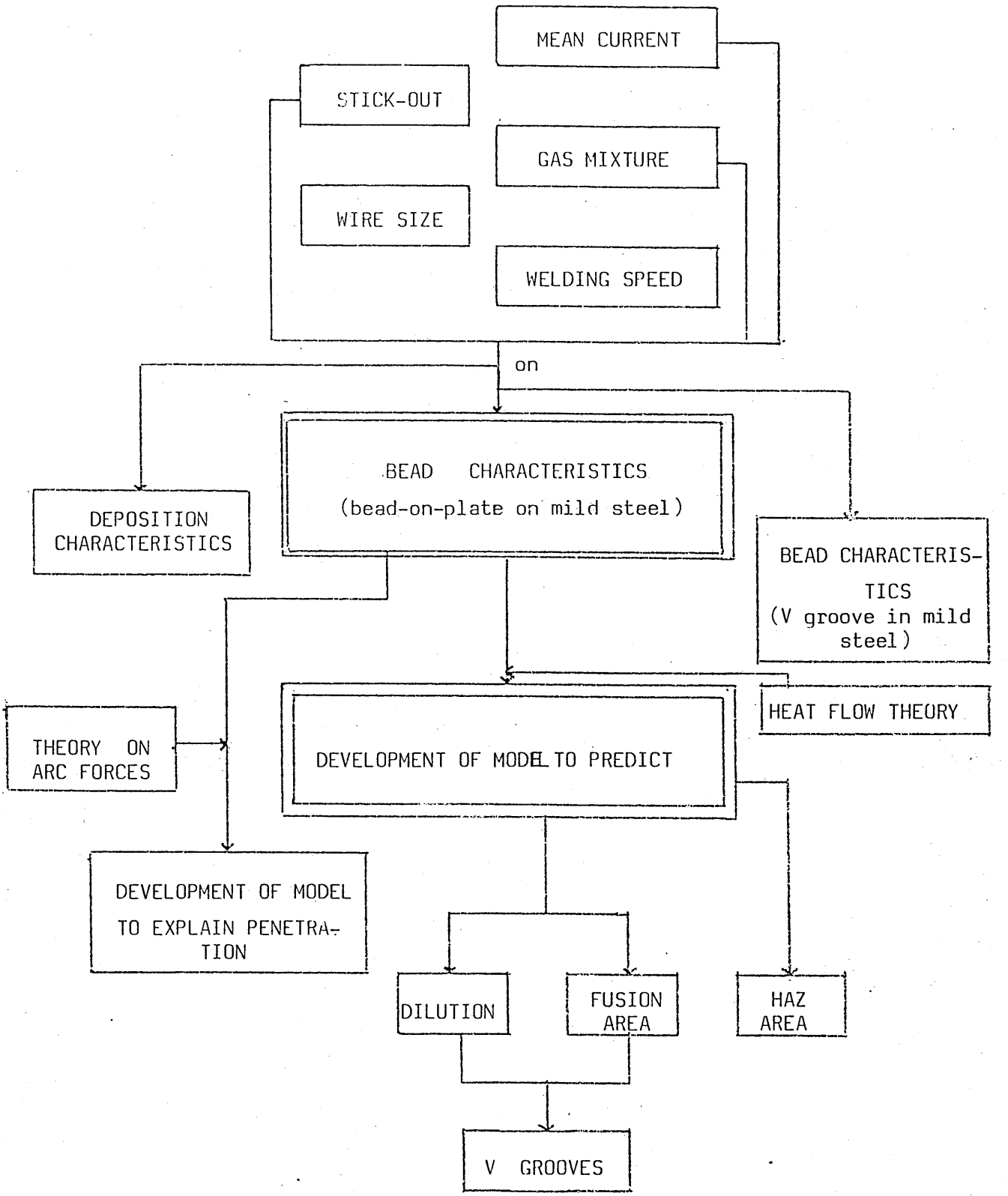

FIG. 33 - Schematic representation of experimental programme

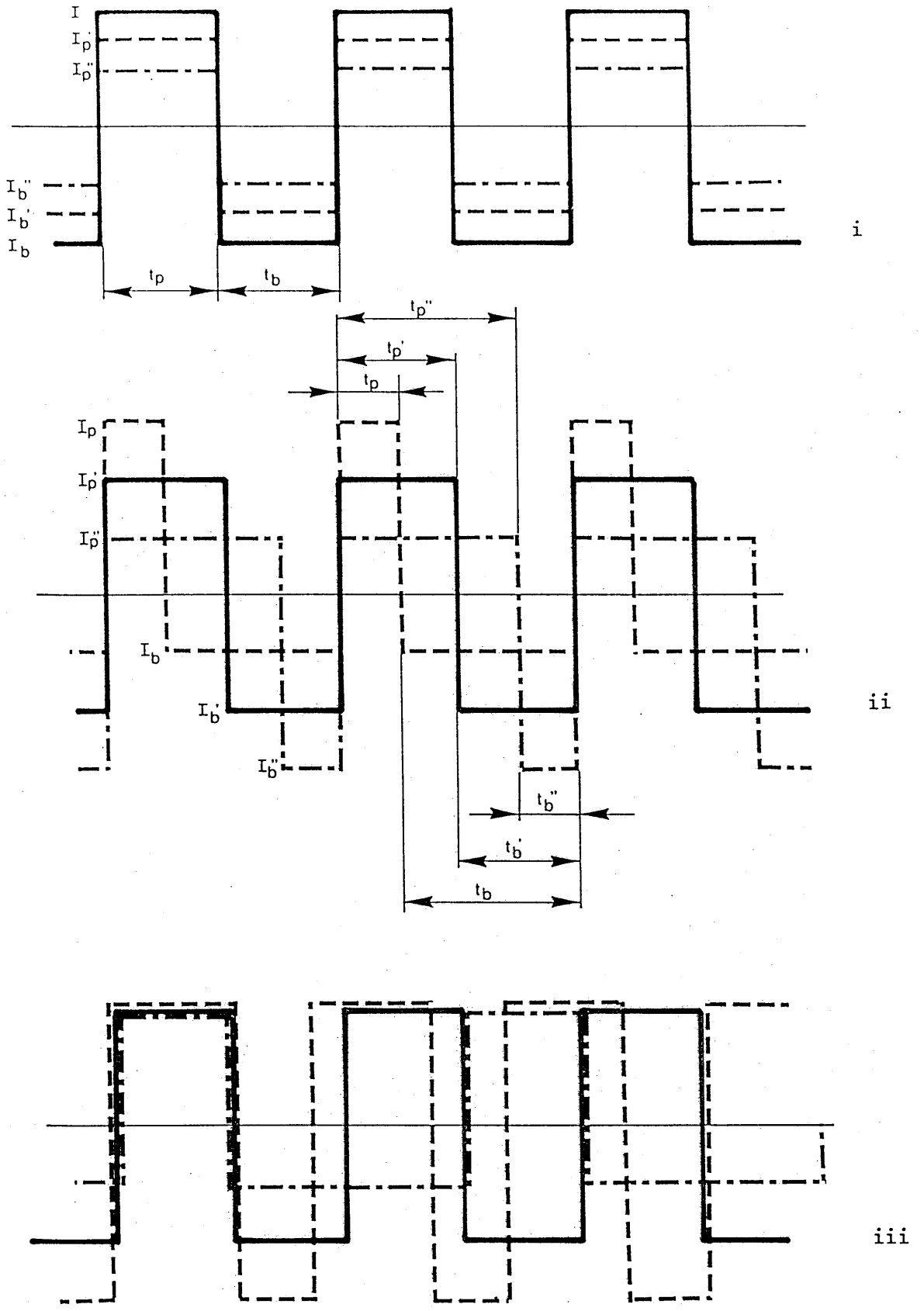

FIG. 34 - Representation of the three different approaches used on the experiments

i) constant $\bar{I}$, t_p, t_b and F, varying I_p and I_b

ii) constant $\bar{I}$ and F, varying t_p, t_b, I_p and I_b

iii) constant $\bar{I}$, I_p and t_p and varying t_b, I_b and F.

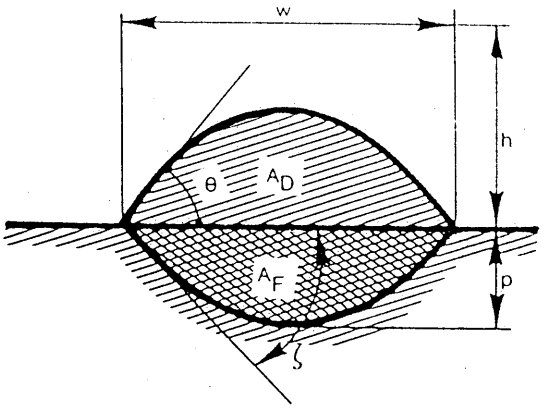

FIG. 35 - Bead areas

P - penetration
h - reinforcement heigth
w - width
A_D - deposited area
A_F - plate fusion area
Θ - wetting angle
ζ - fusion angle
$A_D + A_F = A_T$ - total fusion area

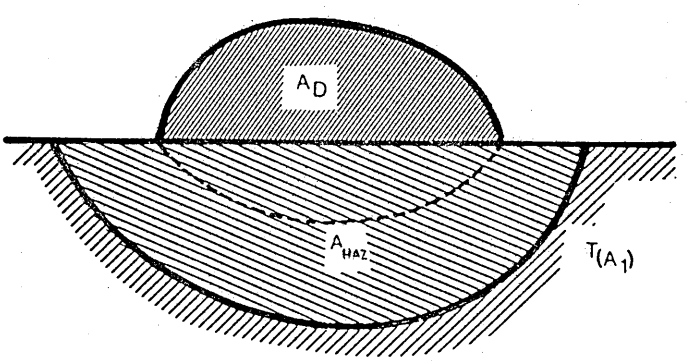

FIG. 36 - Definition of heat affected zone area

A_{HAZ} - Heat affected zone area
$T_{(A1)}$ - isothermal defining heat affect zone area

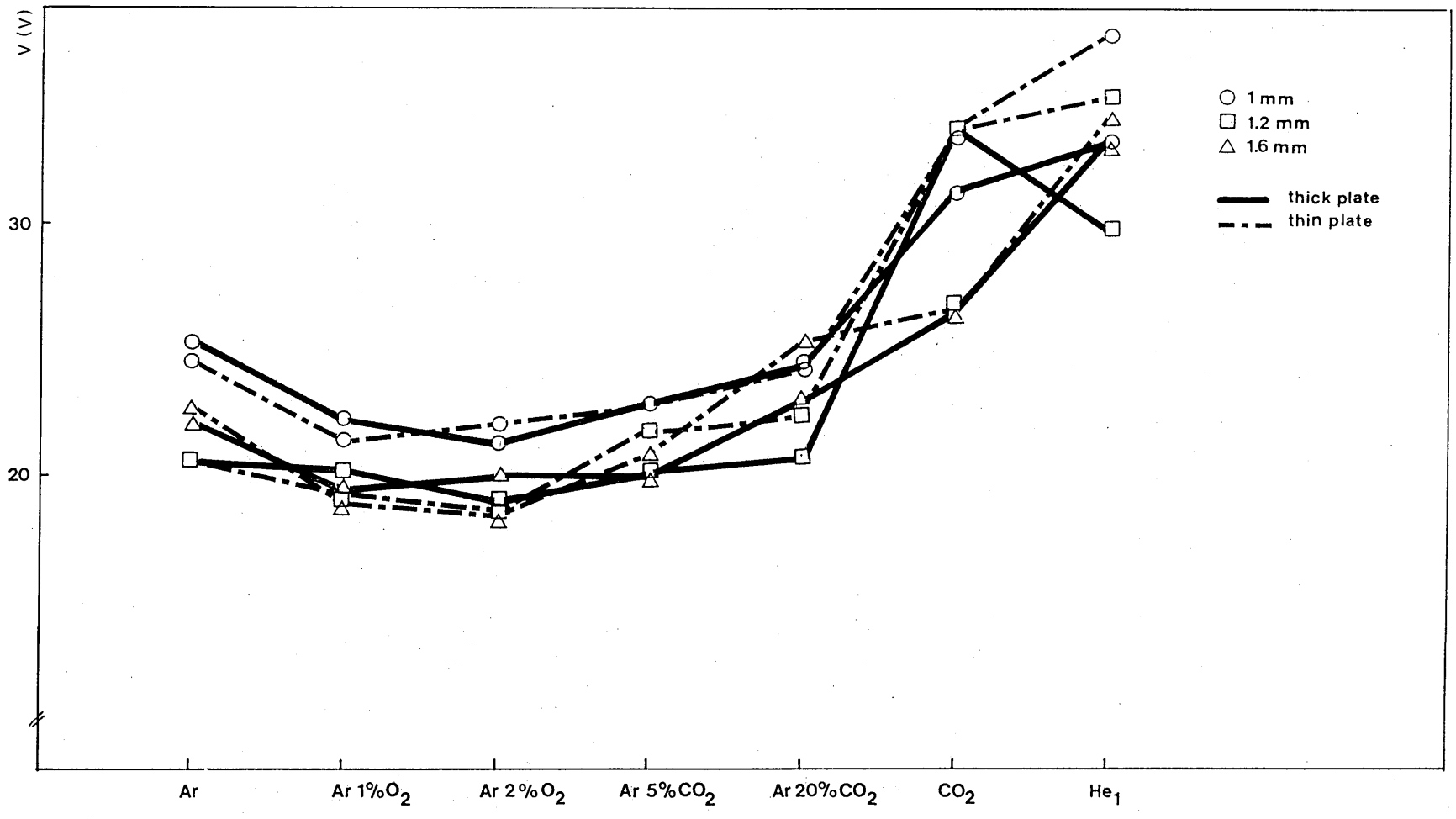

FIG. 37 - Influence of shielding gas composition and wire diameter on arc voltage
($\bar{I}$ = 100 A, ℓ= 15 mm)

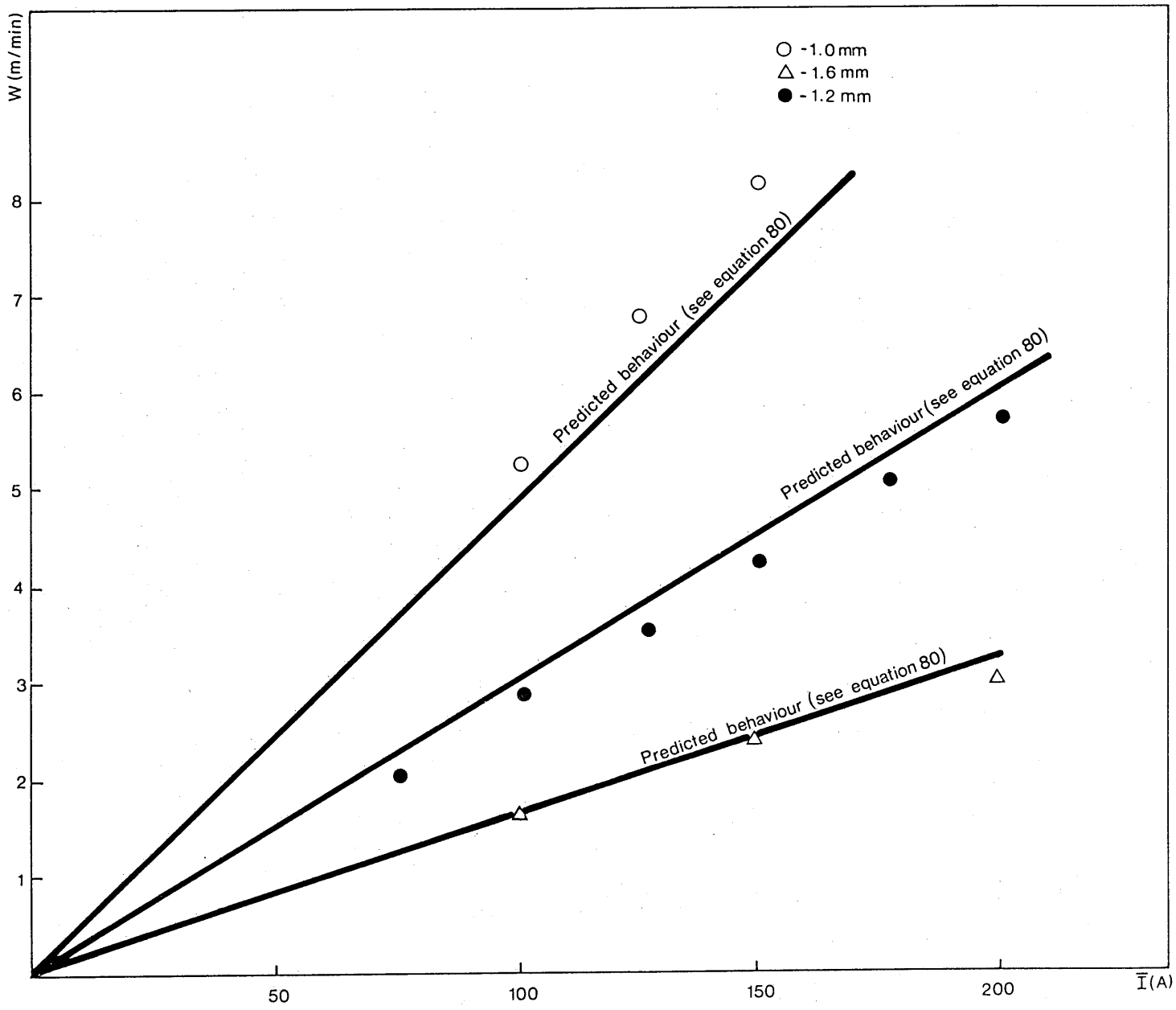

FIG. 38 - Influence of mean current on electrode burn-off rate
(Ar/5% CO_2, ℓ = 15 mm, I_p= 350 A, T_p= 4 ms, F/Ī=50/100)

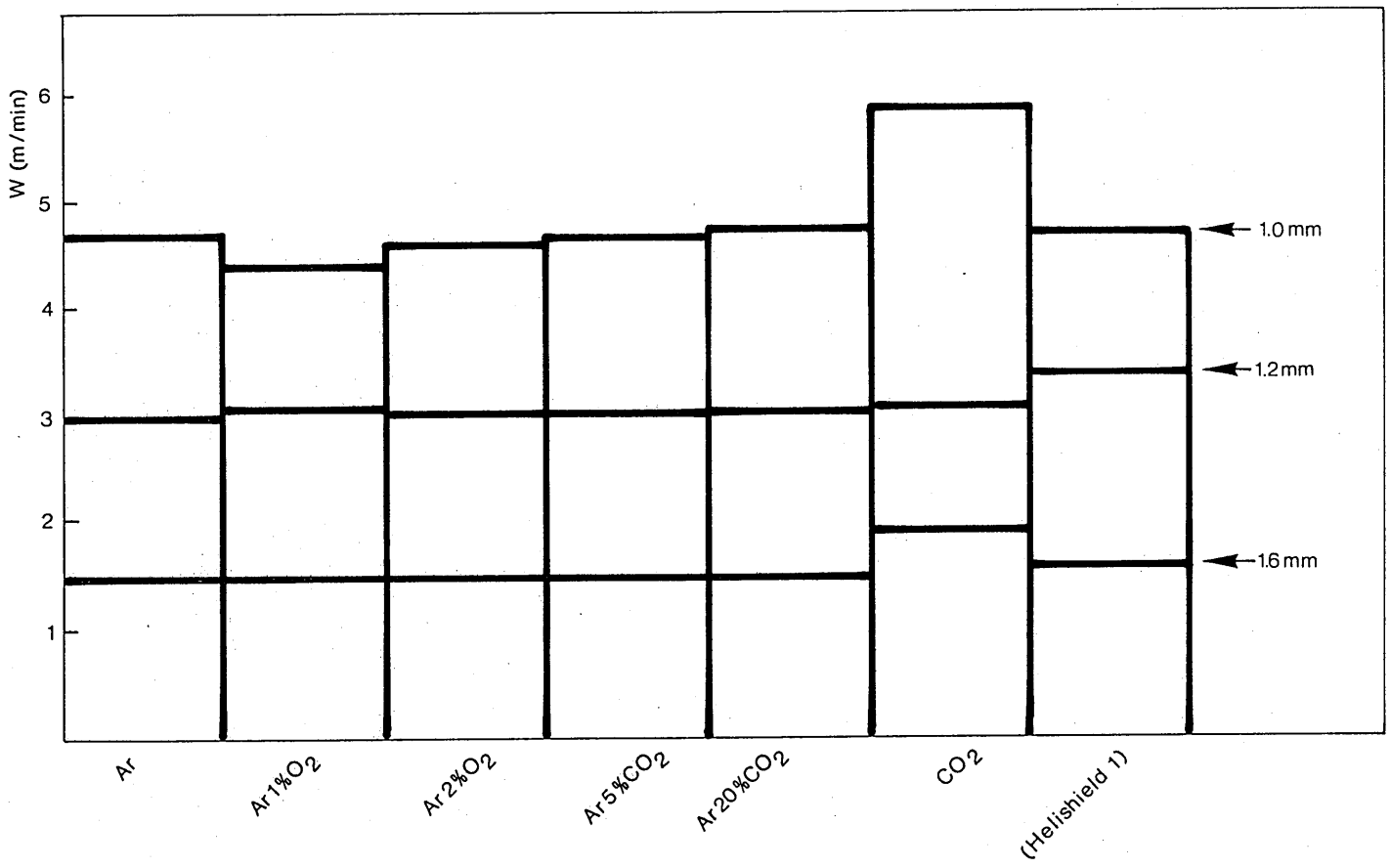

FIG. 39 - Influence of wire size and shielding gas composition on electrode burn-off rate ($\bar{I}$ = 100 A, ℓ = 15mm)

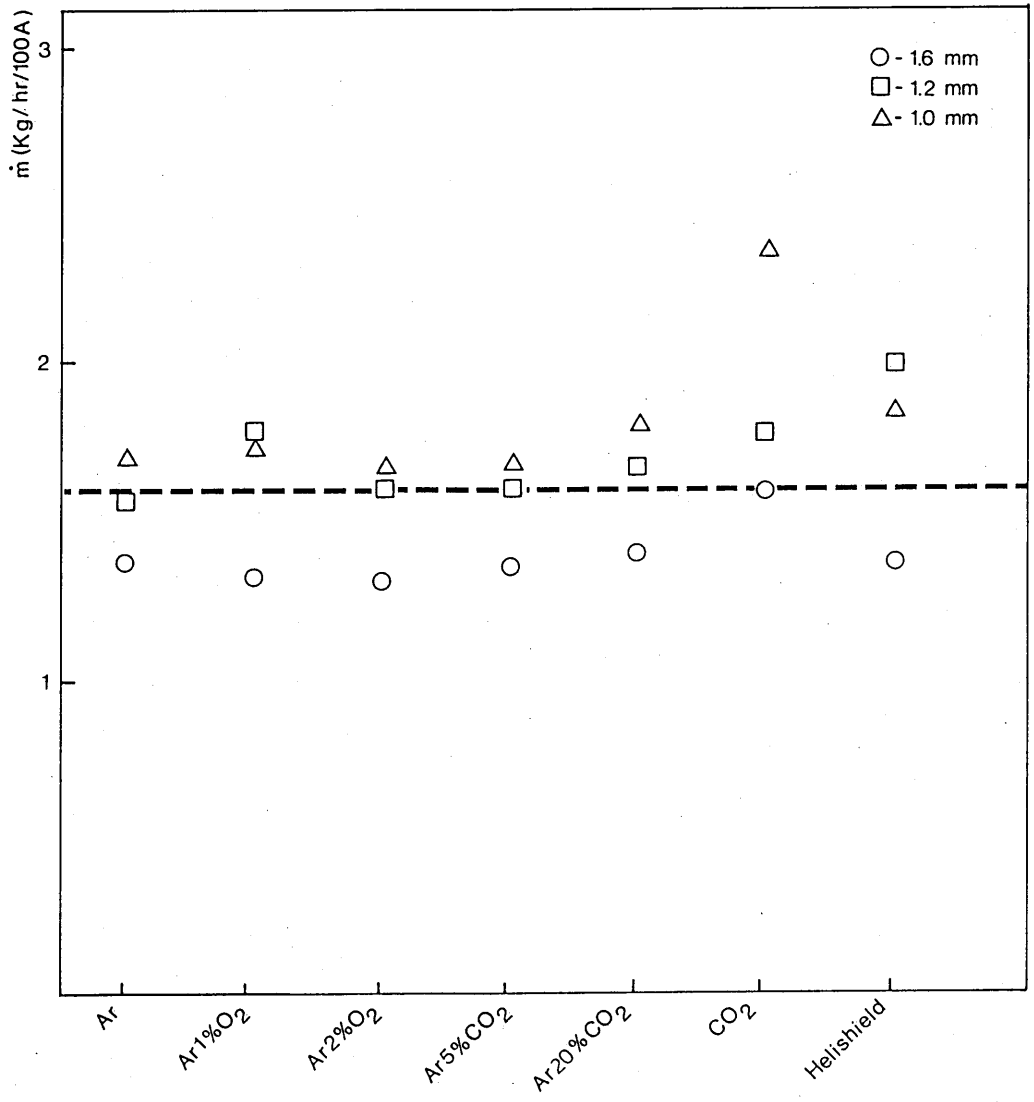

FIG. 40 - Influence of wire size and shielding gas composition on deposition rate ($\bar{I}$ = 100A, ℓ = 15mm)

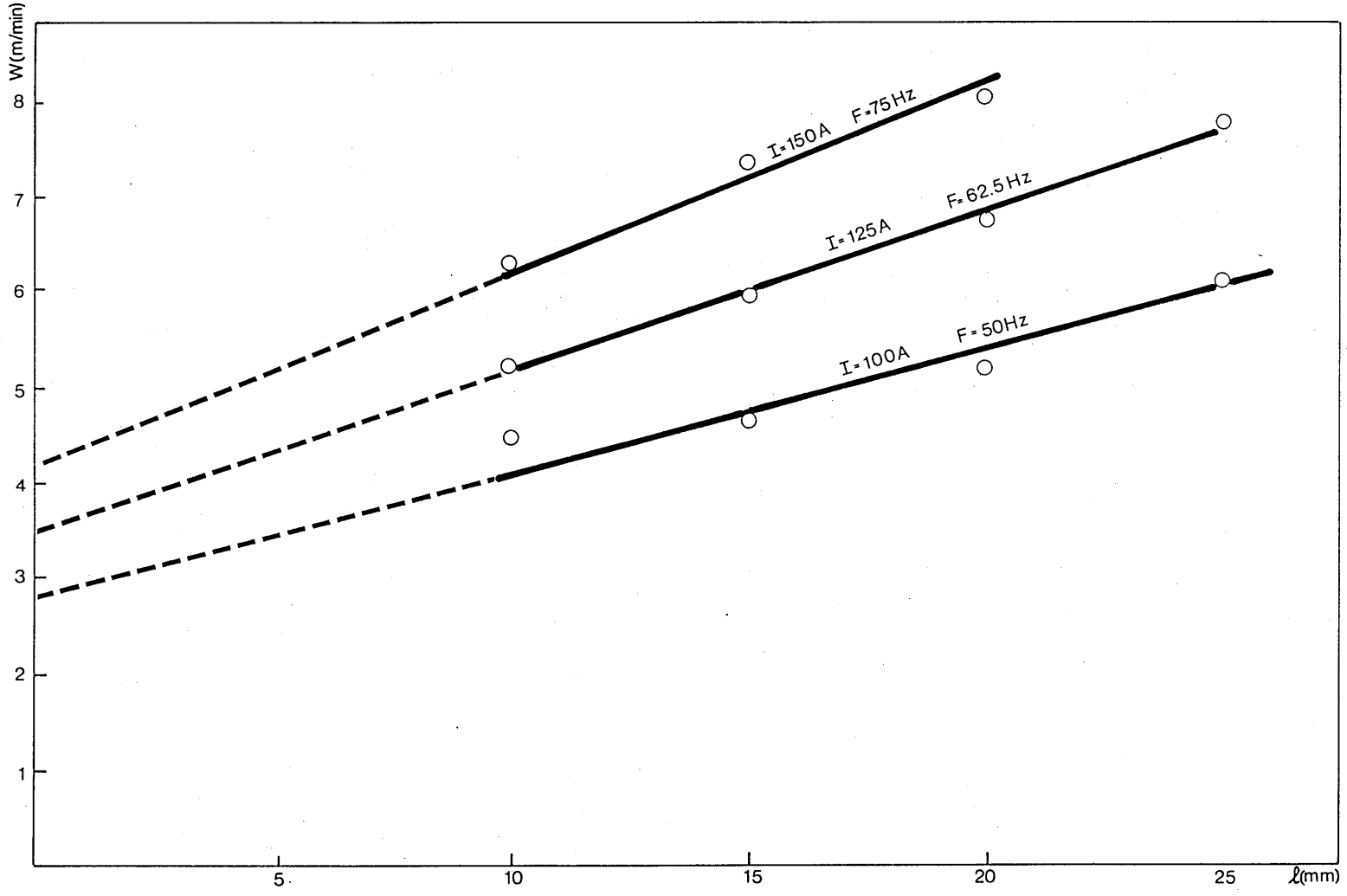

FIG. 4.1 - Influence of electrode extension on burn-off rate
(1.0mm wire diameter, Ar/5% CO_2 shield)

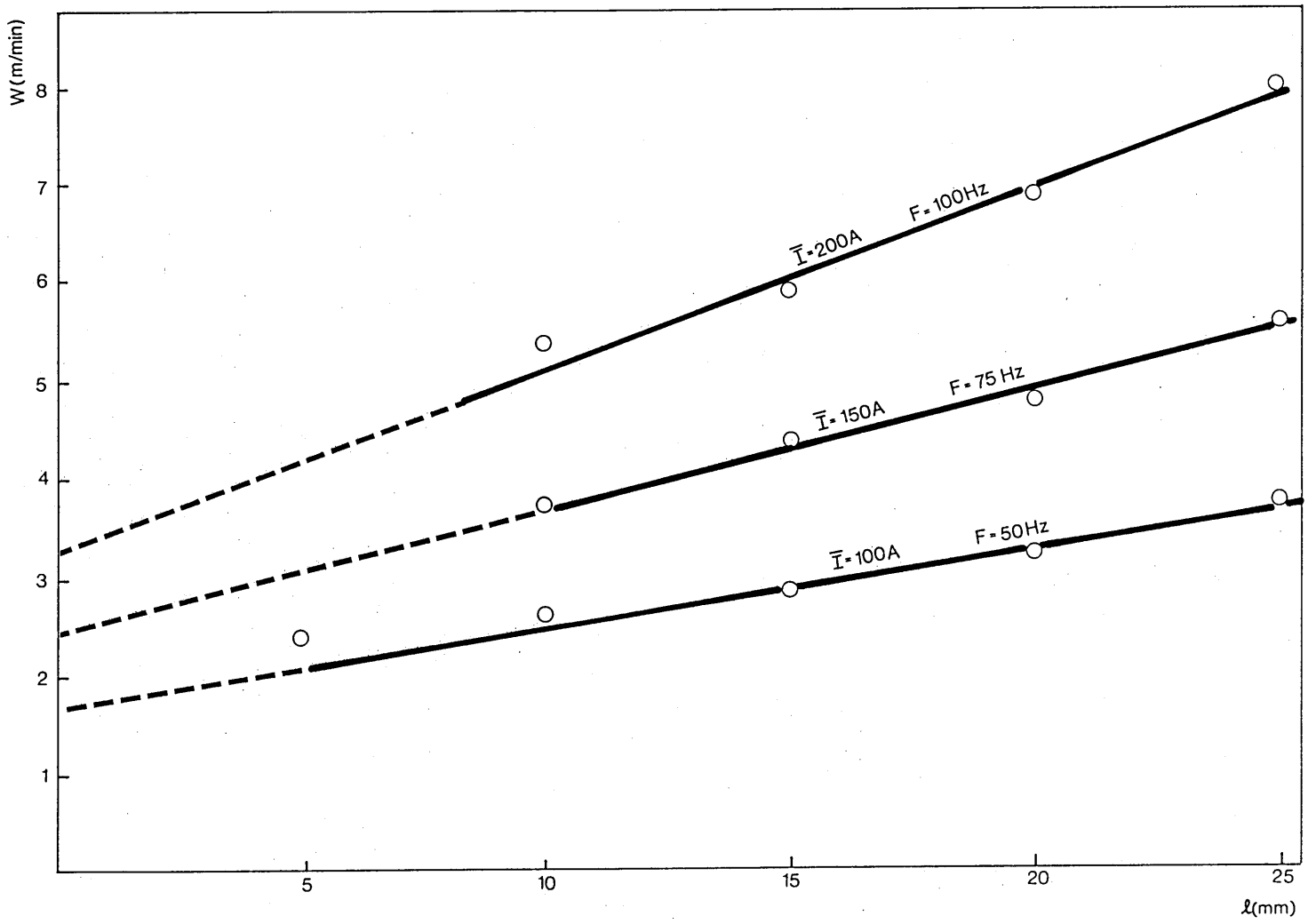

FIG. 42 - Influence of electrode exntension on burn-off rate
(1.2mm wire diameter, Ar/5% CO_2)

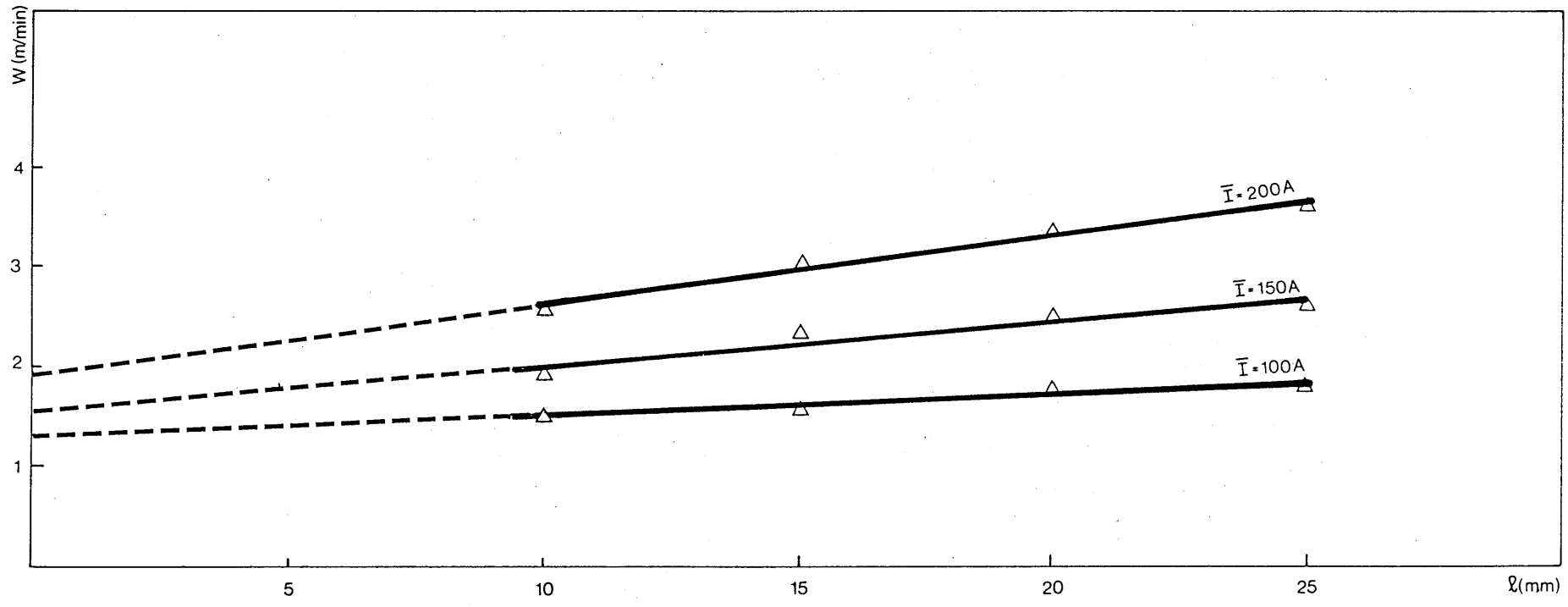

Fig. 43 - Influence of electrode extension on burn-off rate
(1.6mm wire diameter, Ar/5% CO_2)

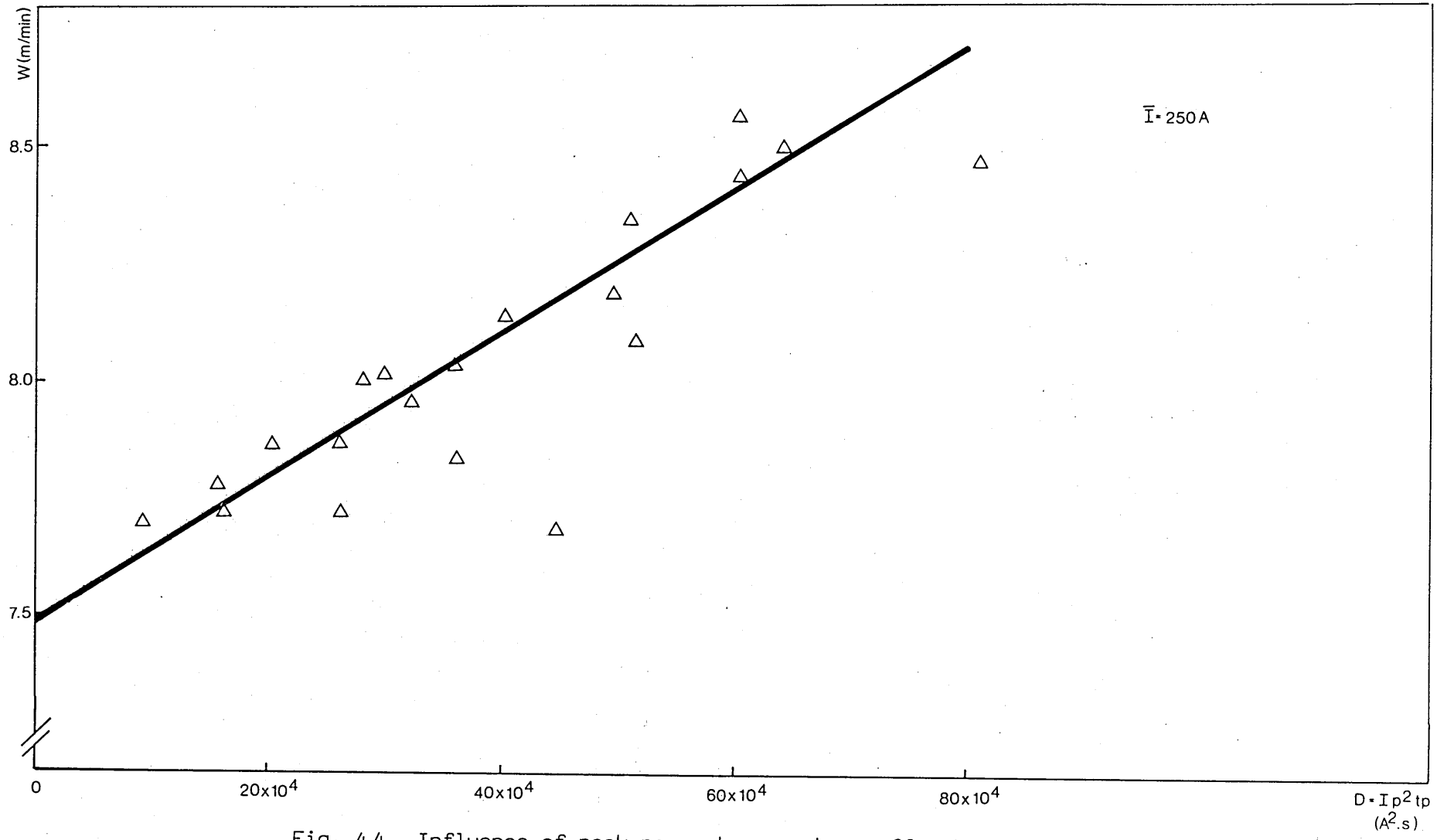

Fig. 44 - Influence of peak parameters on burn-off rate
(1.2mm wire diameter, Ar/5% CO_2, ℓ = 15 mm, $\bar{I}$ = 250 A, F = 125 Hz)

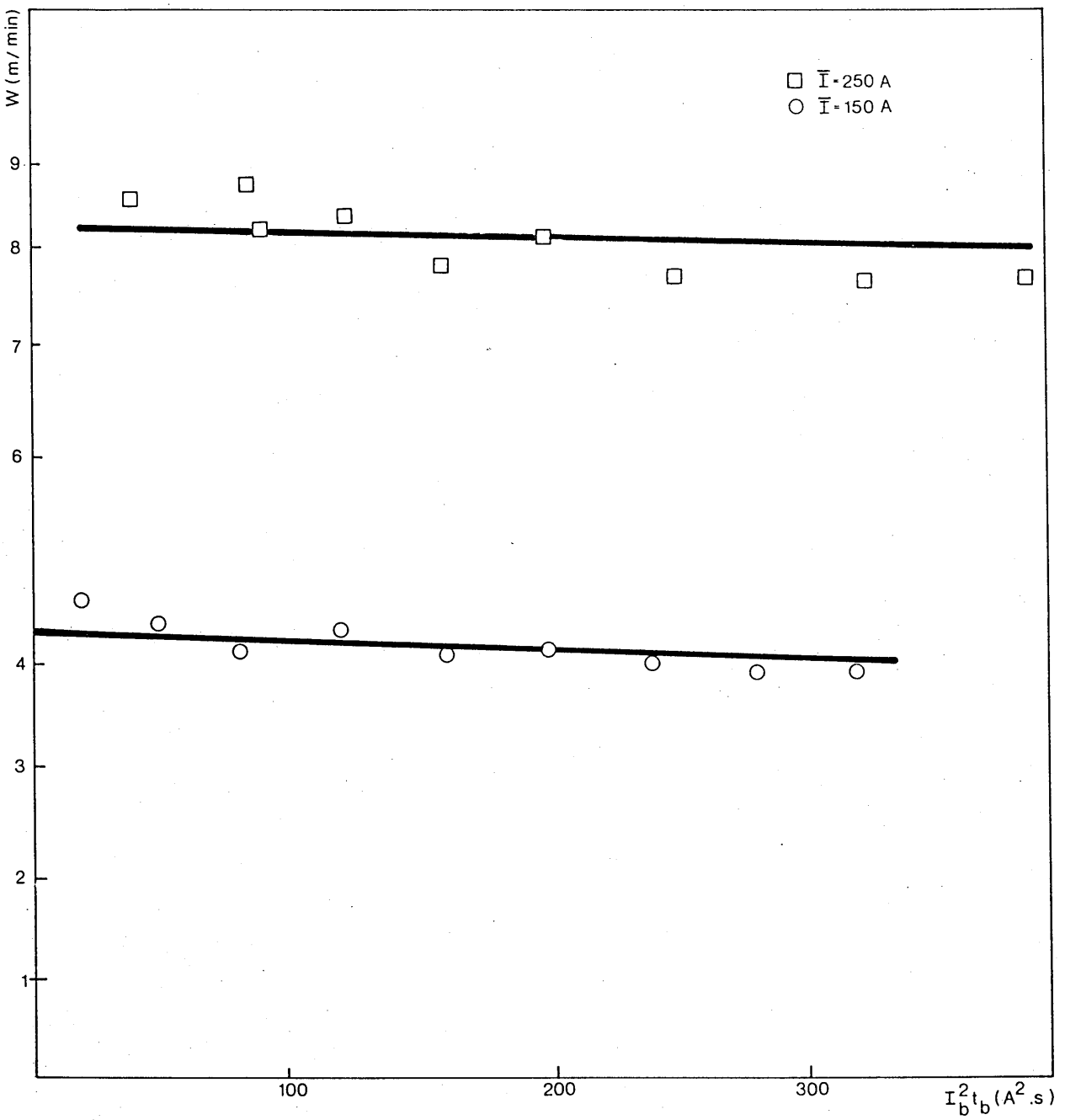

FIG. 45 - Influence of background parameters on burn-off rate
(1.2mm wire diameter, Ar/5% CO_2, ℓ = 15mm, I_p= 350A, t_p= 4ms)

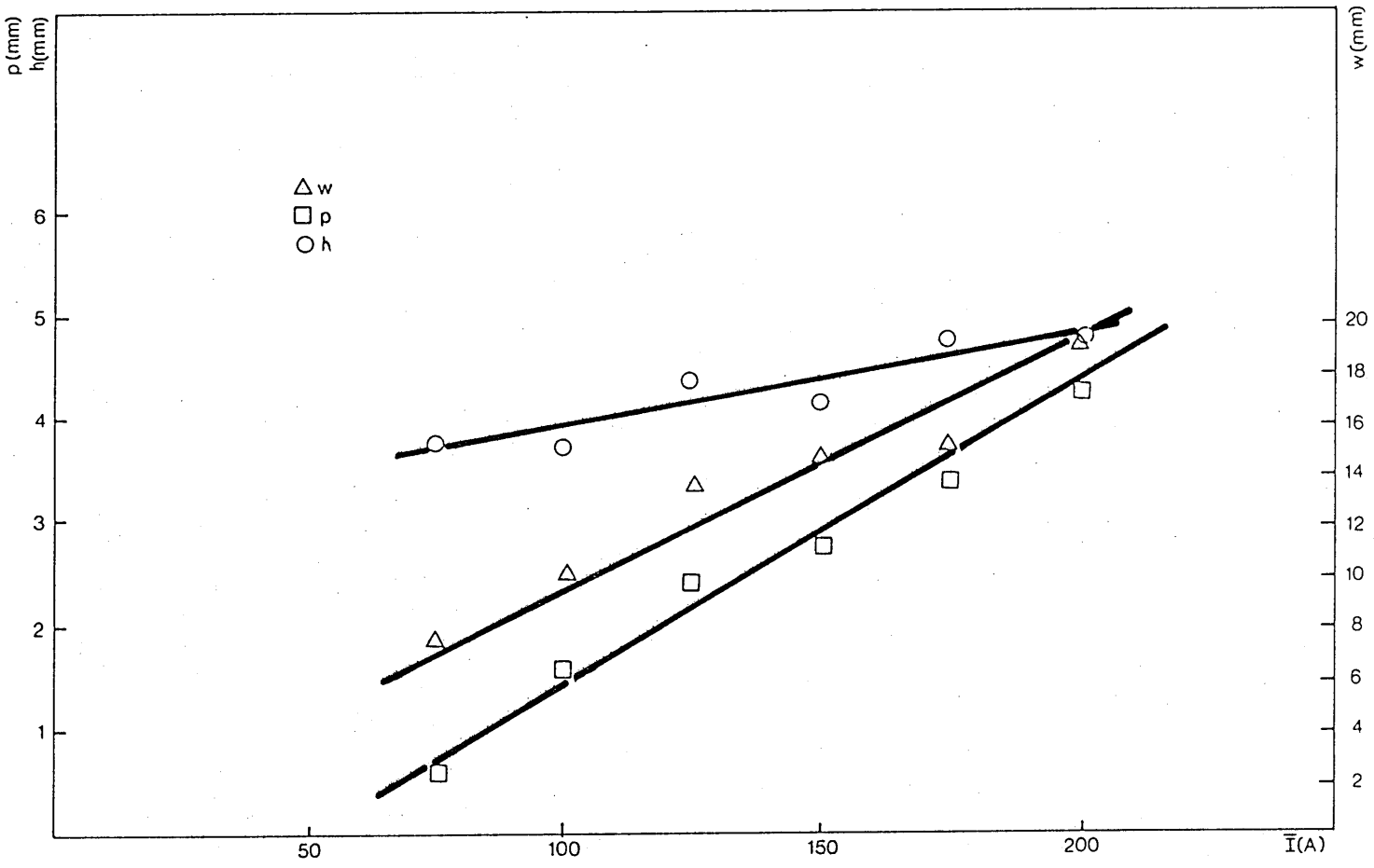

FIG. 46 - Influence of mean current on bead penetration (p), reinforcement height (h) and width (w)

(1.2 mm wire, Ar/5% CO_2, v = 1.53 mm/s, thick plate)

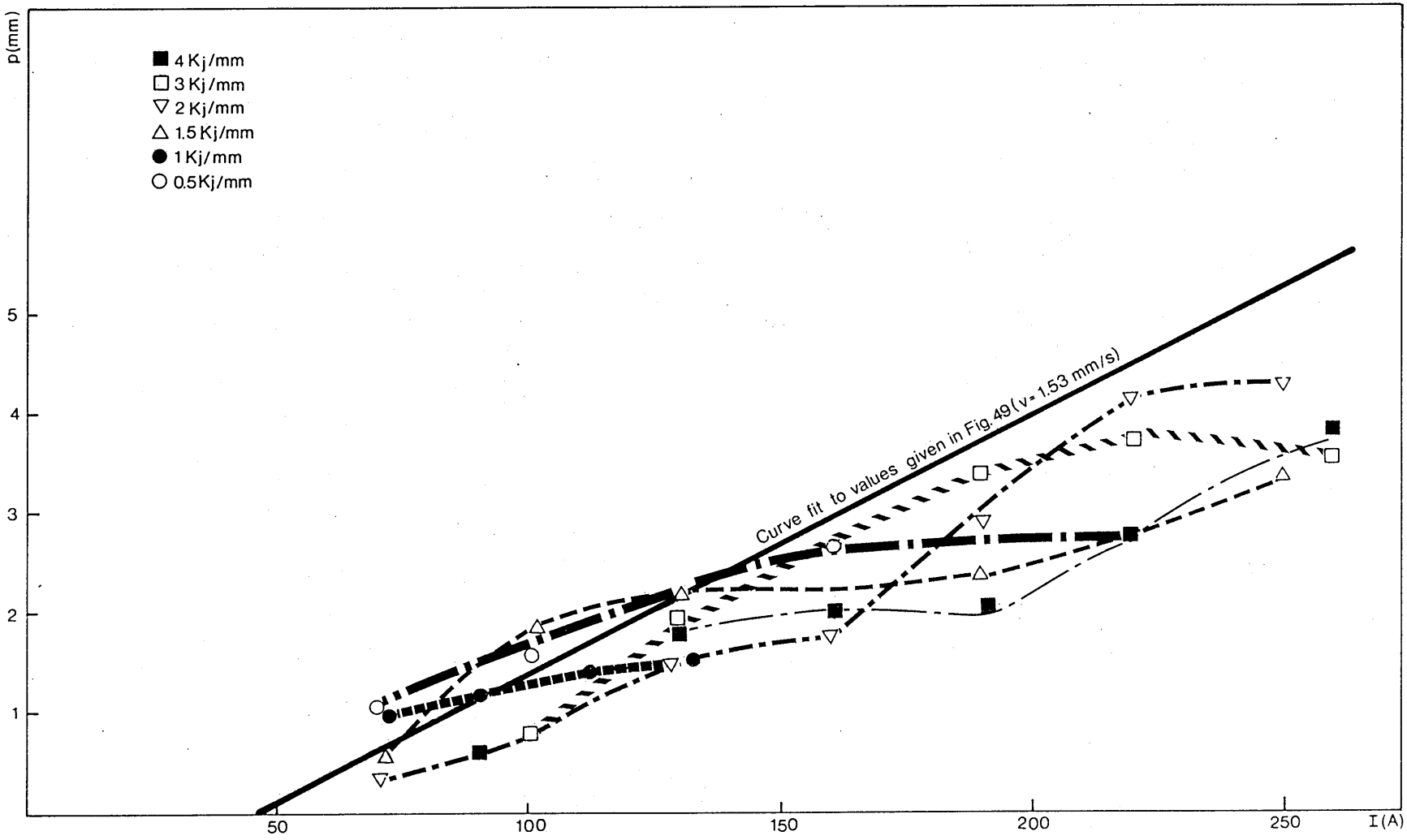

FIG. 47 - Influence of mean current on penetration for different heat inputs
(ℓ = 15 mm, Ar/5% CO_2)

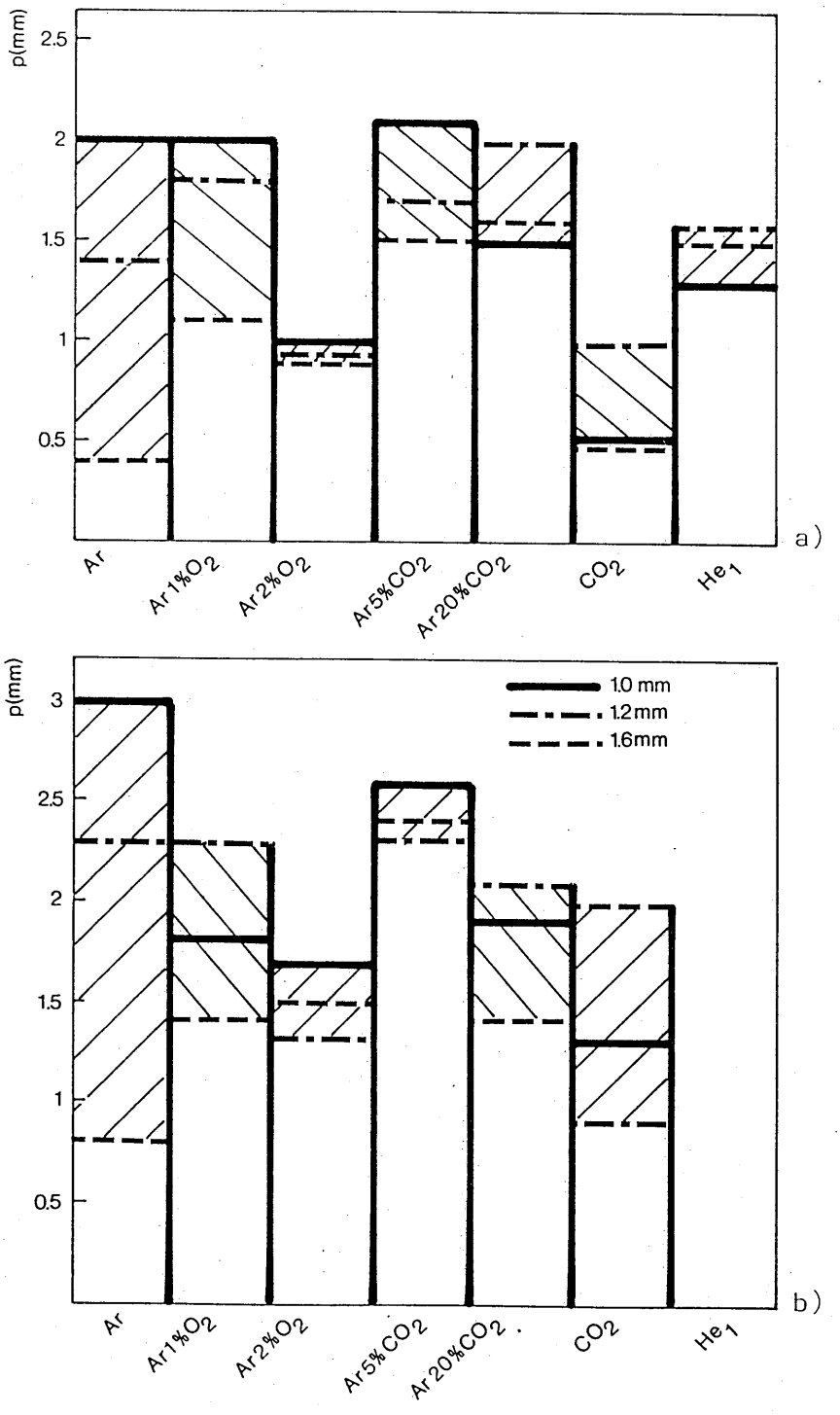

FIG. 48 - Influence of shielding gas composition and wire diameter on penetration (p)

(a) Thick plate
(b) Thin plate

($\bar{I}$ = 100 A, v = 1.53 mm/s, ℓ = 15 mm)

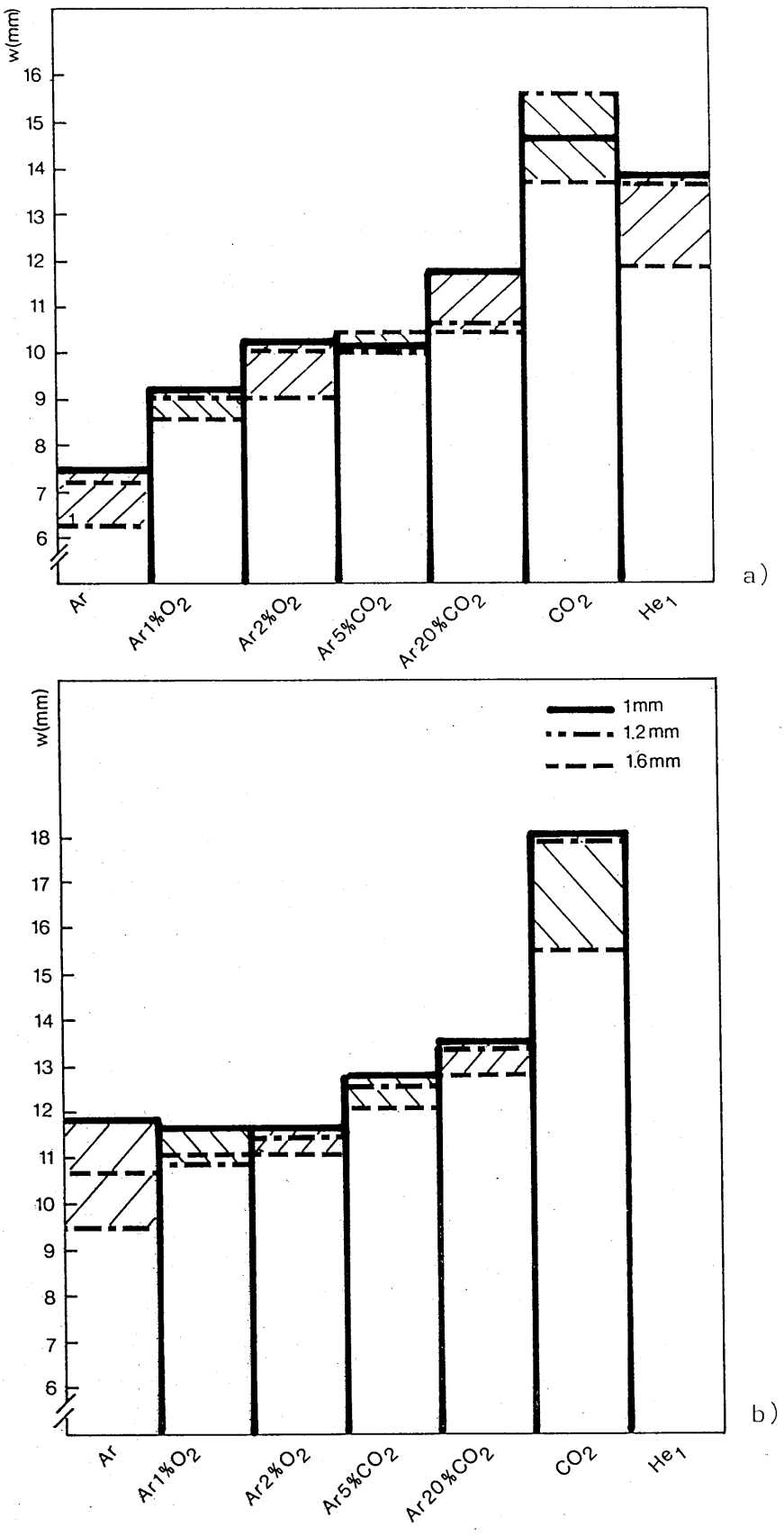

FIG. 49 - Influence of shielding gas composition and wire diameter on width of the bead (w)
(a) Thick plate
(b) thin plate
($\bar{I}$ = 100 A, v = 1.53 cm/s, ℓ = 15 mm)

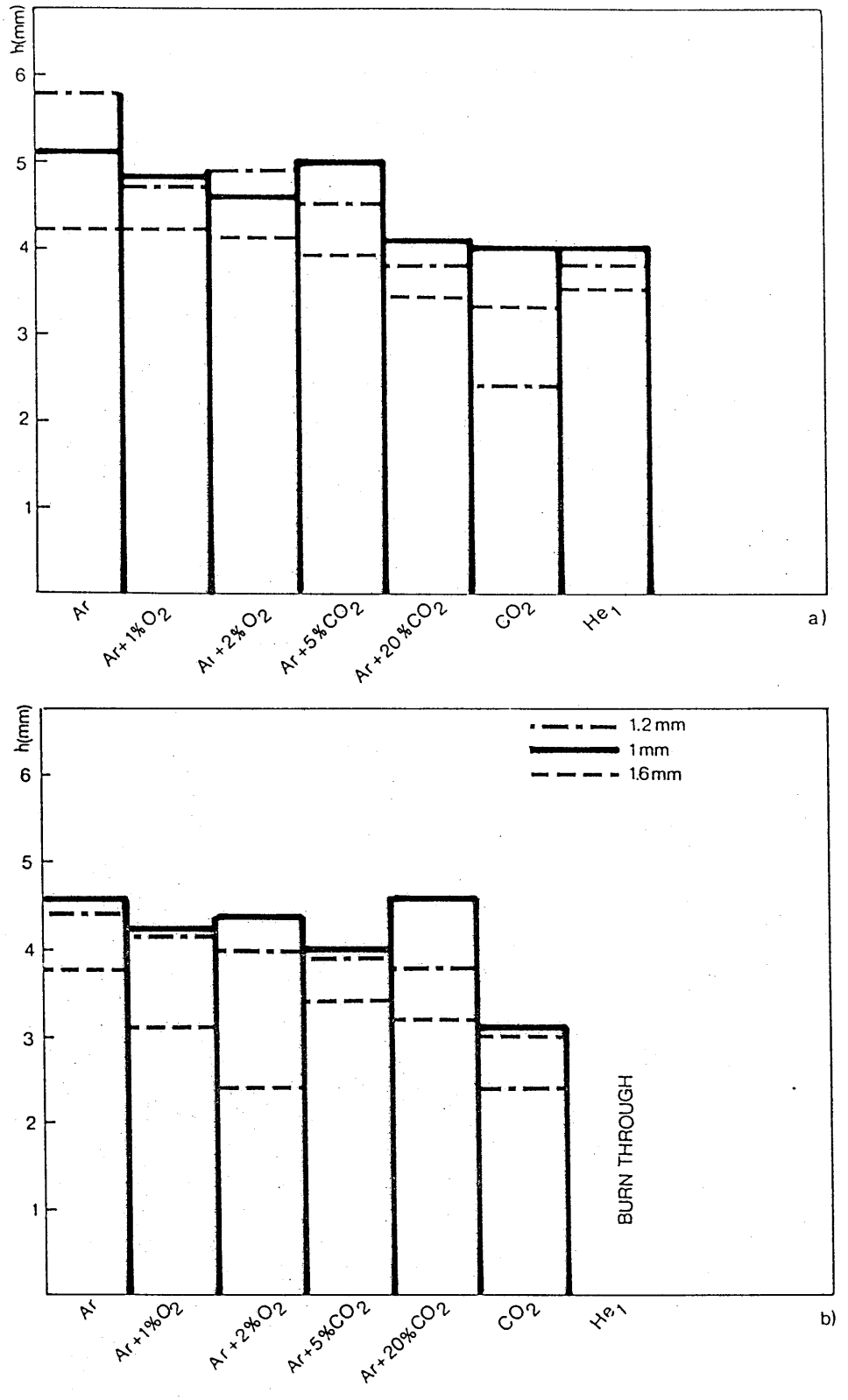

Fig. 50 - Influence of shielding gas composition and wire diameter on reinforcement (h)

(a) thick plate

(b) thin plate

I = 190 A, v = 1.53 m, l = 15 mm

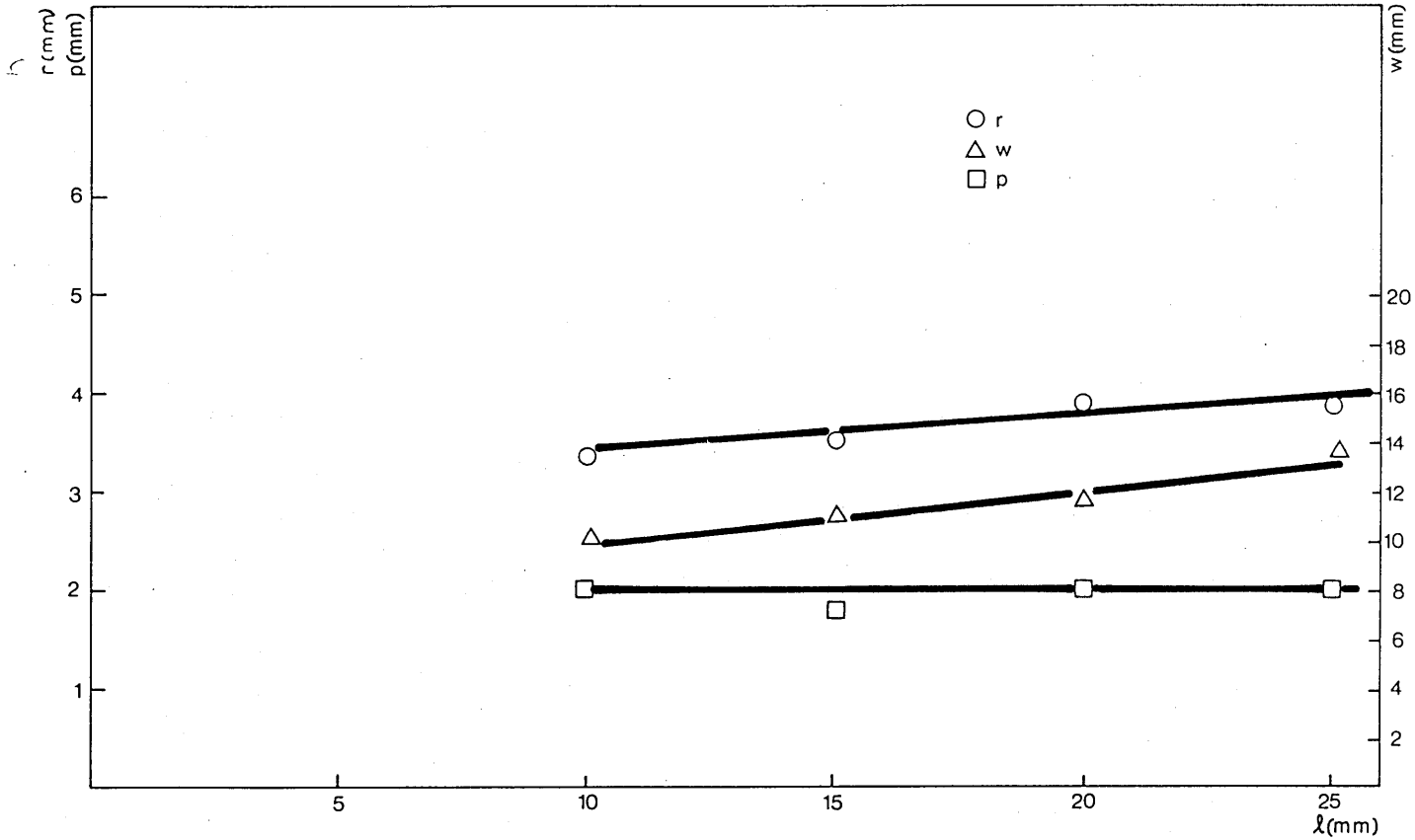

FIG. 5.1 - Influence of electrode extension on penetration (p), width (w) and reinforcement heigth (h)
(1.2 mm wire, Ar/5% CO_2, I_p = 350 A, t_p = 4 ms, $\bar{I}$ = 100 A, F = 50 Hz, v = 1.53 mm/s, thick plate)

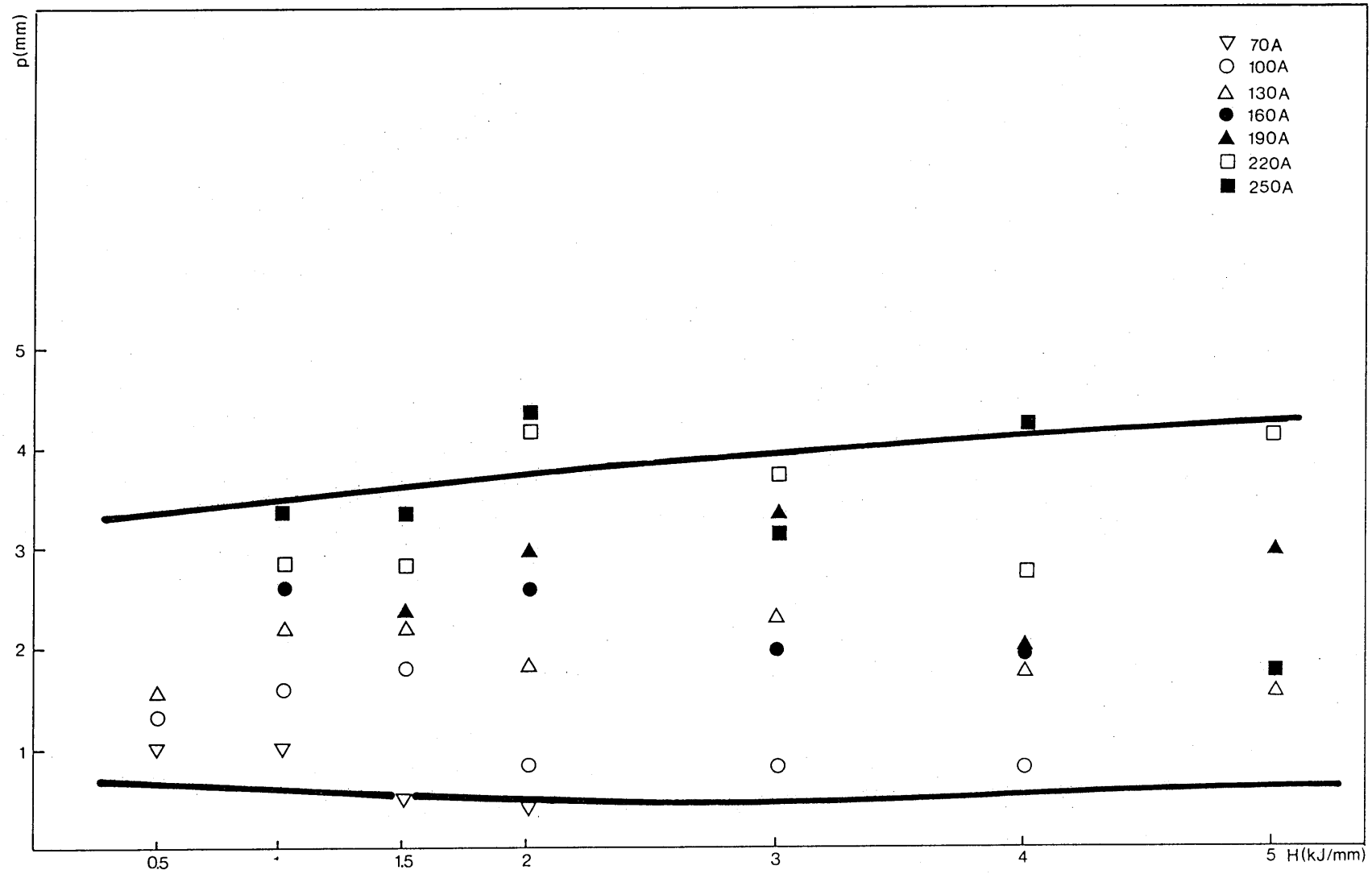

Fig. 52 - Influence of heat input on penetration for a range of mean currents (1.2 mm wire, Ar/5% CO_2, I_p = 350 A, t_p = 4 ms, $\bar{I}/F$ = 2, thick plate)

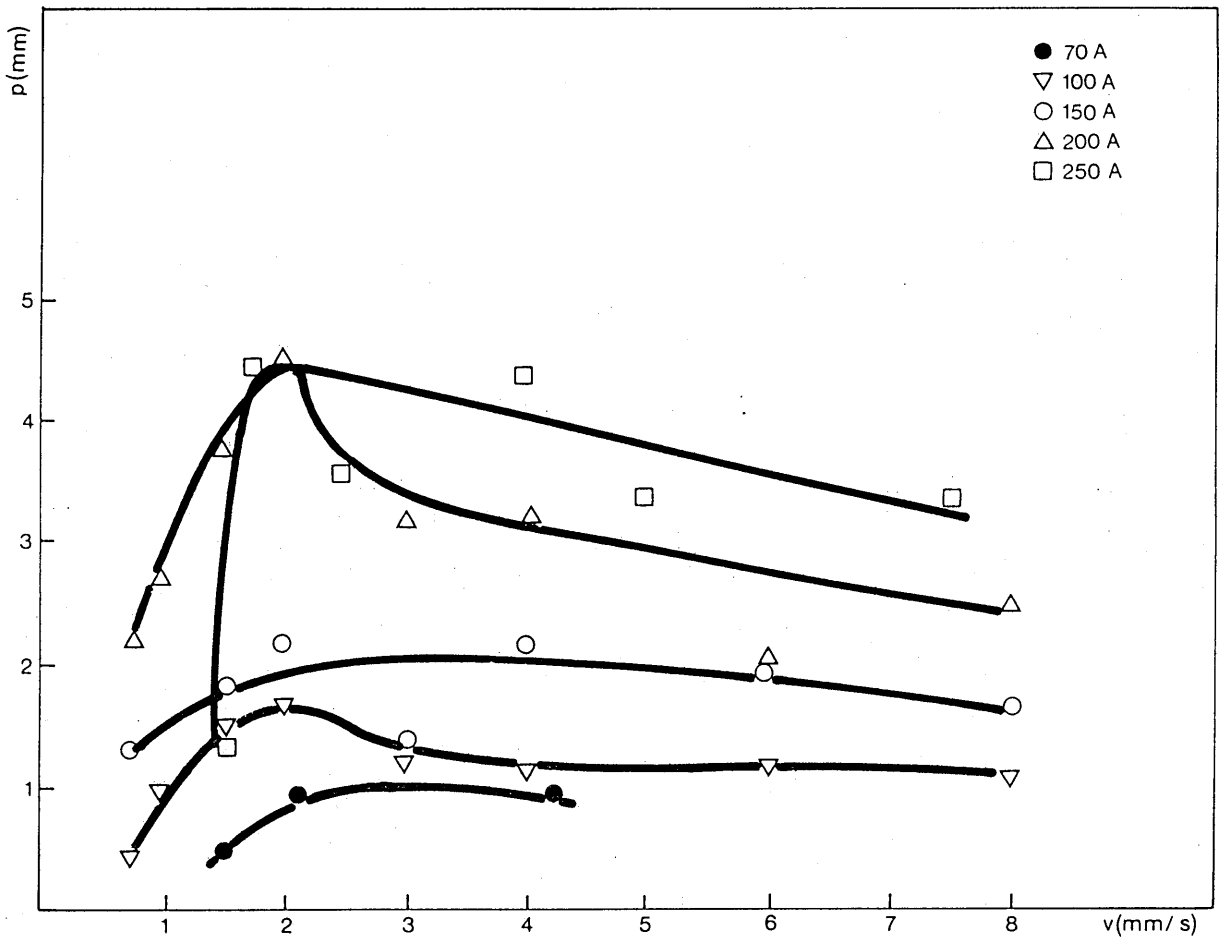

FIG. 53 - Influence of welding speed on penetration (p)
(1.2 mm wire diameter, Ar/5% CO_2)

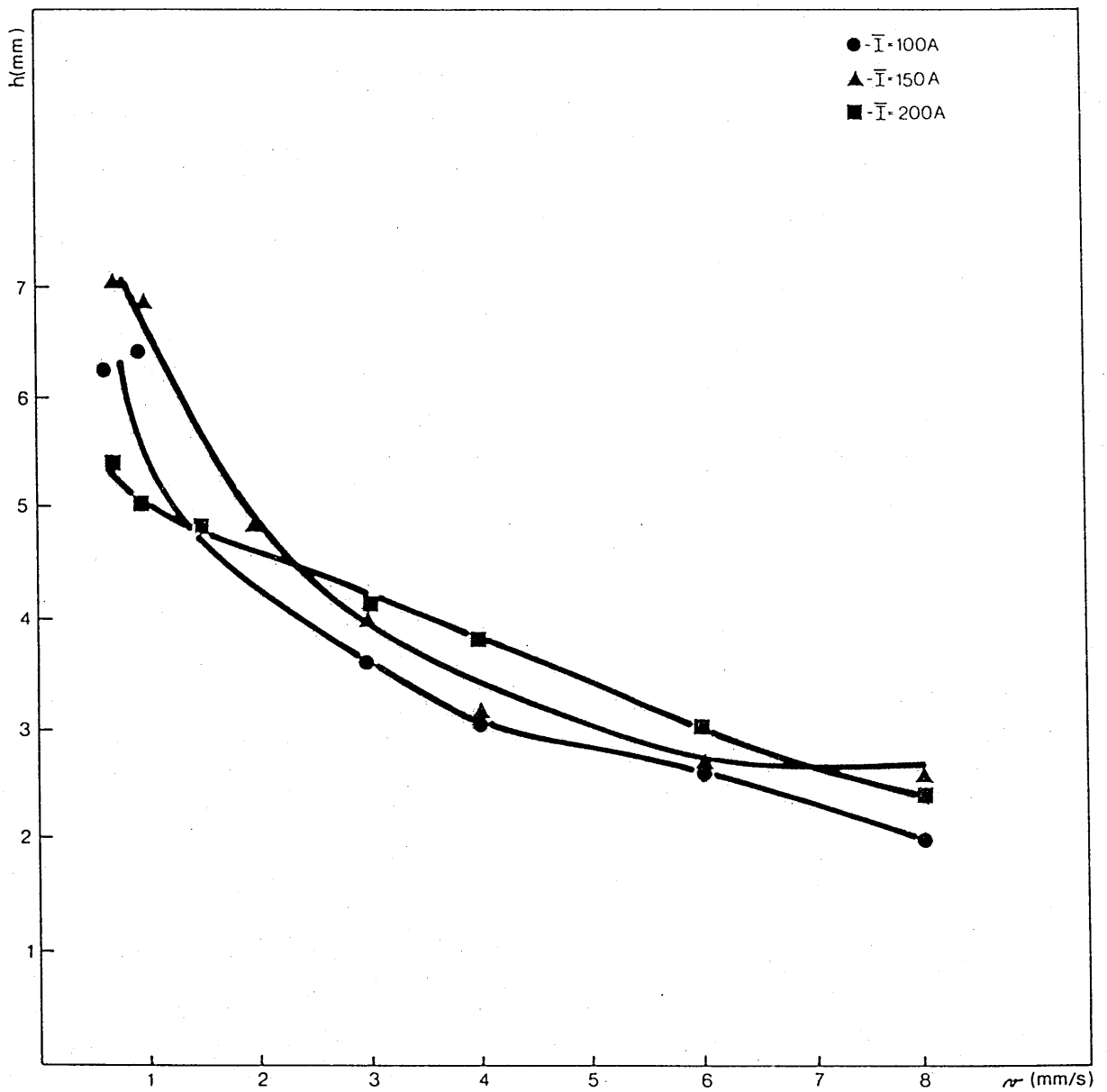

FIG. 54 - Influence of welding speed on reinforcement height (h) of the bead (1.2 mm wire diameter, ar/5% CO_2, shield, ℓ = 15 mm)

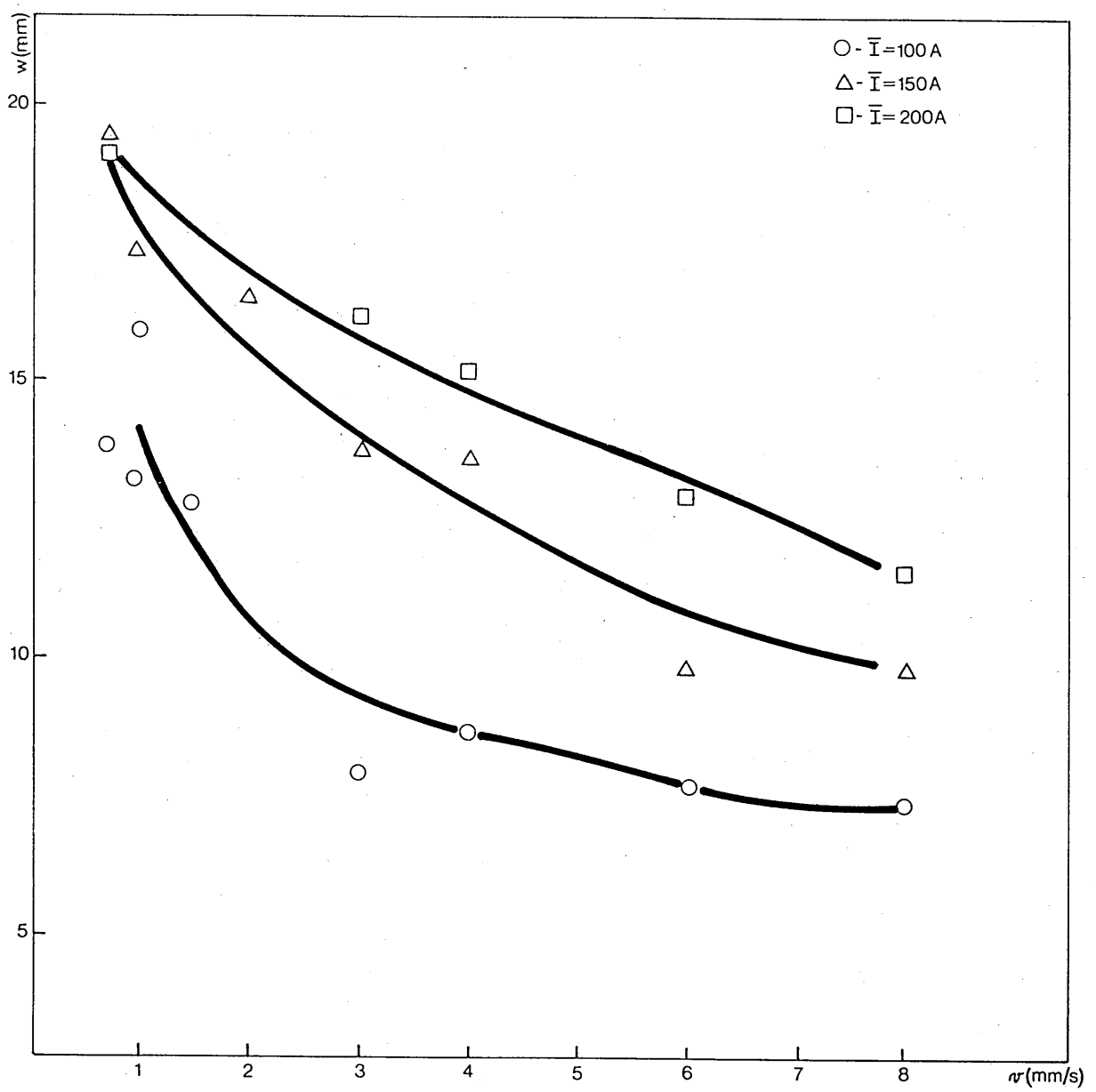

FIG. 5.5 - Influence of welding speed on width (w) of the bead (1.2 mm wire diameter, Ar/5% CO_2 shield, ℓ = 15 mm)

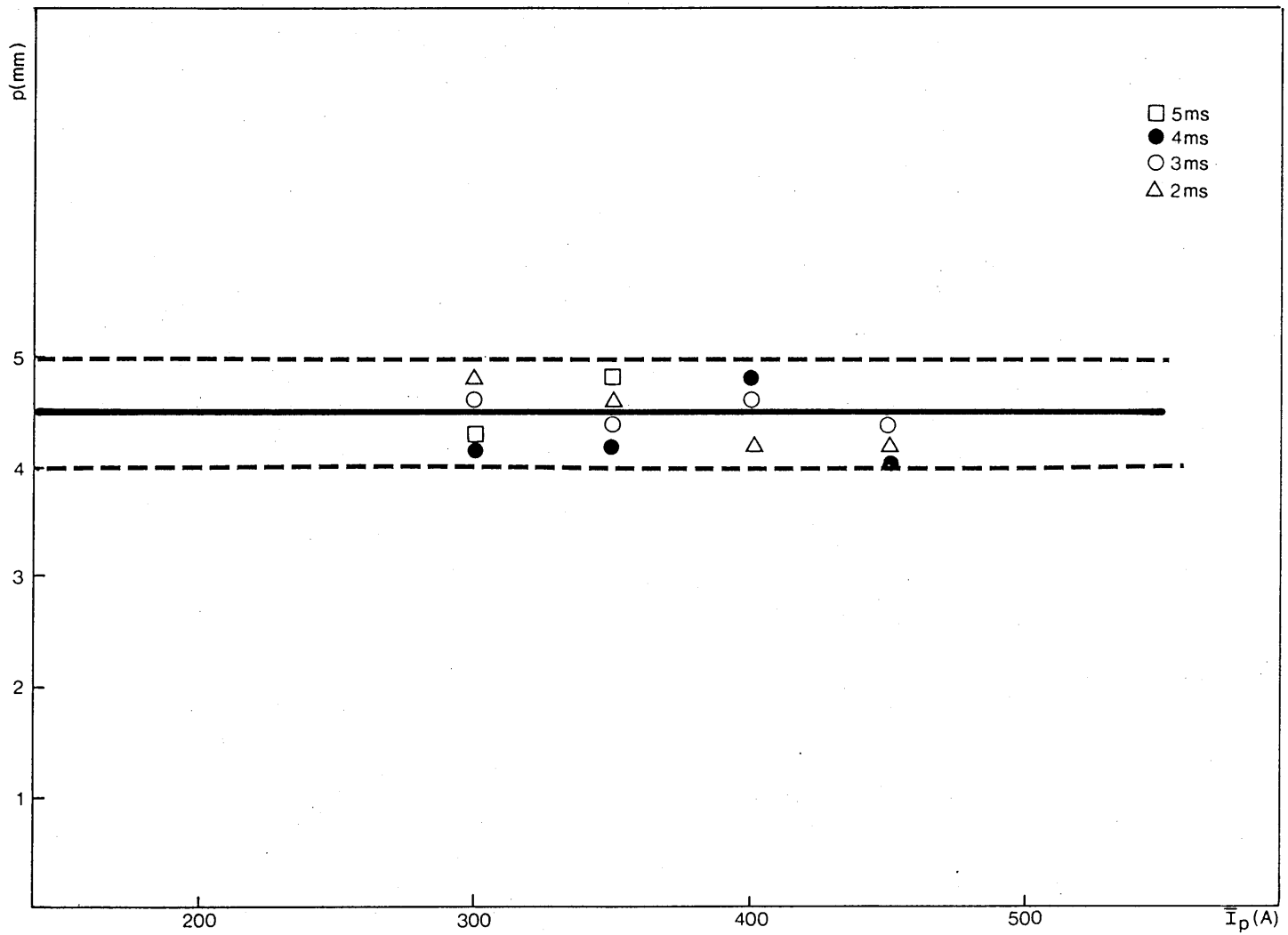

FIG. 56 - Influence of peak current on penetration for 250 Amps mean current,
(1.2 mm wire, Ar/5% CO_2 shield, ℓ = 15 mm)

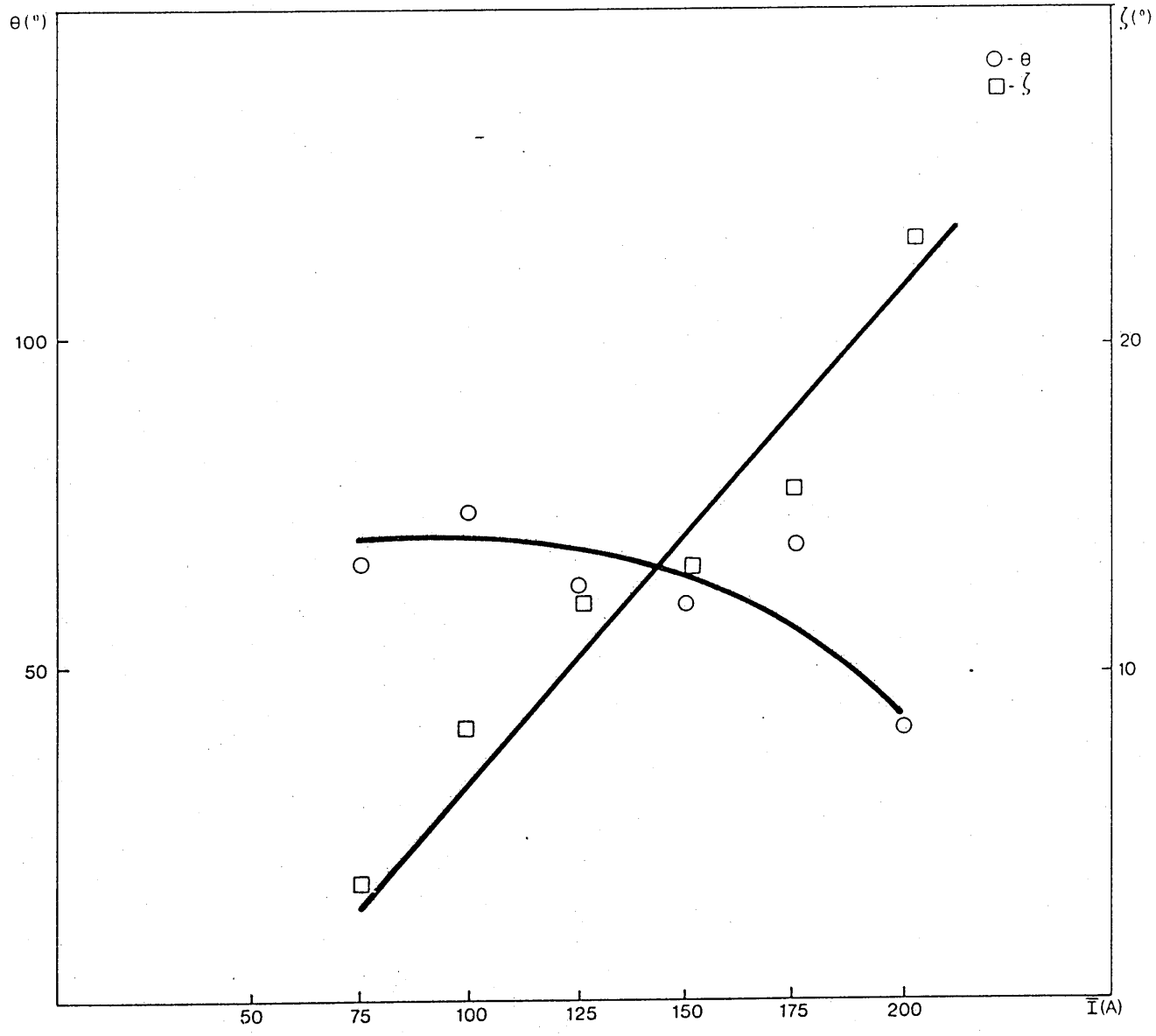

FIG. 57 - Influence of mean current on wetting angle (θ) and fusion angle (ζ)
(I_p = 350 A, t_p = 4 ms, ℓ = 15 mm, Ī/F= 2, Ar/5% CO_2)

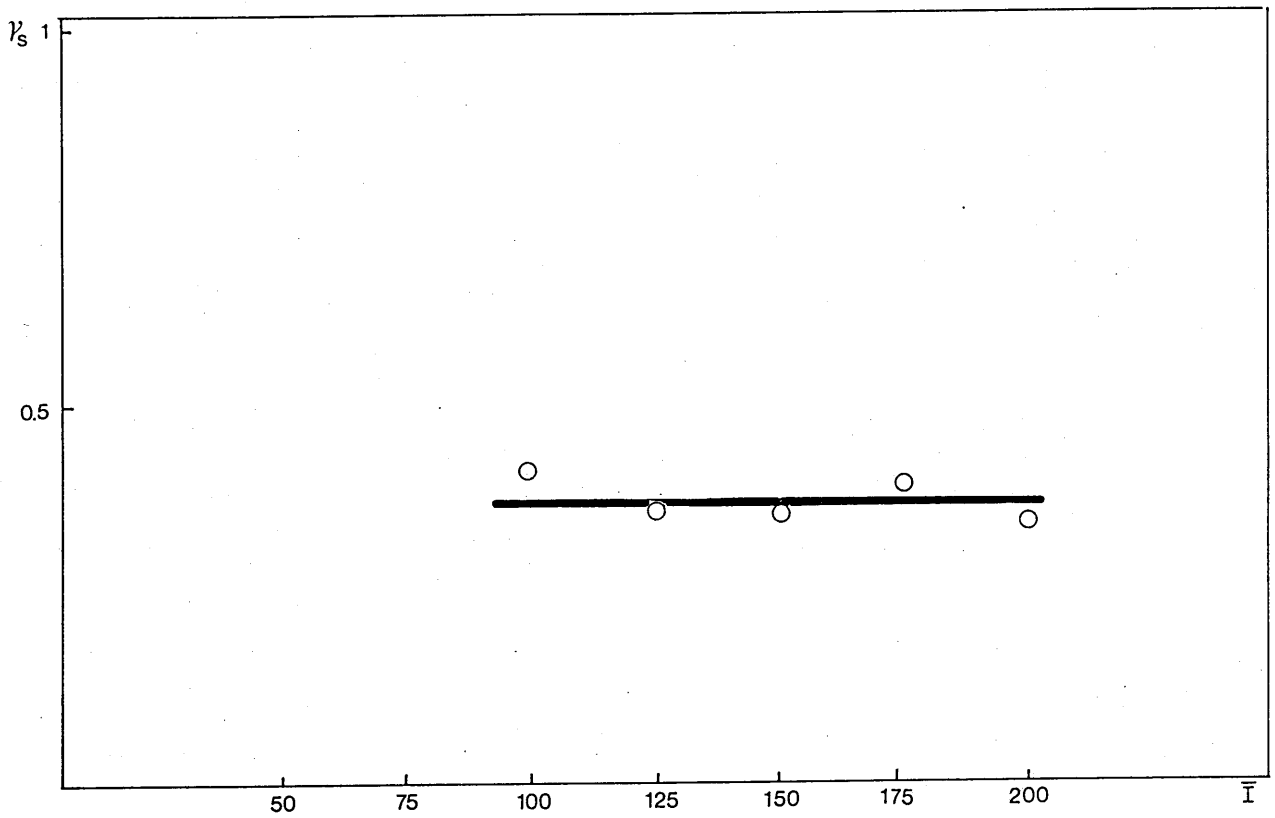

FIG. 58 - Influence of mean current on bead shape factor
(I_p= 350 A, t_p= 4ms, ℓ = 15mm, $\bar{I}/F$ = 2, Ar/5% CO_2)

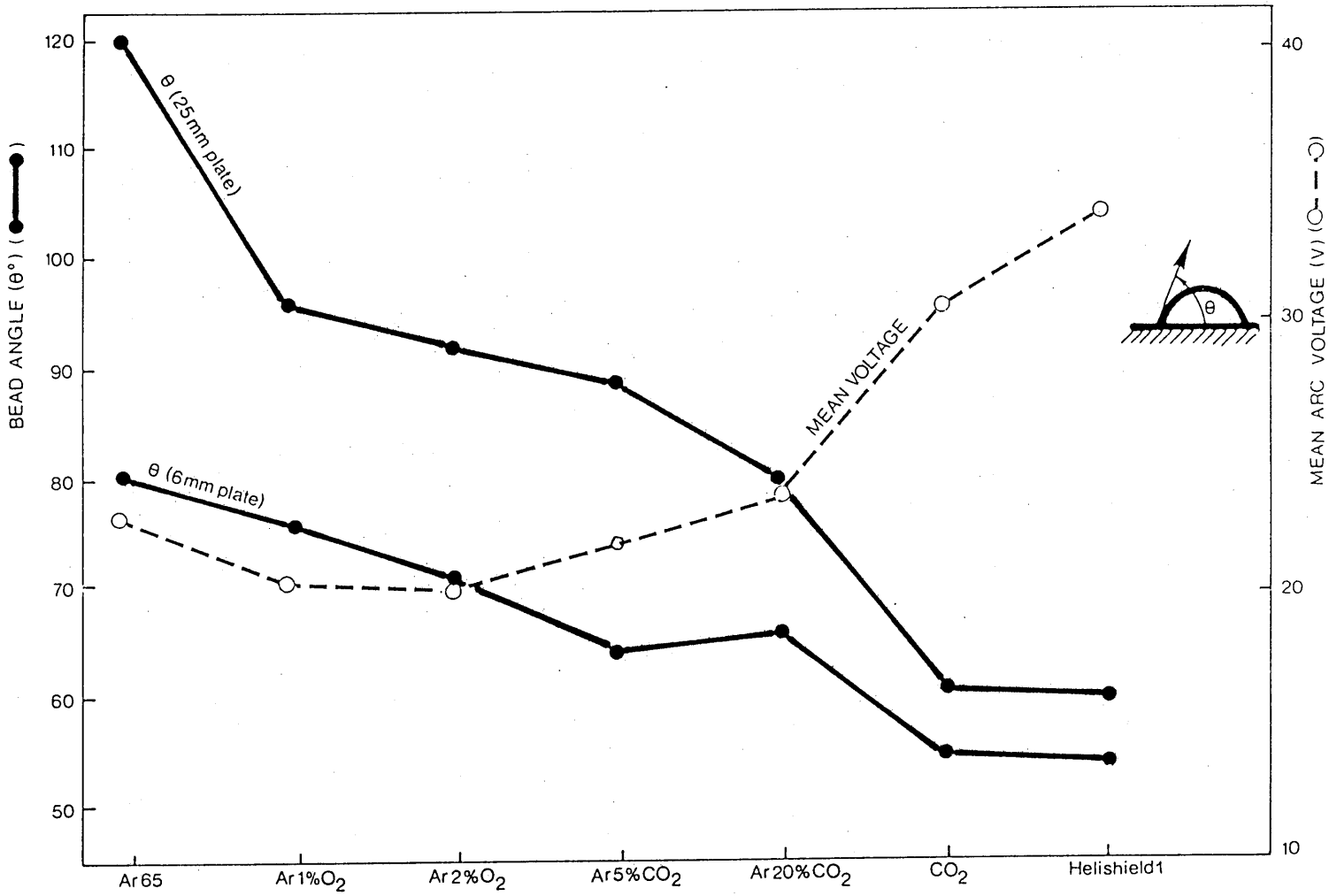

FIG. 59 - Influence of shielding gas composition on bead wetting angle and mean arc voltage (values average over 3 wire sizes)

($\bar{I}$ = 100 A, v = 1.53 mm/s, ℓ = 15 mm)

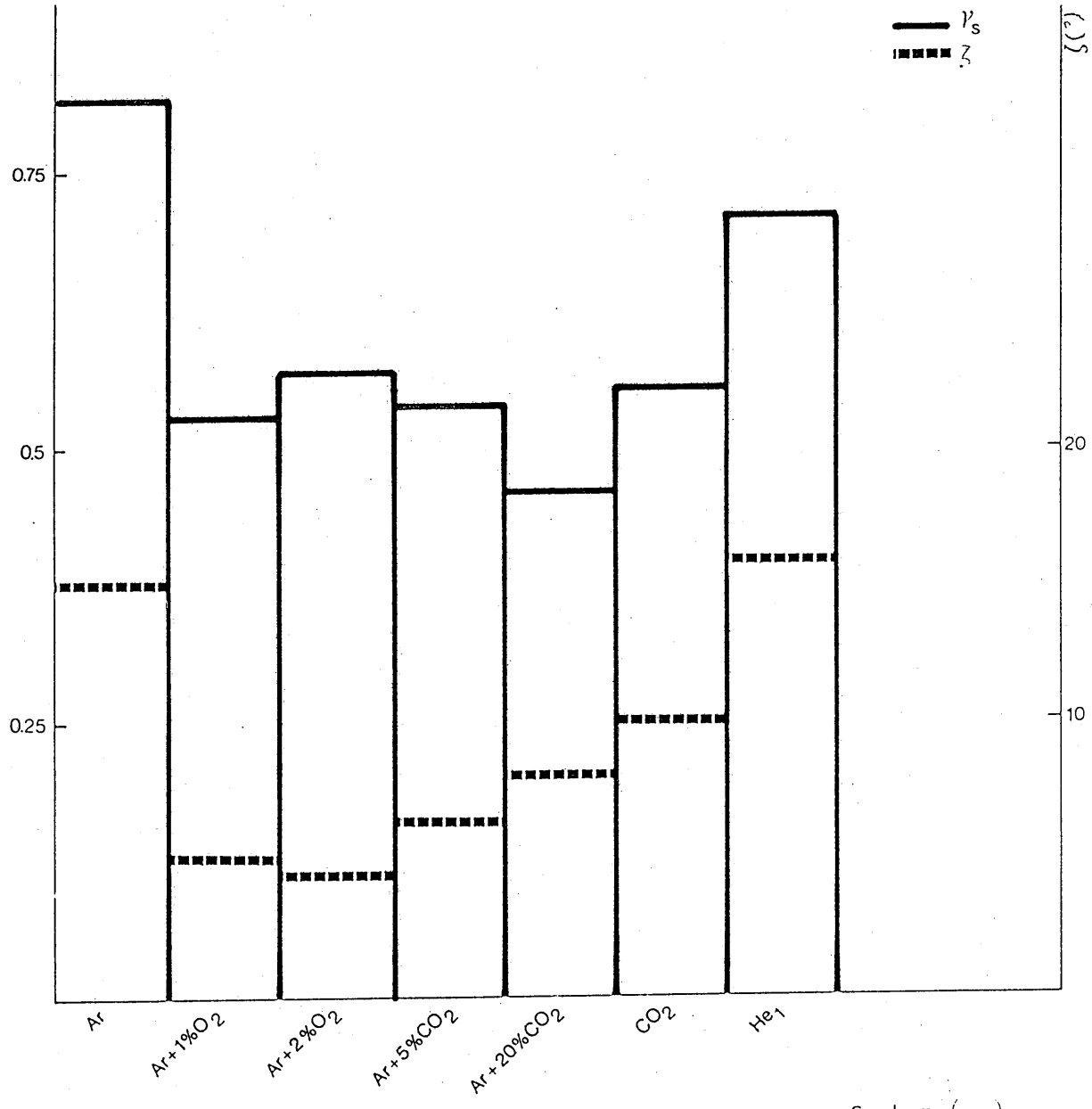

FIG.60 - Influence of shielding gas composition on bead shape factor (γ_s) and fusion angle (ζ)
($\bar{I}$ = 100 A, v = 1.53 cm/s, ℓ = 15 cm)

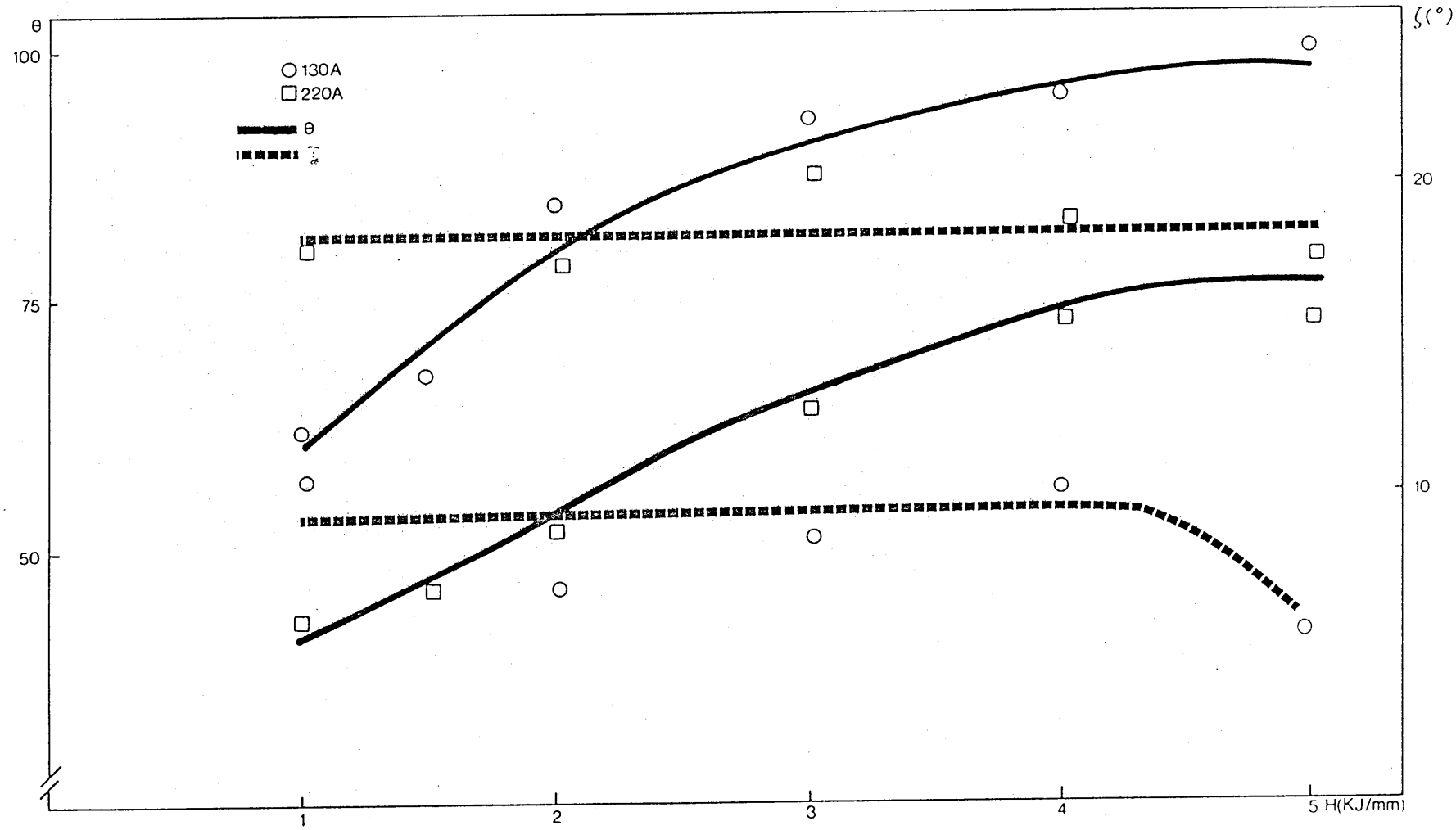

FIG. 61- Influence of nominal heat input on wetting angle (θ) and fusion angle (ζ)

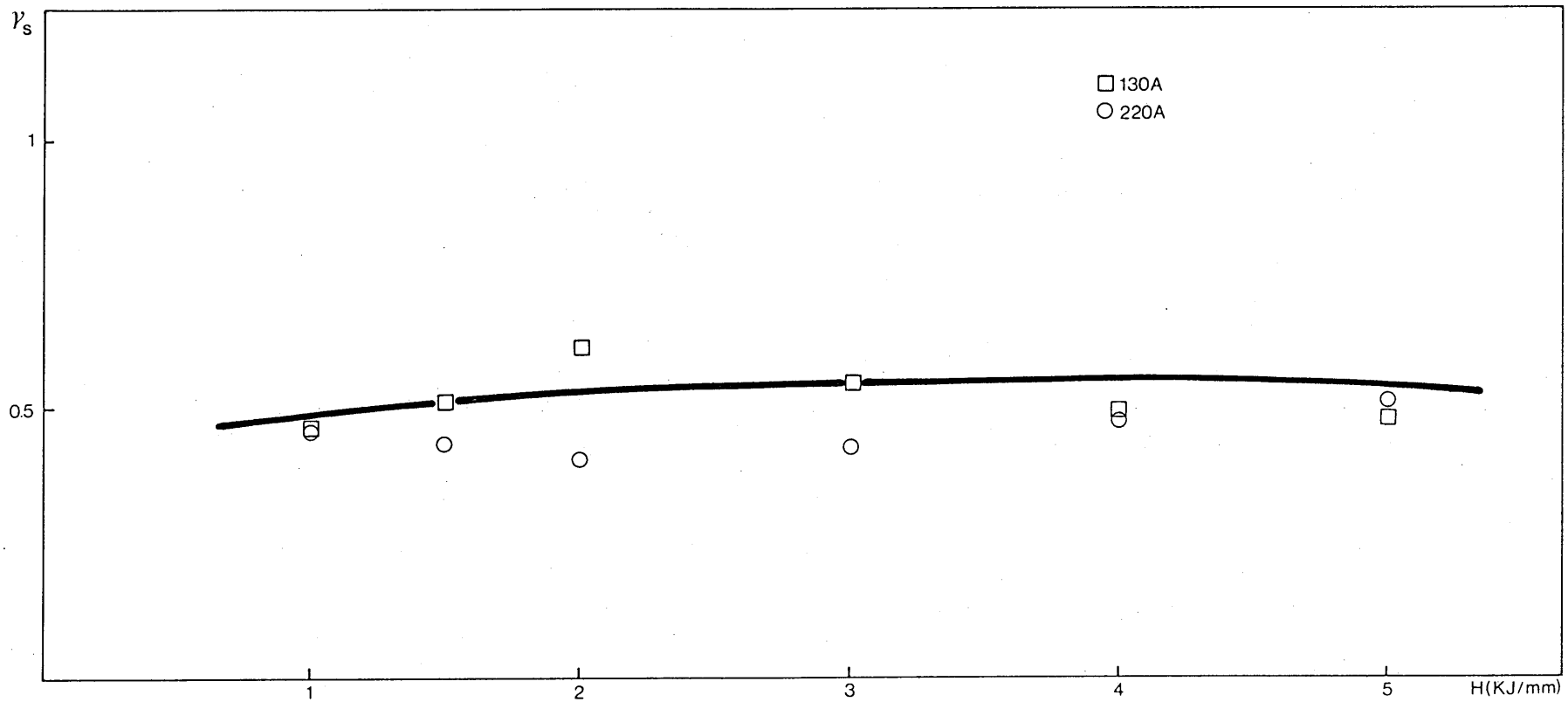

FIG. 62 - Influence of nominal heat input on bead shape factor
(I_p= 350A, t_p= 4ms, $\bar{I}/F$ = 2, ℓ = 15mm, Ar/5% CO_2)

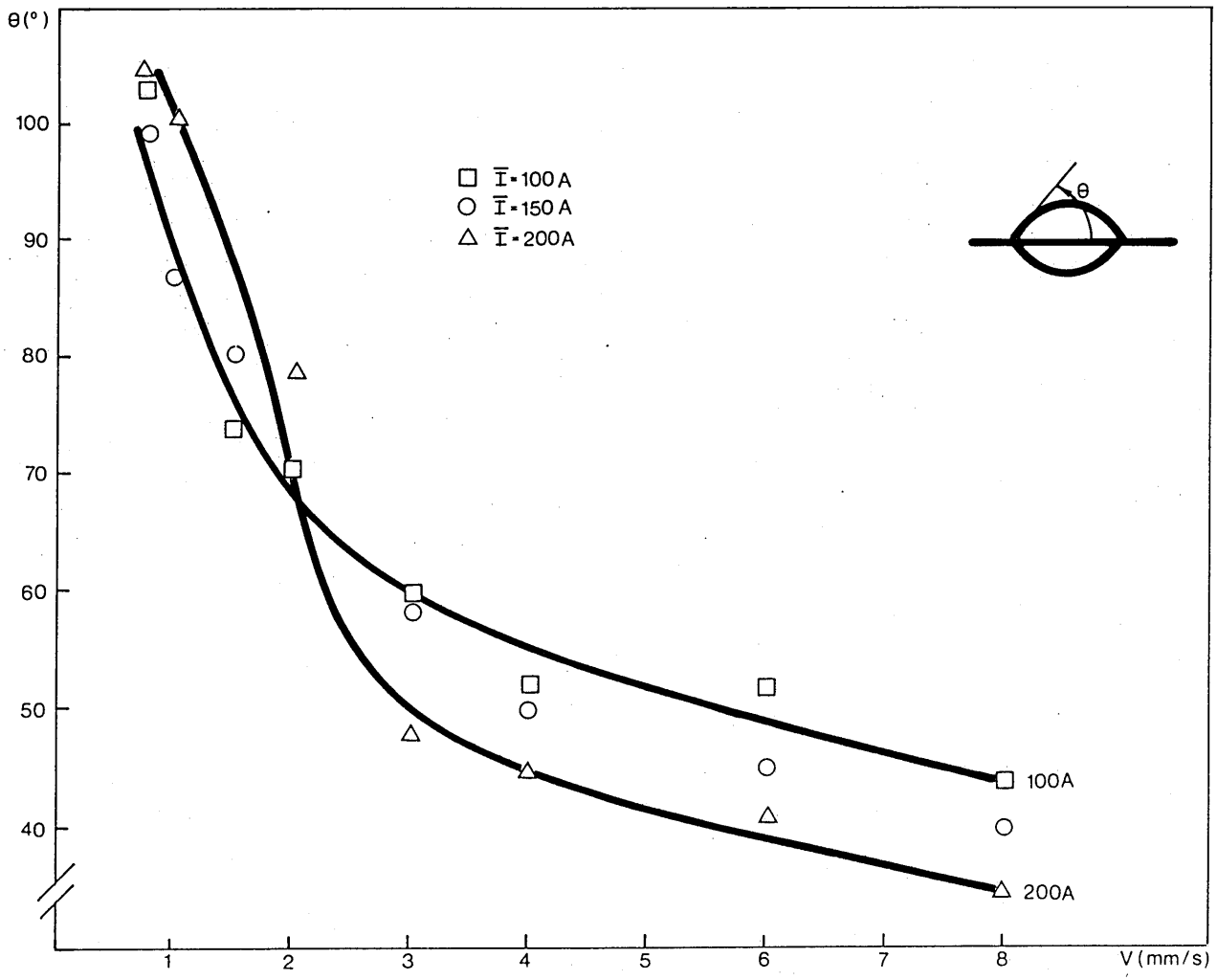

FIG. 63 - Effect of arc current and welding speed on bead plate wetting angle

(ℓ = 15 mm, 1.2 mm wire diameter, Ar/5% CO_2)

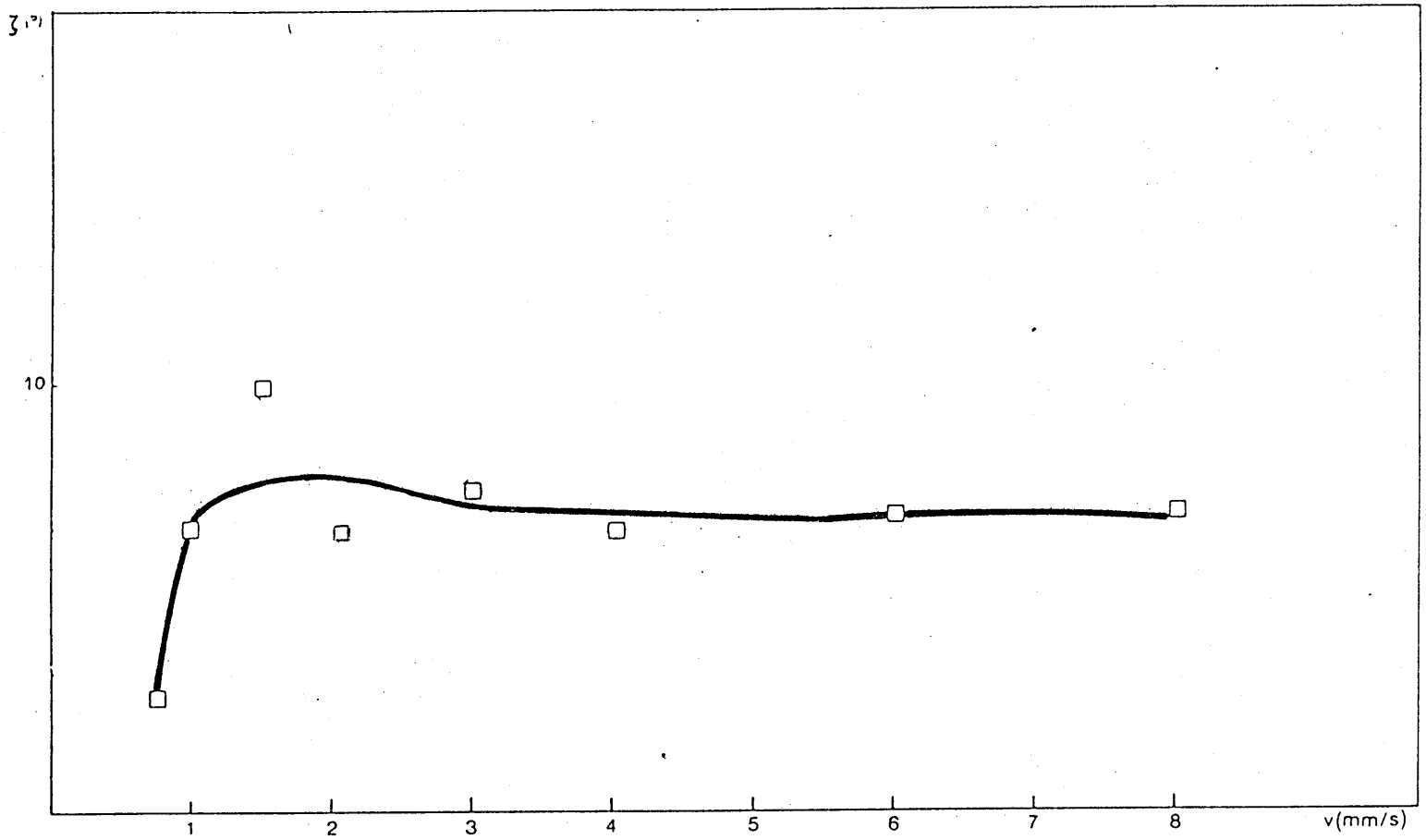

FIG. 64 - Influence of welding speed on plate fusion angle
($\bar{I}$ = 100 A, $\bar{I}/F$ = 2, I_p = 350 A, t_p = 4 ms, 1.2 mm wire diameter)

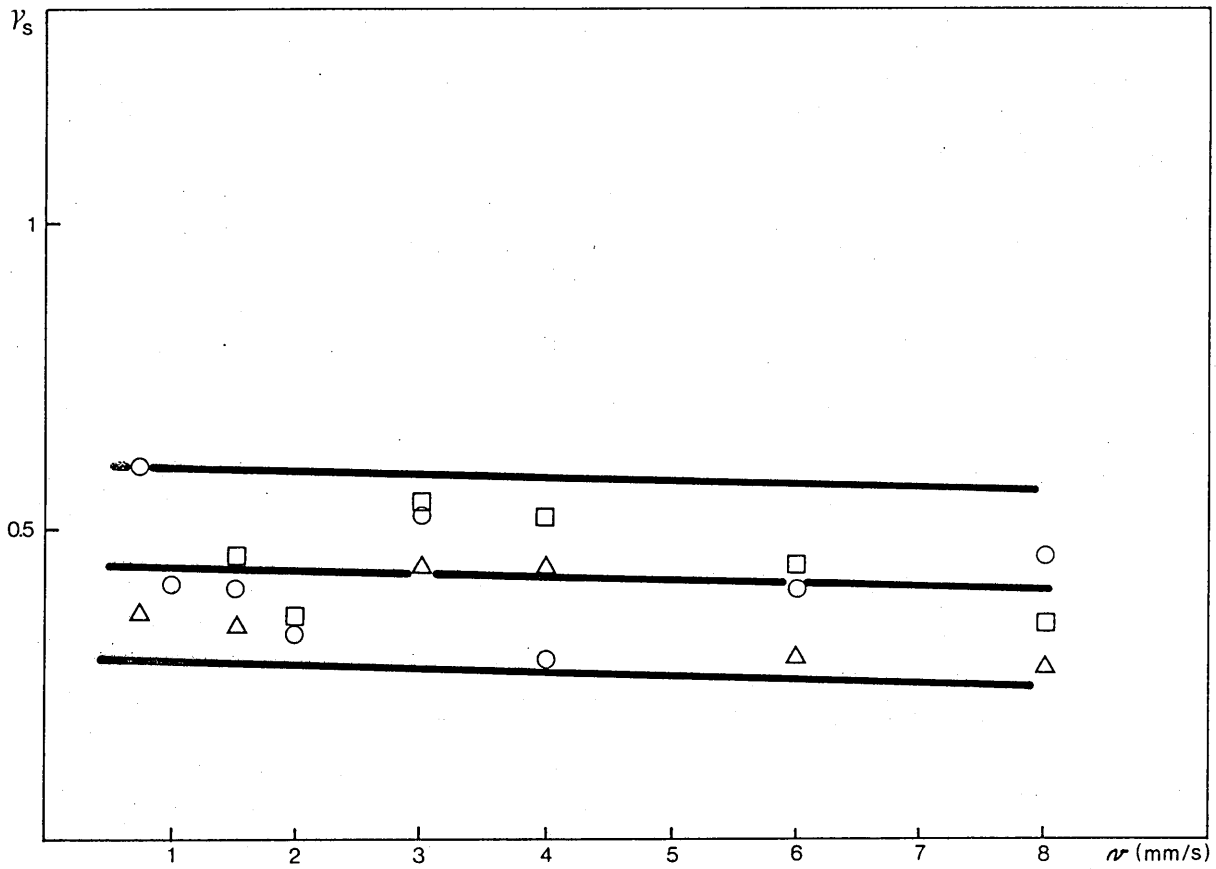

FIG.65- Influence of welding speed on bead shape factor for different mean currents with 1.2 mm wire in an Ar/5% CO_2 shield

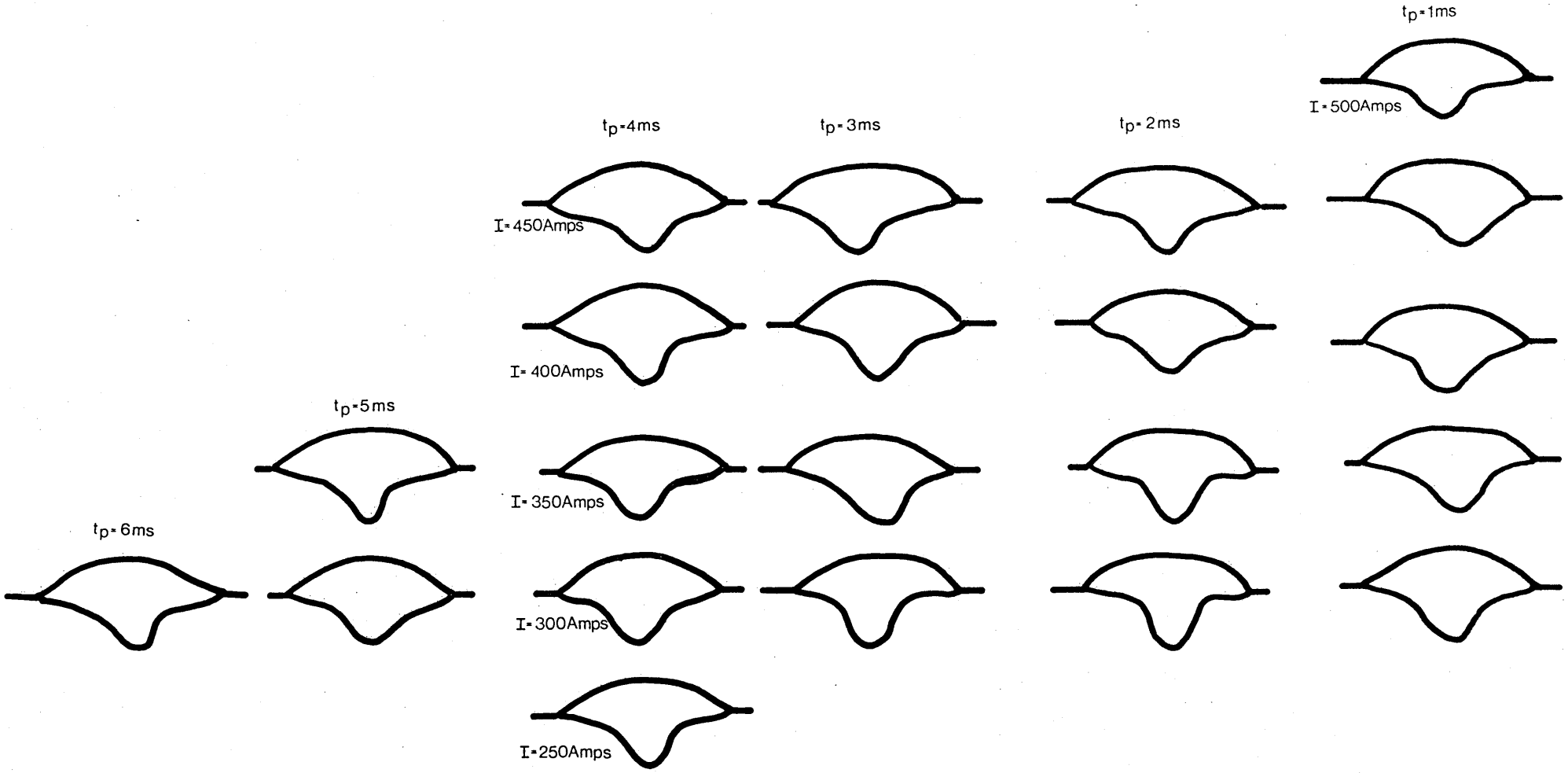

FIG. 66 - Bead shape in mild steel with an Ar/5% CO_2 shield for a 1.2 wire size ($\bar{I}$ = 250A, F = 125 Hz)

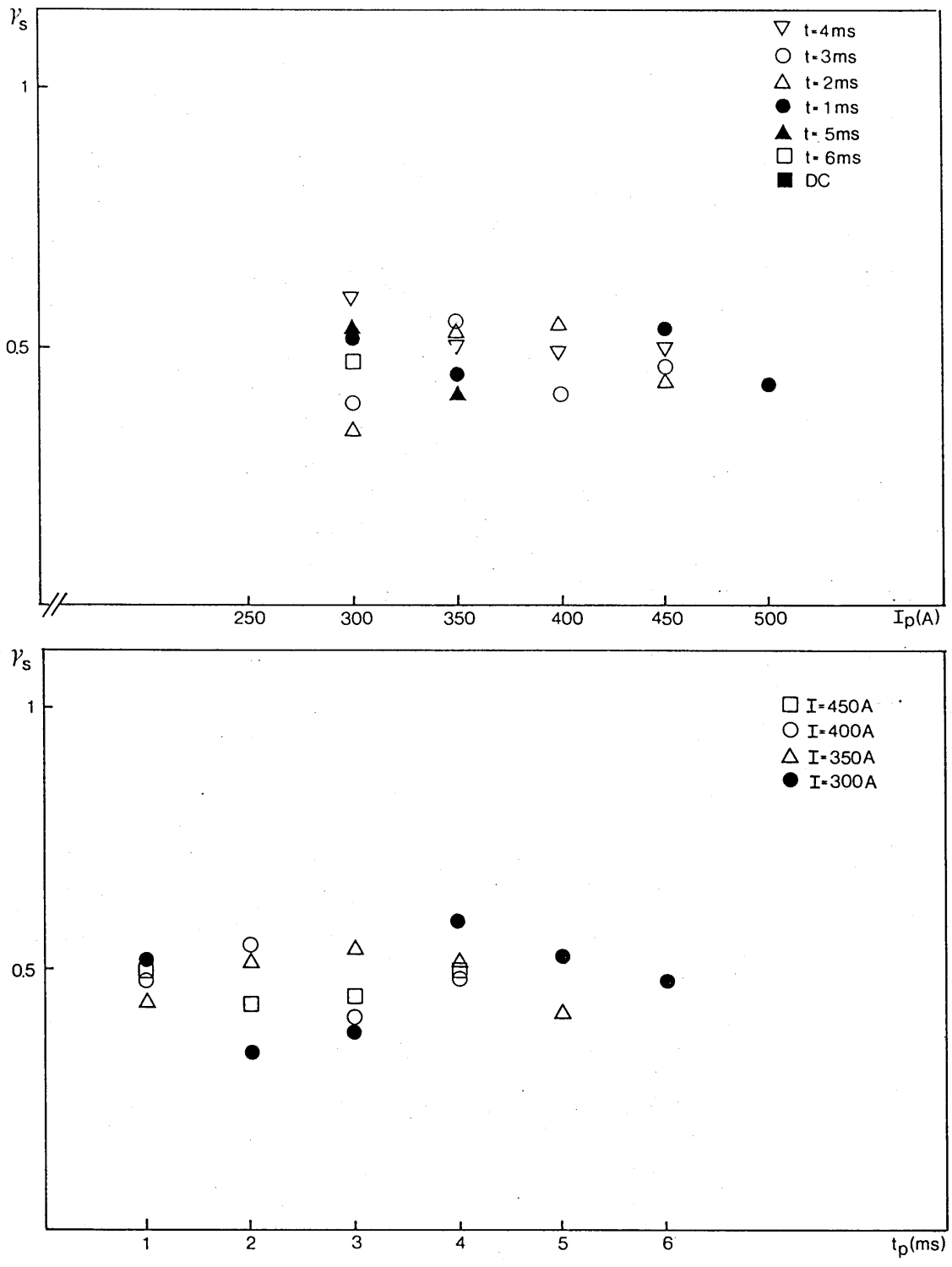

FIG.67- Influence of peak parameters on bead shape factor ($\bar{I}$ = 250 A, F = 125 Hz, ℓ = 15 mm, Ar/5% CO_2)

i) influence of peak current on bead shape factor for different peak durations

ii) influence of peak durations on bead shape factor for different peak currents

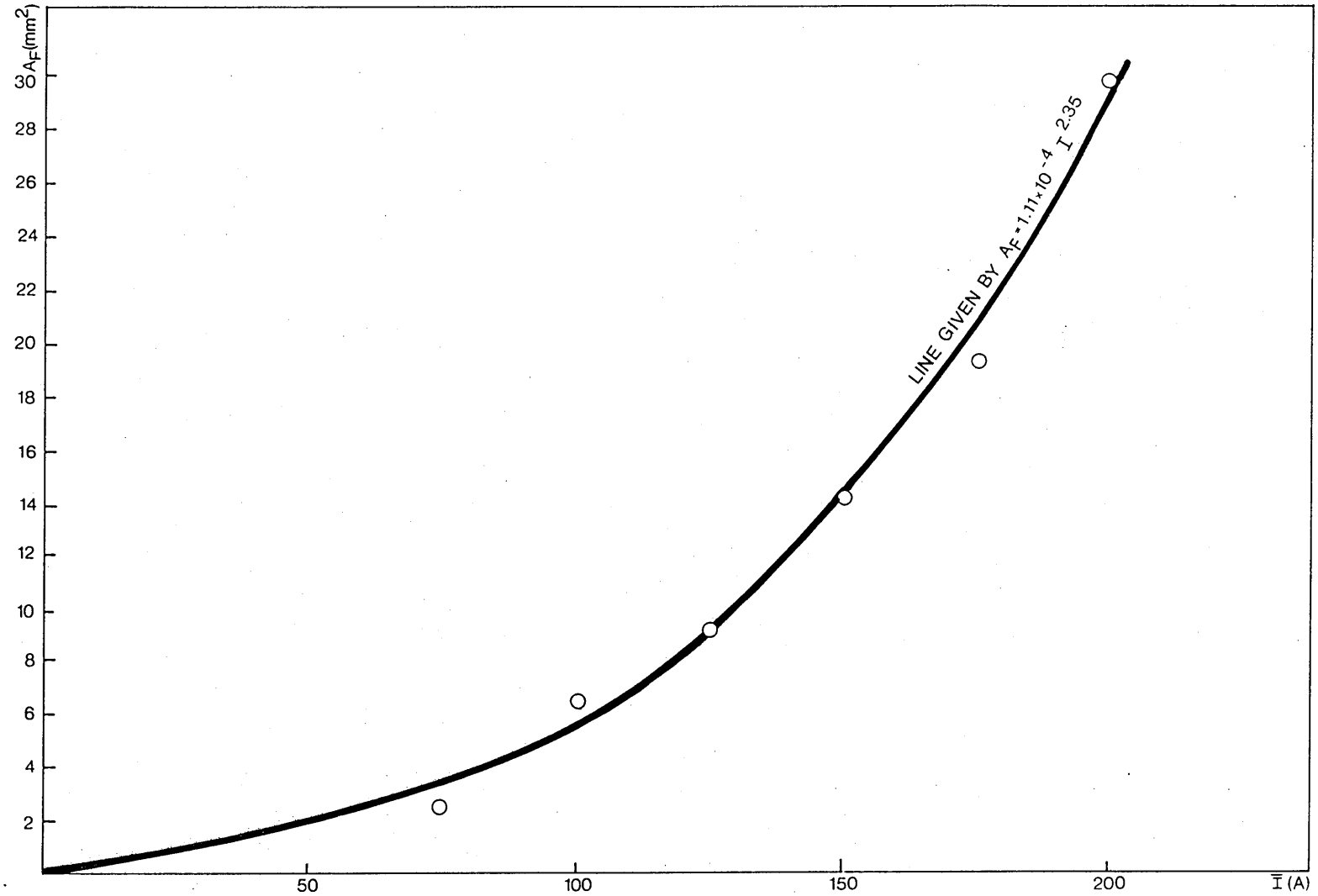

FIG. 68 – Influence of mean current on plate fusion area for 1.2 mm wire size in an Ar/5% CO_2 shield on thick plate (ℓ = 15 mm, v = 1.53 m/s)

(1.2 mm wire diameter, ℓ = 15 mm, Ar/5% CO_2)

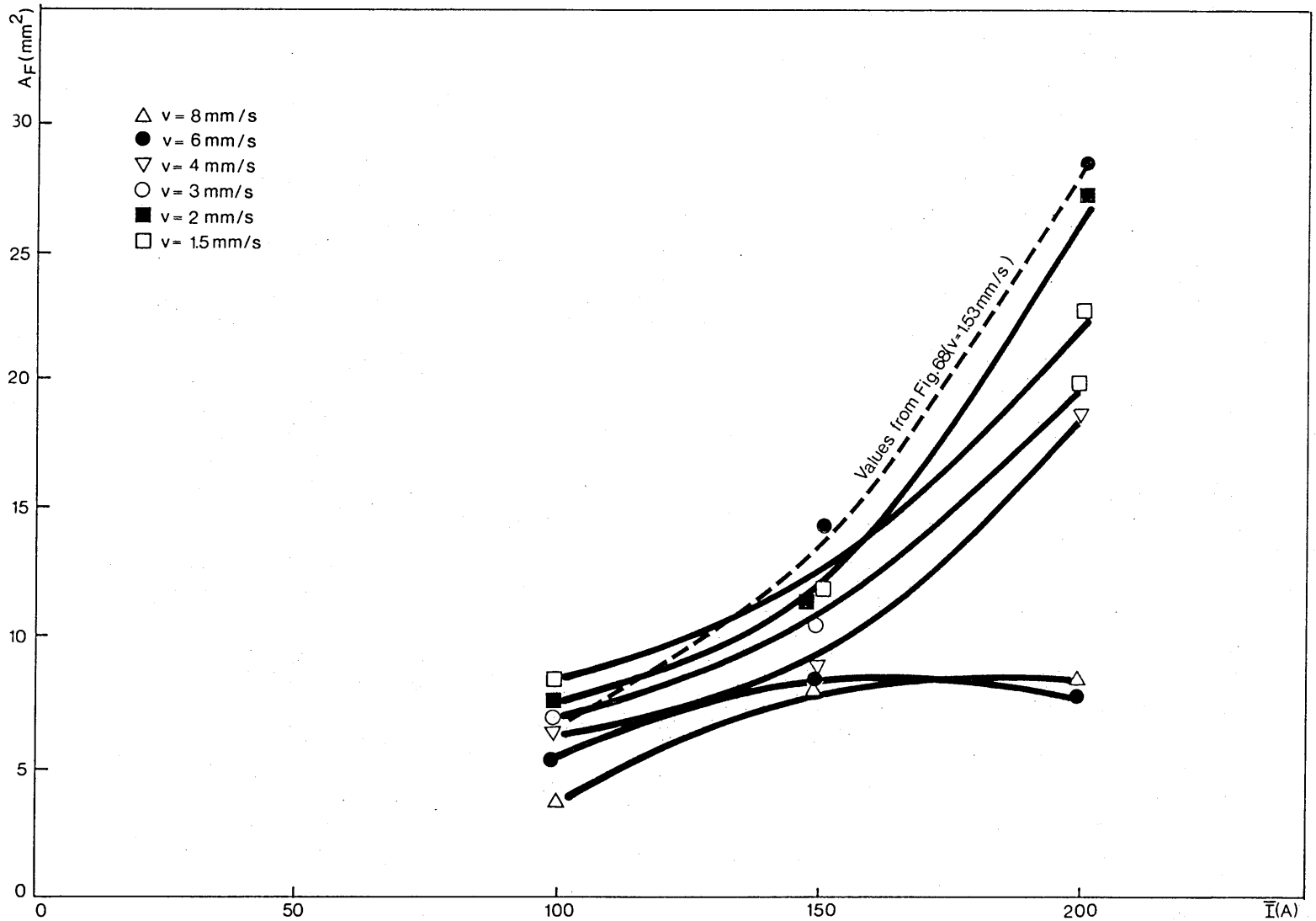

FIG. 69 - Influence of arc current ($\bar{I}$) on plate fusion area (A_F)

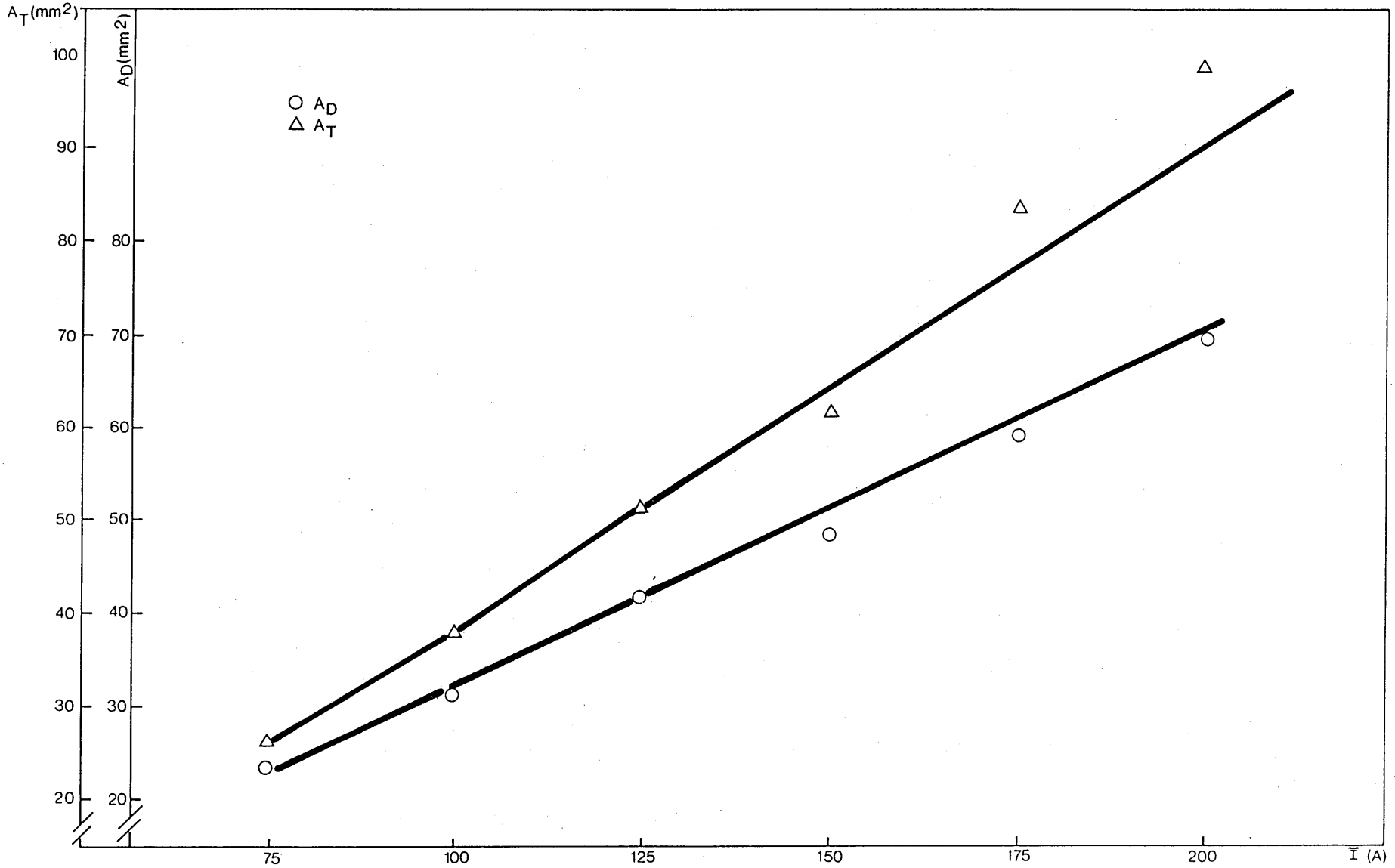

FIG. 70 - Influence of mean current ($\bar{I}$) on total fusion area (A_T) and reinforcement area (A_R) (1.2mm wire, Ar/5% CO_2, I_p= 350A, t_p= 4ms, $\bar{I}/F$ = 2, v = 1.53mm/s)

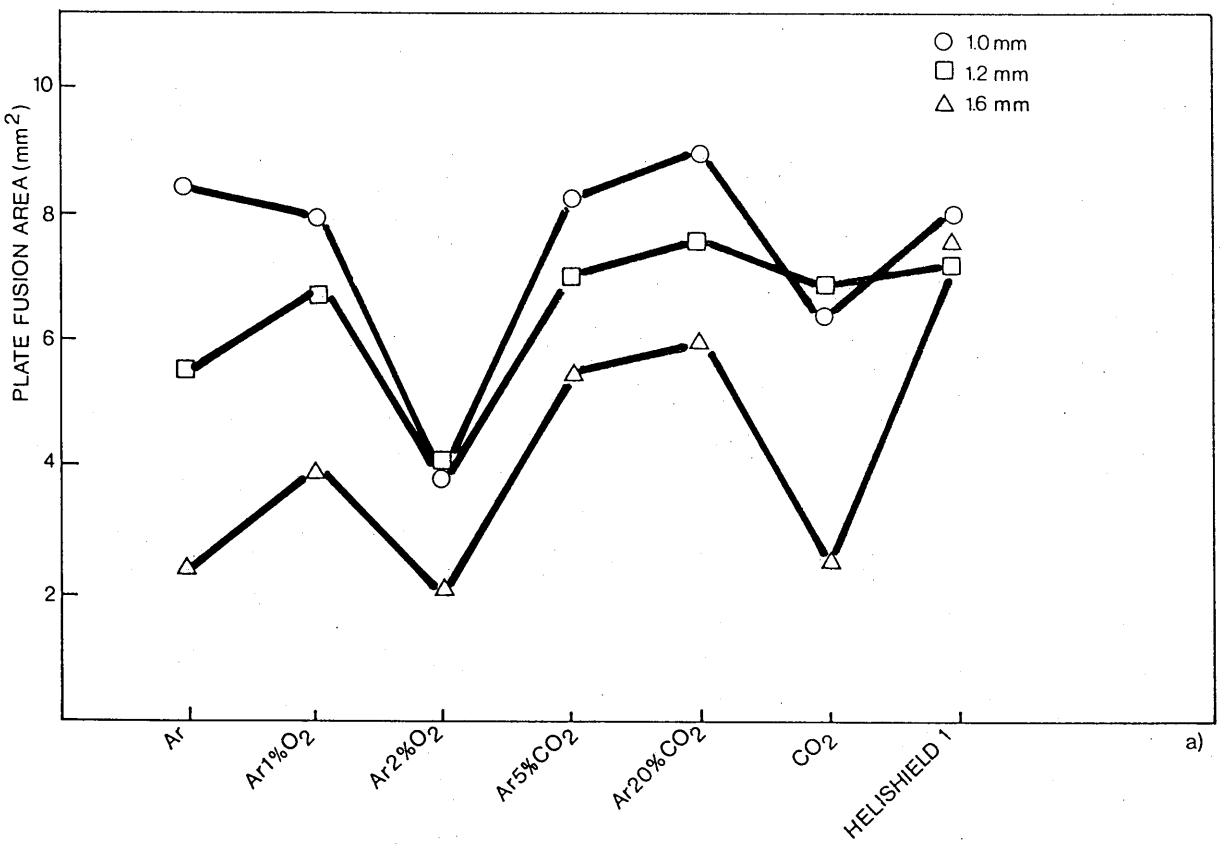

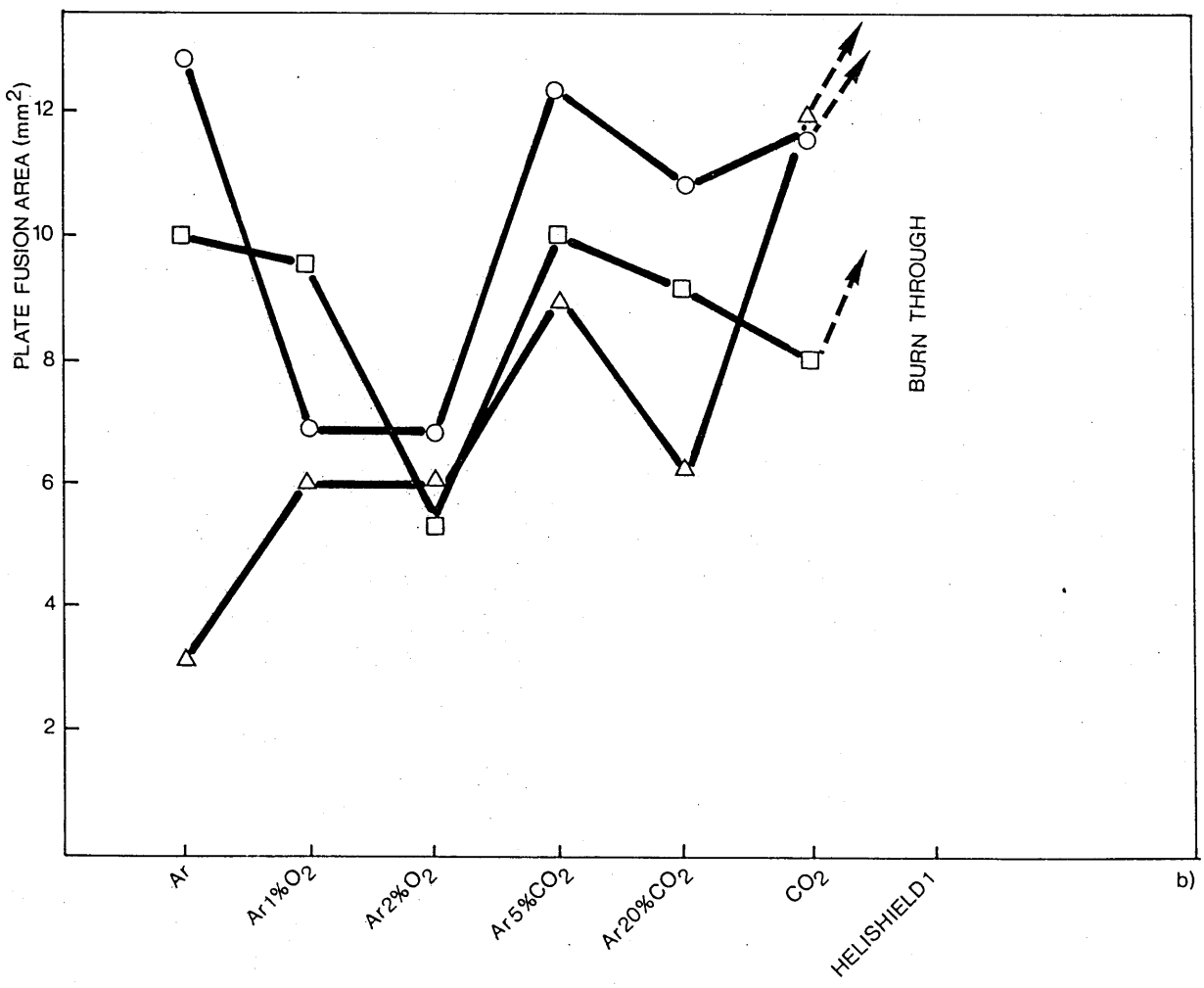

FIG. 7 1- Influence of wire size and shield gas composition on plate fusion area (I = 100 A, v = 1.53 m/s, ℓ = 15 m)

(a) Thick plate (b) thin plate

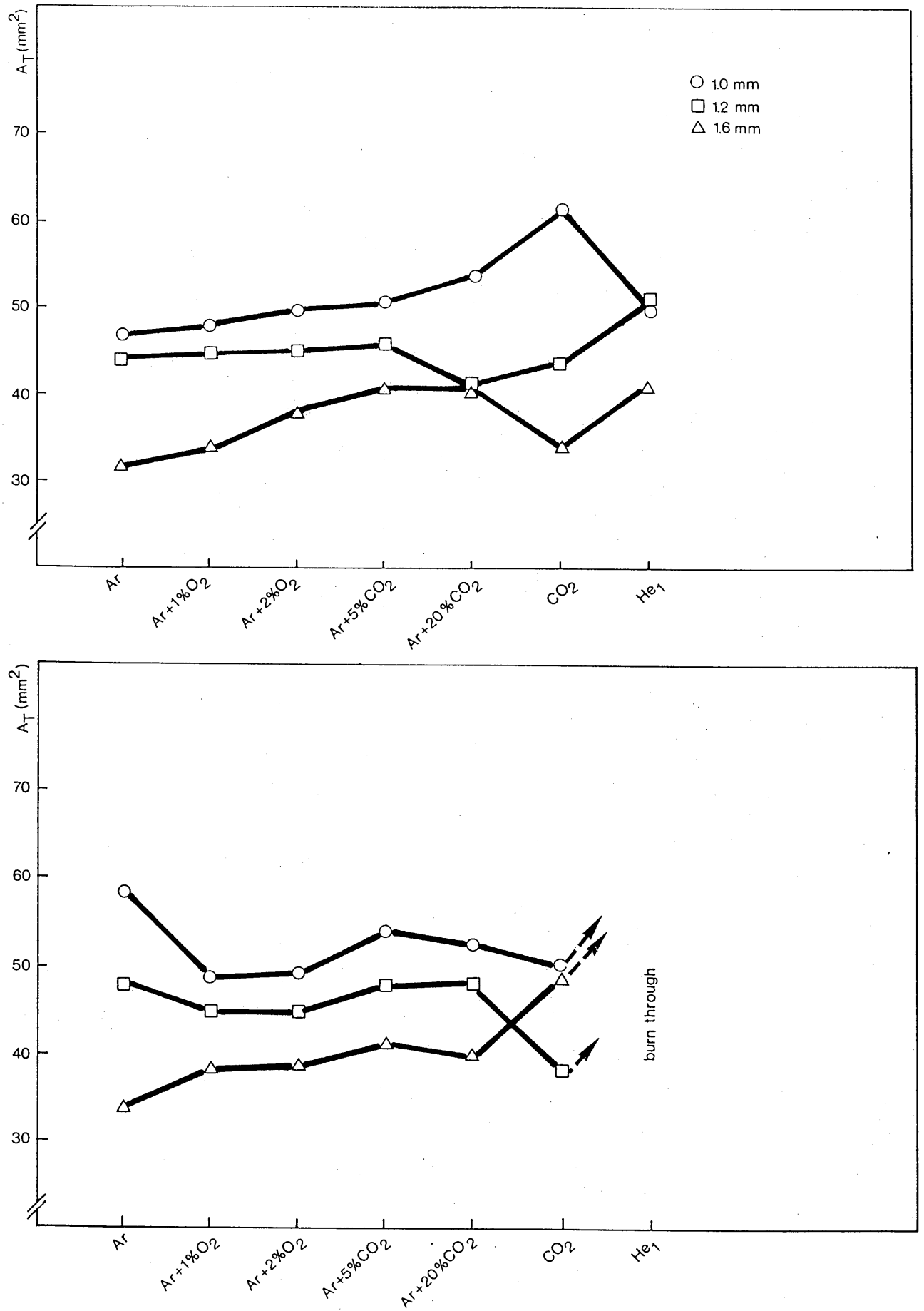

FIG. 72 - Influence of wire size and shielding gas composition on total fusion area
($\bar{I}$ = 100 A, v = 1.53 m/s, = 15 mm)

(a) Thick plate (b) Thin plate

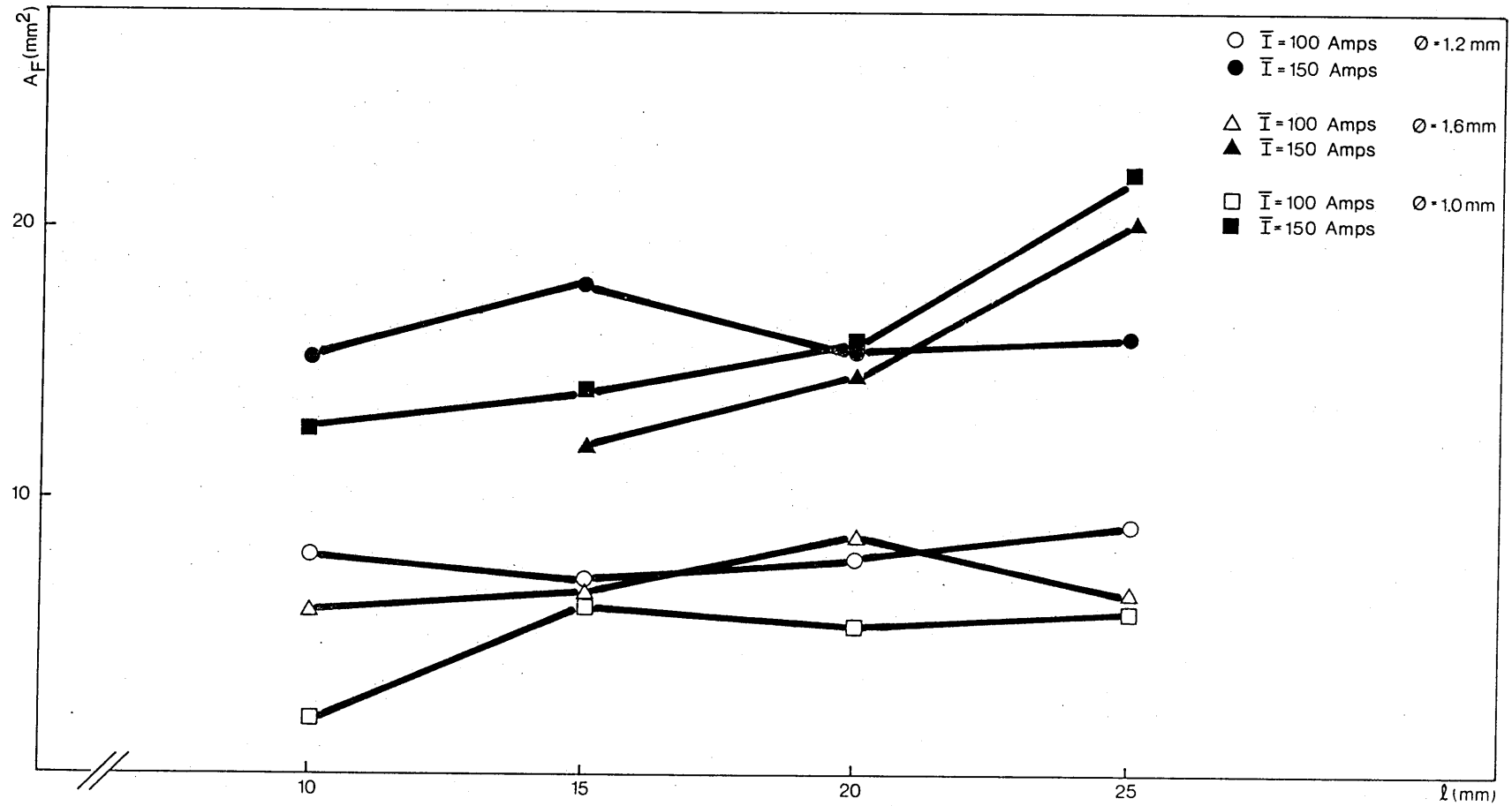

FIG. 7 3 - Influence of electrode extension on plate fusion area for mean currents of 100 and 150 Amps and 1.0, 1.2 and 1.6 mm wire diameters in an Ar/5% CO_2 shield (v = 1.53 mm/s)

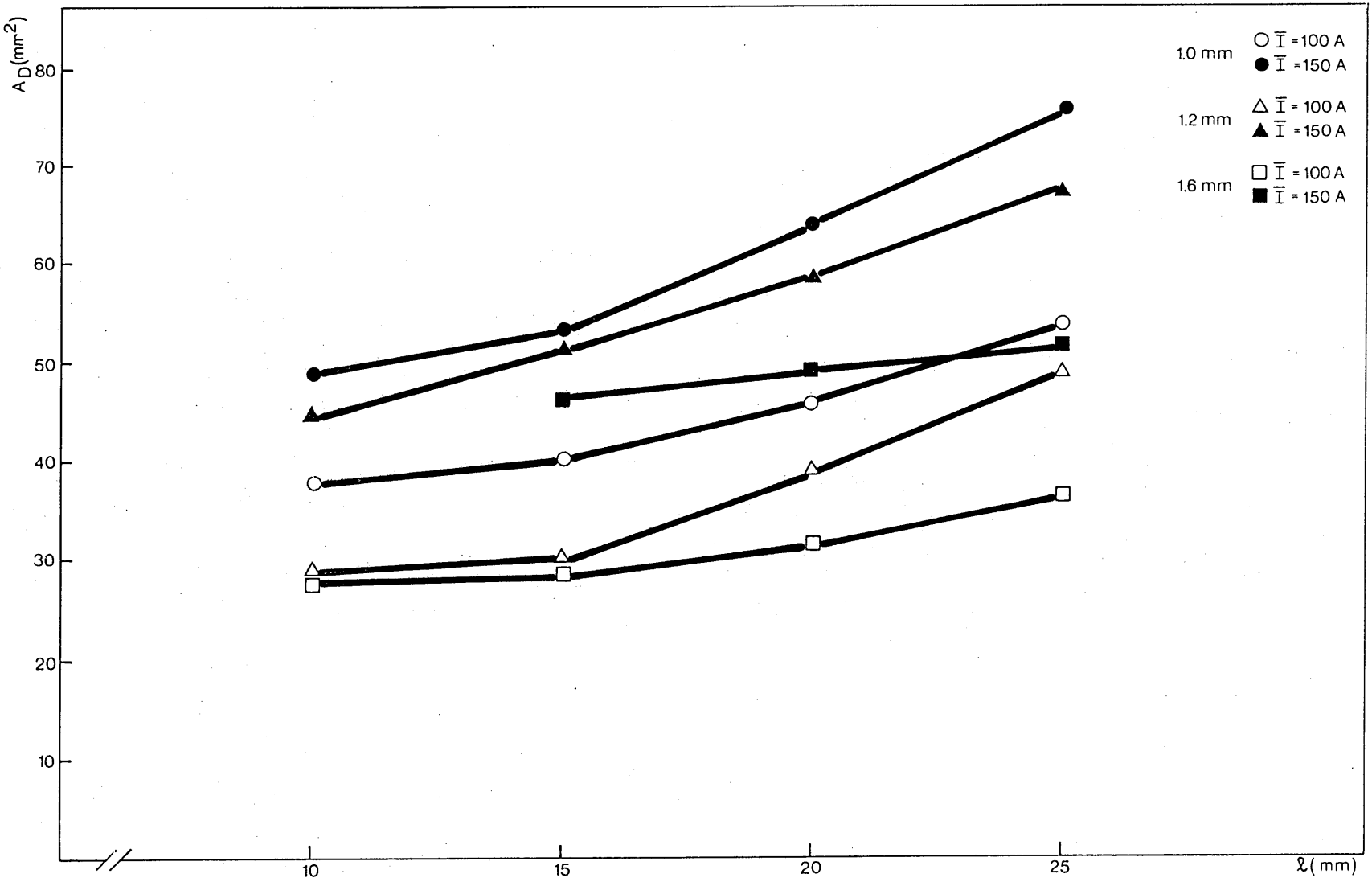

FIG. 74 - Influence of electrode extension on deposited area
(Ar/5% CO_2, v = 1.53 mm/s)

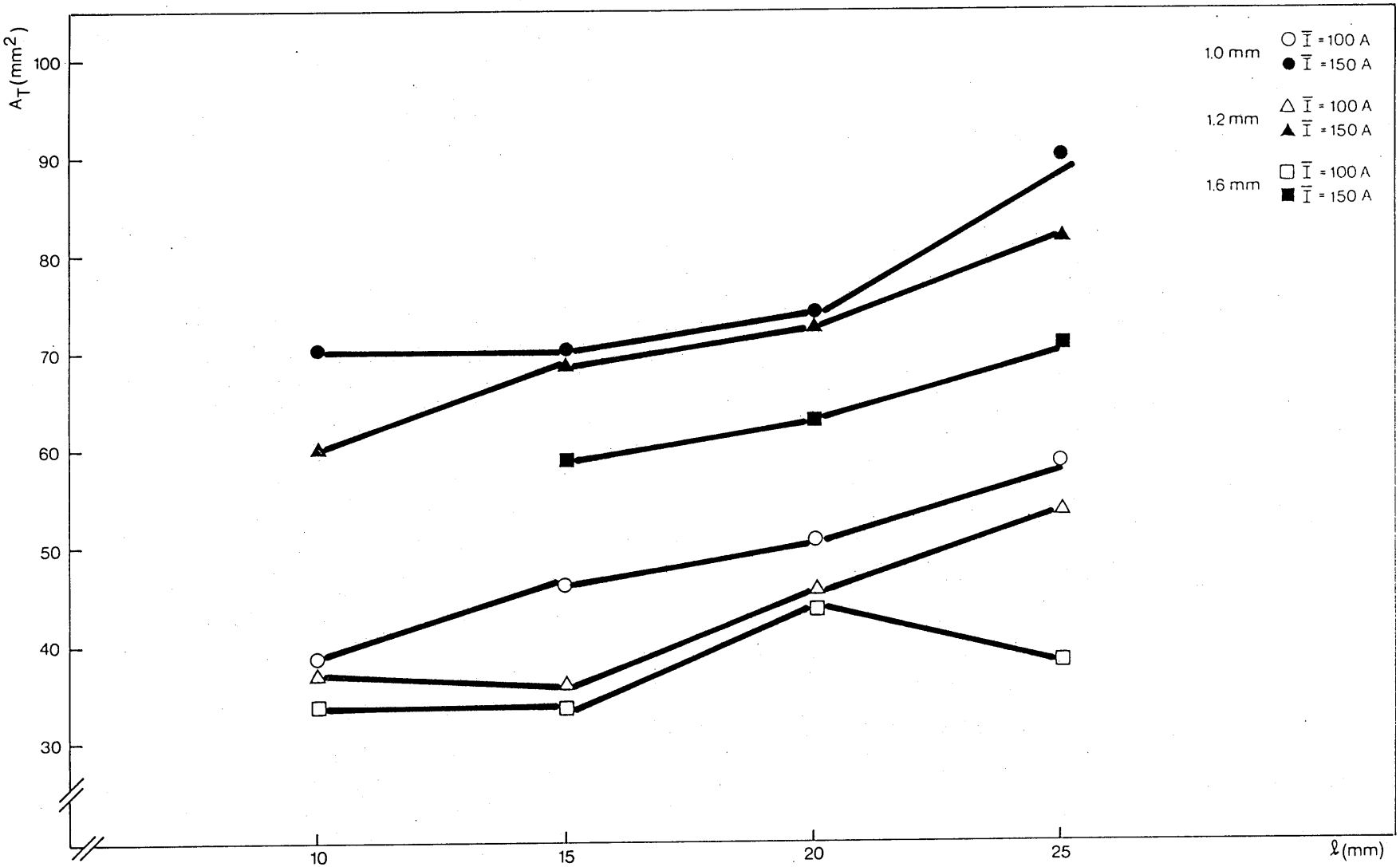

FIG. 75 - Influence of electrode extension on total area
(Ar/5% CO_2, v = 1.53 mm/s)

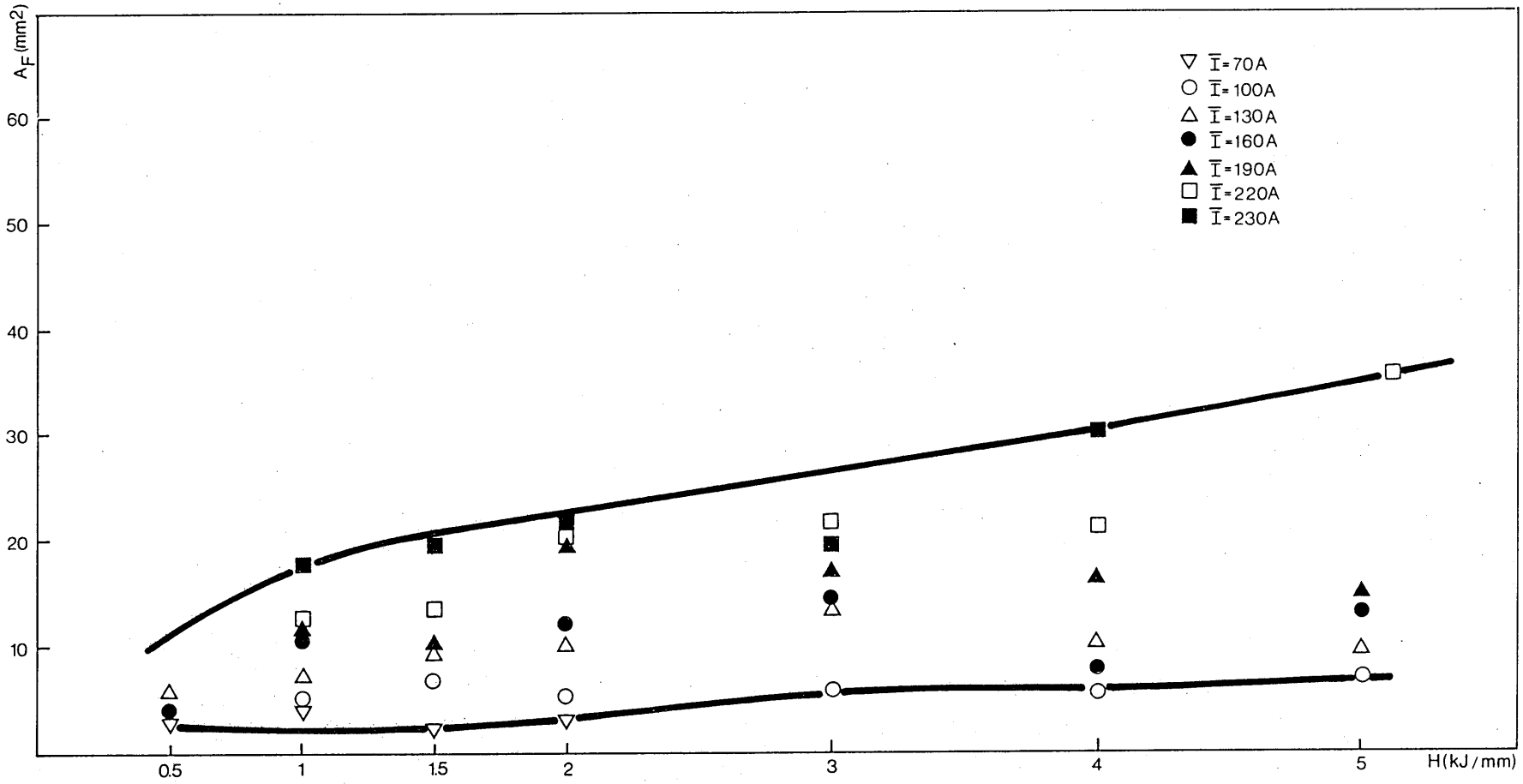

FIG. 7.6 - Influence of nominal heat input on plate fusion area
(I_p= 350A, t_p= 4ms, $\bar{I}/F$ = 2, ℓ = 15 mm)

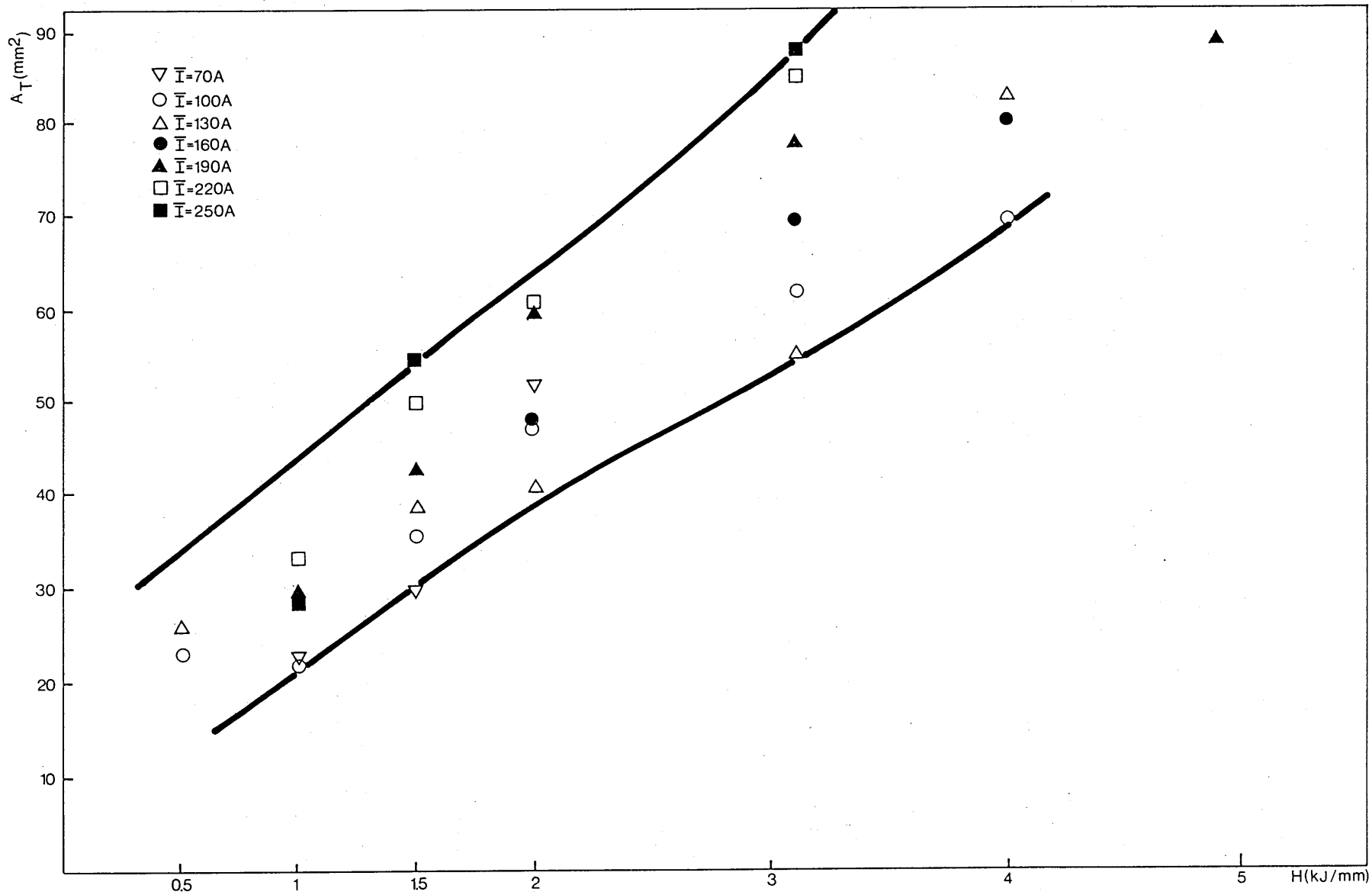

FIG. 7 7 - Influence of nominal heat input on total fusion area
(I_p= 350A, t_p= 4ms, $\bar{I}/F$ = 2, ℓ = 15mm)

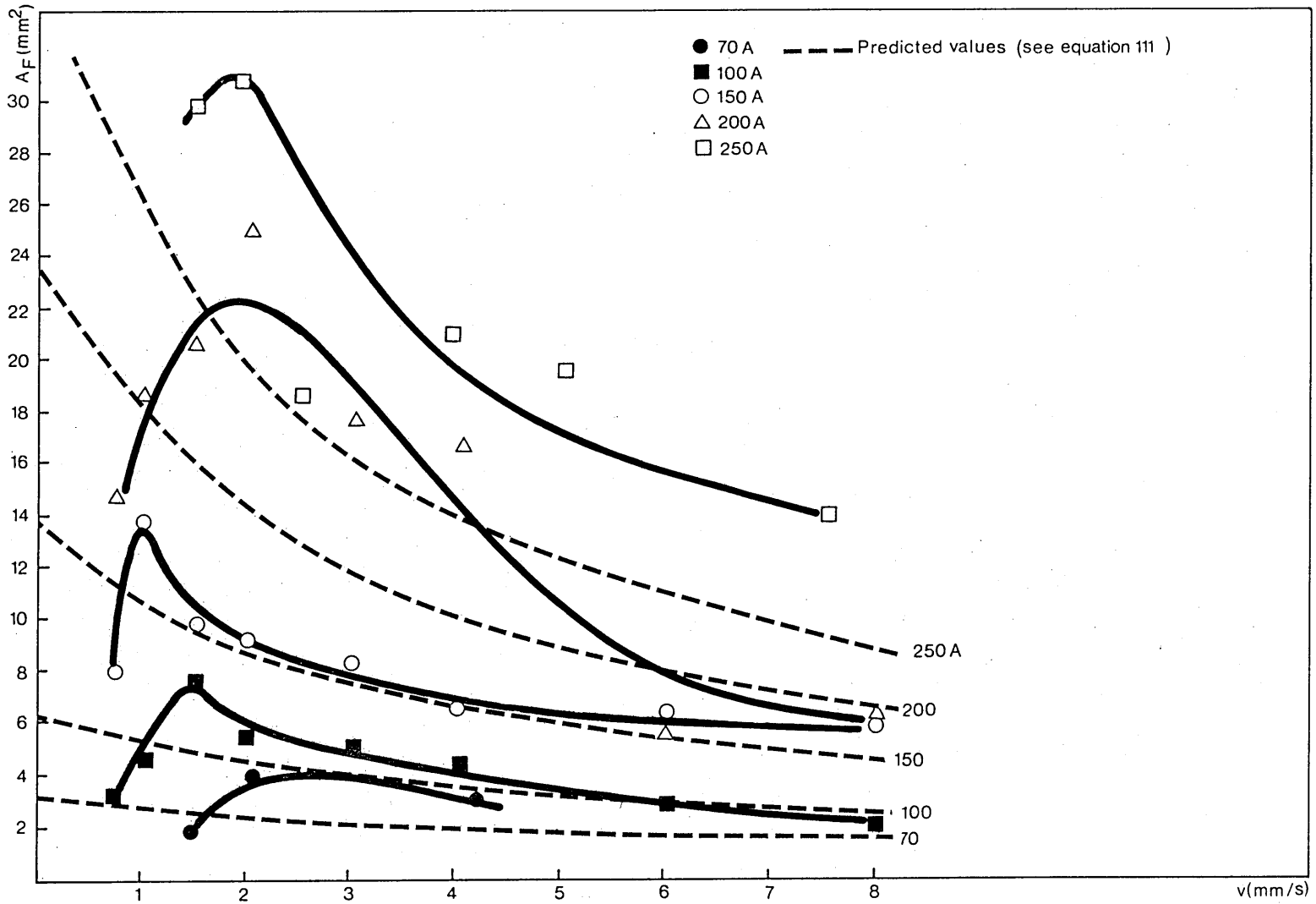

FIG. 78 - Influence of welding speed on plate fusion area (A_F)

(ℓ = 15 mm, Ar/5% CO_2)

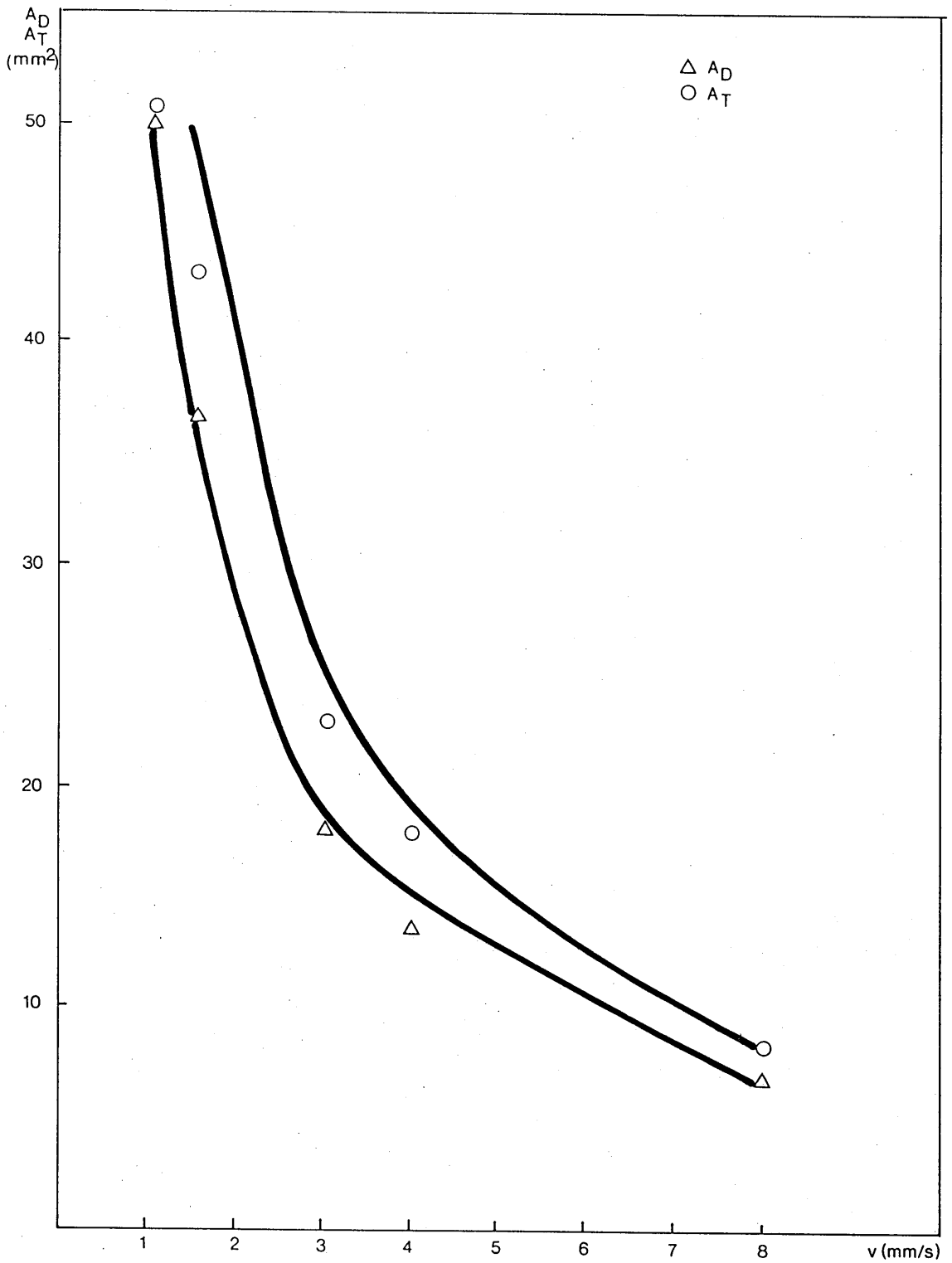

FIG. 79 - Influence of welding speed on total fusion area (A_T) and reinforcement area (A_D) ($\bar{I}$ = 100 A, ℓ = 15 mm, Ar/5% CO_2)

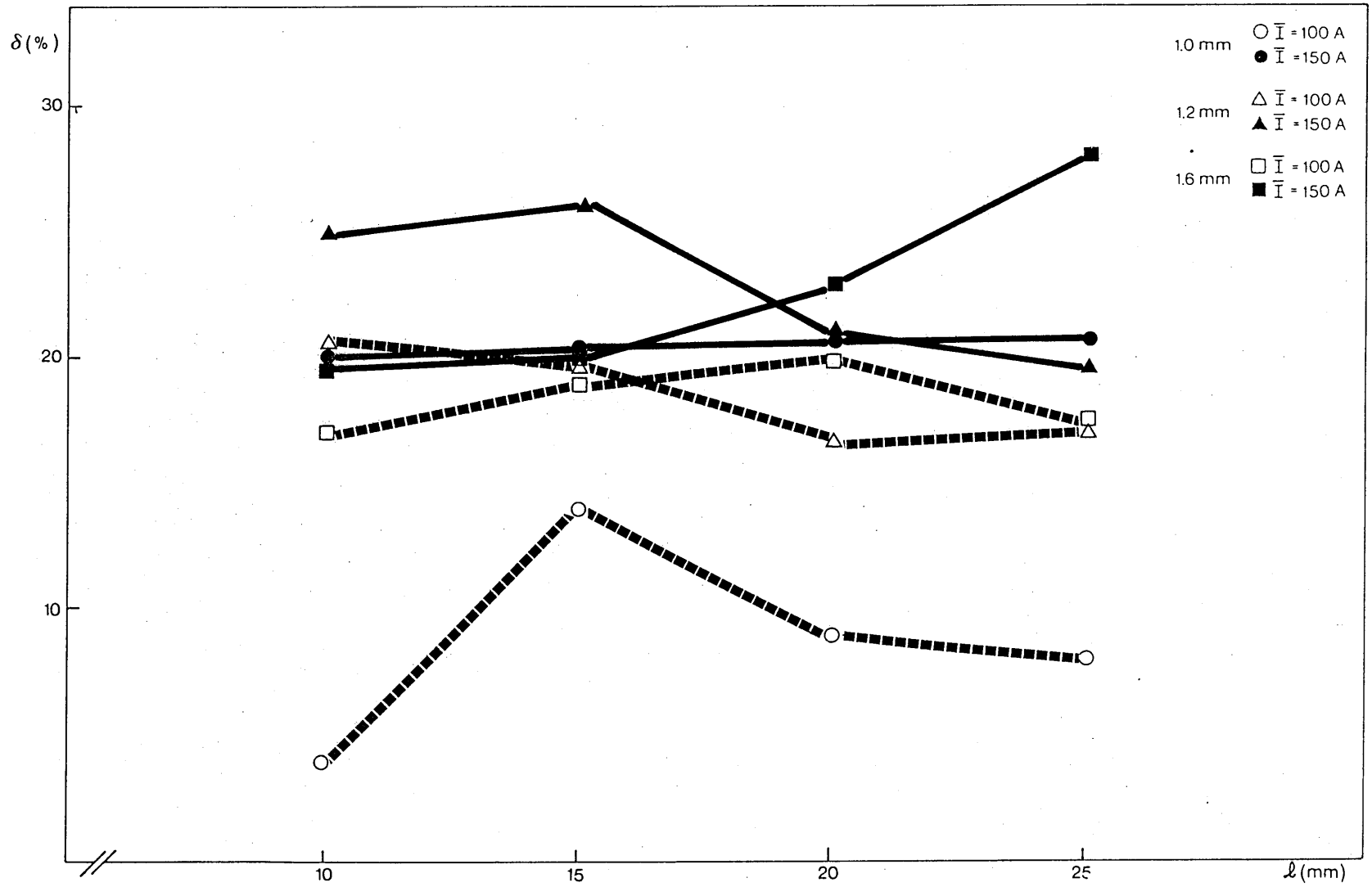

FIG. 80 - Influence of electrode extension on dilution
(I_p = 350 A, t_p = 4 ms, Ar/5% CO_2, v = 1.53 mm/s)

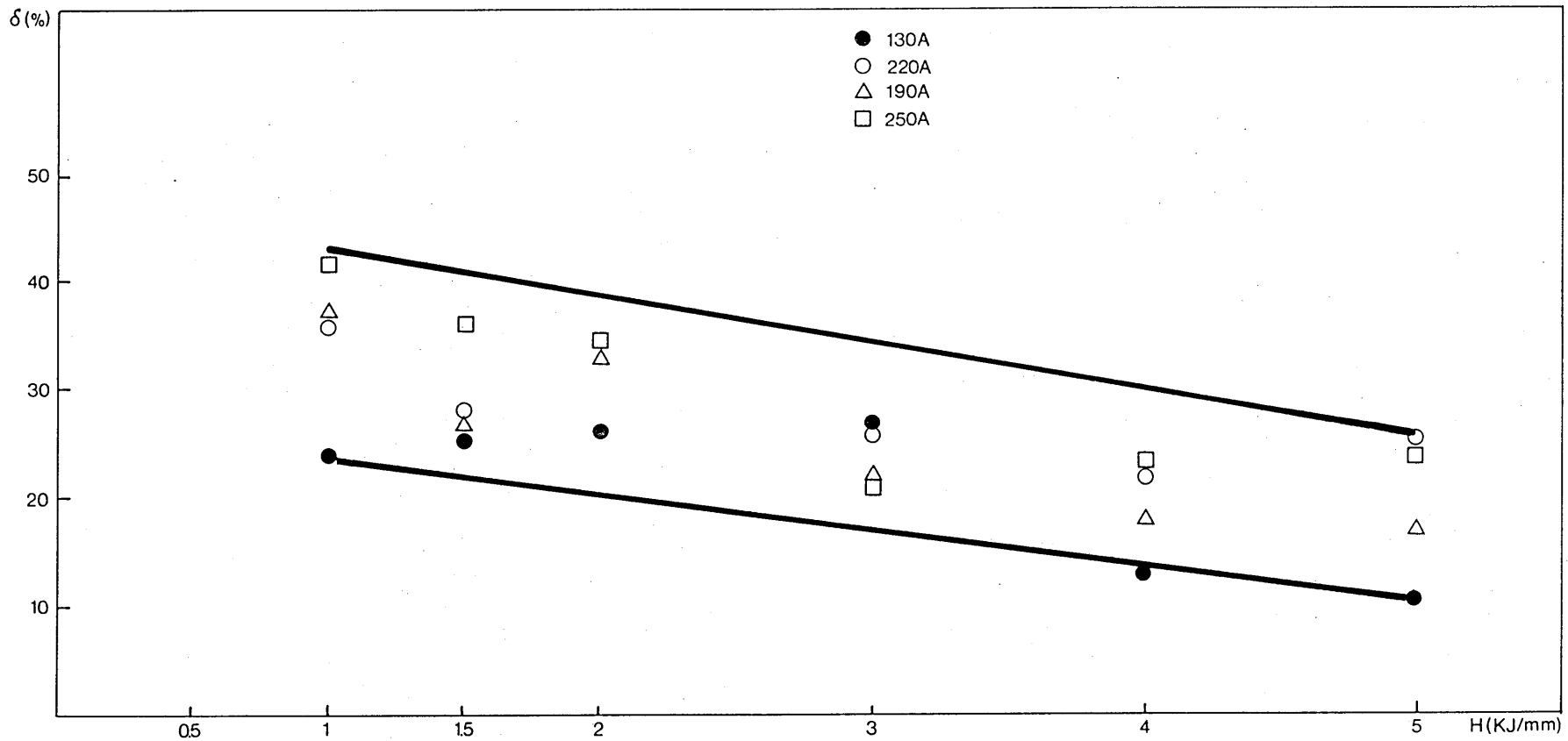

FIG. 8·1 - Influence of nominal heat input on dilution for a range of mean currents (I_p= 350A, t_p= 4ms, $\bar{I}/F$ = 2, ℓ = 15mm, Ar/5% CO_2)

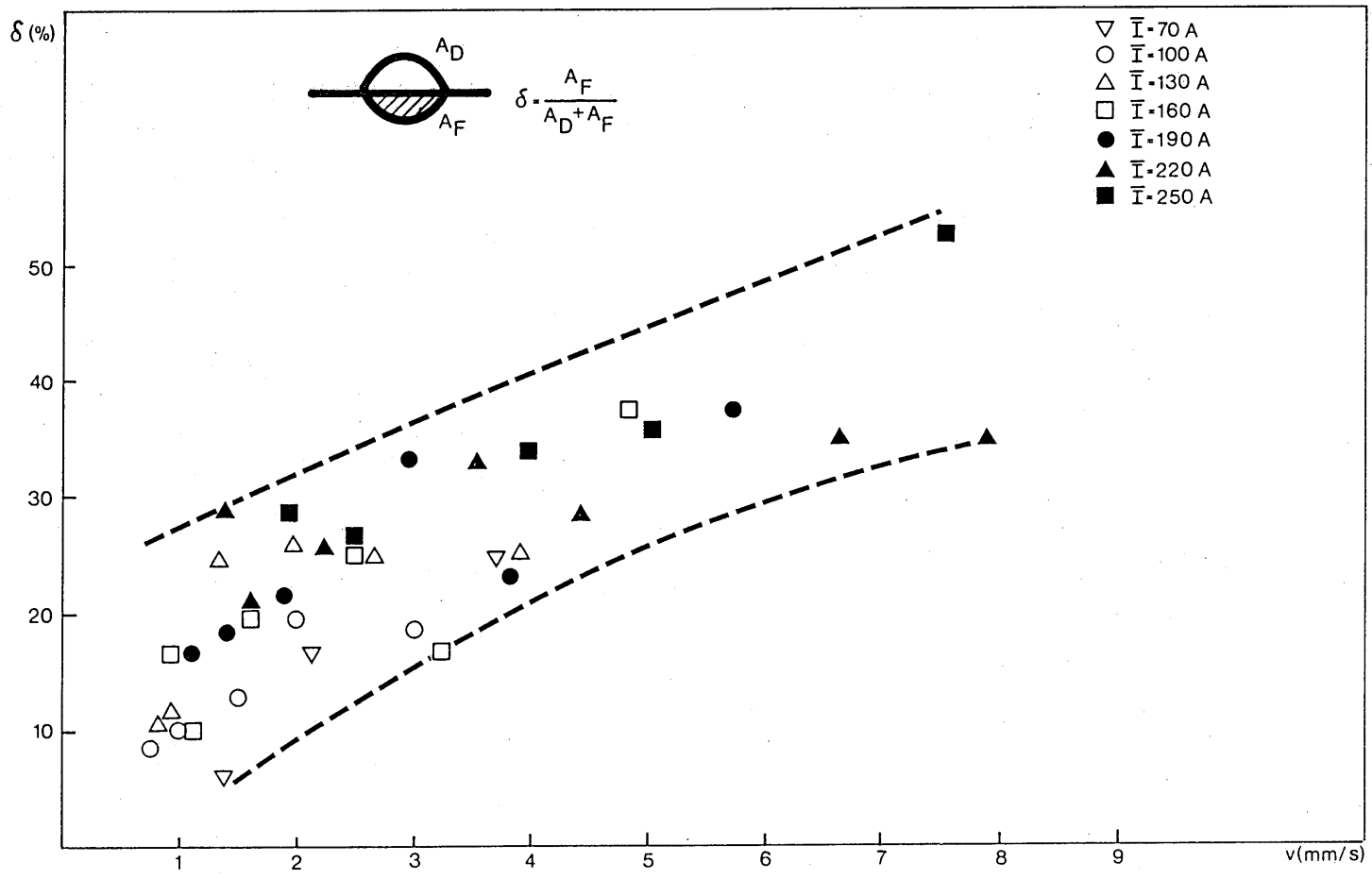

FIG. 82 - Influence of welding speed and arc current on dilution

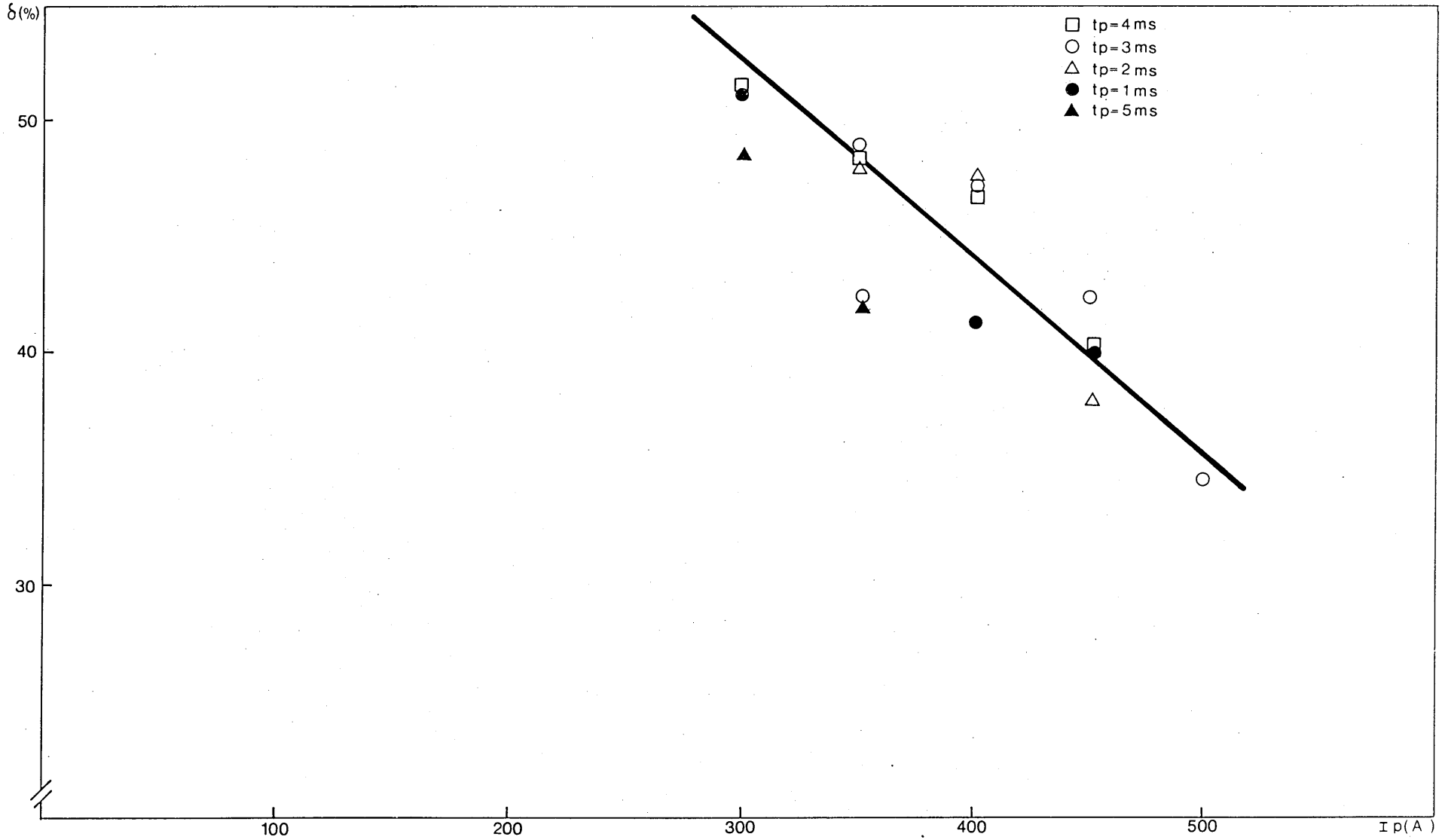

FIG. 83 - Influence of peak parameters on dilution

($\bar{I}$ = 250 A, ℓ = 15 mm, Ar/5% CO_2)

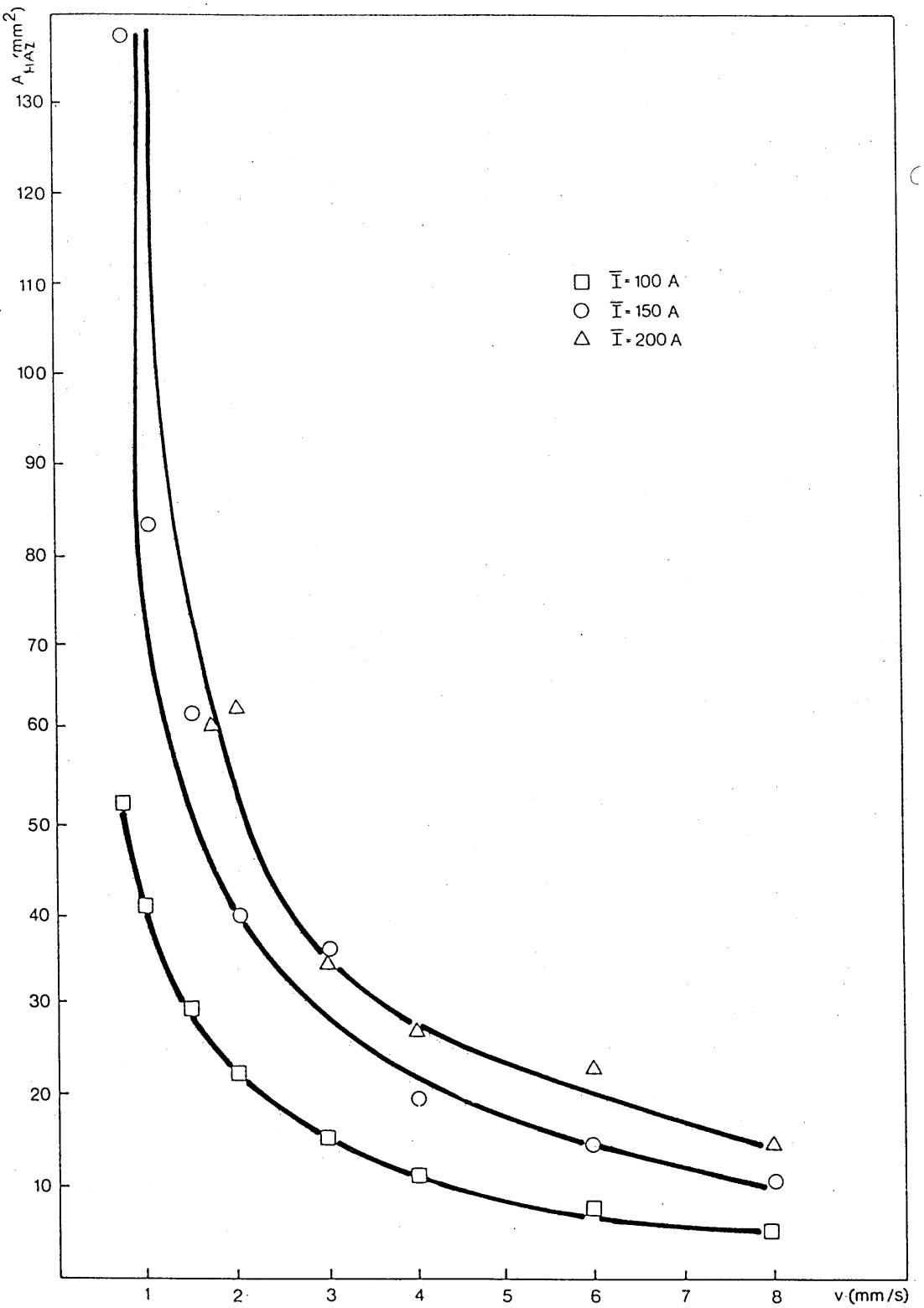

FIG. 84 - Influence of welding speed on heat affected zone area
(I_p= 350A, T_p= 4ms, Ī/F = 2, ℓ = 15mm, Ar/5% CO_2)

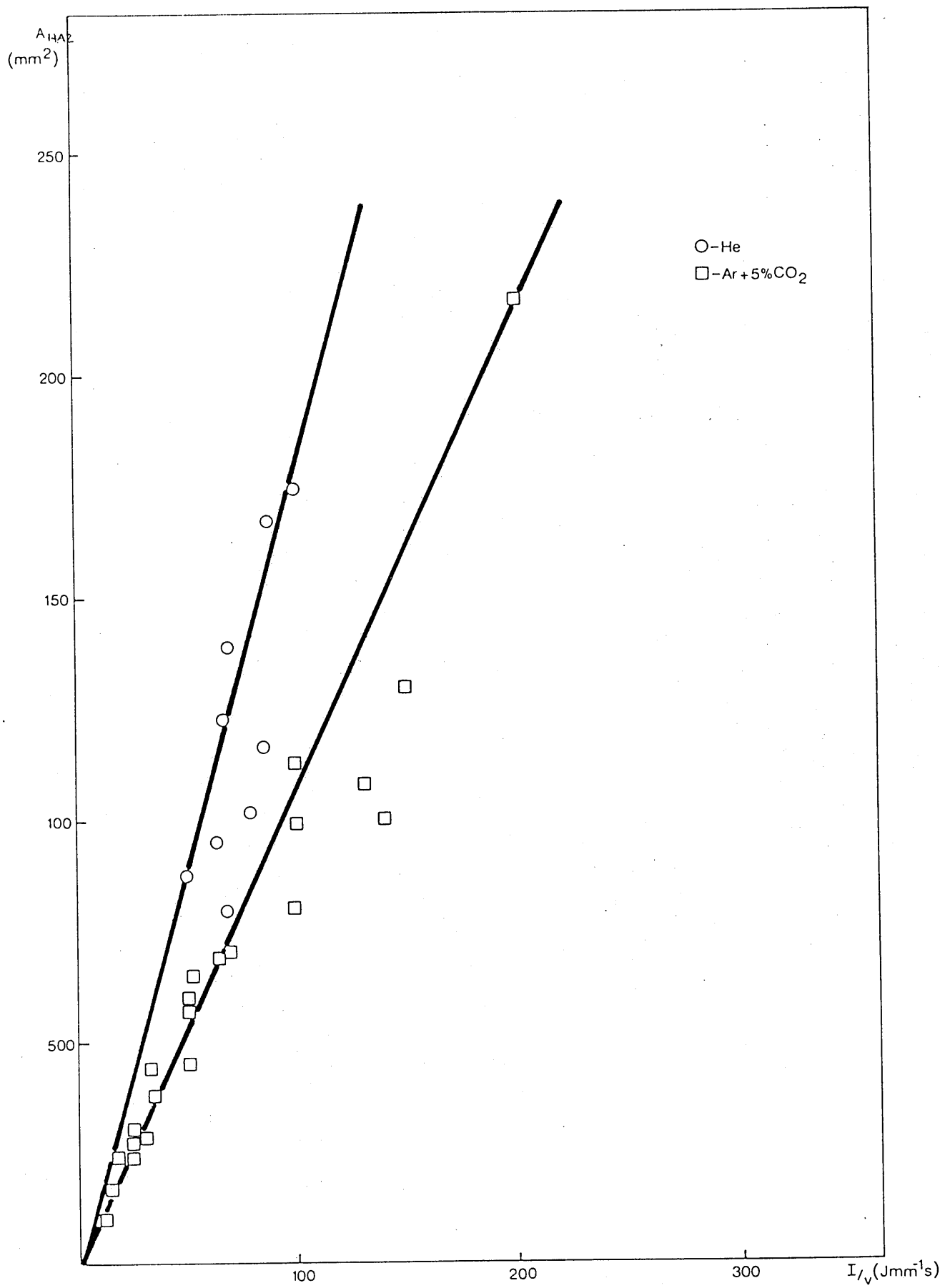

FIG. 85 - Influence of $\bar{I}/v$ on heat affected zone area
(Ar/5% CO_2, l = 15 mm, I_p = 350 A, t_p = 4 ms)

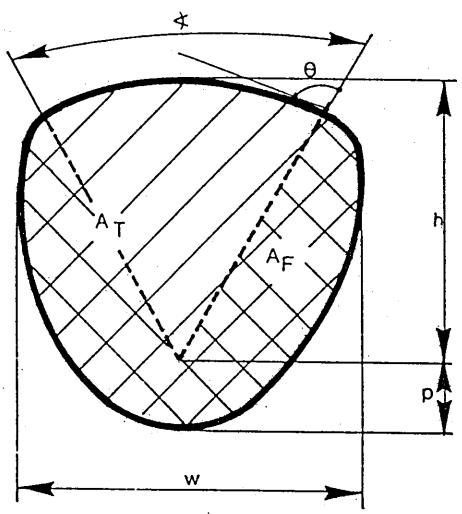

FIG. 86 - Weld bead shape in a V groove

α - V groove angle
θ - wetting angle
p - penetration
h - heigth of deposited metal
w - width
A_F - plate fusion area
A_T - total fusion area

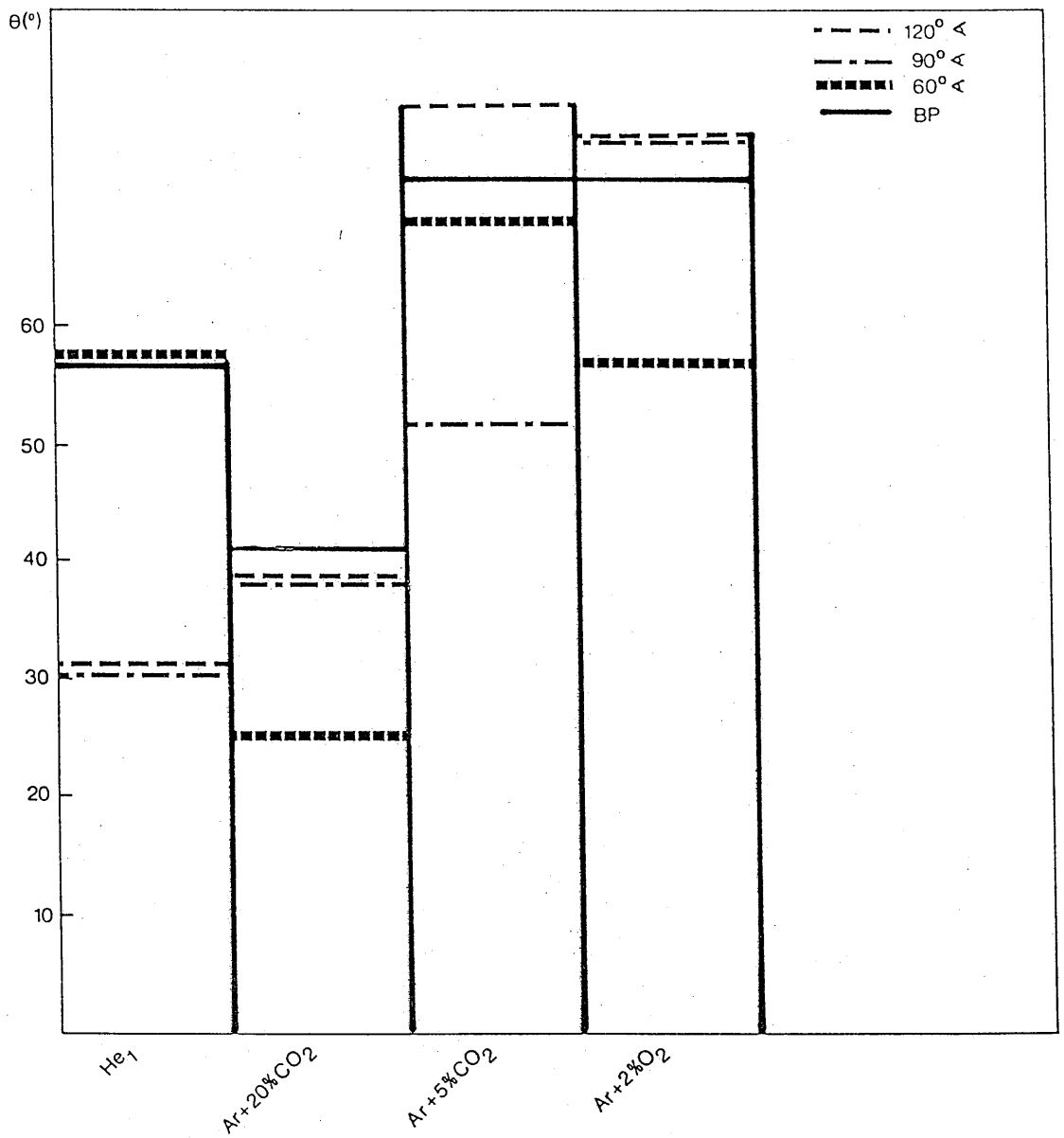

FIG. 87 - Influence of shielding gas composition on wetting angle in V grooves (I = 150 A, v = 2 mm/s, ℓ = 15 mm)

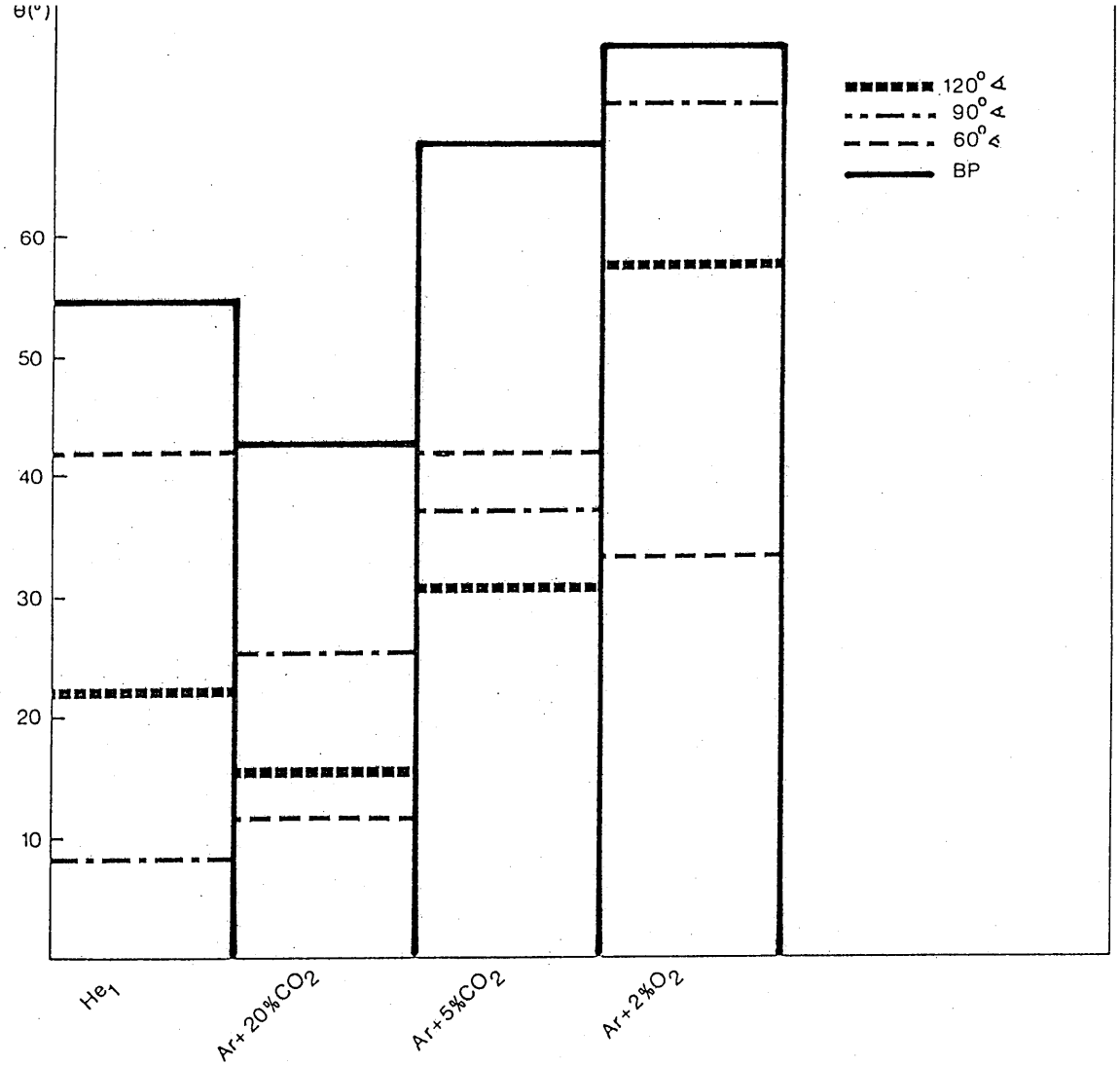

FIG. 88 - Influence of shielding gas composition on wetting angle in V grooves ($\bar{I}$ = 200 A, v = 2mm/s, ℓ = 15 mm)

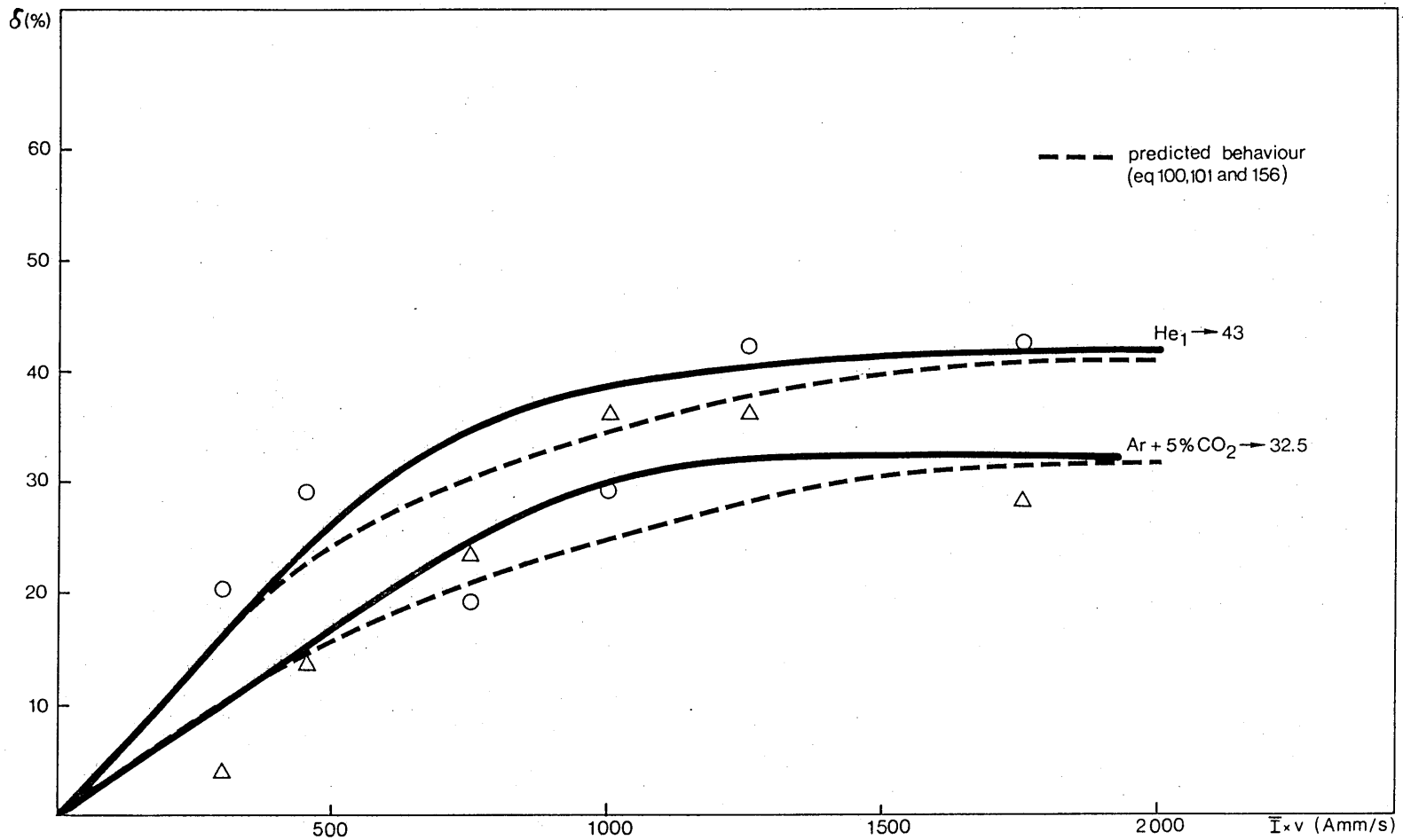

FIG. 89 - Influence of product mean current ($\bar{I}$) x welding speed (v) on dilution (δ)(60^c (1.2 mm wire diameter, ℓ = 15 mm, I_p = 350 A, t_p = 4 ms, $\bar{I}/F$ = 2)

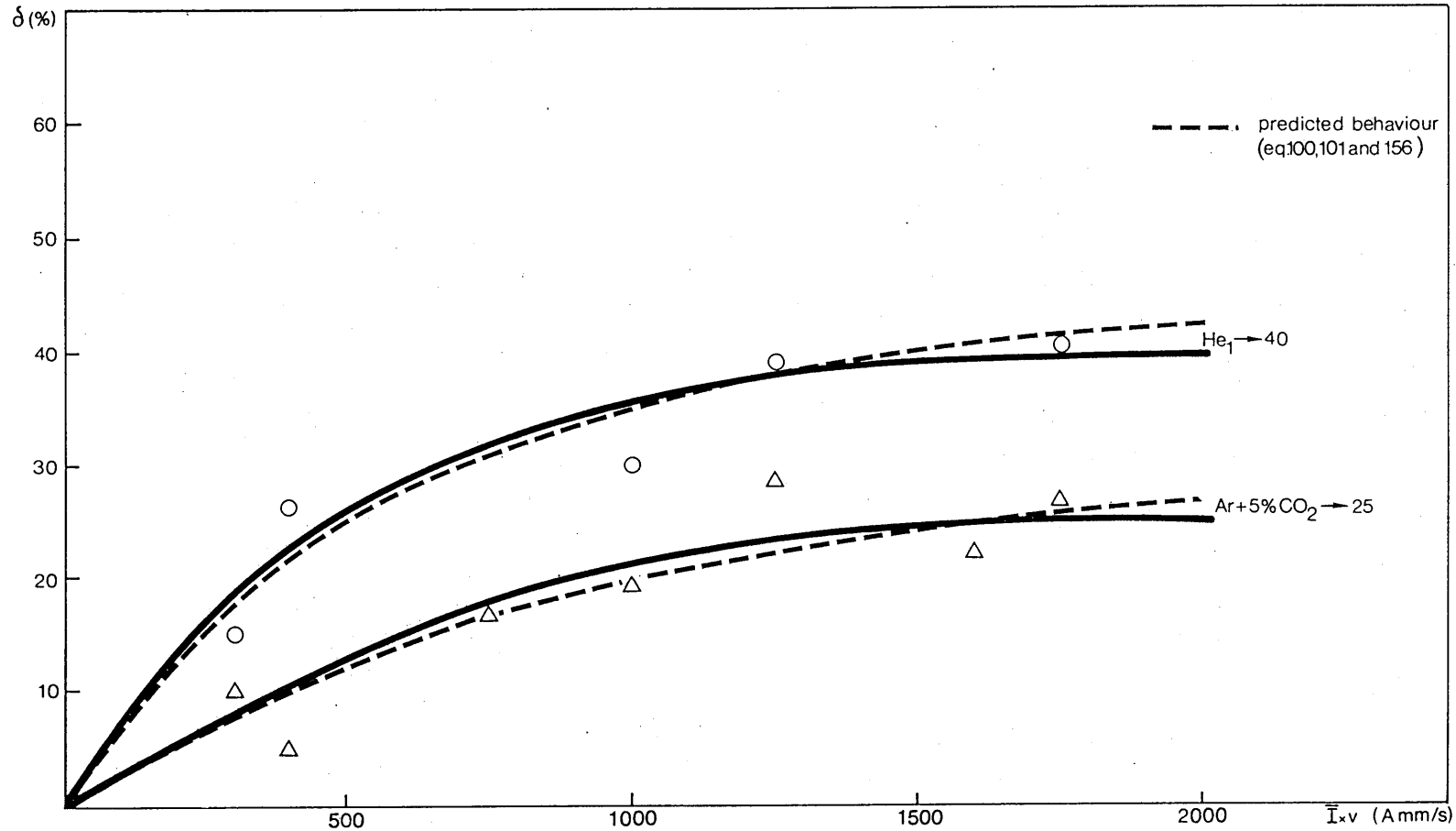

FIG. 90 - Influence of the product mean current ($\bar{I}$) x welding speed (v) on dilution (δ) (90^{o})

(1.2 mm wire diameter, ℓ = 15 mm, I_p = 350 A, t_p = 4 ms, $\bar{I}/F$ = 2)

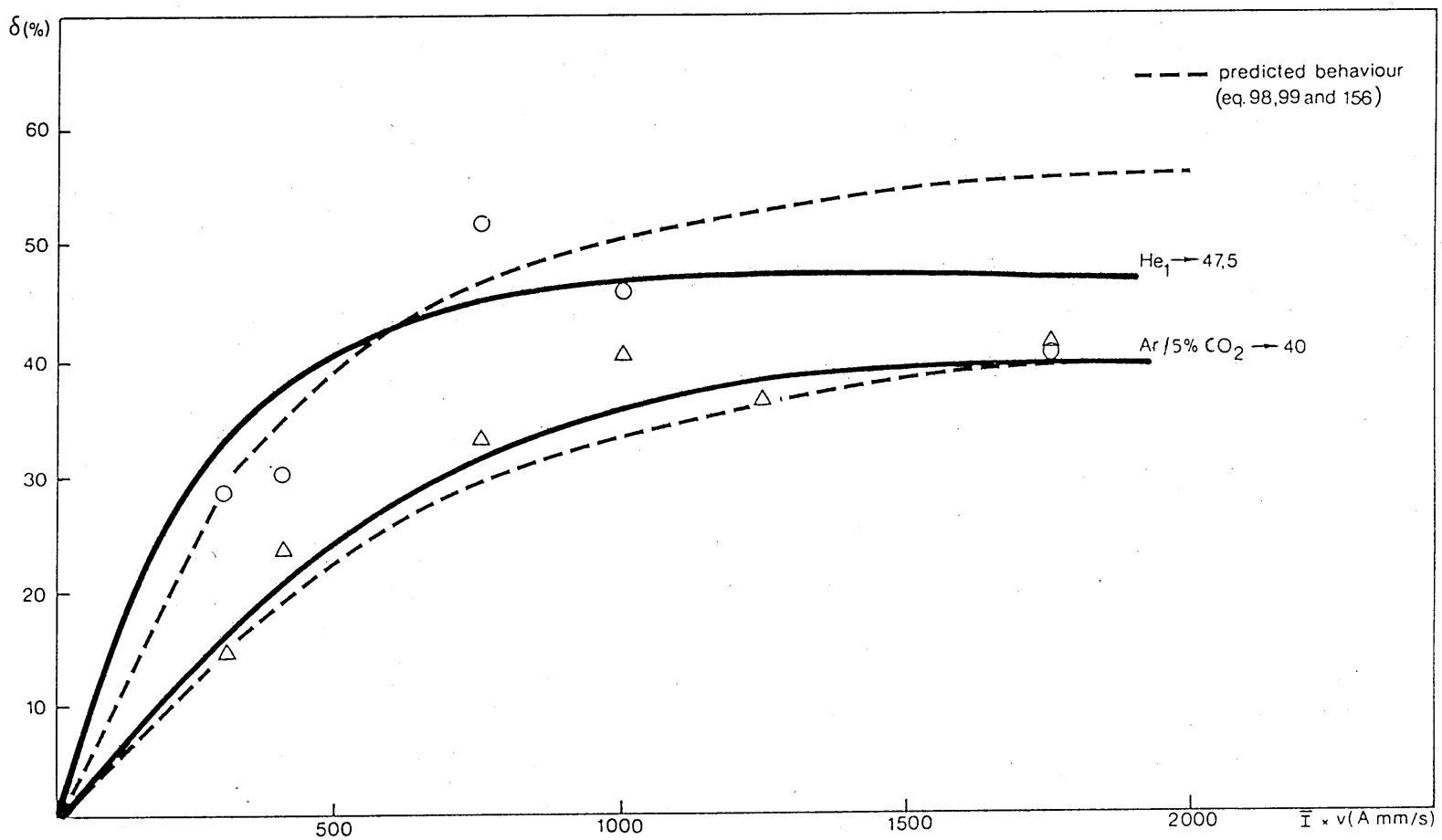

FIG. 91 - Influence of the product mean current ($\bar{I}$) x welding speed (v) on dilution (δ) (120^0)

(1.2 mm wire diameter, ℓ = 15 mm, I_p = 350 A, t_p = 4 ms, $\bar{I}/F$ = 2)

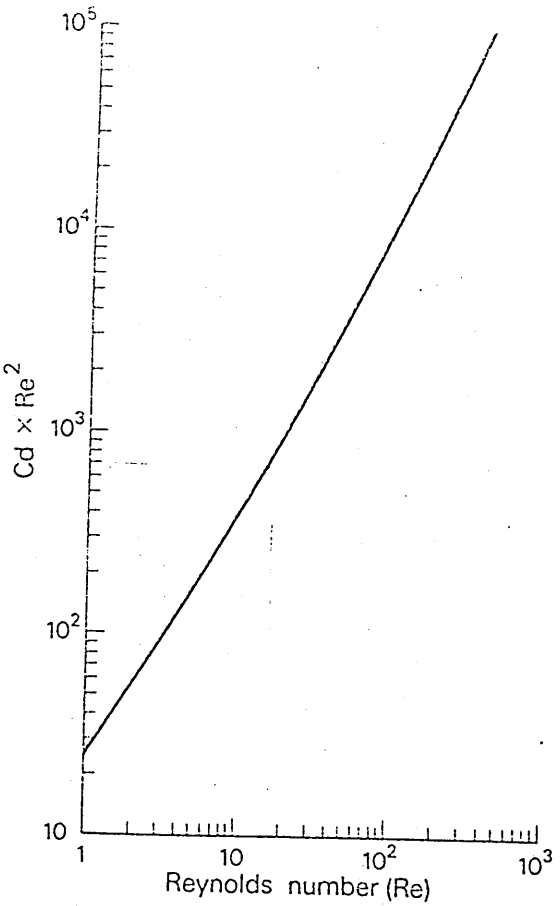

FIG. 92 - The drag coefficient as a function of Re (ref. 44)

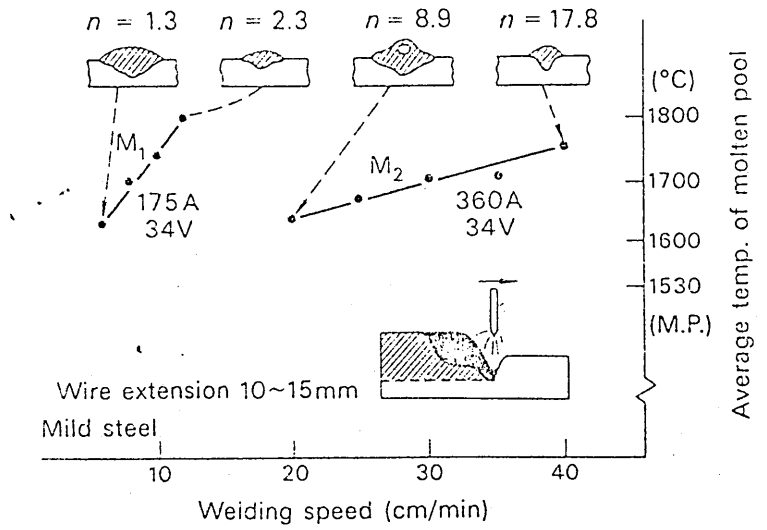

(a) GMA bead welding

FIG. 93 - Average weld pool temperature for GMAW of mild steel (ref. 64)

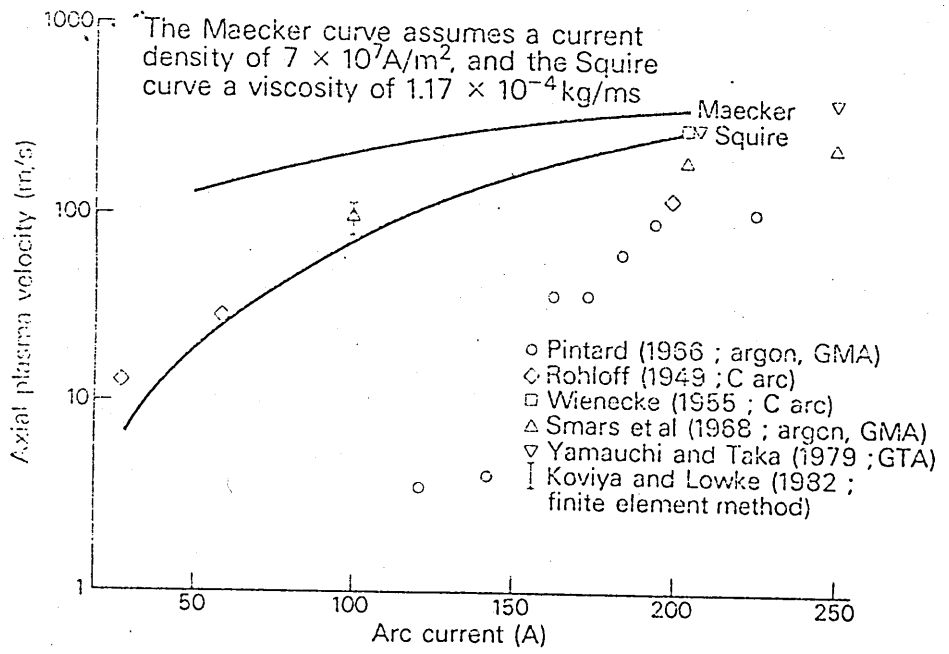

FIG. 94 - Axial plasma velocity 7mm from the electrode tip as a function of current (ref. 64)

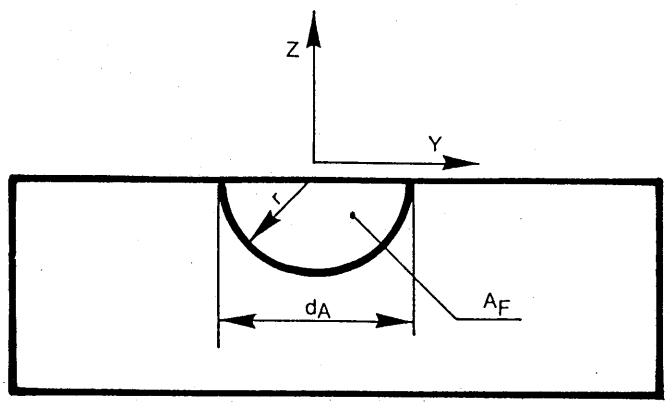

FIG. 95 - Definition of fusion area (A_F)
(d_A - diameter of A_F, r_A - radius of A_F)

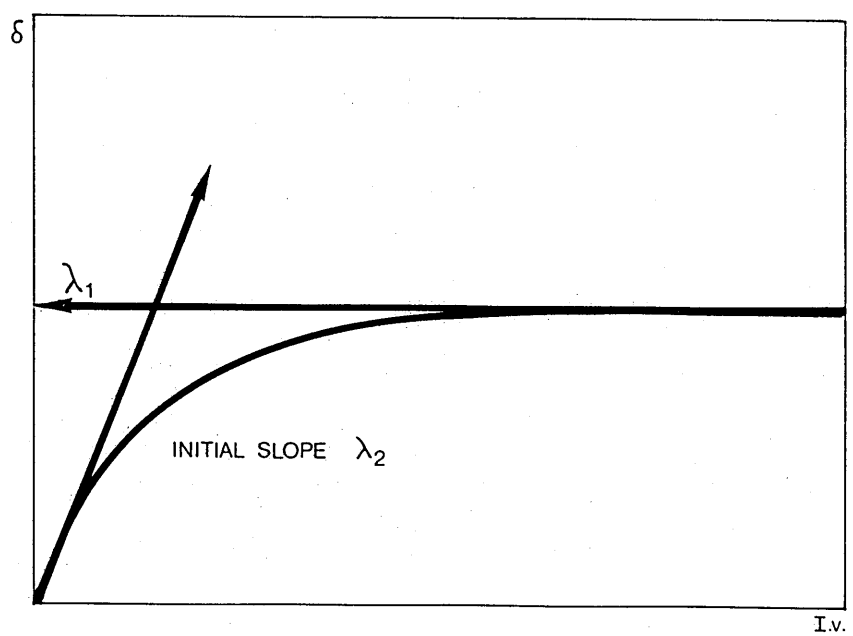

FIG. 96 - Schematic representation of $\delta/\bar{I}.v$
(Relationship given from equations 104 and 105)

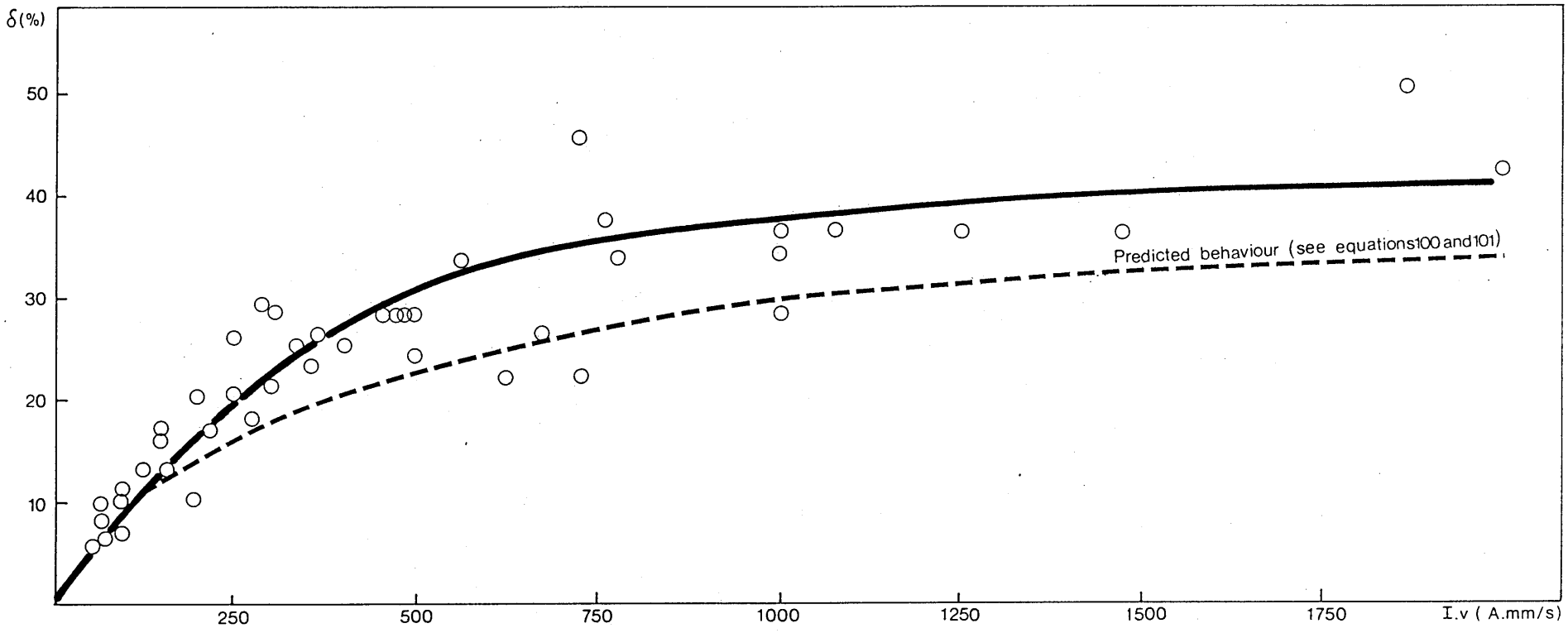

FIG. 97 - Influence of the product mean current ($\bar{I}$) x welding speed (v) on dilution

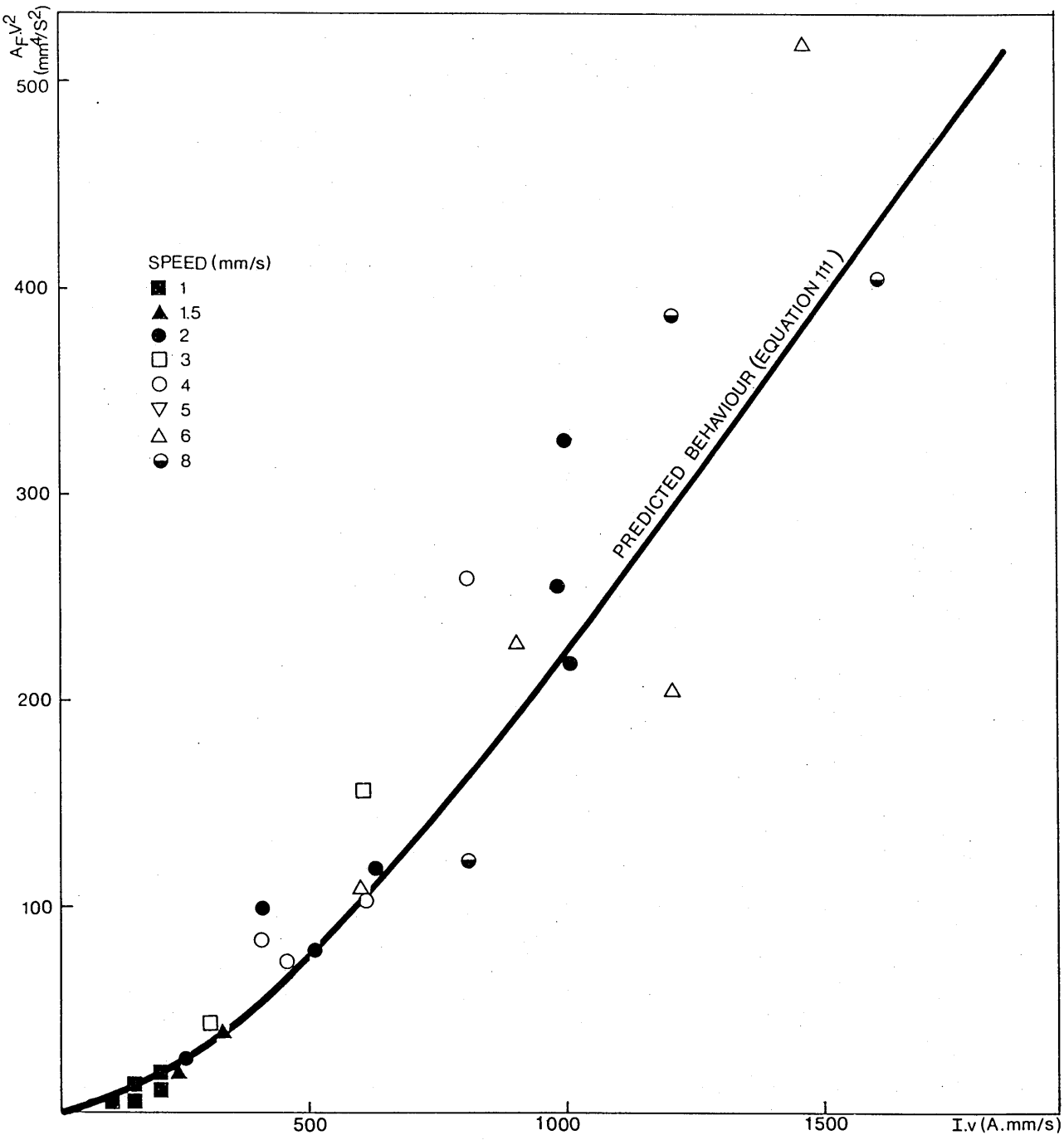

FIG. 98 - Relationship between A_F v^2 and I . v

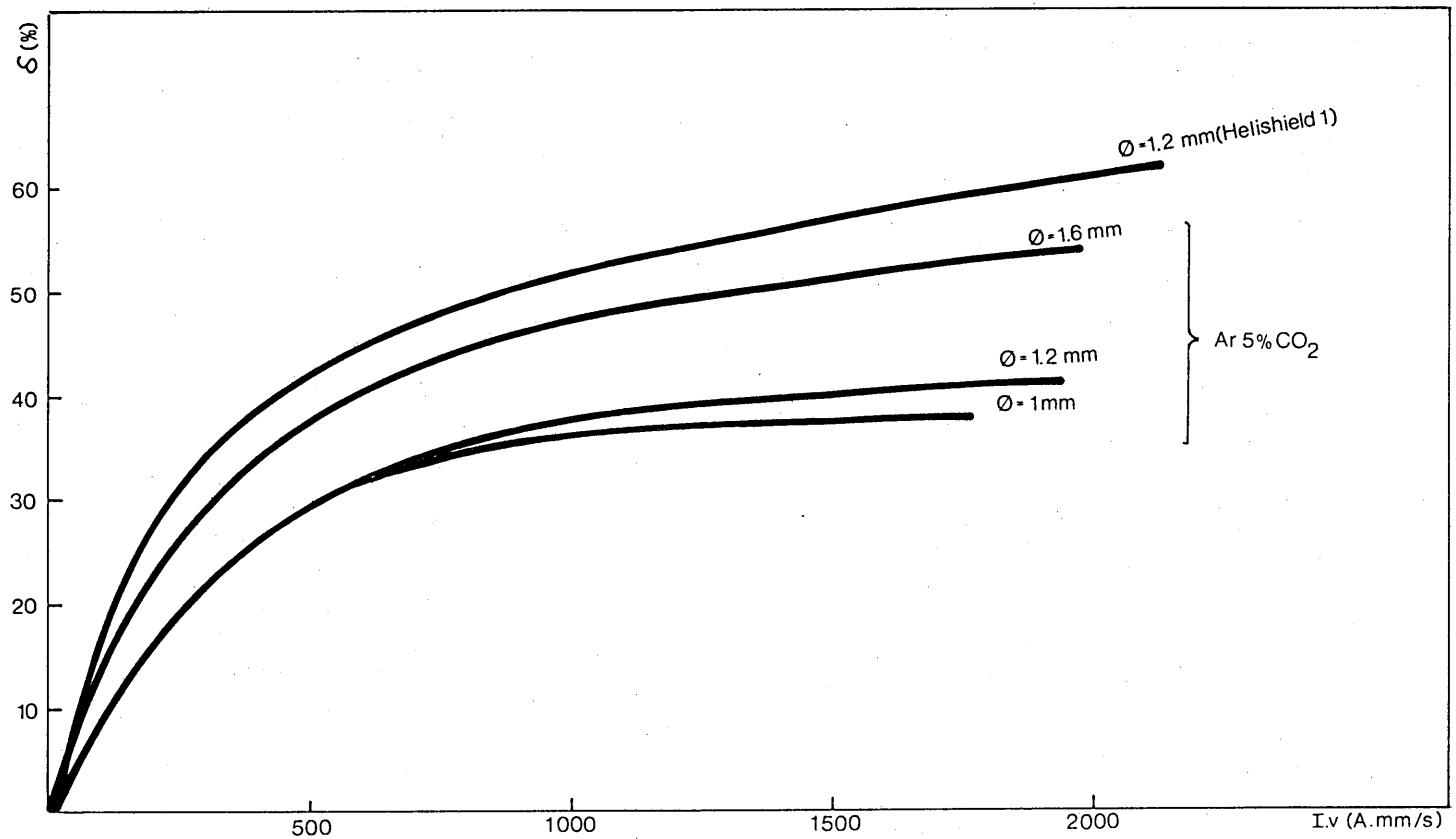

FIG. 99 - Influence of wire size and gas composition on δ

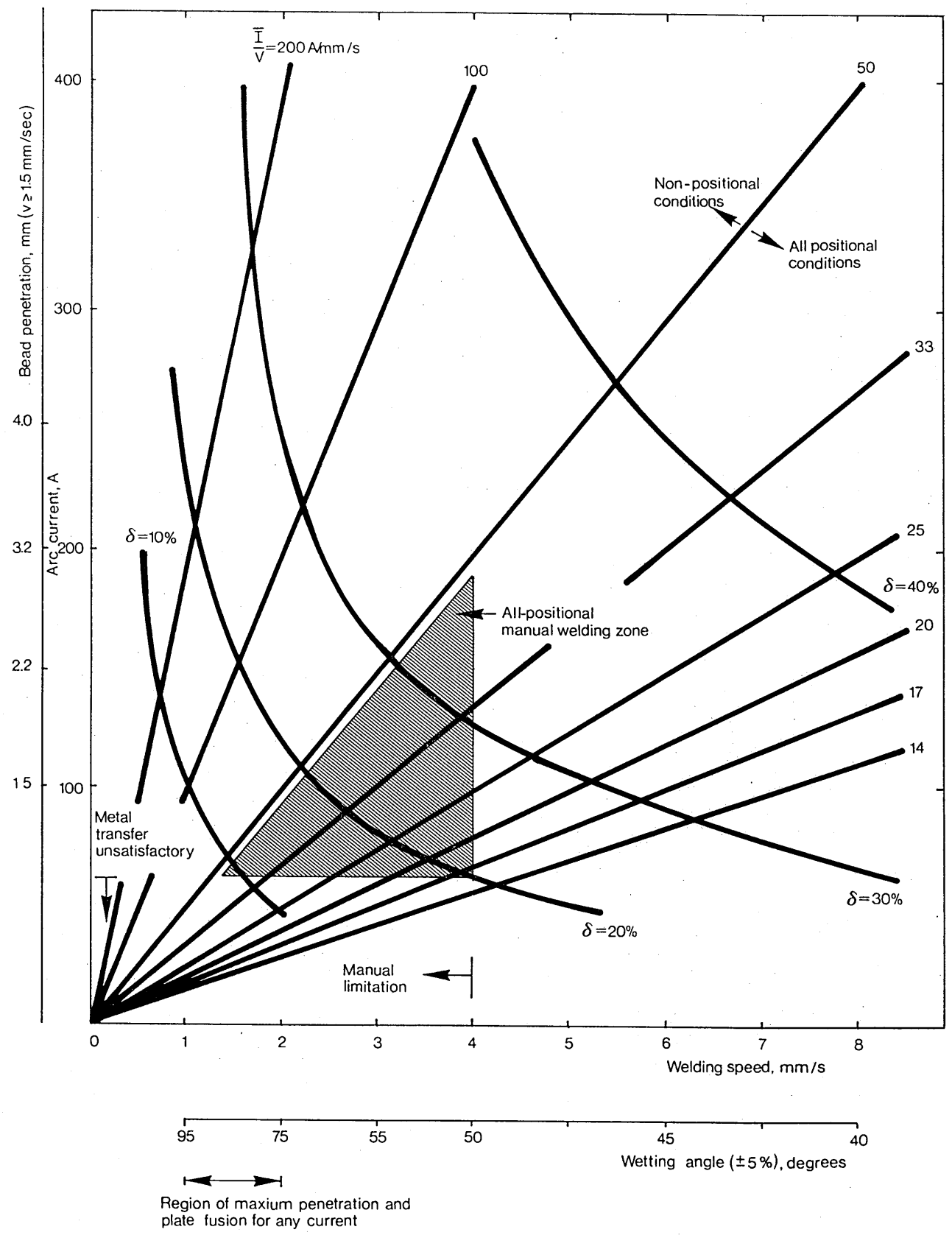

FIG. 100 - Generalized representation of fusion characteristics

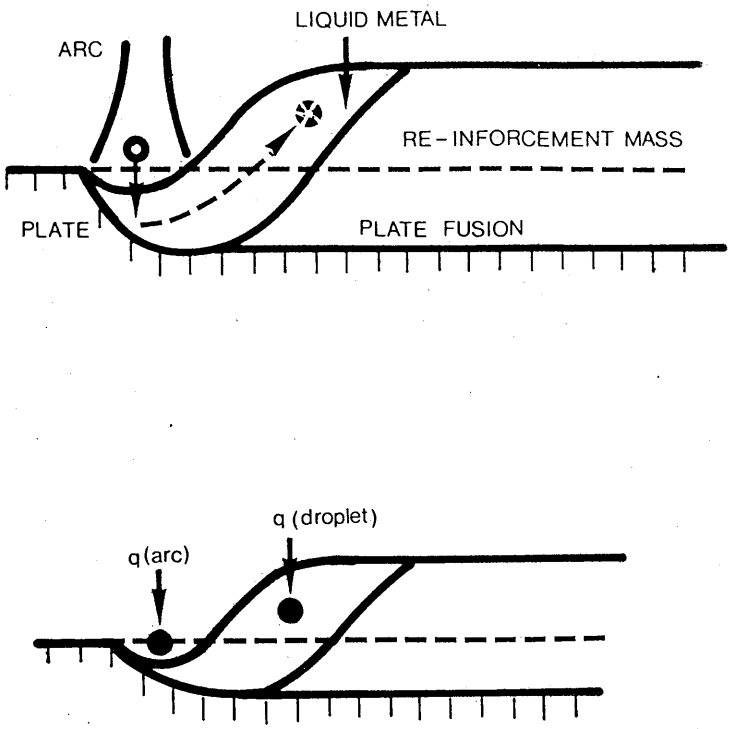

FIG. 101 - Representation of heat source position

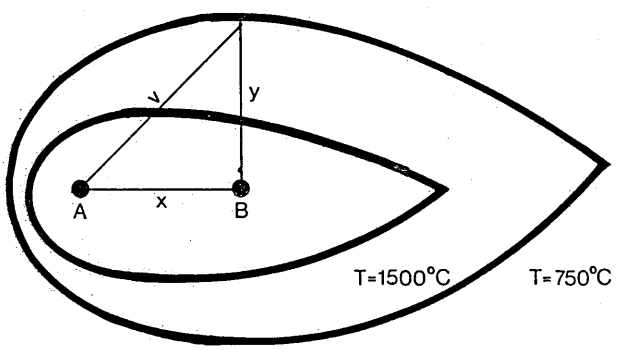

FIG. 102 - Definition of heat affected zone

A - heat source position

B - center of the area defined by the isotherm at 750^{o} C (A_s)

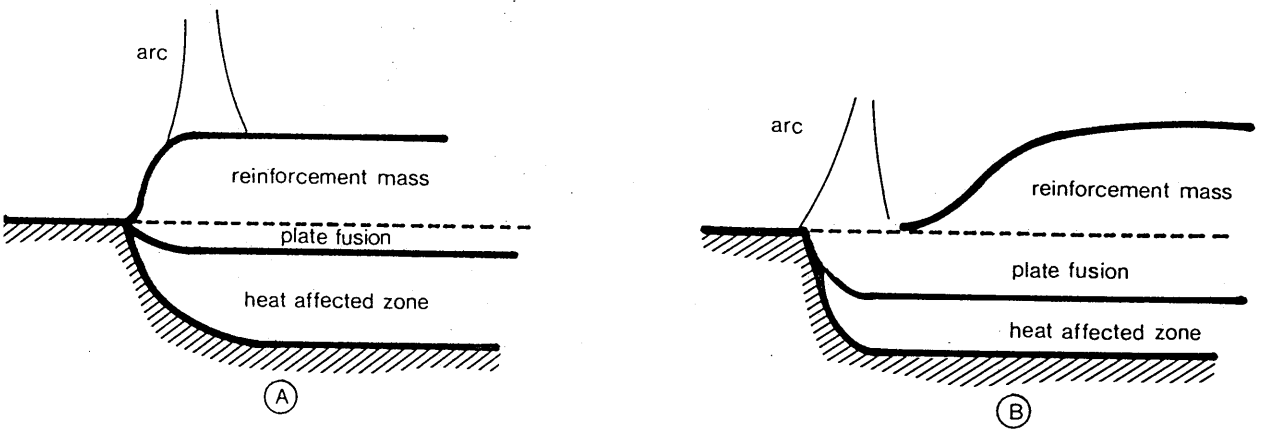

FIG. 103 - Representation of heat source position (extreme cases)

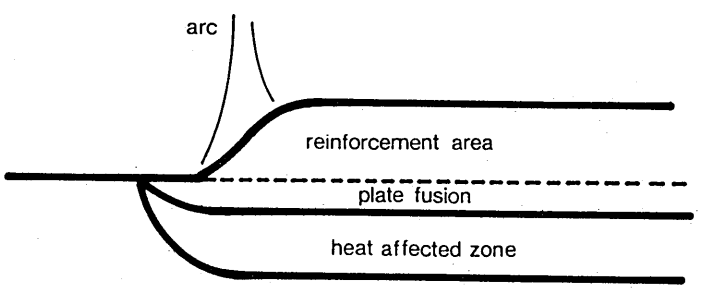

FIG. 104 - Representation of heat source position

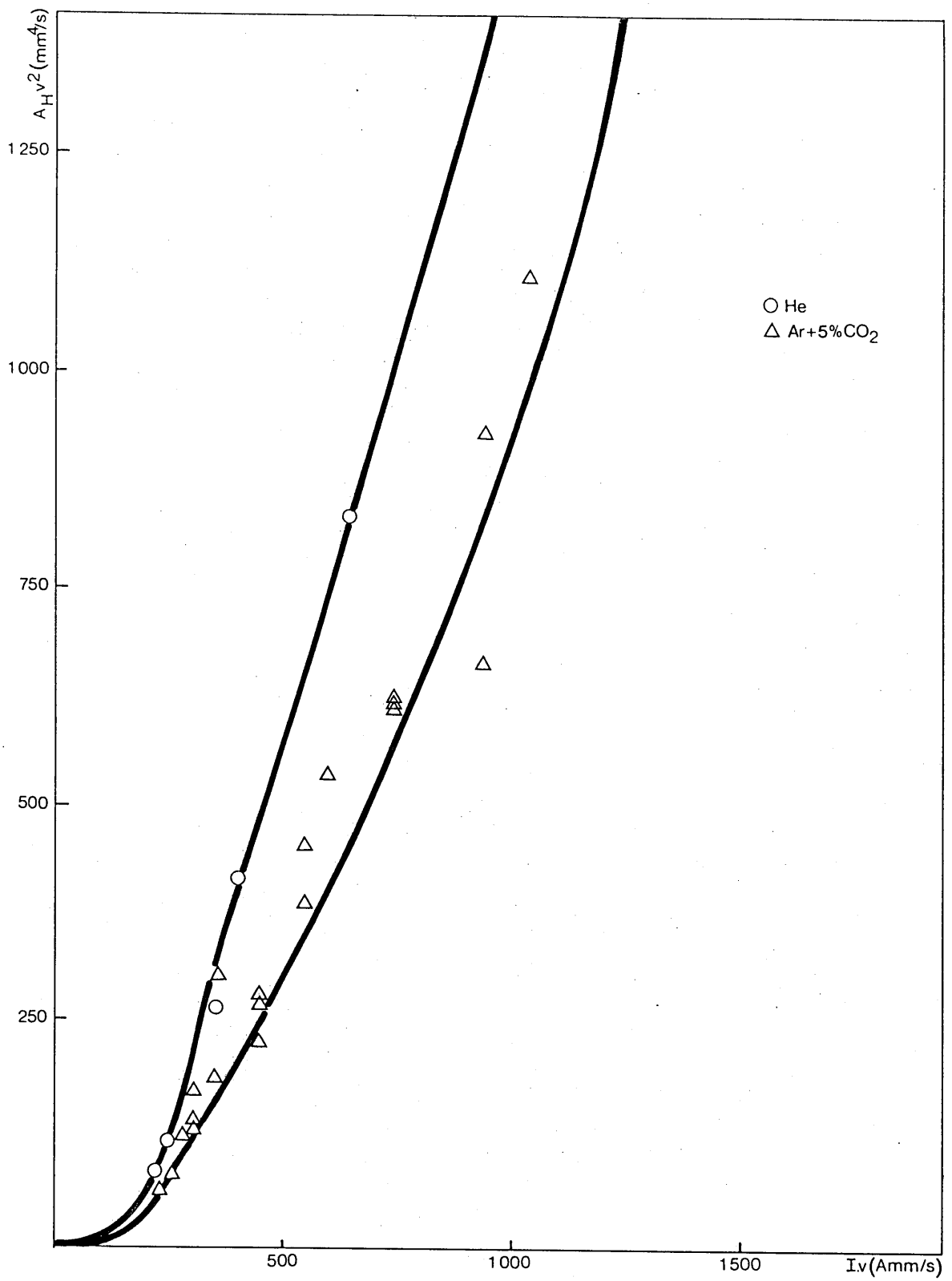

FIG. 105 - Relationship between $A_H v^2$ and I.v
(ℓ = 15 mm, 1.2 mm wire diameter, I_p = 350 A, t_p = 4 ms, $\bar{I}/F$ = 20

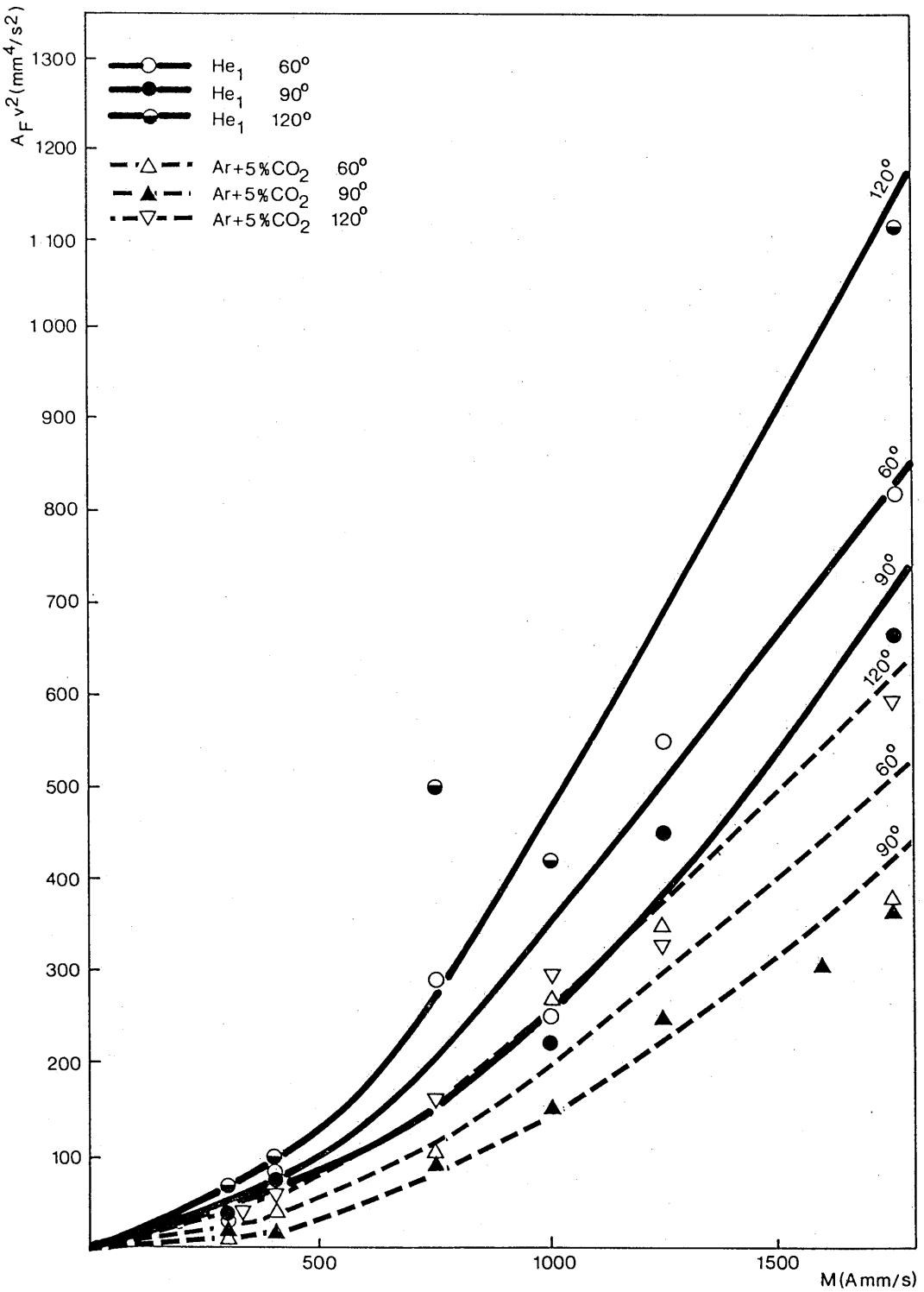

FIG. 106 - Relationship between $A_F v^2$ and I.v in a V groove
(1.2 mm wire diameter, ℓ = 15 mm, I_p = 350 A, t_p = 4 ms, $\bar{I}/F$ = 2)

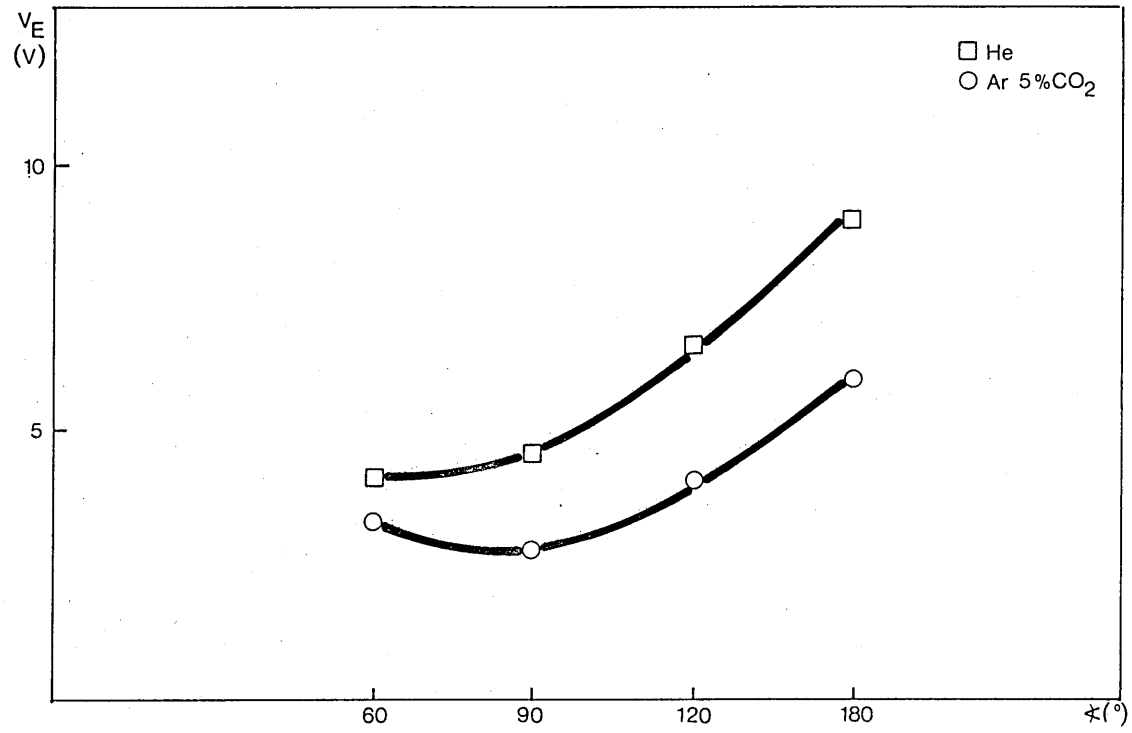

FIG. 107 - Relationship between V_e and V groove angle

- (1.2 mm wire diamter, ℓ = 15 mm, I_p = 350 A, t_p = 4 ms, $\bar{I}/F$= 2) .